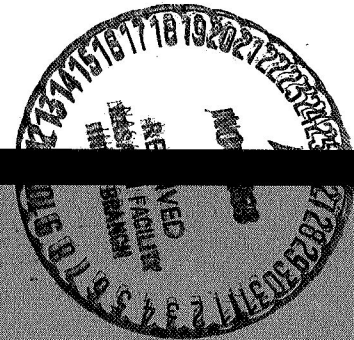# SELECTED TECHNOLOGY FOR THE

ELECTRIC POWER INDUSTRY

A conference held at

LEWIS RESEARCH CENTER

Cleveland, Ohio

September 11 - 12, 1968

NATIONAL AERONAUTICS AND SPACE ADMINISTRATION

SELECTED TECHNOLOGY FOR THE

ELECTRIC POWER INDUSTRY

*The Proceedings of a
Technology Utilization conference held
at Lewis Research Center, Cleveland, Ohio,
September 11 - 12, 1968*

FOREWORD

Large sums of money are currently being spent for aerospace research and development, resulting in a rapid expansion of our knowledge. As our knowledge increases, it is essential that the new information be communicated for general application in our economy as quickly as possible.

Power is an essential ingredient of all space activity. Life cannot be sustained in space without power. Research and development in many areas of power generation is therefore being conducted at the Lewis Research Center and under NASA contract with private industry in support of aerospace activities.

We believe that many aspects of this research in aeronautics and space technology are of interest to the power industry. The program herein was worked out in cooperation with the Edison Electric Institute and was designed to bring you up to date on some of the things we are thinking and doing. We hope you find it interesting and useful.

<div style="text-align: right">

Abe Silverstein
Director
Lewis Research Center

</div>

INTRODUCTION

Walter T. Olson

This Conference on Selected Technology for the Electric Power Industry is intended to acquaint an audience from that industry with some of the technology that derives from the Nation's aerospace activities. The conference is based on the premise that advances made in one technical effort can contribute advances to other fields. Anyone will immediately think of his own examples. For instance, the prime mover that was developed for pumping water out of mine shafts came to propel ships and trains and to generate electricity. And the cycle can close: mine pumps are now driven by electric motors!

Space exploration is a good illustration of a technical effort that, in addition to producing wholly new scientific knowledge, both uses and creates new technology. Space exploration was made possible by the development of rocket propulsion, the computer, and miniaturized electronics. To continue the example, the modern rocket engine has evolved from engines developed for military purposes, and it traces its antecedents to Chinese pyrotechnics. But along the way it has both adapted and helped create turbopump technology, modern metallurgy, sophisticated fluid mechanics and thermodynamics, and advanced control systems.

Based on this premise, then, an attempt has been made to select and to describe technical topics from aerospace activities that might have value in the electric power industry. The technical topics are presented by the staff of the Lewis Research Center and mostly relate to the work of the Center and its contractors. Consequently, a brief description of Lewis and its work provides an appropriate background and setting.

The reader is assumed to have a general familiarity with the national aerospace program as managed by the National Aeronautics and Space Administration. Program components include (1) scientific studies of space phenomena, (2) manned exploration of space, (3) applications of space flight, such as meteorology, Earth resources, navigation, and communications, and (4) extensive research and development both to support present activities and to make future undertakings possible, including advances in aeronautics. Parts of this total NASA program are technically conducted or managed by field Centers, and Lewis Research Center is one of these.

Major tasks of the Lewis Center are research and advanced technology in propulsion and power for flight.

Currently the third largest of NASA's 10 major centers, Lewis has a staff of approximately 4420 people, about 1800 of whom are professional engineers and scientists.

Physically, the Center occupies 350 acres at the southwestern corner of Cleveland, with an auxiliary location of 6000 acres near Sandusky, Ohio, 50 miles west of Cleveland. Lewis comprises extensive laboratories in many buildings for almost every kind of physical, chemical, electrical, and metallurgical research. In addition, unusual tools for propulsion and power technology include such items as space simulation chambers, high-speed wind tunnels of various sizes, engine test facilities that simulate altitude operation, test stands for rockets and components, and radiation sources, including a cyclotron and a 60 000-kilowatt reactor.

The Lewis Center came into being in 1941 as an outgrowth of the powerplants group at the National Advisory Committee for Aeronautics first laboratory at Langley Field, Virginia. During World War II, the Lewis Center made major contributions to reciprocating engine cooling, supercharging, and high octane fuels. The period immediately following saw the development to a high degree of the airbreathing turbojet and ramjet engines. Development of these engines relied heavily on basic results from compressor, fuels, combustion, and turbine research at Lewis. Almost every major U.S. engine powering jet aircraft today has been put through its paces at Lewis to have some item or other of Lewis research incorporated into it. Early work on liquid-fueled rockets, mostly high-energy propellant rockets, paralleled the airbreathing engine program and expanded rapidly in 1957.

Today, the program of the Center is oriented to advancing the technology of chemical, nuclear, and electric rockets and of space electric power for a wide spectrum of power levels. It includes the background research and technology in metallurgy, plasma physics, fluid flow, control dynamics, and other topics pertinent to these engines and to new and unusual propulsion and power generation systems.

Lewis also has had responsibility for development of the operational Atlas-Centaur launch vehicle and for the Thor-Agena and Atlas-Agena launch vehicles. Centaur, an upper stage on Atlas, is propelled with hydrogen-oxygen engines. Hydrogen-oxygen technology was pioneered at Lewis about 12 years ago. The technology of flying liquid hydrogen is vital to many of our future missions, notably Apollo, while Centaur itself is the vehicle that sent the Surveyor spacecraft to soft-land instruments on the Moon. The Atlas-Agena launch vehicle has been used for a variety of important missions, including Nimbus weather satellites, orbiting geophysical observatories, advanced technology satellites, the history-making Ranger and Orbiter photography of the Moon, and the Mariner flights to Venus and Mars.

For the present fiscal year, Lewis expects to account for almost $250 million of NASA's budget. About one-third will be used for salaries, operations, and general

support of in-house projects. The other approximately two-thirds represents contracted research and development work, including a wide variety of projects in universities and industry.

In presenting this Conference, we are contributing to a major NASA effort, namely, to ensure maximum value from national space activities.

At its present level of about $4 billion per year, the space program is a large part of the $17 billion that the Federal Government is spending annually for research and development. Federal research and development expenditures represent about three-fourths of the national total. Thus, it is important that the Nation use the results of all these expenditures as effectively as possible.

A problem of first importance is that of usefully disseminating the technical information being generated in our country, especially when this information is so profuse, so fragmented, and so isolated from many users by company, by industry, by geography, and by other factors, such as the form in which it appears. And so NASA has addressed itself to this problem with a variety of ways of better communicating its results and findings.

This conference is one such attempt at communication. This is only the second time that we have structured a conference for a particular industry. In December 1965, we presented a conference to the petroleum industry. Its success, as measured both by attendance and by continuing follow-on interest and inquiry from companies in that industry, helped to prompt this conference. There are several reasons for having selected the electric power industry for this effort. It is a large industry. It is vital to our Nation's well-being. It is apparent that this industry is in a period in which it is continuously advancing its technology in order to keep up with growing demands for power, for example, the increasing use of atomic energy. And, most compelling, perhaps, technical representatives from this industry expressed the belief that NASA information might be helpful. Because there was this interest, the conference was presented.

Choice of the specific contents of the conference was guided by several meetings and consultations with technical representatives of the electric power industry. In particular, meetings were held first with members of the staff of the Cleveland Electric Illuminating Company and then with a task force of technical executives from several utilities, who were assembled for the purpose under the auspices of the Research Advisory Committee of the Edison Electric Institute. We are grateful for their help, and we thank them for it. They were: Philip A. Salmon, Chairman, Advance Projects Engineer, Electric Engineering Department, Public Service Electric & Gas Company; Edward Hines, Director of Engineering, Research Department, The Detroit Edison Company; Edward C. Kistner, Jr., Engineer in Charge, Power Plant Section, Philadelphia Electric Company; Richard G.

Schuerger, Manager, Civil and Mechanical Engineering, The Cleveland Electric Illuminating Company; and Kenneth L. Wheeler, Manager, Plant Substation, Engineering Department, The Cleveland Electric Illuminating Company. Individual members of the Lewis staff were helped by the Cleveland Electric Illuminating Company and the Detroit Edison Company. The Edison Electric Institute was also helpful in selecting the audience, and the American Public Power Association identified invitees from the public sector of the industry.

The first topics presented (Nuclear Reactors, Rankine Cycle Systems, and Brayton Cycle Systems) have been assembled from a large body of work that the Lewis Center and others have been engaged in over some period of time. Our overall objectives have been, as stated earlier, to advance the art of propulsion or power generation; specific work to this end has produced both detailed improvement in materials and components and greater understanding of the processes and technical subjects involved. Some of these results have been collected, edited, and organized so that the impact and meaning of any single piece of new technology (e. g., a new material, a better compressor, or a cooled turbine) can be seen in terms of its effect on a total power-generation system.

In organizing the material in this way, it was recognized that costs are important, and costs have been kept in mind in relating technology to systems. Parameters have not been plotted against dollars, however, because we are not really close enough to the electric power industry to do that with authority. Nor, for similar reasons, are we presumptuous enough to design power stations of the future in detail; that is the business of the electric power industry. But our technology is discussed in terms of power-generation systems to try to give it perspective and real meaning.

Other specific topics that members of this industry have selected as having potential value are also presented.

CONTENTS

1. NUCLEAR REACTOR HEAT SOURCES
FOR FUTURE POWER GENERATION

Samuel J. Kaufman, Donald Bogart, John V. Miller, and Richard E. Gluyas

The prospects for the continued increase of nuclear energy sources for the generation of electric power has received much attention. This discussion reviews available data pertaining to this question. It then explores the characteristics of the fast-breeder reactor which seems to offer the greatest potential for the power industry.

Most of the experience at Lewis Research Center has been with reactors for space propulsion or space power systems. These reactors are designed to operate at much higher temperatures and for shorter times than those of commercial power systems, and thus the problems are quite different. Therefore, for this discussion, information was gathered (see bibliography) from the power industry, the AEC, and their contractors and consolidated in light of experience at Lewis. Discussion of this information will serve to establish a basis for the material presented at this conference.

Three general areas of fast-breeder reactors are discussed: (1) the difference between breeder reactors and the power reactors now in use, (2) some of the potential materials problems associated with breeder reactors with major emphasis on the fuel-element materials, and (3) the relative merits of gas and liquid-metal coolants for reactors.

FUTURE POWER REQUIREMENTS AND THE BREEDER REACTOR

The Edison Institute's estimate of the electric power capability for this country up to the year 2000 is shown in figure 1-1. The upper curve indicates that during the next 30 years the electric power demands are expected to increase nearly tenfold, doubling every 10 to 15 years. The lower curve shows the estimated nuclear power capability for this same period and indicates that by the year 2000, 50 to 60 percent of the total electric generating capability will come from nuclear power.

If this prediction of nuclear growth in the power industry is assumed to be correct, a very large increase will occur in the amount of uranium required. Figure 1-2

shows the annual uranium requirements during this period if reactors of the type being used today continue to be built to keep pace with the increasing power demand. The refined uranium ore from which reactor fuel is eventually made is U_3O_8. Within 20 years, the annual uranium ore requirement will have risen to over 100 000 tons per year, nearly 10 times the 1967 production.

For the present type reactors, only a small fraction of natural uranium is actually consumed or burned. Only seven-tenths of 1 percent of the natural uranium is uranium 235 (U^{235}); yet this isotope is the one which produces essentially all the power in present-day reactors. Only about 10 percent of the reactor power comes from high-energy fissioning of U^{238}; most of the uranium, the U^{238} isotope, is not used. A large stockpile of this relatively nonfissionable U^{238} will accumulate to satisfy the U^{235} requirement of these "burner" reactors.

One way in which this growing stockpile of U^{238} can be utilized is by converting it in a reactor to the more fissionable fuel, plutonium 239 (Pu^{239}). This process is shown schematically in figure 1-3 which indicates that U^{238} is classified as a fertile material. When one of these fertile nuclei absorbs a neutron from the reactor, it becomes radioactive U^{239}. This isotope has a half-life of 23 minutes, emits a beta particle, and decays to radioactive neptunium 239. This isotope has a half-life of 2.3 days, gives off a beta particle, and decays to Pu^{239} which is a relatively stable fissionable isotope that can be used as fuel in a reactor.

The total process by which the fertile U^{238} is converted to a fissionable fuel in a reactor is called breeding. The breeding ratio is defined as the ratio of the fissionable material produced to the fissionable material consumed in the reactor. When this ratio is less than 1, as it is in the present-day reactors, there is a net consumption of fuel. However, for reactors in which this ratio is greater than 1, there is actually more fuel produced than consumed so that, at the end of a fuel cycle, a net surplus of fuel will exist. Such a reactor is therefore a true breeder.

The doubling time is defined as the time it takes to double the total fissionable inventory within the reactor and within the fuel reprocessing cycle. For example, a typical breeder reactor could have a core loading of 3000 kilograms of plutonium with another 1000 kilograms being processed out-of-core; the doubling time is therefore the time to produce 4000 kilograms of additional plutonium.

The fact that the breeder reactor can produce plutonium from U^{238} means that the uranium ore can be used more efficiently than with present-day reactors. It also means that the net cost of fuel for the breeder reactor will be less than that for burner reactors since the breeder is, in fact, producing rather than consuming fuel. Table 1-I shows a comparison of the fuel costs for a fossil plant, a nuclear burner, and a nuclear breeder. The fuel costs are expressed as fractions of the total cost of generating power. These relative costs are approximate since they vary with geo-

graphic location, type of fuel used, and many other factors. The primary point illustrated is that fuel costs in a breeder reactor are 2 to 3 times less than the fuel costs in nuclear burners or in fossil-fueled plants.

This reduced net fuel cost for a breeder reactor could have an important effect on the overall design philosophy of the breeder system. Since fuel costs are relatively low, thermal efficiency, that is, the efficiency with which fuel is converted to electric power, is less important in a breeder reactor than it is in a nuclear burner or fossil-fueled plant. Therefore, it is possible that, in the design of the breeder reactor, instead of emphasizing thermal efficiency, greater emphasis could be placed on plant cost and system reliability even if a reduction in overall system efficiency were required.

Table 1-II shows a comparison of the breeding characteristics of a present-day burner reactor and a representative breeder reactor. The primary fuel of the burner is U^{235}, while the breeder uses Pu^{239}. Both kinds of reactors have a substantial quantity of the fertile U^{238} present. In the burner reactor, U^{238} is present because the fuel used is only partly enriched in the U^{235} isotope. In the breeder reactor, a large quantity of U^{238} is added to provide a large number of fertile nuclei.

An important difference between the burner and breeder is the average neutron velocity in the two reactors. At present, burner reactors operate most efficiently when neutrons are slowed down to thermal neutron velocities; however, because of the poor nuclear properties of plutonium at thermal neutron velocities, neutrons in a breeder reactor must be prevented from slowing down and kept at high velocity. Reactors which operate on high velocity neutrons are called fast reactors.

Typical breeding ratios for these two types of reactors are 0.6 for the burner and 1.43 for the breeder. The doubling time for such a breeder can be from 8 to 12 years. With this doubling time, the breeder reactors could readily keep pace with the predicted electrical growth of the country.

BURNER AND BREEDER REACTOR CHARACTERISTICS

Today's burner reactors are divided into several classes. Two of the most well known of these are the boiling-water reactor and the pressurized-water reactor. Either type could be used to typify today's reactor systems.

A schematic drawing of a pressurized-water-reactor system is shown in figure 1-4. This plant is composed of a two-loop system: a reactor loop in which nuclear fuel produces thermal energy, and a power-generation loop in which thermal energy is converted to electrical energy. The energy conversion loop is discussed in detail in the papers on Brayton cycle and Rankine cycle systems. In the reactor

loop, pressurized-water coolant enters the reactor at about 550° F, is heated to about 600° F, produces 500° F steam in the steam generator, and is pumped back into the reactor. The net efficiency of the overall system is about 30 percent.

The breeder reactor system and its operating goals, as presently proposed by the nuclear power industry, are shown in figure 1-5. Schematically, this system resembles the pressurized-water system except for an extra loop consisting of a heat exchanger and a pump. Besides the added components, there are some other significant differences. The reactor loop is sodium cooled instead of water cooled. The reason for the change is that water is too good a moderator. Maintaining the high neutron velocities required for an effective breeder makes replacing the water coolant with sodium desirable. Other coolants such as helium and steam are also being considered as fast-breeder coolant candidates, but most of today's emphasis is on liquid-metal cooled systems. In the reactor loop, the sodium enters the reactor at 900° F, is heated to about 1150° F, passes through the heat exchanger where it heats the sodium in the intermediate loop, and is again pumped into the reactor.

The sodium in the intermediate loop enters the heat exchanger, is heated to 1075° F by the sodium in the reactor loop, enters the steam generator where it produces 1000° F steam, and is again pumped back into the heat exchanger. The sodium-cooled intermediate loop was inserted for safety. The reactor loop, which is highly radioactive, can be located within the containment chamber. However, because of the possibility of sodium-water fires, it is desirable to keep the water loop out of the containment chamber. There is still the possibility of a sodium-water fire in the steam generator, but this could be more easily extinguished since it would be located outside the containment chamber.

It should be noted that the outlet coolant temperature in the breeder reactor is 500° F higher than in the pressurized-water reactor in order to produce 1000° F steam for the turbine. The net efficiency in the breeder reactor is 40 percent compared with about 30 percent in the pressurized-water reactor. The high coolant temperature has no effect on the breeding capability of the reactor. As far as reactor performance and nuclear characteristics are concerned, the reactor would be just as effective a breeder at 600° F as it is at 1150° F.

The specific power at which the reactor is operated is among the operating conditions of the breeder which are important to consider because of their influence on performance. Figure 1-6 shows the effect of power density on the breeding characteristics of a typical reactor. The breeding ratio is plotted against the doubling time in years. The parameter shown in the figure is the specific power of the reactor core for 100, 300, and 500 kilowatts (thermal) per liter of core. The shaded band represents the previously discussed 10- to 15-year period during which the electrical power requirements of the country will double. In order for breeder re-

actors to keep pace with this growth, the doubling time of breeder reactors should be equal to or less than this 10- to 15-year period. For a given breeding ratio, it is necessary to operate the reactor at as high a specific power level as possible to minimize the doubling time. For a breeding ratio of 1.43, the specific power of the core must be about 300 kilowatts (thermal) per liter in order to lie in the shaded band. This specific power represents a large increase over present-day burner reactors which operate at power densities of 60 to 90 kilowatts per liter.

This necessity for high power density has some important effects on the operating requirements of materials for fast breeders. The fuel burnup required for a breeder fuel pin would be approximately 10 atom percent of the fuel, whereas present reactors have burnups of the order of 2 to 4 percent. Such high burnups are required in breeder reactors because of the direct relation to high power density and to the need for keeping the refueling interval to about a year. If the fuel burnup were limited to 2 to 4 percent as in the present reactor, the higher specific power associated with the breeder would mean that some of the fuel pins would need to be changed every month or two. This refueling procedure would result in a large percentage of down time for such a system and would reduce the load factor of the plant considerably.

Another important result of the higher specific power of the breeder is the level of neutron exposure which the cladding of the fuel pin must withstand. In the present systems, the cladding receives a total fast flux neutron exposure of about 10^{22} neutrons per square centimeter. This exposure would be increased an order of magnitude to 10^{23} neutrons per square centimeter in the breeder reactor. As shown later, this increase in neutron exposure seriously affects the performance of the cladding material.

Development of the proposed liquid-metal-cooled fast-breeder reactor appears to be much more difficult than was the development of the present-day burner reactors because first, the specific power at which the breeder fuel element must operate is increased; second, the operating temperature is increased; and third, the coolant is to be changed from water to sodium.

MATERIALS PROBLEMS IN BREEDER REACTORS

An examination of the potential materials problem areas can be made by considering the fuel element and its basic component, the fuel pin. A typical breeder reactor fuel pin is shown in figure 1-7. It is made of stainless steel, is 1/4 inch in diameter and 8 feet long, and has a wall thickness of about 15 mils. Oxide fuel pellets are placed in the tube, which is then capped at both ends. The figure shows that

there are two void regions in the pin: one, an annular gap between the fuel and clad; the second, an axial void region above the fuel. The annular gap allows for thermal expansion and fuel swelling; the axial void is used to store fission gases which escape from the fuel.

A breeder reactor contains about 5 times as much fissionable fuel per unit volume of core as a burner reactor. The breeder is therefore very sensitive to small movements of the fuel pins. The possibility of a power excursion, which could result in severe damage, is avoided by preventing the fuel pins from shifting during operation. This is accomplished by bundling a hundred or more fuel pins tightly together into a fuel-element assembly, as shown in figure 1-8. The fuel pins can be spaced by a wire wound spirally around the pin, as shown in the figure, or by some type of ferrule located between the pins. These spacing devices increase pressure losses and can cause "hot spots" which would result in local increases in fuel-element temperature. These factors make design of the fuel elements a major problem.

Numerous fuel-element assemblies are clustered together to form the reactor core. Figure 1-9 is a simplified schematic drawing of the breeder reactor. The reactor consists of a central-core region containing a mixture of U^{238} and the Pu^{239} fissionable fuel; this central section is surrounded by a blanket region containing U^{238}. Breeding of new Pu^{239} fuel takes place in the U^{238} both in the core and in the surrounding blanket. The heat generated in the fuel elements is transferred to the sodium which is pumped through the core.

The number of fuel pins required to dissipate the heat from a reactor is given in figure 1-10. The required number of fuel pins is plotted against reactor diameter for a 1000-megawatt-electric reactor. Curves are shown for three pin diameters, 1/4, 3/8, and 1/2 inch. There are about 200 000 1/4-inch fuel pins in the breeder reactor - about 4 or 5 times the number used in the present burner reactor. A considerable portion of the increased number comes from using the small-diameter fuel pins proposed for the breeder reactor. The justification for the small-diameter pin is discussed later.

For the breeder reactor, the large number of fuel pins, the high burnup, the high neutron exposures, and the high temperature require high performance materials. The fuel-pin materials that are in the most advanced stage of development are oxide fuel and stainless-steel cladding. The oxide fuel consists of a mixture of uranium oxide and plutonium oxide. The stainless steels being considered are the 300 series, austenitic type, particularly 304 and 316 stainless steel.

However, some alternate fuels and cladding materials also are being considered. The alternate fuels are a mixture of uranium and plutonium carbides and a mixture of uranium and plutonium nitrides. Uranium-plutonium metal fuels also are a pos-

sibility but are less promising than the ceramic fuels and are not discussed further. The alternate cladding materials (nickel alloys, vanadium alloys, and the refractory metals, including niobium alloys and molybdenum alloys) offer higher strength than stainless steels if higher strength is required.

Fuels

Three properties of a fuel are most important in determining its suitability for use in a breeder reactor: thermal conductivity, swelling under irradiation, and compatibility with cladding materials.

The thermal conductivity affects the maximum fuel temperature in the fuel pin for given operating conditions of heat flux and coolant temperatures. Figure 1-11 is a plot of maximum fuel temperature against thermal conductivity for typical breeder reactors being considered. The curves are calculated values for 1/4-, 3/8-, and 1/2-inch-diameter pins.

The maximum allowable fuel temperature is set at about 4000° F to prevent the fuel from melting. With the indicated thermal conductivity of oxide fuel, a 1/4-inch-diameter fuel pin is the maximum allowable size.

Both carbide and nitride fuels have considerably higher thermal conductivities, as indicated in figure 1-11. Therefore, pins containing these fuels could be as large as 1/2 inch in diameter without exceeding the fuel temperature limit of 4000° F. Earlier, mention was made of 200 000 1/4-inch oxide fuel pins required in large breeder reactors. Use of 1/2-inch carbide or nitride fuel pins could reduce this number by a factor of 4 and thereby greatly reduce the fuel fabrication costs. If preferred, the higher thermal conductivity of the carbide and nitride fuels could be used to reduce the fuel temperature. Keeping the diameter of the fuel pins at 1/4 inch, for example, would limit the maximum temperature of a carbide or nitride fuel pin to less than 2500° F.

Fuel swelling under irradiation is a particularly severe problem with breeder-reactor fuel pins because of the high fuel burnups required. That nuclear fuels swell under irradiation because of the generation of fission products is well known. This fuel swelling must be allowed for in fuel-pin designs to prevent external dimensional changes in the fuel pin which could restrict cooling flow and could lead to pin failure.

There are many factors that influence the rate of fuel swelling. These factors are not fully understood for breeder-reactor fuels because only a few irradiation tests have been completed on the mixed uranium-plutonium ceramic fuels. Therefore, existing swelling data on uranium-bearing fuels (particularly UO_2) must be heavily relied on in predicting fuel swelling for the mixed U-Pu fuels.

The seriousness of the swelling problem is illustrated in figure 1-12. Predicted swelling of fully dense uranium dioxide in the temperature range of interest is plotted as a function of fuel burnup under conditions where no fission gas can be released from the fuel. As the figure shows, breeder-reactor fuels which are subjected to about 10 percent burnup may swell as much as 17 percent in volume. The swelling would be much less in burner reactors - about 5 percent in volume because of the lower burnup of about 3 percent.

At the reactor operating temperatures, some of the fission products that cause this swelling are solid and others are gaseous. But the gaseous products (such as krypton and xenon) cause most of the problem. Thus, release of these fission gases from the fuels could greatly reduce the amount of swelling. At the same time, high stresses in the cladding of the fuel pin could be prevented by providing enough void space in the pin so that the released fission gases can be collected without building up high pressures.

Most of the fission gases are released from oxide fuel; very little is released from carbide fuel. Measurements have been made of fission gases released from uranium dioxide and uranium carbide test specimens that were irradiated to about 5 percent burnup at surface temperatures of 1100° F. The uranium dioxide released nearly 90 percent of its fission gases, but the carbide released only about 5 percent. This large difference is related to the difference in thermal conductivities of the fuels. The poorer thermal conductivity of the oxide resulted in much higher central temperatures and a larger temperature gradient in the oxide specimens than in the carbide specimens of the same diameter. These temperature conditions increased the mobility of the fission gases in the oxide fuel and allowed them to be released into the void space.

The interplay amoung fuel conductivity, fission gas release, and fuel swelling introduces a high degree of complexity into fuel behavior and selection. A fuel with low thermal conductivity will tend to release a high percentage of fission gas and will be limited to small-diameter pins. Larger diameter pins can be used with high conductivity fuels to reach comparable temperatures, but temperature gradients will be lower and fission gas release may not be as great. This would perhaps still leave a swelling problem.

Differences in fission gas release and swelling behavior between the low- and high-conductivity fuels will affect the fuel-pin design. They will require that some-what different design approaches be used for oxide fuels than for carbide or nitride fuels. Because the carbide or nitride fuels will retain more of their fission gases, they will swell more than oxide fuels. Therefore, some void space must be provided within the fuel pin to allow for the swelling without straining the cladding. Void space is also required in oxide fuel pins to allow release and collection of the

fission gases at low pressures. However, the locations of the required void spaces differ, as shown in figure 1-13. Schematic illustrations are shown of the cross sections of parts of pins containing oxide fuels and carbide or nitride fuels. The dots in the fuel area represent porosity initially fabricated into the fuel and the fission gas bubbles.

In the case of the oxide, the high temperature and the large temperature gradient cause porosity in the fuel to migrate to the hottest zone at the center and form a central void which usually extends the full length of the pin. The fission gases also migrate to the hottest region and into this central void. Once there, the fission gases can move axially into collection chambers provided at the ends of the fuel pin. These void spaces at the ends of the pins also provide space for some axial swelling of the fuel which occurs because of the solid fission products and residual unreleased fission gas. This design approach was used recently for a test pin containing U-Pu oxide fuel that was irradiated to about 12 percent burnup. About 83 percent of the fission gases were released to the collection chamber and the oxide fuel swelled about 7 percent axially, but the most important observation was that the external diameter of the fuel pin did not change.

For carbide or nitride fuels, which do not release as much of their fission gases, an annular void space between the fuel and cladding appears to be necessary, as shown in figure 1-13. This space should allow swelling of the fuel without imposing high stresses on the cladding. However, this annular void (or gap) introduces a problem in heat conduction across the gap. This problem may be remedied by using either high-pressure helium or liquid sodium to increase the thermal conduction across the gap. This design approach currently is being tested in several irradiation specimens containing mixed U-Pu carbide fuels. Only a few specimens have been examined so far, and these were irradiated to fuel burnups of less than 5 percent. However, the results appear encouraging in that no appreciable increase in pin diameter was found.

The third area of concern with respect to fuel selection is its compatibility with pin cladding; that is, the fuel and the cladding should not react excessively with each other. Compatibility data available in the literature have been evaluated and the results show that there is good compatibility of the oxide, carbide, and nitride fuels with the various cladding materials considered. However, this is so only if the stoichiometry of the fuel is precisely controlled, because changes in fuel composition can lead to fuel-clad reactions. The stoichiometric composition of UO_2, for example, is exactly two atoms of oxygen for each atom of uranium.

Stoichiometric effects seem to be more important for carbide and nitride fuels than for the oxide fuel. For example, figure 1-14 indicates the effect of fuel stoichiometry on compatibility with cladding for carbide fuels of uranium and plutonium.

The depth of attack of the fuel on the cladding is shown to vary with the carbon content of the fuel. The stoichiometric mixture is that at the minimum. Lowering the carbon content leads to the formation of free uranium and free plutonium which can alloy with the cladding. Raising the carbon content can lead to carburization of the cladding. Therefore, the composition of carbide fuel must be carefully controlled to maintain near-stoichiometric composition to minimize the depth of attack.

In summary of the fuels discussion, oxide, carbide, and nitride all have merit as breeder-reactor fuels. The oxide fuel is the prime candidate because of the experience with uranium dioxide and because the compatibility of oxide with clad materials is not sensitive to small changes in fuel stoichiometry. Carbide and nitride have better thermal conductivity and hence offer the potential of using larger and thus fewer fuel pins. However, the choice of fuel will ultimately be made on the swelling characteristics and the ability to accommodate the swelling by adequate fuel-pin design. This type of information is being obtained in extensive fuel irradiation tests throughout the country.

Cladding

The fuels, however, are only one part of the fuel element, the other aspect is the cladding material. As mentioned earlier, austenitic stainless steels are currently considered the prime candidates for use as fuel-pin claddings. However, alloys of nickel, vanadium, niobium, and molybdenum are also being studied for this use.

In selecting a cladding material for fuel pins, many factors must be considered, but three are most important.

(1) The first of these is material strength, particularly its long-term creep strength at the maximum operating temperatures. The cladding must be able to withstand the high internal stresses generated by the swelling fuel along with any fission gases released by the fuel. These stresses must be borne by the cladding without any appreciable strain.

(2) The effects of the cladding material on the operating costs of the reactor must be considered. Not only the cost of the material itself, but also its effect on the breeding ratio and doubling time of the reactor must be considered.

(3) The third major factor concerns the effect of irradiation on cladding materials. In fast-breeder reactors, cladding materials will be subjected to very high neutron exposures because of the high fuel burnup levels and the long operating times. Thus, neutron exposures of more than 10^{23} neutrons per square centi-

meter can be expected. Under these high neutron exposures, the claddings must remain ductile, must maintain good strength, and also must maintain dimensional stability.

Figure 1-15 compares the long-term creep strengths of alloys typical of each class of material. The stress to produce 1 percent strain in 10 000 hours is plotted as a function of temperature for type 316 stainless steel and for selected alloys of nickel, niobium, vanadium, and molybdenum. At 1200° F, stainless steel has a strength of about 10 000 psi, which is probably adequate for use as fuel-pin cladding at this temperature. However, hot spots in the fuel pins could push the cladding temperatures to 1400° F or higher. And, at these temperatures, 316 stainless steel has very little strength. Thus, it would be desirable to lower the operating temperatures of the fuel pins if stainless-steel claddings are used. Alternatively, the higher strength alloys shown in figure 1-15 could be used at higher operating temperatures.

Using these higher strength alloys can increase the cost of the power produced in two ways; the initial cost of the material and its fabrication, and the breeding ratio. Both these factors are shown in table 1-III. The estimate of the relative costs of tubing for typical alloys of each group is listed. For this comparison, the current cost of stainless-steel tubing was used as a base line, and the future costs of the less common alloys were predicted by assuming a normal advance in technology and experience with these alloys. These estimates show that nickel alloys, such as the Hastelloys, should be comparable in price with stainless steel. However, the other alloys are much more expensive primarily because of their scarcer supply and the more difficult fabrication processes involved.

Consideration must be given to the effects of these materials on the reactor breeding ratio, which can be greatly affected by changes in the cladding. The highest breeding ratios can be attained with either stainless steel or vanadium alloys, the next highest with nickel alloys. But the use of the other alloys involves a penalty in breeding ratio. The magnitude of this penalty is important in terms of increased doubling time for the fuel cycle. Because of the slightly lower breeding ratio for nickel alloys, the fuel doubling time increases from 12 to 15 years. And the very low breeding ratios for the refractory alloys of niobium and molybdenum will cause the fuel doubling times to increase, by a factor of 3, to about 35 years.

It is apparent that stainless steels are the most attractive cladding materials from the cost viewpoint provided that the fuel element can be limited to low enough

temperatures. If higher strengths are required, fuel cycle costs will limit the practical alternatives to alloys of nickel or vanadium.

The effects of irradiation on these clad materials must also be considered. Results of in-pile testing are beginning to show that there is a major problem associated with the irradiation of stainless steels, for they become seriously embrittled under neutron bombardment. This is illustrated in figure 1-16 where ductility (expressed as percent uniform elongation) is plotted against test temperature for 304 stainless steel. The upper curve shows the typical behavior of unirradiated 300 series stainless steel; the ductility decreases at temperatures above 1000° F but it remains at tolerable levels at temperatures up to 1500° F. However, material which was irradiated at 1000° F to a neutron exposure of 1.72×10^{22} neutrons per square centimeter has lower ductility even at low temperatures and drops to intolerably low levels at higher temperatures. Furthermore, the embrittling effects increase with higher neutron exposures, and exposures nearly 10 times greater than those seen in this test are expected in fast-breeder reactors.

In addition to this problem of severe embrittlement of the cladding, irradiation to higher neutron exposures can also cause swelling of stainless steel. This problem is indicated in figure 1-17 which shows volumetric swelling measured in 316 stainless steel as a function of neutron exposure in the temperature range of 680° to 1080° F. This range is below the 1200° F reference temperature, but data are not available for 1200° F. There was very little growth at neutron exposures up to about 10^{22} neutrons per square centimeter. But in the extra decade of exposures that are required for materials in fast-breeder reactors, stainless steel actually increased nearly 10 percent in volume. This amount of swelling can cause serious problems in fuel-element claddings. Not only is the strength decreased, but gross dimensional changes can occur amounting to a 3-inch increase in the length of an 8-foot fuel pin and a diameter change of as much as 8 mils for a 1/4-inch-diameter fuel pin. However, there is still hope that by modifying the stainless steel the swelling problem can be eliminated. Some basis for this hope is shown by the triangular data points in figure 1-17. These particular points were obtained on 20-percent cold-worked stainless steel and show much lower swelling than annealed stainless steel for which the curve is shown. Although the data are limited, behavior of this type does indicate that there may be ways of reducing the irradiation-induced swelling of stainless steel.

Thus, it is apparent that there are some serious problems associated with the use of stainless steels as fuel-pin claddings in fast-breeder reactors. Many studies to overcome these problems are currently underway in various laboratories, particularly by the AEC and its contractors. As a result, researchers now have a fairly good knowledge of what causes embrittlement and swelling. The embrittle-

12

ment and swelling at lower temperatures appear to be the result of clustering of irradiation-induced vacancies in the metal lattice. This microscopic vacancy-clustering eventually leads to macroscopic voids and the resultant swelling. This might explain the smaller swelling of cold-worked stainless steel. The microstructure of cold-worked stainless may slow the clustering of vacancies. The problem is compounded by the formation of helium bubbles at higher temperatures. The helium originates from the irradiation of some impurities in the stainless steel but the helium atoms produced do not collect to form bubbles until higher temperatures are reached.

Now that the causes of swelling and embrittlement under irradiation are being better defined, there is hope that methods of overcoming these effects can be found for stainless steels. However, because of these irradiation effects, more consideration is being given to alternate nickel and vanadium alloys as cladding materials. Unfortunately, the irradiation problems found in stainless steels are also being found with nickel alloys. It has been suggested that the similar behavior of both materials is a result of their having face-centered-cubic crystal structures. The vanadium alloys, on the other hand, have a body-centered-cubic crystal structure, and the current theory indicates that this structure should be more resistant to irradiation embrittlement. To date, only a few irradiation tests have been run on vanadium alloys, but the limited data do support the theory. It is observed that vanadium alloys withstand irradiation much better than stainless steels, so that work on vanadium alloys is being accelerated.

In this discussion on cladding materials, austenitic stainless steels are considered the prime candidates because of their low cost and the wide-spread experience with them. However, the strength of these alloys will limit their operating temperature, and they may severely embrittle and swell under irradiation. Thus, either an improved stainless steel must be developed or an alternate material, such as a vanadium alloy, must be used.

Liquid-Metal Corrosion

Another potentially serious materials problem is associated with the use of liquid sodium, which can be very corrosive if it is not used carefully. This corrosion can be detrimental to the fuel-element claddings, the reactor structural members, and coolant loop components, including piping, heat exchangers, and pumps. The presence of impurities like oxygen or carbon or the presence of two or more different metals in the same system can have large effects on corrosion rates.

Ideally, sodium corrosion should not be much of a problem in a single metal

system at the planned reactor operating temperatures of about 1200° F. Figure 1-18 shows estimates of the upper temperature limits at which various alloys might be compatible with sodium. These estimates are based on laboratory-scale tests in which operating conditions are very closely controlled. This figure indicates that sodium corrosion should not be a problem with stainless steel at temperatures below about 1500° F.

However, these limits are very difficult to attain in practical large-scale systems because there are many factors which increase the corrosive effects of sodium. The prime factor is the amount of oxygen impurity in both the sodium and the container materials. The effect of oxygen on the corrosion rate of sodium on stainless steel as a function of temperature is shown in figure 1-19. The three curves indicate probable corrosion rates for sodium containing about 10, 50, and 1000 ppm oxygen. The 10- and 50-ppm curves are based on data obtained in various types of tests. The 1000 ppm curve is estimated. It is apparent from these curves that increasing oxygen content greatly decreases the useful temperature for the system. For example, a corrosion rate of about 1 mil per year is considered the maximum tolerable level for fuel-pin claddings. At this rate, oxygen levels of less than 10 ppm are needed to prevent severe corrosion of fuel-pin hot spots which may be at temperatures of about 1400° F.

This low level of oxygen puts heavy demands on the reactor and system designers, builders, and operators. Therefore,

(1) Reactor designers must insist on procurement of materials with the lowest oxygen content practically attainable.

(2) Extra cautious handling techniques must be used during construction to prevent contamination of either the sodium or the container materials. For example, welding procedures must not introduce impurities like oxygen or carbon.

(3) Gradual oxygen contamination of the sodium during the long reactor operating times will require continual cleanup of the sodium during operation. This requirement leads to complications in the coolant loops because small bypass loops must be added for continual oxygen analysis and purification. Developing components for purification and analysis becomes a major problem. These components must reliably maintain the oxygen content in the sodium below 10 ppm to provide good corrosion resistance.

As mentioned earlier, the presence of dissimilar metals in contact with sodium can aggravate corrosion problems. Dissimilar metals are usually used in coolant loops because of strength, cost, or other factors. However, use of dissimilar metals can lead to transfer of certain alloying elements from one material to another through the sodium. This mass transfer can lead to compatibility problems or to changes in the properties of the materials.

The microstructure of a molybdenum specimen, heated in a sodium-filled nickel container for 100 hours at about 1800° F, is shown in figure 1-20. As a result of this test, a nickel-molybdenum (Ni-Mo) alloy layer about 2 mils thick was formed on the surface of the molybdenum. The Vickers hardness number test indentations indicate that the Ni-Mo layer is much harder than the molybdenum substrate. This hard surface layer could decrease the ductility of the molybdenum and could render it useless for further operation under high strain conditions.

The net effect of using dissimilar metals in sodium loops is to lower the maximum temperature at which they can be used. Figure 1-21 shows the revised estimates of the compatibility limits of various metals in high-purity sodium. The lower, darker portions of the bars indicate the range in which we think the metals should be usable in dissimilar metal systems, for example, in a system where stainless steel is used with a ferritic steel or where a nickel alloy is used with stainless steel. These estimates indicate that stainless steels or nickel alloys used at temperatures of about 1200° F in fast-breeder reactors would be operating in a region near their compatibility limits if other metals are present. Then a potentially dangerous situation would arise that would not allow for any hot spots in reactors nor changes in other effects which could also increase the corrosion rates.

Therefore, sodium-cooled systems that use stainless steel or nickel-alloy components should be limited to operating temperature of 1000° F or lower to ensure hot-spot temperatures less than 1200° F. Since sodium corrosion may limit the operating temperatures of breeder reactors, the use of a less corrosive coolant should also be considered.

BREEDER REACTOR COOLANTS

The choice of coolant for fast-breeder reactors is an area which has received much attention. Gas, steam, and liquid metal have all been considered as possibilities, although much effort is presently being directed toward the use of liquid metals. Some factors which must be evaluated in selecting a coolant are heat-transfer and pumping-power characteristics, the effect on the breeding ratio, and the safety aspects of a loss-of-cooling accident. Several other factors should also be considered.

Although steam, gas, and liquid metal are being considered as coolants, the potential breeding ratio with steam is lower than that of the other coolants. It is somewhere in the area of 1.1 to 1.2 so that the doubling time for a steam-cooled breeder reactor would be well over 25 years. Therefore, this discussion is limited to the two most promising coolants for fast-breeder reactors, sodium and

helium. Sodium, like most liquid metals, has excellent heat-transfer properties, but potentially serious corrosive characteristics. Therefore, helium must be considered as a candidate reactor coolant even though it is a poorer heat-transfer medium than sodium. Comparable heat transfer can be obtained with helium by using high pressure and high velocity. High velocity results in large pressure losses and increases the pumping power requirements of the system.

This point can be illustrated by comparison of two identical reactors operating at the same power level; one reactor is cooled with sodium and the other with helium. Figure 1-22 shows how the surface temperature of the fuel pins will vary in these two reactors if the same inlet and exit coolant temperatures are maintained. While such a comparison may not represent the optimum conditions for either coolant, it does serve to demonstrate the effects. In this figure, the surface temperature is plotted along the length of the fuel pins with the flow of coolant from the inlet at the left to the outlet at the right. The lower curve is for the system where sodium was used as the coolant; the upper curve is for the helium-cooled system.

The maximum cladding temperature of the helium-cooled system is about 200° F higher than the sodium-cooled reactor. In addition, the relative pumping power across the reactor core is twice as great for the helium-cooled system. However, since the pumping power requirement for a typical sodium-cooled reactor loop is less than 1 percent of the power output of the plant, even a factor of 2 on pumping requirement may be an acceptable value.

There are several ways of improving the heat-transfer characteristics of a gas-cooled reactor. One is to roughen the surface of the fuel pin in the region of high clad temperature. This will improve the heat transfer and reduce the surface temperature of the fuel pin. Surface roughening is only done to the portion of the pin where the temperature is high because roughening the fuel pin increases the pressure drop and pumping power requirements. In the example shown here (fig. 1-22), the relative pumping power across the core has increased by about 50 percent as the result of roughening only the hot portion of the fuel element. However, the maximum surface temperature has been reduced to less than 100° F over that of the sodium-cooled system.

Achieving even this moderately good heat transfer required the use of relatively high-pressure helium (1250 psi). This will introduce some additional design problems for the helium-cooled system, but these must be weighed against the problems involved in using a potentially highly corrosive liquid metal.

Another problem is that of the hot spots associated with the fuel pin spacer, which was mentioned earlier. Because of the power heat-transfer characteristics of helium, this problem would be more severe than in the sodium-cooled reactor.

It can be concluded that the use of helium instead of sodium probably will re-

sult in an increase in the surface temperature of the fuel pin. In addition, the pumping power required for a helium system will be higher than for the sodium system. Also, helium must operate at a pressure which is considerably higher than that required for sodium. The magnitude of these problems does not, however, rule out the use of helium as a possible fast-reactor coolant.

The use of helium as a fast-breeder coolant enhances the breeding characteristics of the reactor, as shown in table 1-IV. Because helium is much more transparent to high-velocity neutrons than to sodium, there are less-parasitic captures in the helium. For every 1000 neutrons in a sodium-cooled reactor, 30 are absorbed by the coolant. In a helium-cooled system, less than 1 out of every 1000 neutrons would be absorbed in the coolant. This fact, coupled with other neutronic effects of helium relative to sodium, increases the breeding ratio from 1.43 for sodium to about 1.55 for a comparable helium system.

This increase in breeding ratio could be used to offset the poorer heat-transfer-pumping characteristics of the helium-cooled system. For example, the helium-cooled reactor could operate at a power density 20 percent lower or about 240 kilowatts per liter compared with 300 kilowatts per liter in the sodium-cooled reactor and still have the same doubling time.

The reason that the safety aspects of a loss-of-coolant flow must be considered in comparing coolants can be explained with the use of figure 1-23 showing a normal reactor power decay following shutdown. For a considerable period of time after initiation of shutdown, the actual power generated in the reactor is appreciable. After a few hours, for example, about one-tenth of 1 percent of the original power is still being produced. Because the thermal power required for a 1000-megawatt-electric system is 2500 megawatts, about 2.5 megawatts of thermal power still are being generated 2 hours after shutdown.

In the sodium-cooled reactor shown in figure 1-9, even the rupture of a coolant pipe would still leave the reactor submersed in coolant, and heat could be dissipated by conduction and natural convection of the coolant.

In a high-pressure gas-cooled system, however, a break in a line would result in loss of coolant in a very short time and there would be no effective means of removing the heat from the reactor core. One could consider using a reserve gas coolant which would be pumped from an external storage container through the core for as long as necessary. The amount of gas required for such a procedure makes this method of core protection unattractive. A more likely approach would be to spray the core with water. However, to assure that the introduction of such an effective nuclear moderator into the core did not result in a nuclear excursion, the water would have to contain a soluble neutron absorber.

The safety aspect of a loss-of-coolant flow seems to be a major problem with

the use of a gas coolant. A system would have to be designed which either precluded the possibility of such an accident or was protected in the event of such an occurrence.

Several other coolant considerations can be mentioned. The use of an inert gas elimenates the fire hazards associated with the use of sodium. Second, helium does not become radioactive as sodium does. The high level of radioactivity of sodium may require as much as a 10-day waiting period after shutdown before access to the containment area can be made. There is more operating experience with sodium than there is with gas for cooling fast reactors. However, if experience with all types of reactors, heat-transfer loops, and other systems were included, a far greater amount is available on gas systems than on liquid-metal systems.

Helium could be an attractive alternate for a fast-reactor coolant and offers some real advantages. If helium were used, it could be used in a one-loop system transferring heat directly from the reactor to the steam system. This would eliminate the intermediate loop required by a sodium system because the isolation requirement for the intermediate loop in the sodium system is eliminated. However, the single helium loop could become contaminated by fission products leaking from ruptured fuel pins which would pose a radiation hazard around components of the steam system. Finally, the consequences of a loss-of-helium-flow accident pose the problem of how to ensure removal of afterheat from the core to prevent excessive overtemperatures in the fuel elements.

If the hazard of the loss-of-coolant-flow accident in the gas system is really an insurmountable problem, helium could be used in another way. It could be substituted for sodium as the coolant in the intermediate loop (fig. 1-24). Then, the possibility of any reactions between the sodium and the water would be eliminated because they would be physically separated by the inert loop. Also, many of the problems which result from leaks in the sodium steam generator would be solved. Of course, the use of a gas coolant instead of a liquid metal would probably increase the size of the heat exchanger and steam generator and, as in the reactor, would increase the pumping power requirement of the system. However, the use of helium in the intermediate loop does offer some potential advantages.

CONCLUDING REMARKS

This discussion has shown that many of the operating conditions of fast-breeder reactors are much more severe than those for current burner reactors. Therefore, major advances must be made before fast-breeder reactors become a commercial reality. For breeder reactors to be economically competitive, they must

(1) operate at much higher power densities, 300 kilowatts per liter instead of 60 to 90; (2) require higher levels of fuel burnup, 10 percent rather than 2 to 4 percent; and (3) withstand higher neutron exposure, 10^{23} instead of 10^{22} neutrons per square centimeter. These factors make fuel-element development for breeder reactors a more difficult task than for burner reactors.

Because of the large fuel swelling associated with the high levels of fuel burnup, the best choice of fuel material is not clear. More data on fuel swelling of oxide, carbide, and nitride fuels is needed before the decision can be made.

The additional neutron exposure encountered in breeder reactors causes problems of swelling and loss of ductility in austenitic stainless steel. Thus, more radiation-resistant stainless steel must be developed or a more expensive cladding material such as vanadium alloys must be considered.

The use of sodium as the coolant presents the possibility of serious corrosion problems at reactor operating temperatures of 1100° to 1200° F. Because these corrosion problems would be greatly eased at lower temperatures, a drop in reactor operating temperature should be seriously considered for breeder-reactor power systems. The lower temperatures would also ease some of the fuel and cladding problems. Of course, lower temperatures will require some penalty in power-conversion efficiency. But since operating costs of nuclear power systems are not as sensitive as fossil-fueled plants to small changes in efficiency, a drop in system operating temperature seems to be economically feasible in order to increase the reliability of the fuel elements.

Last, the use of helium as the coolant is an attractive alternate to sodium for both the reactor and the intermediate loop. Helium would overcome the problems of sodium corrosion and sodium-water reaction problems; however, it also introduces a potential safety problem in the event of a loss-of-coolant accident. If methods of overcoming this safety problem can be developed, helium should be more seriously considered as a coolant.

BIBLIOGRAPHY

Anon.: Alkali Metal Coolants. Proceedings of the Symposium on Alkali Metal Coolants: Corrosion Studies and System Operating Experience. International Atomic Energy Agency, Vienna, 1967.

Anon.: An Evaluation of Four Design Studies of a 1000-MWe Ceramic-Fueled Fast Breeder Reactor. Rep. COO-279, Reactor Eng. Div., Chicago Operations Office, U.S. A.E.C., Dec. 1, 1964.

Anon.: Fast Breeder Reactor Report. Edison Electric Institute, Apr. 1968.

Anon.: Large Fast Reactor Design Study. Rep. ACNP-64503, Allis-Chalmers Mfg. Co. and Babcock Wilcox Co., Jan. 1964.

Anon.: Liquid Metal Fast Breeder Reactor Design Study. Rep. CEND-200, vols. 1 and 2, Combustion Engineering, Inc., Jan. 1964.

Anon.: National Power Survey: Federal Power Commission-1964 - Part I. U.S. Government Printing Office, Oct. 1964.

Anon.: Proceedings of the Conference on Breathing, Economics and Safety in Large Fast Power Reactors. Rep. ANL-6792, Argonne National Lab., Dec. 1963.

Brown, F. L.; Neimark, L. A.; Koprowski, B. J.; Kittel, J. H.; Ayer, J. E.; and Kruger, O. L.: Performance of Mixed-Carbide Fuel Rods Under Fast-Reactor Conditions. Trans. ANS, vol. 10, no. 2, Nov. 1967, pp. 473-475.

Daniel, R. C.; Bleiberg, M. L.; Meieran, H. B.; and Yeniscavich, W.: Effects of High Burnup on Zircaloy - Clad Bulk UO_2, Plate Fuel Element Samples. Rep. WAPD-263, Westinghouse Electric Corp., Bettis Atomic Power Lab., Sept. 1962.

Hoffman, E. E.; and Manly, W. D.: Corrosion Resistance of Metals and Alloys to Sodium and Lithium. Rep. ORNL-2271, Oak Ridge National Lab., Apr. 9, 1957.

Holmes, J. J.; and Irvin, J. E.: Effect of Fast-Reactor Irradiation on the Tensile Properties of Type-304 Stainless Steel. Trans. ANS, vol. 10, no. 2, Nov. 1967, pp. 487-488.

McNelly, M. J., ed.: Liquid Metal Fast Breeder Reactor Design Study. Rep. GEAP-4418, vols. 1 and 2, General Electric Co., Atomic Power Equipment Dept., Jan. 1963.

Olmsted, Leonard M.: 15th Steam Station Cost Survey. Electrical World, Oct. 16, 1967, pp. 99-114.

Perry, K. J.; Nelson, R. C.; and Rubin, B. F.: High Burnup Performance of Mixed-Oxide Fuel to 120,000 MWD/T. Trans. ANS, vol. 10, no. 2, Nov. 1967, pp. 461-462.

Steck, R. B., comp.: Liquid Metal Fast Breeder Reactor Design Study. Rep. WCAP-3251-1, Westinghouse Electric Corp., Atomic Power Div., Jan. 1964.

TABLE 1-I. - COMPARISON OF

FUEL COSTS

Type of powerplant	Fuel costs / Total generation costs
Fossile	0.48
Nuclear burner	.37
Nuclear breeder	[a].16

[a]Estimated for 1985.

TABLE 1-II. - COMPARISON OF

BREEDING CHARACTERISTICS

	Burner	Breeder
Primary fuel	U^{235}	Pu^{239}
Fertile material	U^{238}	U^{238}
Average neutron velocity	Thermal	High
Typical breeding ratio	0.6	1.43
Doubling time, yr	--------	8 to 12

TABLE 1-III. - FACTORS AFFECTING

CHOICE OF CLADDING MATERIAL

Material	Relative tubing cost	Breeding ratio
Stainless steel	1	1.43
Nickel alloy	1 to 2	1.35
Vanadium alloy	5 to 10	1.43
Niobium alloy	15 to 20	1.14
Molybdenum alloy	20 to 25	1.14

TABLE 1-IV. - EFFECT OF COOLANT

ON BREEDING RATIO

Coolant	Coolant captures per 1000 neutrons	Breeding ratio
Sodium	30	1.43
Helium	1	1.55
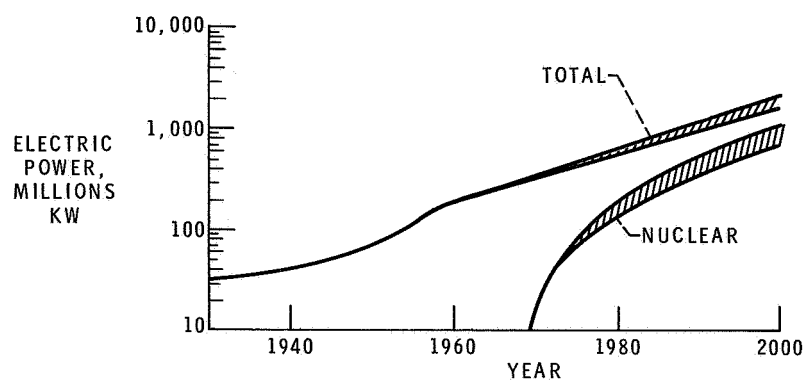
Figure 1-1. - Estimated electric power trends.
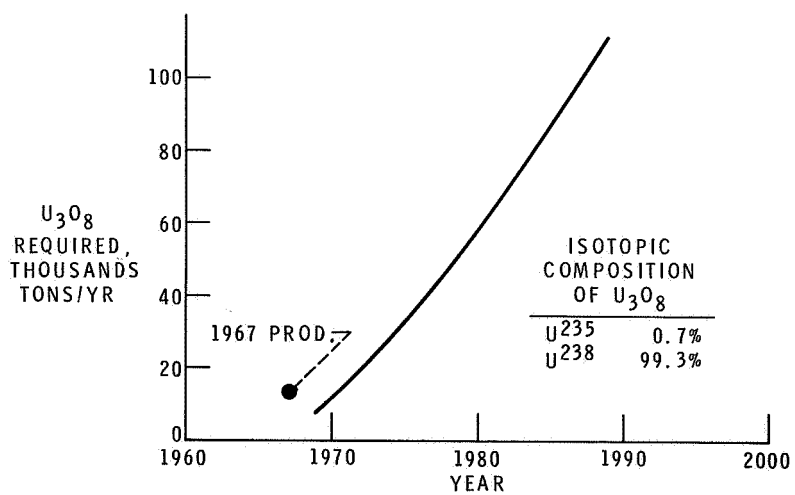
Figure 1-2. - Annual U_3O_8 requirements using present reactors.
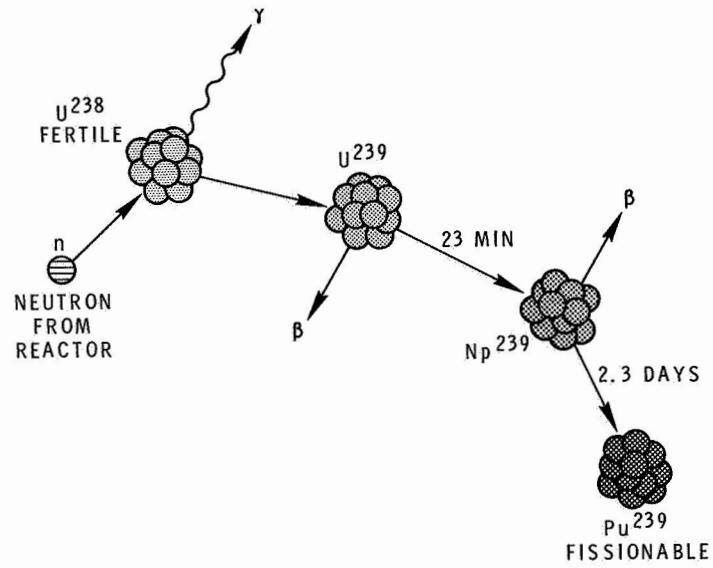
Figure 1-3. - Plutonium 239 production in a reactor.
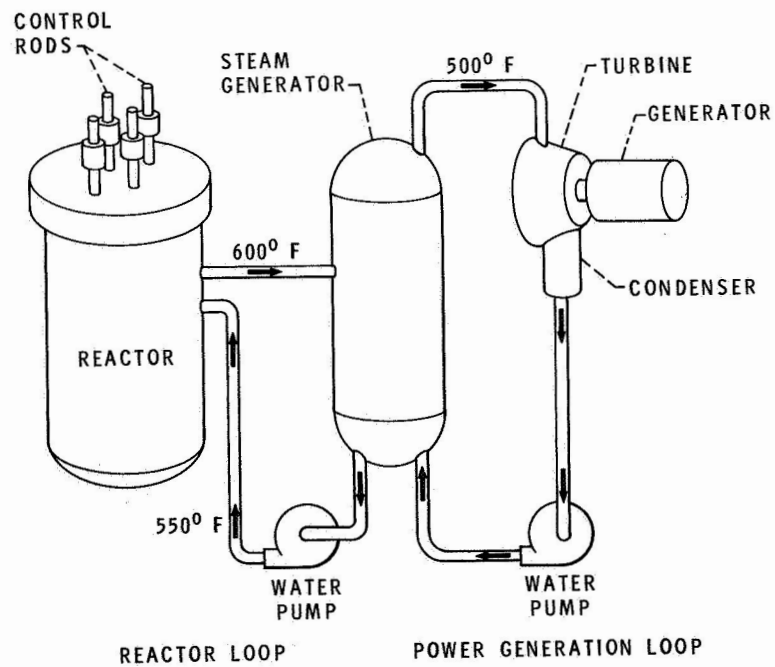
Figure 1-4. - Pressurized-water burner-reactor system.
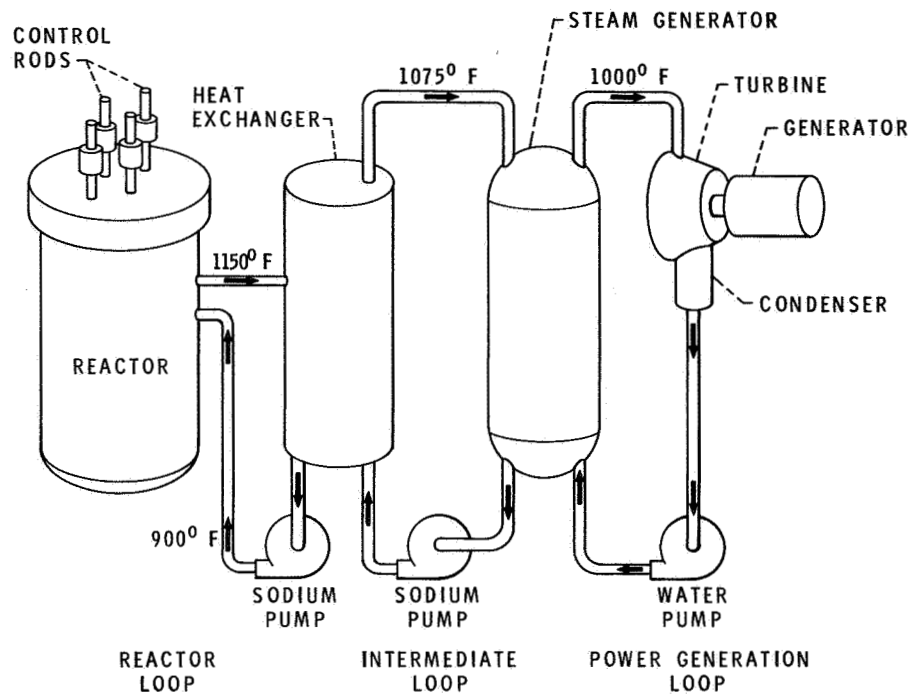
Figure 1-5. – Liquid-metal breeder-reactor system.
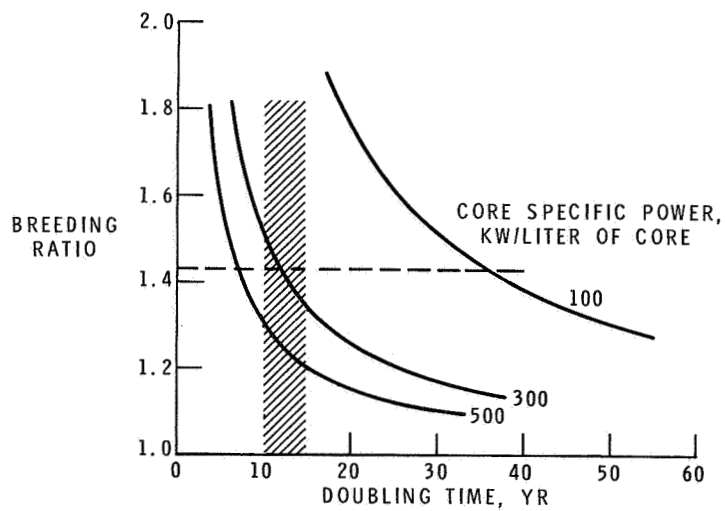
Figure 1-6. – Effect of power density on breeding characteristics of a typical reactor.
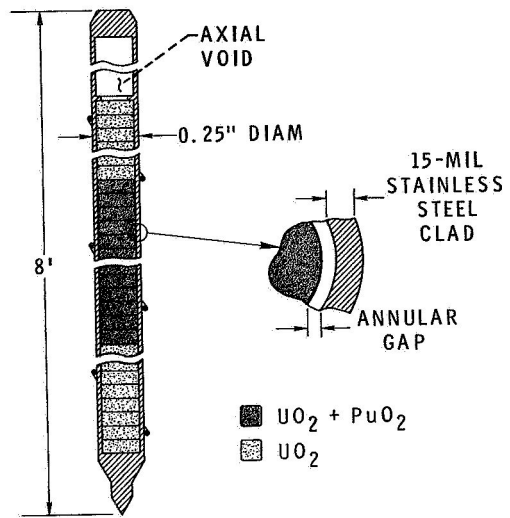
Figure 1-7. – Typical breeder-reactor fuel pin.
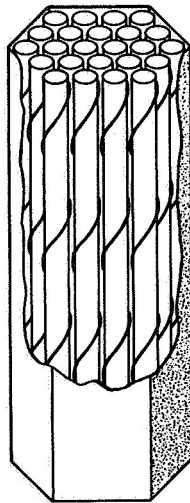
Figure 1-8. – Fuel-element assembly.

26

COVER GAS

REACTOR VESSEL

U²³⁸ + Pu²³⁹ (CORE)

U²³⁸ (BLANKET)

SODIUM COOLANT

CS-47679
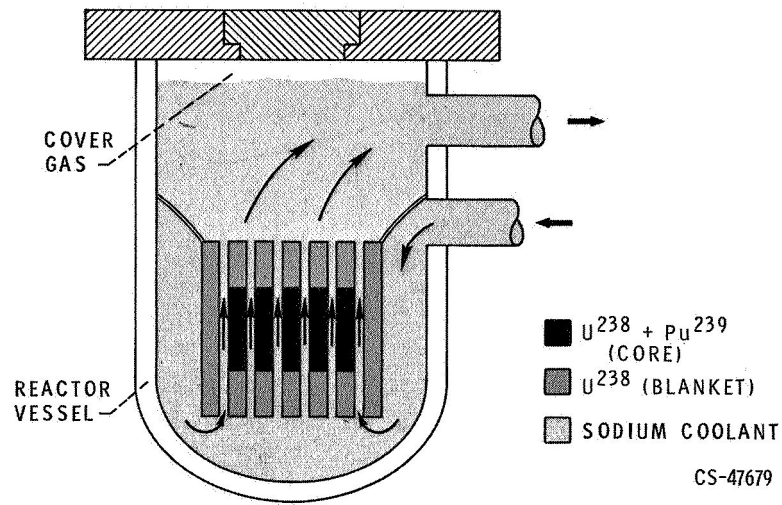
Figure 1-9. – Breeder reactor.

FUEL PIN DIAM

1/4"

3/8"

1/2"

BREEDER

BURNER

NO. OF FUEL PINS

500,000

400,000

300,000

200,000

100,000

0

10   15   20

REACTOR DIAM, FT
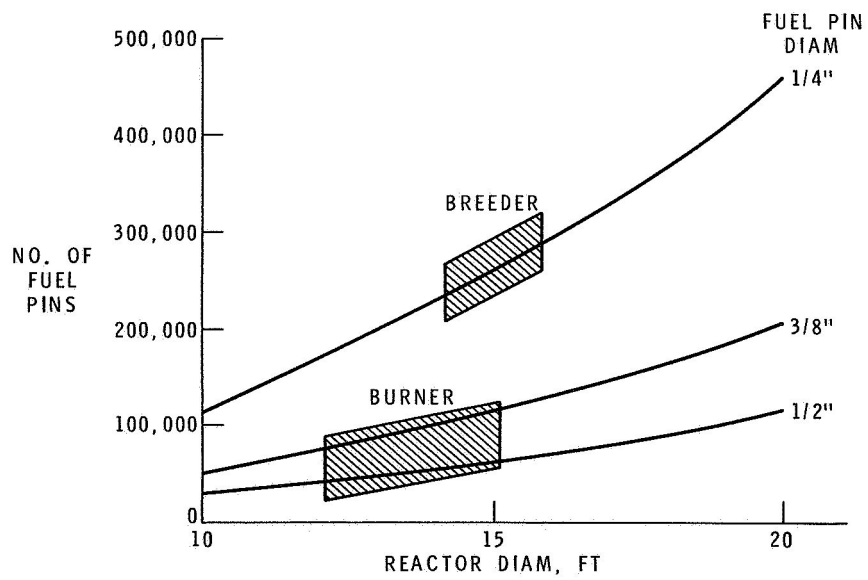
Figure 1-10. – Number of fuel pins required for 1000-megawatt-electric reactors.
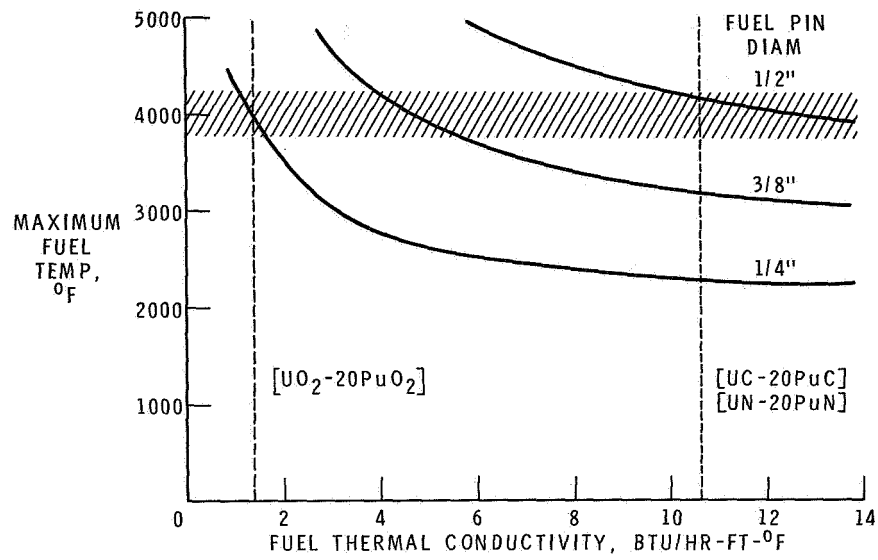
Figure 1-11. - Thermal conductivity and allowable fuel-pin diameter at 300 kilowatts per liter.
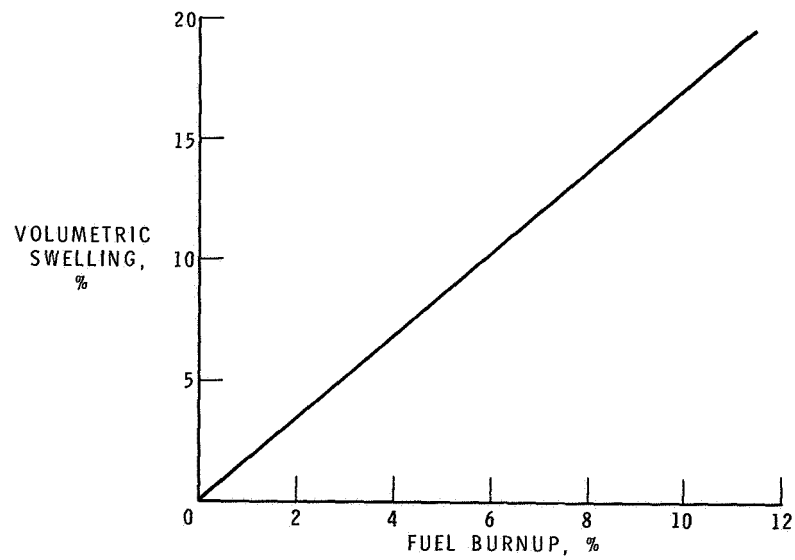
Figure 1-12. - Irradiation swelling of dense oxide fuels with no gas release.

28
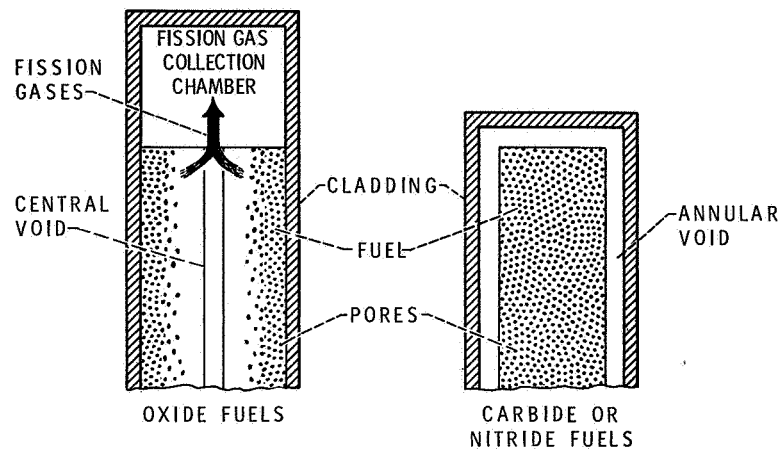
Figure 1-13. - Fuel-pin configurations.
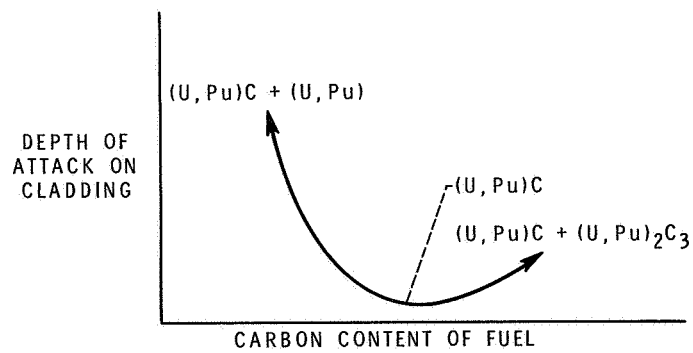
Figure 1-14. - Effect of fuel stoichiometry on compatibility with cladding.
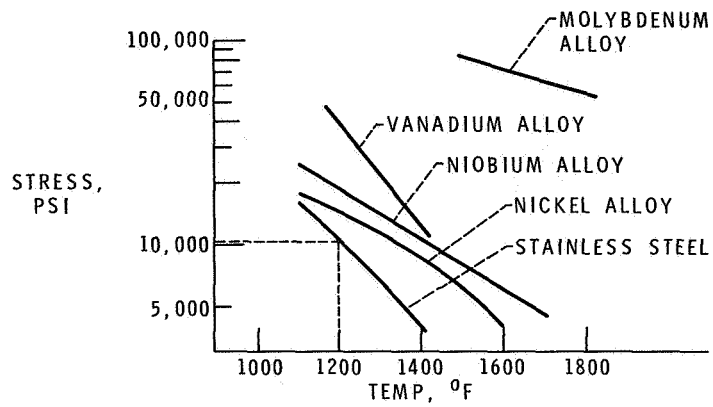
Figure 1-15. - Creep strength of cladding alloys. Stress to produce 1 percent strain in 10,000 hours,
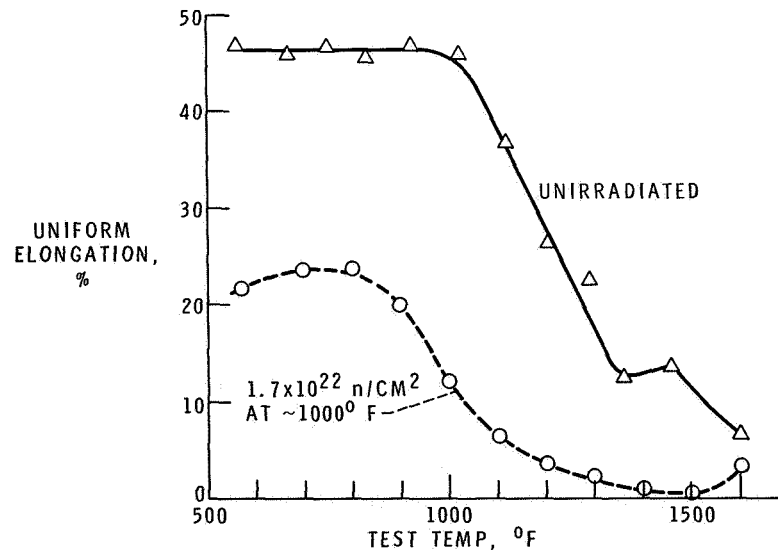
Figure 1-16. - Effect of irradiation on ductility of stainless steel.

30
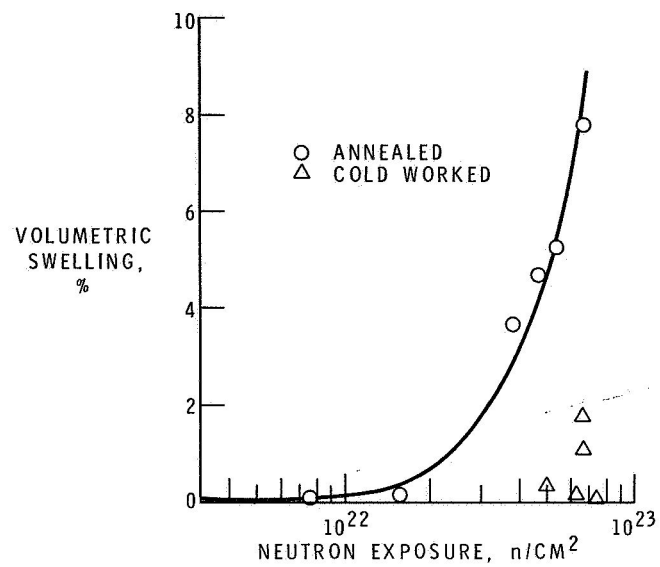
Figure 1-17. - Irradiation swelling of 316 stainless steel. Irradiation tempera-
ture, 680° to 1080° F.
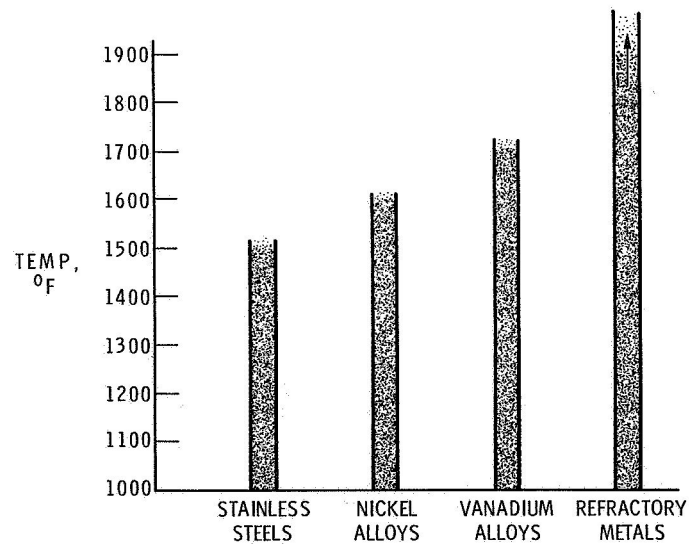
Figure 1-18. - Estimated compatibility limits of metals with high-purity sodium.
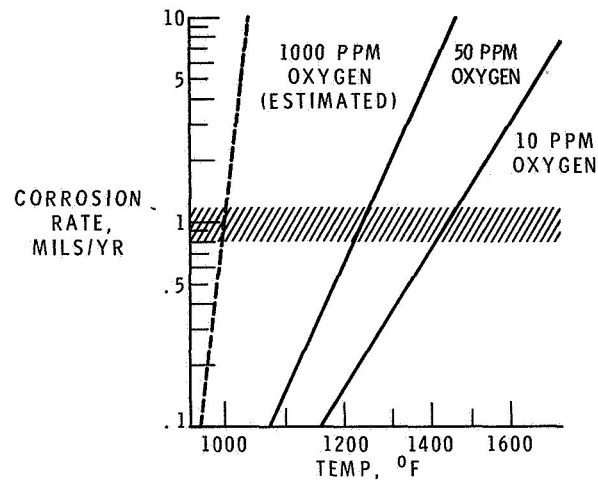
Figure 1-19. - Effect of oxygen on corrosion rates of stainless steel in sodium.
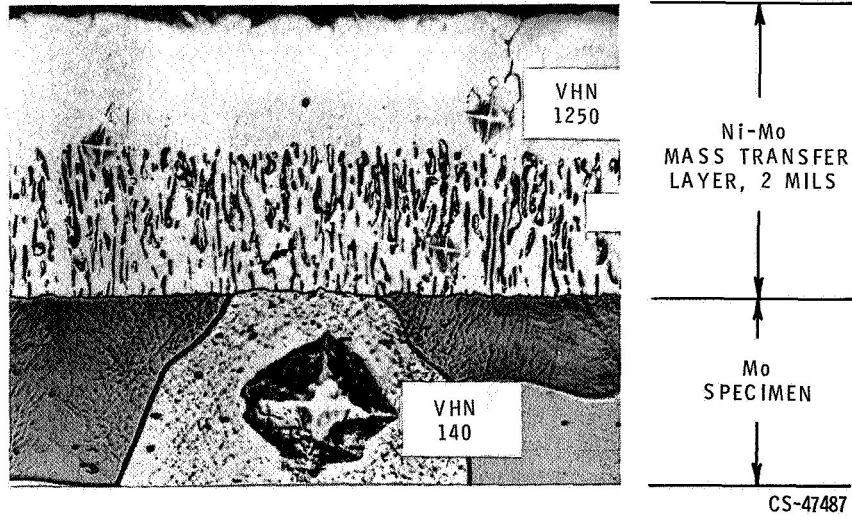
Figure 1-20. - Mass transfer of nickel to molybdenum for 100 hours in sodium at 1830^0 F.

32
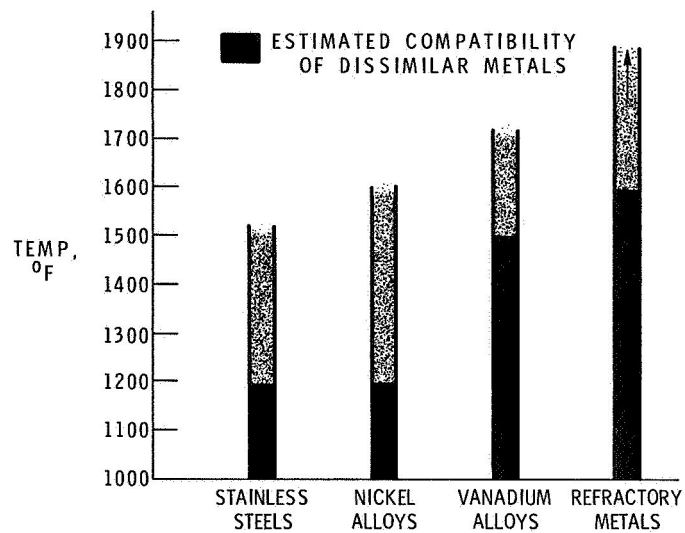
Figure 1-21. - Effect of dissimilar metals on compatibility with high-purity sodium.
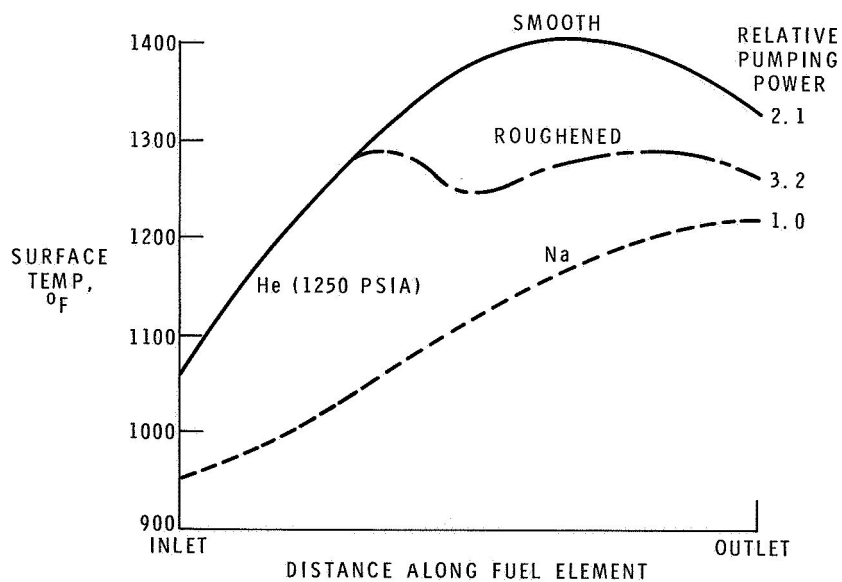
Figure 1-22. - Fuel-pin surface temperature distribution. Outlet temperature, 1200° F; coolant temperature rise, 250° F.
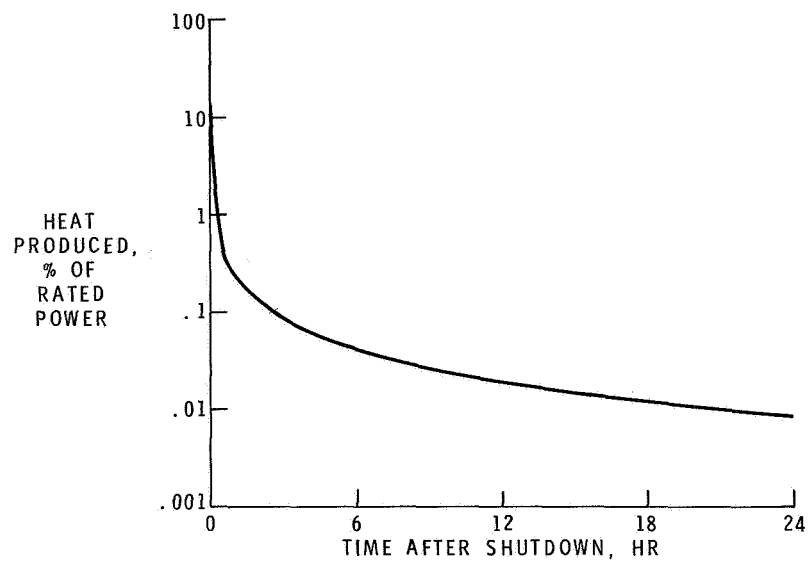
Figure 1-23. – Reactor power decay after shutdown.

SODIUM
REACTOR
LOOP

HELIUM
INTERMEDIATE
LOOP

STEAM POWER
GENERATION
LOOP
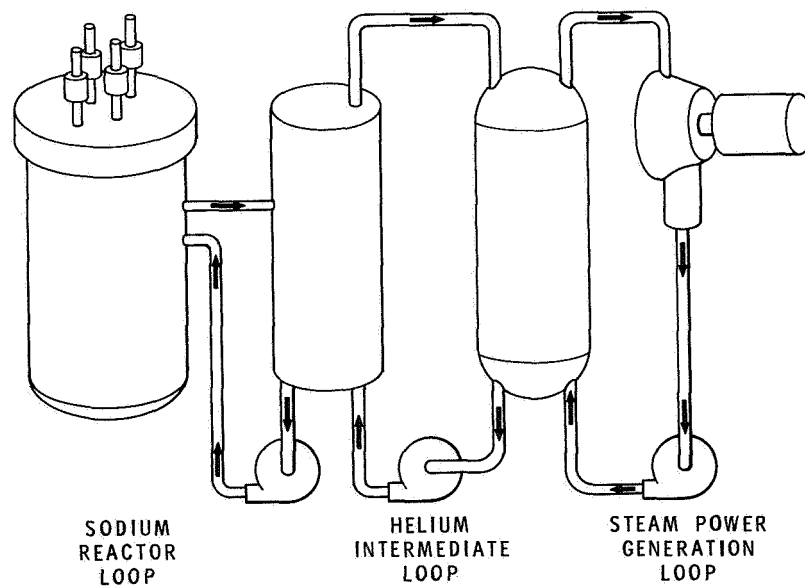
Figure 1-24. – Breeder reactor system.

34

2. TOPICS ON RANKINE CYCLE POWER
SYSTEMS TECHNOLOGY

Martin J. Saari, Jack A. Heller, Robert G. Dorsch, Phillip L. Stone,
Herbert G. Hurrell, Martin V. Gutstein, and Cavour H. Hauser

The preceding discussion on nuclear reactors dealt with some of the technical
aspects of the thermal energy source and transport of this energy to the power con-
version system. The purpose of the following discussion is to review selected top-
ics associated with that part of the Rankine power system that converts the thermal
energy into the mechanical energy used to drive the electric generating equipment.
The substance of this discussion has been accumulated through research and devel-
opment programs conducted at the Lewis Research Center and under NASA con-
tracts and grants to industry and universities. All this effort has been targeted at
the development of power systems for space flight applications.

The space Rankine system (fig. 2-1) has a fundamental similarity to the
ground-based power system (fig. 2-2) but differs substantially in size, weight, and
power output. The basic difference in cycle operating conditions results from the
fact that in the space environment waste heat from the system must be dissipated
by radiation rather than by convection as in the ground-based system. Thus, since
the size (and weight) of the radiator is a function of the fourth power of the radiating
temperature, there is a strong incentive to operate the heat rejection radiator at as
high a temperature as possible. To maximize cycle efficiency it is necessary to
elevate the peak cycle temperatures (at the turbine inlet) to the highest levels com-
mensurate with material limitations. Typically, then, the Rankine space-power sys-
tems operate at turbine inlet temperatures between 1200° and 2000° F, depending on
the working fluids used. In contrast, the ground-based steam-power systems char-
acteristically operate at temperatures below 1200° F.

Because of the high temperatures, the space-power systems utilize liquid met-
als as working fluids to minimize the peak pressure levels which reflect in reduced
system weight. The peak cycle pressure levels thus range between 50 and 300 psia
for the working fluids currently under consideration. The peak pressures in the
steam systems, on the other hand, range between 1000 to 5000 psia.

Despite the differences in temperatures, pressures, working fluids, and physi-
cal size between the space-power system and ground-based powerplant, the basic

thermodynamic and hydrodynamic processes that occur within either system are, nonetheless, governed by the same physical principles which provide the path for cross fertilization of technological advances in either direction. In fact, many of the liquid metal heat-transfer and fluid dynamic problems have been investigated experimentally by using water or organic fluids because of the similarity of behavior characteristics and the relative ease of handling these fluids.

The pressing necessity for minimum weight and size of space-power systems has stimulated an extensive search, during the past decade, for ways and means of maximizing performance from each pound and each cubic inch of hardware without losing sight of the crucial reliability and long-life requirement. The Rankine system technology has, for the most part, been acquired through the Systems for Nuclear Auxiliary Power Development (SNAP) programs and more recently through research activities directed toward the development of advanced nuclear Rankine space-power systems.

The discussion is presented, not on the pretense of having a pat answer to any specific related problem, but hopefully for the purpose of stimulating further thought and inquiry into potential application of ideas to either the conventional fossil-fuel or reactor-powered ground-based electric generating systems. The subjects to be considered include the following:

(1) Thermal design considerations and stability of compact once-through boilers

(2) Turbine-blade erosion

(3) Some cogent materials considerations

(4) Pump technology

(5) Analysis of system dynamics by computer simulation

TECHNOLOGY OF COMPACT ''ONCE-THROUGH'' BOILERS

In a ''once-through'' boiler, the boiling fluid enters as a liquid, discharges as a saturated or superheated vapor, and flows directly to the turbine without the need for liquid-vapor separation or liquid recirculation. In space boilers, the heating fluid enters the boiler, as shown in figure 2-3, in the region of the vapor outlet. The heating fluid then flows opposite to or countercurrent to the flow of the boiling fluid and discharges in the region of the boiling fluid inlet. A typical temperature profile in such a boiler is also shown in figure 2-3. The temperatures of both the heating and the boiling fluids are plotted as a function of distance along the boiler. The heating fluid, in passing through the heat exchanger, transfers heat to the boiling fluid. Consequently, its temperature decreases continuously. The boiling fluid, entering opposite to the heating fluid, is quickly heated to its boiling temper-

ature corresponding to the local pressure. Thereafter, in the boiling region, the temperature decreases somewhat. This temperature decrease is due to the pressure loss incurred by the boiling fluid and to the fact that the temperature is related to the pressure in a two-phase fluid. At the end of the boiling region, further additions of heat cause the temperature of the boiling fluid to increase. This region is called the superheated vapor region.

The temperature difference between the heating and boiling fluids at the boiler inlet is generally very large, of the order of several hundred degrees. This temperature difference decreases rapidly, however, and reaches a minimum at the point where boiling first initiates. This minimum temperature difference between the heating and boiling fluids is called the "pinch-point" temperature difference. In the boiling region, the temperature difference increases again. In the super-heated vapor region, the temperature difference decreases.

As the boiling fluid undergoes a transformation from a liquid to a vapor, its character changes radically. This can be explained by reference to figure 2-4, which shows a schematic of a simple once-through hollow-tube boiler. The heating fluid flows in the annulus, and the boiling fluid flows in the central tube opposite in direction to the heating fluid. As the boiling fluid is heated, bubbles are produced at the tube wall and these are swept into the center of the tube. This flow regime is called the "bubbly" flow regime. Further downstream, the bubbles agglomerate into single large bubbles which almost fill the entire cross section of the tube. This regime is called the "plug" or "slug" flow regime. With further heat addition, the plugs tend to enlarge and burst open, leaving a ring or annulus of liquid at the tube wall and droplets traveling with the vapor in the core. This regime is frequently labeled the "annular" or "annular-mist" flow regime. Eventually, the liquid layer at the wall is boiled or evaporated, and a "dry-wall" condition exists along with droplets flowing in the vapor core. This flow regime is called the "mist" or "fog" flow regime. Figure 2-4 also shows schematically the heat flux distribution along the length of the single-tube boiler. At the inlet, the heat flux in the liquid convective region is moderately high but decreases with length. This decrease is due to the reduction of temperature difference between the heating and boiling fluids. In the boiling region, the heat flux increases to a maximum. The maximum flux generally occurs at the end of the annular flow regime. Thereafter, the flux decreases substantially to values typical of vapor convection. This is not unexpected since a continuous liquid layer at the tube wall does not exist in this region of the boiler. The heat flux decreases with length due again to the decrease in temperature difference between the heating and boiling fluids. Because of the poor heat-transfer characteristics at this location, extraordinarily long tube lengths would be required to evaporate most of the entrained liquid droplets flowing in the vapor.

Space boilers are made more compact not only by bringing the parts of a boiler closer together, such as by reducing the separation between tubes, but also by increasing the average heat flux. Higher average heat fluxes are achieved by separating the liquid and vapor phases within the tubes by swirling the flow as shown in figure 2-5. When a swirl is induced in the flow, the liquid droplets are centrifuged to the tube wall where efficient boiling heat transfer can take place. Moreover, when the liquid is separated out, the vapor then has a relatively large, unobstructed passage for it to flow to the outlet of the boiler. The effect on the heat flux distribution is also shown in figure 2-5. The heat fluxes in the liquid and low-quality regions for the two cases are comparable. The biggest difference occurs in the boiling region. The swirl effect on the liquid droplets causes the boiling region to extend to higher qualities, and thereby the average heat flux is increased substantially. In the vapor region, the swirl effect increases the effective velocity which raises the local heat-transfer coefficients and hence the heat flux. This increase in the heat flux can be significant depending on the requirements for dryness and superheat.

To swirl the flow, inserts such as those illustrated in figure 2-6 are placed inside the tubes of a boiler. The twisted tape, fabricated from a flat strip of sheet metal and then twisted, is thus one of the simplest inserts. However, the tape divides the tube into two distinct flow passages. If the insert is fabricated or installed improperly, the hydraulic resistance of the two passages can differ substantially, and this may lead to maldistributions of flow and heat transfer. To avoid this potential problem, the helical vane on a center rod has been employed in boiler tubes. This insert has the advantage that the vane extends along a tube radius and not a diameter. Consequently, it swirls the boiling fluid without dividing the tube into two flow passages. Both the twisted tape and the helical vane have surfaces along the tube axis where the centrifugal forces are small or nonexistent. As a result, some of the liquid in the boiling fluid can flow along these surfaces and thus bypass the tube wall. If the insert extends to the outlet end of the boiler, it is possible that some of this liquid could flow the entire length of the boiler and exit with the vapor. Frequently these inserts are terminated upstream of the boiler exit. The liquid will then flow off the insert, be centrifuged to the tube wall, and then be evaporated before exiting the boiler.

The helical wire coil insert has been employed in boilers because of its ease of manufacture and installation. The coil is placed inside a tube in an extended condition and then allowed to relax, expand radially, and thus engage the tube wall. In addition, liquid bypassing of the tube wall is minimized since this insert has no surfaces near the tube centerline. The combination of a wire coil and a center rod is employed in the liquid and low-quality regions of a boiler to increase the fluid

velocities and hence the heat-transfer coefficients.

A comparison of the performance of a given boiler tube both with and without a swirl-generating insert is shown schematically in figure 2-7. The curves shown in this figure represent a composite of experimental data obtained with conventional fluids, such as boiling water and organic fluids, and with liquid metals, such as boiling potassium. Local heat-transfer coefficients are plotted as a function of length along the tube. Generally, the tube with an insert has higher heat-transfer coefficients and a longer boiling region than the tube without an insert. Moreover, at the outlet, the tube without a swirl insert discharges an intermediate quality mixture of liquid and vapor. For example, conventional fluids discharge from a short hollow-tube boiler with a maximum exit quality of about 60 percent. High conductivity fluids, such as potassium, discharge at an exit quality as high as 90 percent. However, the same tube with an insert discharges a superheated vapor, superheated by as much as 200° F. The length of the hollow-tube boiler would have to be substantially greater than that of the boiler with an insert to discharge a vapor with the same superheat. For a given length, the tube with an insert has a much larger pressure drop than the tube without an insert. However, the hollow tube, to achieve an exit superheat of 200° F, for example, would be much longer than the tube with an insert. Its pressure drop, therefore, may not be much different from the tube with an insert. In general, the pressure drop penalty associated with the use of inserts must be evaluated for each individual boiler.

The reduction in length of space boilers made possible through the use of swirl-generating inserts is shown in figure 2-8. The length of the boiler with hollow tubes has been taken as unity. The boiler that contains inserts in its tubes is shown to have a length one-fourth or less that of the hollow-tube boiler. The specific volumes (i.e., the volume of a boiler per kilowatt of heat transferred) or three typical boilers: a fossil-fueled central power station boiler, a sodium-steam boiler of a nuclear central power system, and a liquid metal-to-liquid metal space-power boiler are compared in figure 2-9. The specific volume of the sodium-steam boiler is roughly one-tenth that of the fossil-fueled boiler. This is primarily attributable to the superior heat-transfer characteristics of liquid metals as compared to the combustion gases. Space boilers also employ liquid metals, but their specific volumes are still smaller than the sodium-steam generator, as shown in the figure. Part of this reduction of specific volume is due to the lower working pressures of the liquid metal boiling fluid (well below critical pressure) which permits the use of thin-wall tubing. (The thin-wall tubing offers lower resistance to the transfer of thermal energy.) A substantial portion of this reduction in volume of space boilers, however, is due to the application of swirl-flow technology and the use of inserts, as described previously. It is possible that ground-based boilers may be made

more compact through the use of this same technology. However, the magnitude of the reduction in boiler size depends on the characteristics of each boiler and, thus, must be individually determined.

Figure 2-10 shows a boiler now being tested for the SNAP-8 space-power system. The boiler is a once-through counterflow heat exchanger. The heating fluid is a sodium-potassium alloy (NaK), and the boiling fluid is mercury. The mercury flows in seven tubes contained within the shell. Each tube possesses a swirl-generating insert. Approximately 500 kilowatts of heat are transferred at a mercury vapor exit temperature of nearly 1300° F. The coiled configuration of the boiler reduces thermal stresses and facilitates installation of the boiler on the spacecraft. The diameter of the coil is 48 inches, and the height is approximately 36 inches.

The SNAP-8 boiler has a feature which may be of interest for the design of the sodium-steam generator of the ground-based reactor powerplant. The tubes of this boiler are designed with double containment - that is, with two walls separating the boiling fluid from the heating fluid. In the sodium-steam generator, such a design would reduce the likelihood of mixing water with sodium. In the SNAP-8 system, double containment minimizes the possibility of mixing the mercury with the heating fluid which is the reactor coolant.

The double containment feature is shown in figure 2-11. This figure shows a cross section of the SNAP-8 boiler. The outer pipe is the shell which contains the flowing NaK heating fluid. Inside the shell are the seven double-walled tubes. Mercury boils inside the inner wall and nonflowing NaK fills the space between the walls. A leak between the flowing NaK and the static NaK would not affect the operation of the boiler. A leak between the mercury and the static NaK would allow the higher pressure mercury to flow into the static NaK but not into the NaK that passes through the reactor. Although the double containment concept is somewhat complicated, it does provide greater reliability and safety than single containment.

BOILER INSTABILITIES

High-flux short-tube boilers are known to exhibit a wide variety of flow, pressure, and steam void fluctuations and oscillations. These disturbances are generally referred to as boiler instabilities. However, these instabilities are caused by a variety of different mechanisms, depending on the boiler and system operating conditions and on the particular hardware characteristics. It is necessary, therefore, to identify the specific type of instability which is occurring before an attempt can be made to reduce or eliminate it.

Three frequently encountered types of boiler instabilities, which will be used as examples, are the following:

    (1) Acoustic

    (2) Heat-transfer coupled

    (3) Feed-system coupled

        (a) Excursions

        (b) Dynamic oscillations

The acoustic type is an example of a channel flow disturbance; the heat-transfer coupled is typical of an instability which is internally coupled within the boiler; and the feed-system coupled is an example of a system-coupled instability.

Acoustic disturbances in boiler tubes or heated channels are related to the fact that a very low speed of sound exists in a boiling fluid. The propagation velocity of a pressure wave through the very low-quality subcooled boiling region is shown in figure 2-12 as a function of the amount of steam present in the form of bubbles in the liquid. The curve is based on data taken by Karplus at Armour Research Foundation under government sponsorship. With no steam bubbles present, the wave velocity through the liquid is about 4800 feet per second. This velocity decreases sharply to 300 feet per second with only $1\frac{1}{2}$ percent steam in the tube. This happens because the presence of even a small amount of vapor causes a very large increase in compressibility of the fluid. At 40 percent steam, the velocity is down to only 60 feet per second.

The low speed of sound in the subcooled boiling region makes it possible for "organ-pipe" type pressure wave resonances to occur in very short tube lengths. For a 30 cps resonance, for example, these lengths are of the order of 1 to 5 feet as compared to 80 feet for a liquid-filled tube. These resonant pressure waves can be self-sustaining under some conditions.

The low acoustic speed in a boiling fluid also permits another type of disturbance to occur in the higher quality net vaporization region, that is, between 50 and 100 percent steam by volume. In this region the sonic velocity and the fluid velocity in the tube can be comparable in magnitude particularly at high weight flow rates. Thus, choked flow conditions can occur. In fact, it is possible for the fluid velocity to actually be higher than the acoustic velocity and have local supersonic flow accompanied by shock waves. Thus, in an unsteady flow situation, there is a mechanism for intermittent choking and/or shock wave formation. The resultant pressure wave disturbances may also cause water hammer effects through the evaporation of droplets and the collapse of vapor bubbles as they travel through the boiler tube.

Acoustic disturbances are encountered mostly in startup or transient situations and usually do not cause serious operating-point instabilities. This is because the

disturbances occur mostly at high frequencies (between 20 and 400 cps) or are random with time. In either case, they cannot couple with the other system components. When these acoustic disturbances do occur, they may cause problems in the boiler such as inducing mechanical vibration of the boiler tubes. Adjustments in either the tube flow rate, the subcooling, or the heating rate may sometimes be necessary to reduce or eliminate an acoustic disturbance.

The second example is the heat-transfer-coupled instability. This instability has been experienced during developmental testing of the SNAP-8 boiler. It is an oscillatory type of instability; that is, it manifests itself as periodic oscillations in boiler exit pressure. This instability results from a coupling process internal to the boiler because it has been observed when all the boiler input variables, such as liquid flow, were constant. It seems to be caused by an interaction between the heat flux within the boiler and the vapor generation rate. This is believed because the pressure oscillations correlate quite well with the pinch-point temperature difference, which is a measure of heat flux.

As noted earlier (in the discussion of fig. 2-3), at the end of the subcooled region where boiling starts, the fluids are separated by a rather small temperature difference, or pinch-point ΔT. Experimental correlations between the exit pressure oscillations and the pinch-point ΔT are shown in figure 2-13. The amplitude of the boiler exit pressure oscillation is plotted against the pinch-point ΔT for three different flow rates of the boiling mercury. At large values of the pinch-point ΔT, the amplitude was only 1 or 2 percent of the mean pressure. However, the amplitude was found to increase sharply as the pinch-point ΔT was decreased for a given mercury flow rate.

The frequency of this pressure oscillation was in the range of 0.1 to 1 cps. As the figure suggests, the effect of this instability can be kept at a tolerable level by operating the boiler with a high value of pinch-point ΔT.

It should be mentioned that the pinch-point temperature difference ΔT should not be increased indiscriminately, because an excessively large temperature difference has an adverse effect on heat transfer. The upper and lower limits on pinch-point ΔT are influenced by the working fluids and boiler tube geometry.

The third example is the feed-system-coupled instability, which involves an interaction between boiler pressure and the liquid flow into the boiler tubes. In the excursive type of feed-system-coupled instability, a flow excursion can occur because of the peculiar relation which exists between boiler pressure and weight flow rate at some operating conditions. A typical plot of steady-state boiler tube inlet pressure against weight flow rate for a hollow-tube boiler is shown in figure 2-14. The curve is for constant heat input, and for simplicity, the exit pressure is assumed to remain constant. The inlet pressure is, of course, equal to the exit

pressure plus the pressure drop in the tube at each flow rate. At low flow rates, the boiler tube exit quality is high and the tube contains mostly high velocity vapor. It is the high velocity vapor which accounts for most of the pressure drop in the tube. The pressure drop caused by the low velocity liquid is small. At low increasing flows, the inlet pressure, therefore, at first increases rapidly with an increasing weight flow. However, as the weight flow into the boiler tube continues to increase, the exit quality begins to decrease because less of the inlet flow is vaporized. This results in increasingly smaller fractions of high velocity vapor in the tube. At some point, therefore, the pressure starts to decrease and continues to do so until the flow becomes so large that there is only hot liquid in the tube. In the all-liquid region the pressure again increases with weight flow. The region in which the pressure decreases as the weight flow increases is called the negative-resistance region. It is bounded by positive-resistance regions on each side.

The implications of the positive- and negative-resistance regions on static stability are now examined. Portions of the boiler curve in these regions are replotted in figure 2-15 along with corresponding curves for the boiler feed water supply system.

First, the high-quality region with positive boiler resistance is examined (see fig. 2-14). A portion of this region is shown in detail on the left side of figure 2-15. The system is considered to be operating at the intersection point. The flow into the boiler is assumed to increase a small amount or ΔW. The boiler inlet pressure tends to become greater than the supply pressure and decelerate the flow. The increase in flow, therefore, cannot be maintained and the system returns to the operating point at the end of the transient. The system is thus statically stable.

Now the negative-resistance region of the boiler is examined (fig. 2-14). A portion of this region is shown in the center of figure 2-15. With the feed-system characteristics indicated, it is not possible to operate at the intersection point because a small flow increase ΔW would cause the boiler inlet pressure to begin to drop below the supply pressure. The flow would therefore accelerate and continue to increase. The system, which is thus unstable and would undergo a flow and pressure excursion, ends up in the stable positive-resistance region at high weight flows.

The third set of curves in figure 2-15 are now considered. The hydraulic characteristics of the feed system have been changed to give a steeper feed-system supply curve as indicated. The boiler and feed-system combination is not statically stable even though the boiler is operating in the negative-resistance region. The system is stable about the operating point because with a flow increase ΔW the supply pressure now cannot provide the higher pressure demanded by the boiler. The flow thus decelerates, and the system returns to the operating point. Conse-

quently, a boiler can be statically stabilized in the negative-resistance region by using a pump with a steeper slope or by adding a pressure drop orifice at the inlet to the boiler tube or by doing both.

From what has been discussed so far, feed-system-coupled instabilities would be expected when the boiler is operated in the negative-resistance region. In addition, it is often assumed that a once-through boiler having high-quality steam output and operating in the positive-resistance region will be stable. This assumption results from analyzing the system only from a steady-state viewpoint. However, in practice, feed-system-coupled boiler instabilities that are often encountered in the positive-resistance operating region are the dynamic type. They are oscillatory and occur at particular frequencies. The reason that dynamic oscillations can occur in the positive as well as in the negative-resistance region is that the pressure oscillation can lag behind the flow oscillation. It can lag to the point where the pressure is actually decreasing when the flow is increasing. That is, a negative-resistance condition can exist at a particular oscillation frequency. The lag is principally caused by the fact that it takes time for the liquid flow into the boiler to vaporize and thereby affect the boiler pressure.

In order to predict the occurrence of this type of instability the dynamic characteristics of the boiler must be known. Because relatively little is known in this area, fundamental research studies on the dynamic characteristics of simple heat exchanger boiler configurations are being conducted at the Lewis Research Center.

The boiler dynamics research rig is shown in figures 2-16 and 2-17. The boiler test section is a single-tube boiler heated by hot water. The liquid Freon pumped through the boiler tube is vaporized, and then it flows through a large diameter pipe to a large water-cooled condenser. This provides constant boiler exit pressure. Stable steady-state conditions are established in the boiler and then the Freon inlet flow is sinusoidally perturbed about its mean value by the controllable throttle valve. Boiler inlet perturbation pressures and flows are measured at the location shown in figure 2-16.

Forced-flow and pressure oscillations are measured at the boiler inlet and are shown schematically in figure 2-18. From data of this kind the amplitudes of the flow oscillation (A_F) and the pressure oscillation (A_P) are obtained at each imposed frequency. Further, at each frequency, the amount (in degrees) that the pressure oscillation lags behind the flow oscillation is determined.

Required at each frequency is the ratio of the sinusoidal pressure perturbation to the sinusoidal flow perturbation. This ratio, which is known as the boiler inlet impedance, is analogous to the ratio of voltage to current in an ac circuit.

It is convenient to plot this ratio in the polar form shown in figure 2-19. At a particular frequency the distance from the origin to the curve is the amplitude ratio

(A_P over A_F), and the angle measured from the positive axis is the pressure os-
cillation lag in degrees. When the amplitude ratio and lag angle are plotted for a
series of different frequencies in the range of interest, a curve of the type shown is
obtained. The curve starts at steady state (or zero frequency) with no lag between
pressure and flow. This is therefore called the positive-resistance axis. The am-
plitude vector rotates clockwise with increasing frequency. At the point where the
curve crosses the axis, the pressure oscillation lags behind the flow oscillation by
180°; thus, the pressure is decreasing when the flow is increasing and vice versa.
That is, the boiler has pure negative resistance at this frequency.

A similar plot of actual frequency response data taken on the boiler dynamics
rig is shown in figure 2-20. A hollow single-tube boiler was operating stably at a
point in the positive-resistance steady-state region, and forced oscillations were
imposed at frequencies between 0.04 and 1.5 cps. The experimental results are
shown by the solid curve. Shown as a broken curve are the analytical results cal-
culated with the aid of a simple model. The shapes of these frequency response
curves are dependent on the boiler tube geometry and on the particular operating
conditions of the boiler. Therefore, all parameters used in the analytical calcula-
tions were evaluated at the operating point from the steady-state characteristics of
the boiler tested.

The analytical model used is analogous to a short electric transmission line
with a current time delay device located near the inlet end of the line. The agree-
ment between the analytical results and experimental data is very good for a short
hollow tube boiler of this type.

Both the experimental and the analytical curves indicate that the inlet impe-
dance of the boiler has a negative-resistance component for frequencies between
0.2 and 1.2 cps. Further, at a frequency of about 0.5 cps the inlet impedance con-
sists entirely of negative resistance. Thus, the boiler tested is a potential source
of feed-system-coupled instabilities in this frequency range.

In order to determine whether an instability will actually occur, the impedance
of the feed system at these frequencies must also be considered. The boiler inlet
impedance curve from figure 2-20 is shown in figure 2-21 along with a correspond-
ing polar plot of the feed-system impedance. Like the boiler, the feed-system im-
pedance varies with frequency. However, it has a positive-resistance component at
all frequencies. For the frequencies of interest, between 0.2 to 1.2 cps, this feed
system is almost entirely resistive; that is, the feed-system impedance vector
falls within the shaded area and has a magnitude R_F.

With the constant pressure exit condition, a feed-system-coupled instability
would be expected to occur if, at some frequency, R_F is equal to or less than the
boiler negative resistance R_B. The net resistance in the system would then be

either zero or negative at that frequency. Examination of the two curves within the shaded regions shows that this is possible at a frequency of about 0.48 cps.

It was possible to experimentally verify the validity of this stability criterion with the boiler dynamics test rig itself. In this frequency range, R_F was determined primarily by the hydraulic resistance of the controllable throttle valve. Normally R_F was larger than R_B, so that the net resistance was positive and the system was normally stable. Now, with the valve oscillating device turned off, it was possible to gradually open the valve beyond its normal set point and decrease R_F. When R_F became equal to or slightly smaller than R_B, the system spontaneously went into natural oscillation as shown by the flow and pressure traces of figure 2-22. The frequency of the natural oscillation was 0.48 cps, which agrees with the predicted frequency. Also, the pressure lags the flow by 180°; that is, the pressure oscillation is at a minimum when the flow oscillation is at a maximum indicating that there is indeed a negative-resistance condition at this frequency.

Further, as the experiment demonstrates, this type of instability can be avoided by providing sufficient feed-system hydraulic resistance close to the boiler inlet. And, there is a means of deciding how large this resistance must be. In a practical system, the feed-system resistance can be made sufficiently large by providing orifices at the inlet to the boiler tubes, for example.

This discussion has been mostly about single-tube boilers. However, the same principles apply to individual tubes fed from a header in a multitube heat exchanger boiler as well as to a parallel bundle of boiler tubes coupling as a unit with the feed system.

TURBINE EROSION

A problem common to nonorganic Rankine system turbines is the blade erosion that results from liquid impingement. The NASA is investigating, both analytically and experimentally, the turbine blade erosion problem in its liquid metal systems as a consequence of the erosion experienced in steam turbines. It is recognized that the efficiency of the Rankine system can be improved by expanding the vapor in the turbine to the lowest possible pressure and temperature. But, this condition is accompanied by increased moisture content in the latter turbine states. It is in these latter wet stages that liquid impact erosion becomes a serious problem. In a current potassium Rankine system under study at NASA the exit moisture would be approximately 20 percent if no moisture separation or reduction devices were provided in the turbine.

The droplet formation in the latter stages of the turbine is examined to obtain a

physical picture of some of the major elements involved in the liquid impact erosion problem. For orientation purposes, figure 2-23 shows a cross section of a typical low-pressure split spool steam turbine. The steam flow enters at the center and is expanded equally in both spools. A portion of the last-stage stator and rotor blades of this turbine is shown in figure 2-24. Wet vapor from the preceding stage enters the stator blades where a small fraction of the fine condensate in the vapor collects on the stator surfaces. The fine condensate moves along the stator surfaces within the slow-moving boundary layer to form larger droplets and puddles. This liquid is eventually swept to the stator trailing edge where the drops break away. The larger drops then undergo a second breakup by the shearing action of the main vapor flow. While most of the droplets impact the rotor, it is only the larger drops, moving at or above some threshold velocity relative to the rotor, that actually erode the rotor leading edges.

The formation and the breakaway of droplets have been observed and recorded on film using the simple technique illustrated in figure 2-25 on small steam turbines. Rocketdyne, under NASA Contract NAS7-391, has prepared a number of such high-speed films in connection with the experimental work of the NASA on droplet formation and subsequent rotor material damage. In another experimental investigation, the behavior of solids under multiple liquid impacts, using a rotating wheel- and-water-jet apparatus, is being performed by Hydronautics, Inc. under NASA Contract NASw-1608.

In addition to experimental work on various aspects of turbine erosion, the NASA is also pursuing analytical investigations of the erosion problem as it applies to the liquid metal systems. Westinghouse, under NASA Contract NAS7-390, has completed a mathematical model of the liquid impact erosion process. The model is based on experimental observations and on the results of previous analytical studies of condensation in the vapor flow. A computer program, which has been written for the mathematical model, contains these major elements that contribute to the erosion process:

(1) Expansion of the vapor from the turbine inlet to condensation in the bulk vapor at the desired turbine stage

(2) Prediction of the fraction of fine condensate that collects on the stator-blade surfaces

(3) Determination of the detachment mode and breakup of the droplets in the stator wake, and a prediction of the resultant number and respective sizes of the droplets

(4) Calculation of the velocity and impingement angle of the respective droplets impacting the rotor

(5) A prediction of rotor-blade material removal for the desired service life
based on the rotor-blade material erosion rate

For verification, Westinghouse applied the analysis to the ninth-stage rotor of
the Yankee steam turbine. This last stage operated at an exit moisture of 15 per-
cent and at a temperature of 97° F. At these steam conditions and a service time
of 13 000 hours, the analysis predicted the following:

(1) The zone over which erosion would take place would be along the last
4 inches of the blade-tip leading edge.

(2) The maximum depth in this eroded zone would be 16 mils.

Comparing these predictions with the actual damage, as obtained from limited
data reported during a field inspection of the turbine, the erosion zone extended
along 2 inches of the blade tip as shown in figure 2-26, which is a sketch of a typical
damaged blade. With regard to the maximum depth of erosion in the Stellite shields,
181 blades had less than 60 mils and the remaining 15 had more than 60 mils. The
Stellite 6B shields on these 15 blades had to be replaced. While the predicted max-
imum depth of erosion was less than the observed maximum depth, the general re-
sults are encouraging in that this analysis is the first to predict quantitatively any
erosion at all in a turbine. On this basis, work on improving the mathematical
model is continuing, particularly in the area of predicting droplet breakup and re-
sultant size distribution in the turbulent stator wake flow. A simplified form of the
present mathematical model is being used in the design of new steam turbines to
limit erosion damage while attempting to further increase turbine output.

As part of the advanced nuclear Rankine cycle space-power-system technology
program, General Electric at Evendale, Ohio has been awarded several contracts
to investigate experimentally erosion damage in potassium vapor turbines. Under
NASA Contract NAS5-1143 General Electric ran a two-stage turbine for 5000 hours.
Figure 2-27 shows the leading edges of a portion of the second-stage rotor after the
test. The inlet temperature was about 1400° F, and the inlet quality to this blade
row was calculated to be 96 percent. Most of the blades were fabricated from the
nickel-base alloy U-700, and the remainder were from the molybdenum-base alloys
TZM and TZC. No droplet impact erosion was experienced in any of the blades.
This result is in agreement with the Westinghouse analytical erosion model which
predicted negligible droplet formation at this moisture level.

Currently, a more severe moisture erosion test is in progress at General
Electric under NASA Contract NAS3-10606. Figure 2-28 shows the rotor assembly
of a three-stage turbine which is being tested at a third-stage rotor inlet tempera-
ture of about 1200° F and at a calculated quality of 90.4 percent. At the conclusion
of the tests, the extent of erosion damage will be compared with the anlytically pre-
dicted values.

CAVITATION IN PUMPS

Cavitation, which is the formation and collapse of vapor within a flowing system, occurs in regions of pump blading where a combination of low ambient pressure and high local velocities are obtained. In a region of high velocity, if the static pressure drops below the vapor pressure of the liquid, vapor bubbles are formed. As these bubbles move with the flow to regions of higher pressure they can collapse violently.

Cavitation is a problem in a pump for two reasons. The implosions of collapsing bubbles can damage the pump blading or casing. Also, when cavitation is severe it can disrupt the flow through the pump, and thus performance is affected adversely.

The effect of increasing cavitation on the performance of a pump is illustrated in figure 2-29, where pump pressure rise for a given speed and flow is shown to depend on the margin of inlet pressure above the vapor pressure or net positive suction head (NPSH). The point of cavitation initiation occurs at a pressure well above that for which performance is affected. At this point it already produces noise and can be detected with a stethoscope on the pump casing. When vapor forming on the pump blade surfaces caused the flow to separate from the blades, the pump output deteriorates rapidly. Large vapor formations are present in the pump when this performance curve becomes vertical.

The flow in an axial flow pump rotor operating in water is shown in figure 2-30. Cavitation-free flow, moderate cavitation at the point of performance dropoff, and extensive cavitation associated with a large performance loss are illustrated in figures 2-30(a), (b), and (c), respectively. With moderate cavitation (fig. 2-30(b)) where the pump operated just above the point of severe performance falloff, both blade-tip cavitation and suction-surface cavitation are evident. Although the blade-tip cavitation is quite prominent, it had no appreciable effect on pump-blade performance. As inlet pressure was reduced, blade-surface cavitation continued to grow (see fig. 2-30(c)). With this large amount of vapor present on the suction surface, the pump no longer operated effectively.

Photographs of the cavitation formations in a centrifugal pump were taken with the camera oriented as indicated in figure 2-31. A typical illustration of cavitation is shown in figure 2-32. These photographs of cavitation were taken in pump rotors that might be used in turbopumps for rocket engines where cavitation damage is not a problem because the duration of engine operation is so short. However, cavitation damage is a problem in the pumps for a turbogenerator electric power system, which must operate reliably for long periods of time. In this case, liquid sodium or potassium may be the working fluid. Since it is not economical to subcool the

condensate, it must be pumped by the condensate return pump in a near-boiling condition. Cavitation damage in this pump is the primary concern.

The problem is evident from the cavitation damage observed on a mixed-flow impeller which was tested at the Pratt & Whitney CANEL installation in liquid potassium at 1400° F for 350 hours. The mixed-flow impeller shown in figure 2-33 is about 7 inches in diameter. The damage (fig. 2-34) occurred on the rear surface of the blade near the trailing edge. The severe pitting would have been followed shortly by blade failure. Some of the pits are 1/16 inch in depth.

Cavitation damage occurs on a fluid-containment surface, such as a pump blade, where adjacent vapor cavities rapidly collapse. Although various studies have shown that pure vaporous cavities can collapse rapidly and at high energy levels, the basic mechanics of damage by imploding vapor bubbles is not clearly established. Recent research, however, has revealed one way in which cavitation damage occurs. Figure 2-35 shows the successive phases of an imploding cavitation bubble near a solid surface. Figure 2-35(a) shows a cavitation bubble adjacent to a surface somewhat as it would appear moving along the suction surface of a pump blade. As the bubble moves into a zone of higher pressure, the vapors within condense rapidly, and the collapsing bubble takes odd shapes. As a bubble collapses (figs. 2-35(b), (c), and (d)), a jet of liquid is formed, which pierces the bubble and impinges on a small area of the adjacent blade surface. The center of the jet appears in the photographs as a dark core which extends above the bubble.

Lewis Research Center has sponsored research on materials that resist cavitation damage. Studies of cavitation damage with the use of alkali-metal pumps are supplemented by work with a magnetostrictive vibratory device which closely simulates pump-blade damage. This device (fig. 2-36) consists of two principal parts - a magnetostrictive vibrator, and a test specimen that is driven by the vibrator. Cavitation damage is produced on the surface of the 0.5-inch-diameter circular specimen, which is submerged in liquid and caused to vibrate at high frequency. On each upstroke vapor bubbles are formed near the surface of the specimen. These bubbles collapse with high energy on the ensuing downstroke. The device provides a practical method for making rapid, accurate, and detailed measurements of the rate of weight loss for a given material.

The cavitation erosion rates for a number of materials, tested over a range of conditions, are presented in figures 2-37 and 2-38. The curves for 304-L stainless steel and 316 stainless steel are similar in that the damage rate is small initially, rises sharply, and then falls off to a constant steady-state zone. The damage rate differs for the various materials. In water, for example, soft aluminum is eroded by cavitation about 60 times faster than stainless steel. The resistance of several refractory alloys - TZM, T-222, and columbium 132M - has been

studied in liquid sodium. These alloys maintain their strength at the high temperature of interest in space-power systems. In 400° F sodium, the resistance of these materials to cavitation damage (based on steady-state values) is comparable with that of 316 stainless steel. Stellite 6B, a cobalt-base alloy, is remarkably resistant to damage. After 14 hours of exposure, weight loss was only beginning to become measurable. Because of its high cost and the difficulty of fabrication, it is impractical to fabricate an entire pump rotor of Stellite. An inlay of Stellite in the most damage-prone area of the blading, however, might greatly extend pump life.

In order to determine which physical properties of the material are important in determining the resistance to cavitation damage, it is important to consider the mechanism of damage. Basically, the containment material is exposed to the jet impingement and pressure shock waves of imploding bubbles on or very near its surface. Damage resistance, then, is a measure of the capacity of a material to absorb this mechanical attack before fracture or pitting occurs. Thus, high values of yield strength, ultimate tensile strength, hardness, and ductility (percentage of elongation to fracture) are beneficial in providing resistance to cavitation damage.

In space-power systems, operation at high-temperature levels is desirable; thus, it is important to consider the effect of fluid temperature on the rate of cavitation damage. The rate of damage for three materials immersed in liquid sodium at 400°, 1000°, and 1500° F are compared in figure 2-39. All the data presented were obtained with the liquid sodium at atmospheric pressure. The greatly reduced rate of damage observed at 1500° F occurs despite the fact that the specimen materials have less strength at this higher temperature.

The decreasing damage at higher temperatures is caused by a change in the properties of the liquid and vapor. To understand the process, the flow in the passage between two pump blades as illustrated in figure 2-40 is considered. A cavitation bubble forms near the suction or low-pressure surface of one blade. This bubble is then swept across the passage to the surface of the adjacent blade where the pressure is higher. There must be a violent, rapid collapse of the bubble close to the blade surface to cause damage.

At relatively low temperature, as in room temperature water, the rate of bubble collapse is limited only by the inertia of the liquid surrounding the bubble. At higher temperatures closer to the boiling point, however, the rate of bubble collapse is controlled by thermal limitations - the rate at which the saturated vapor within the cavity can be condensed on the surrounding liquid interface.

The vapor pressure of sodium as a function of temperature is plotted in figure 2-41. The curve rises steeply at higher temperatures. Bubble collapse is slower and therefore less damaging at high temperatures for two reasons. First, the density of the saturated vapor in the bubble is proportional to vapor pressure.

Thus, a given size bubble will contain a greater mass of vapor at high temperature. The greater mass of vapor takes a longer time to condense. Also, condensation is a heat-transfer process. As a bubble moves across the passage it goes through a pressure change ΔP. Initially the bubble is filled with saturated vapor at the temperature of the surrounding liquid. In the high-pressure region the temperature of the saturated vapor inside the bubble is greater than that of the surrounding liquid by the condensing ΔT (fig. 2-41). At the higher temperature, because of the greater slope of the curve, the ΔT corresponding to the same pressure difference is much smaller. This lower ΔT reduces the rate of condensation and contributes to a slower bubble collapse.

These two effects - a greater mass of vapor in the bubble and the smaller temperature difference between the vapor and the ambient liquid - combine to cause a much slower bubble collapse and therefore less damage at high temperature. At the high temperature of operation of space-power systems, about 1500° F, damage rates are so low that some pump cavitation may be tolerable. However, at temperatures of about 1000° F sodium shows a cavitation damage rate comparable to that of room temperature water. It will probably be necessary, therefore, to operate the sodium pumps in stationary powerplants at a pressure level and flow condition for which cavitation is avoided.

HIGH-TEMPERATURE LIQUID METAL PUMPS

The utility companies use, almost exclusively, the submerged pump for liquid metal service. These pumps, using conventional motors, have overall efficiencies of over 80 percent. They do, however, require a dynamic seal between the motor and the liquid metal cover gas. Space-power high-temperature liquid metal loops cannot tolerate any contaminants, and this has required the development of totally sealed pumps.

Two types of liquid metal pumps being developed are the canned motor pump and the electromagnetic or EM pump. An example of the canned motor pump is the SNAP-8 sodium-potassium (NaK) pump shown in figure 2-42. The pump and a 400-cycle motor are mounted on one shaft and are wholly contained within a welded housing. The pump inlet and exit are welded into the liquid metal loop forming a single, completely sealed unit. No shaft seals are required since both pump and motor are submerged in the same NaK fluid. The high-temperature pumped NaK is separated from the cooler NaK in the motor cavity by a short annular thermal barrier. The pivoted pad journal bearings and double acting pivoted-pad thrust bearings are also lubricated and cooled by cavity fluid. To protect the electrical ma-

terials from chemical attack by the liquid metal, both rotor and stator are encapsulated within welded Inconel cylinders or "cans."

This pump delivers 100 gallons per minute of NaK at an overall efficiency of 35 percent. The low efficiency is due to the small size of the rotor and the presence of the Inconel cans.

One of these units recently completed over 10 000 hours of trouble-free operation. The endurance test included over 800 scheduled start-stop cycles, attesting to the physical integrity of the bearing pads and ball pivots. While the motor hot-spot temperature was maintained at 450° F, the electrical materials used are designed for 1000° F hot-spot service. If this high-temperature material technology is used, a canned motor pump might be developed for sodium service without the need for an external cooling system.

The electromagnetic pump is simpler in concept than the canned motor pump in that the EM pump has no moving parts. Because of the EM pump's simplicity, and despite its lower efficiency, it provides liquid metal systems the maximum in pumping reliability for long duration, unattended space missions. A cross section of a helical induction pump is shown in figure 2-43.

The liquid metal enters the pump at the right into an annular passage. The helical induction EM pump is analogous to an induction motor except that the rotor has been replaced by a liquid metal filled annular passage. The rotating magnetic field imparts a force on the liquid causing it to rotate circumferentially in the annulus. Since the fluid is constrained to flow within the helical channel in the annulus, the fluid moves from one end of the pump to the other. At the same time, the fluid static pressure increases along the helical channel. The high-pressure fluid makes a 180° turn at the end of the annulus and exits the pump at the right through the center pipe. With both fluid connections at the same end of the pump, the stator and cooling passages can be removed, if necessary, without disturbing the sealed liquid metal loop.

NASA has contracted with the General Electric Company to develop a boiler feed pump of the type shown in figure 2-43. The pump is being designed to deliver 33 gallons per minute of potassium at 1000° F. The pump has a calculated efficiency of 18 percent. The stator hot-spot temperature will be limited to 1200° F by using a potassium coolant. All the electrical materials used in the pump, except for the stator end turn connections, have been successfully tested to 1300° F for 10 000 hours. This pump is now in the final stages of assembly, preparatory to testing.

In spite of the lower efficiencies, the canned motor and electromagnetic pumps may provide highly reliable, long-life service for secondary applications in central power stations.

MATERIALS

The current SNAP-8 boiler, described previously, utilizes tantalum as the mercury containment material because of its excellent corrosion resistance and 316 stainless steel as the heating fluid containment material. During the early part of the SNAP-8 development program, however, extensive use was made of 9Cr-1Mo steel throughout the system including the boiler. This material (most often referred to as Croloy 9M or Sicromo 9M) is commonly used in steam systems, primarily in the reheaters.

As the SNAP-8 program progressed, a change was made to a material developed by the Timken Roller Bearing Company called modified 9M, which was considerably stronger than the standard alloy. The improved strength was achieved primarily by a slight chemistry modification and also by a 1900° F normalize and 1350° F temper heat treatment. The chemistry modification consisted of the addition of very small amounts of columbium, vanadium, boron, nitrogen, and zirconium (the total elemental addition being less than 1/2 of 1 percent).

The improved strength properties are clearly illustrated in figure 2-44 in which modified 9M in the normalized and tempered condition is compared with standard 9M, 304 stainless steel, and 315 stainless steel (all in the annealed condition). Plotted is the ASME Boiler and Pressure Vessel Code maximum allowable stress values for each material against temperature. The 321 stainless steel would fall below but near the 316 stainless steel. There are no code values for modified 9M at this time; however, the curve shown was constructed using the same ground rules under which the curves for the other materials were constructed (i.e., 1/4 ultimate tensile strength and 60 percent of 100 000-hr rupture strength). Over the temperature range shown, the modified 9M is much stronger than 9M, stronger than 304 stainless steel, and is stronger than 316 stainless steel up to at least 1100° F. The material has indicated no instabilities even after approximately 18 000 hours of stress rupture testing at 1100° F.

A thorough welding study of the material was conducted at Lewis Research Center. No noticeable difference between it and the standard 9M was observed. The material requires a postweld heat treatment, just as do 9M and the other low and medium chrome steels. As is the case with standard 9M, the material can be utilized up to about 1300° F without excessive scaling.

Because of the improved strength of the modified alloy, it could be used in reheaters in place of 9M. Being able to use a considerably thinner wall would result in a significant cost saving.

The modified alloy could also be used in high-pressure superheater applications in place of 304, 321, 347, or even 316 stainless steel at the same wall thickness if

the postweld stress relief does not impose significant constraints. The cost savings in this case would be very significant as shown in figure 2-45. There is a factor of 2 between modified 9M and 304 stainless steel, a factor of $2\frac{1}{2}$ between it and 321 stainless steel, and a factor of >3 between it and 316 stainless steel.

As noted, the modified 9M has already been used in SNAP-8 boilers. It has also been used in a high-temperature conveyor application. It is likely there are many applications where it could be substituted for more costly materials currently being used.

Stellite 6B, a cobalt-base alloy, is commonly used as blade shielding in the final stages of steam turbines. The use temperature is normally less than 200° F. Stellite 6B has also been considered for service in other areas in steam turbines. One such area is as the nozzle block material for the first stages where significant erosion has been observed in some installations. The temperature in these areas can be as high as 900° to 1100° F, and because of these higher temperatures there is a need for caution based on past experience.

Stellite 6B was utilized in the SNAP-8 turbine shown in figure 2-46. This turbine is a four-stage impulse-type machine, 10 inches in diameter and 20 inches long. The Stellite was used as the nozzle-diaphragm and wheel-blade material in all four stages. It was selected since it was one of the most erosion-resistant materials known.

All available information indicated no potential danger in utilizing Stellite 6B at elevated temperatures. The first turbine, however, failed catastrophically in less than 1000 hours. Examination of the failed parts revealed extremely brittle fracture. The shattered first-stage wheel is shown in figure 2-47.

Subsequent metallurgical studies at Aerojet-General Corporation determined that the material was unstable over the entire operating temperature range of the turbine. Carbide precipitation, which increased the hardness from a normal R_c of 40 to as high as 50 was found to occur. There was also a tendency toward transformation of the crystal structure from face centered cubic (FCC) to hexagonal close packed (HCP) accompanied by a volume decrease. These metallurgical changes resulted in a significant decrease in the material's ductility and resistance to impact. The two hardness extremes are compared in figure 2-48 in terms of the tensile elongation as a function of temperature.

The upper curve is representative of the condition in which the material would normally be put into service. The lower curve is representative of the condition of the material after thermal aging in service occurs. A turbine designer would not utilize a material of such low ductility if he knew about it in the beginning.

A comparison of the impact strengths of the original and thermally aged material is shown in the following table:

Hardness, Rockwell C	Crystal structure	Impact strength, ft-lb
40	FCC	4.2
50	HCP	1.2

Only relative values are important since subsize specimens were used. The R_c 50 material in the HCP crystal structure had approximately one-third the impact strength of the R_c 40 material in the FCC crystal structure.

The metallurgical study also showed that some lots of Stellite 6B were considerably more stable than others. It was determined that the stability of a given lot of material depended on its chemistry, prior processing history, and prior heat treatment. As a result of the study, however, Stellite 6B was eliminated as the SNAP-8 turbine material.

The foregoing does not entirely rule out Stellite 6B for elevated temperature service. It does, however, caution potential users to test thoroughly, at the service temperature, the particular lot or lots of material planned to be used. This would be particularly true if the material is to be exposed to mechanical or thermal shock or both.

COMPUTER SIMULATION OF SYSTEM DYNAMICS

A previous discussion treated some dynamic problems that involve one or two components of the powerplant. Some aspects of boiler stability and dynamic coupling of the boiler with its feed system were discussed. It was shown that sometimes a relatively simple mathematical analysis can indicate the way to avoid trouble. However, there are other dynamic problems that involve all the components of the powerplant. Here the mathematical analysis is much more complicated. Therefore, these system dynamic problems are studied by simulating the powerplant with a computer.

Computer simulation, of course, is not new. It has been used widely in both industry and government in recent years. Therefore, this discussion does not dwell, to any extent, on the techniques involved in puting a simulation together or on the mathematical methods used. Instead, the discussion is focused on a particular application in which a computer simulation was very useful.

This application was in the development of an automatic startup system for the

space powerplant shown schematically in figure 2-49. This is the SNAP-8 system, which is currently being developed. It is a three-loop nuclear Rankine powerplant with mercury as the fluid in the vapor loop. When this system is put into space, the entire startup will be controlled by an electrical programmer. The design of this programmer required detailed information on the startup transients. In obtaining this information, extensive use was made of a computer simulation of the powerplant.

The type of computer simulation used to study the startup transients is illustrated in figure 2-50. The computer depicted in this figure is a large-capacity general-purpose one. The input information includes the many equations that represent the individual components of the powerplant. It also includes the computing logic that provides for the component interactions of the real system. The role of the computer is to take over the big job of solving the many equations. The output of the computer, of course, is the system information. The startup transients can be displayed in the form of tables or graphs. Plots of variables against time are especially convenient, since they are usually recorded in this manner during startups of the actual system.

The advantage of the large-capacity computer was that it simplified the job of writing the component equations. Because the computer was able to handle many equations, the complicated components were subdivided into parts that were easy to analyze. As mentioned previously, the mathematical analysis will not be discussed in detail. However, it should be pointed out that this approach of subdividing complicated components does give good results. The reactor was one component treated in this way. In simulating the reactor, three basic subdivisions were used - control, nucleonics, and heat transfer. The heat-transfer part was broken down into 22 segments.

The reactor model was compared with test data. An example comparison is shown in figure 2-51. The data were obtained from the North American Rockwell Corporation who is the developer of the reactor. For the testing, the operation of the reactor was disturbed by making step increases and step decreases in coolant flow rate. The disturbances were 500 seconds apart. The same disturbing function was imposed on the computer model. The resultant response of the nuclear power is shown: the solid curve is for the real reactor, and the dashed curve is for the computer model. The maximum difference between the curves is about 1/2 percent of the average power level.

The startup procedures for the SNAP-8 system are somewhat similar to the startup procedures used for ground-based powerplants. The main difference is that injection starting of the vapor loop is used. This is done because of the zero-

gravity environment in space. With no gravity force available, the boiler feed pump has no suction head until a sufficient pressure builds up in the condenser. Therefore, the mercury pump cannot be used in the initial startup of the boiler and turbine. Instead, during startup the initial feed rate needed by the boiler is supplied by injection from a pressurized external reservoir (see fig. 2-49). The mercury pump has to take over the job of feeding the boiler when the injection process ends. As stated before, the computer simulation was a valuable tool in defining these startup procedures and the required controls. One startup problem worked out with the computer simulation was to find the proper feed rate schedules for the injection of mercury into the loop.

This problem can be explained with the aid of figure 2-52 where some results are plotted from two different computer runs. The solid curves are for one run, and the dashed curves are for the other run. Three variables are shown for the first 3 minutes of the vapor-loop startup. They are reactor exit temperature, turbine speed, and boiler feed rate. The boiler feed rate schedules were the input variables for the two runs.

The shaded area under the solid plot of the boiler feed rate represents the amount of mercury to be injected into the loop. If this amount was injected with the rapid schedule shown, then the turbine was accelerated to its rated speed of 12 000 rpm well before the injection process stopped. The arrow on the speed curve marks the end of injection. This boiler feed rate schedule, however, resulted in critical rates of change of reactor temperature. The slope of the solid reactor temperature curve exceeds the allowable value at the point indicated. This problem could be corrected by injecting the same amount of mercury over a longer period of time. For this slower injection, the boiler feed rate schedule shown by the dashed line was used. The resulting satisfactory response of reactor temperature is shown by the dashed curve.

However, there was now another problem. With this slower schedule of boiler feed rate, the turbine acceleration was much slower, as shown by the dashed curve for turbine speed. In fact, the turbine was considerably below its rated speed at the time injection was finished; this time is marked by the arrow on the dashed speed curve. Therefore, the speed of the boiler feed pump, which was driven by the turbine generator, was also well below its rated value, and the pump could not deliver enough flow to sustain the operation after injection was over. Therefore, the turbine speed came down as shown in the figure, and the system failed to start.

With the computer, however, many boiler feed rate schedules could be studied. Eventually, schedules within these extremes were found that accelerated the turbine

and at the same time gave satisfactory reactor temperature transients.

As yet the complete SNAP-8 system has not been tested. However, there have been test versions of SNAP-8 which included everything but the reactor and the radiator. One such version used a gas-fired heat source and rejected its waste heat in an air-cooled heat exchanger. Startup tests were made with this system in which the flight-type procedures were followed as far as possible. Therefore, data from these tests were used to check the computer simulation. In doing this, of course, it was necessary to make some changes in the computer program in order to have it represent the system tested.

Some comparisons between computer results and test data are shown in figure 2-53. All parts of this figure represent the same startup run. Several of the more interesting variables are displayed for the first 10 minutes of the vapor-loop startup transient. The injection process began at time zero, and the end of the injection process is indicated by the vertical dashed lines.

The boiler feed rate schedule used in the test run and programmed into the computer is shown in this figure. The turbine speed and the temperature of the heating fluid leaving the boiler are also shown. In a complete SNAP-8 system, this would be the temperature transient fed toward the reactor. The other transients shown - the boiler exit pressure (on the vapor side of the boiler), the generator power, and the liquid weight in the condenser - were simulated quite well with the computer. The largest errors were in the latter part of the boiler temperature transient and in the generator power transient. The generator simulation was optimistic by about 10 kilowatts.

In general, the agreement between the computer results and the test data is good. Since these transients represent some of the most critical events of the startup, it can be concluded that a computer simulation can be used with confidence in the analysis of startup transients. It should also be mentioned that system transients involved in shutdown and load-following operations can also be studied advantageously with a computer simulation.

A computer simulation of a powerplant is a useful tool in designing controls and establishing operating procedures for large-excursion transients, such as startup. A computer simulation is also useful in defining emergency procedures, since many things can be tried that would be too hazardous in a real system. In addition, a computer simulation can be used to generate information pertaining to the structural requirements of the system and its components during off-design operation. The use of a computer simulation as a training aid for powerplant operators should also be considered. A training simulator much like the ones used to train pilots or astronauts could be set up by means of computer simulation.

SUMMARY

The discussion of Rankine power conversion system technology has touched upon a variety of topics. It is evident that potential economics in once-through boiler size, weight, and cost can be realized by the improvement of heat flux associated with the use of internal flow control inserts that separate the liquid and vapor phases within the boiler tubes. Space-power-system boilers using swirl inserts have been built and tested, and the results verify the applicability of the technology to the design of compact boilers.

A scheme for incorporating double containment within the boiler component was described. Boilers utilizing this concept have been built and operated and they have proven effective in avoiding operational hazards associated with the intermixing of boiling and heating fluids in reactor-powered systems.

The boiling instability phenomena were characterized. In general, the attenuation or elimination of instabilities requires identification of the type of instability and then making appropriate adjustments of the operating variables having influence on the particular instability encountered. Experimentally verified analytical techniques for predicting boiling instabilities are effective tools for guiding the thermodynamic and fluid dynamic design of boilers and coupling requirements of the boiler feed system.

The progress toward the understanding of the turbine blade erosion mechanisms and the analytical modeling of the process for purposes of predicting erosion damage rates has been reviewed.

The consequences of pump cavitation in terms of structural damage to the pump impeller and pump performance were discussed in some detail. Although adequate net positive suction head (NPSH) can normally be maintained in ground-based systems to avoid cavitation, there are distinct pump impeller materials choices to be made to provide added insurance against premature pump failure from cavitation damage.

Two types of high-temperature pump designs were described. These concepts, while having lower efficiencies than the more commonly used submerged pumps, provide compact noncontaminating units for special applications.

The virtues of a modified 9Cr-1Mo steel were examined relative to other materials commonly used in power systems with a view toward the economics of system or component construction. The results, though still rather preliminary, are encouraging. Since caution is necessary when using Stellite 6B at elevated temperatures, the user should thoroughly understand the characteristics of the particular lot of material to be used.

60

The value of computer simulation for the analysis of system transient behavior was described briefly. The technique provides a means for definition of complete system dynamics over a much broader range of conditions than could safely be attempted with the actual system as well as the definition of efficient and safe-operating procedures and the establishment of effective control logic. Furthermore, once the system is properly modeled on a computer, the simulation can be utilized for the training of operating personnel.
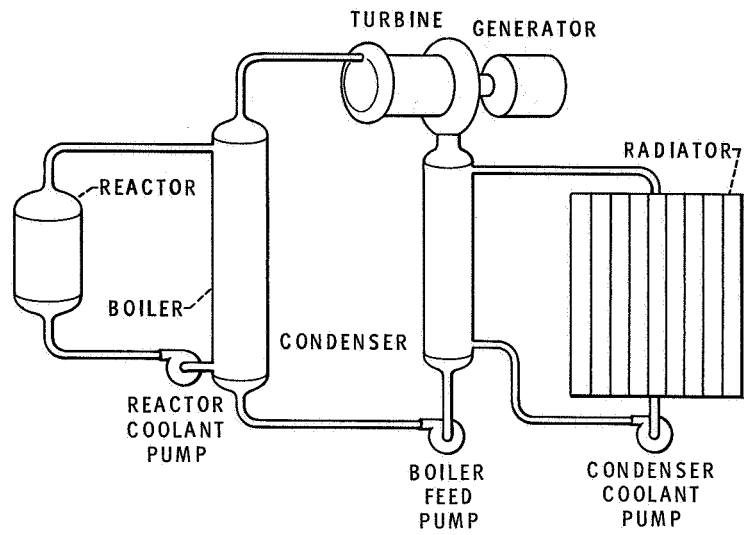
Figure 2-1. - Space nuclear power plant.
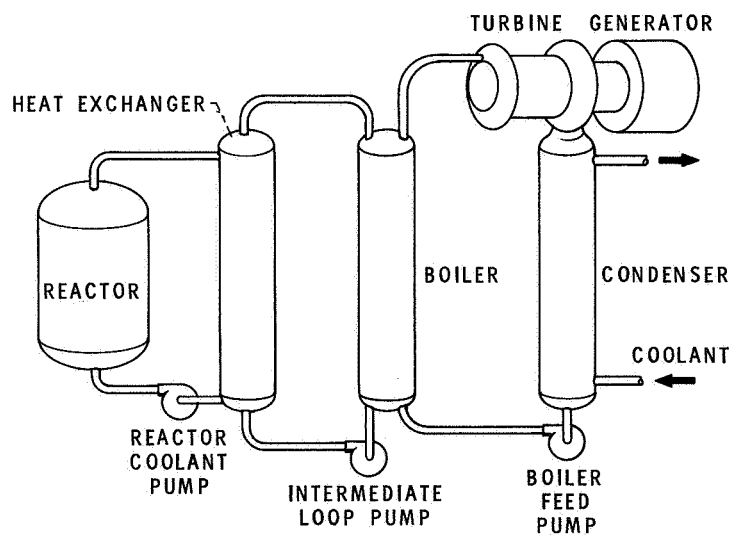
Figure 2-2. - Ground nuclear power plant.
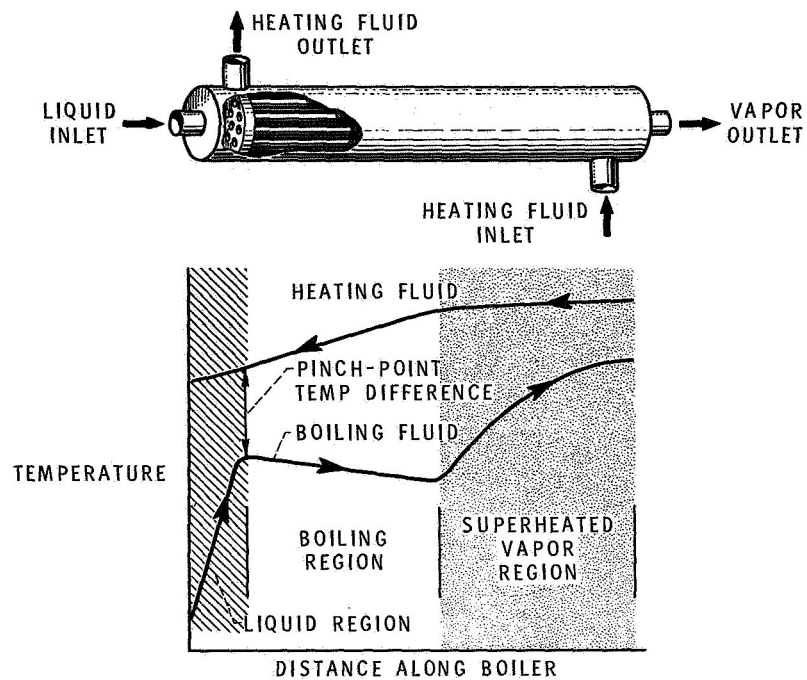
Figure 2-3. – Temperature distribution in "once-through" boilers.
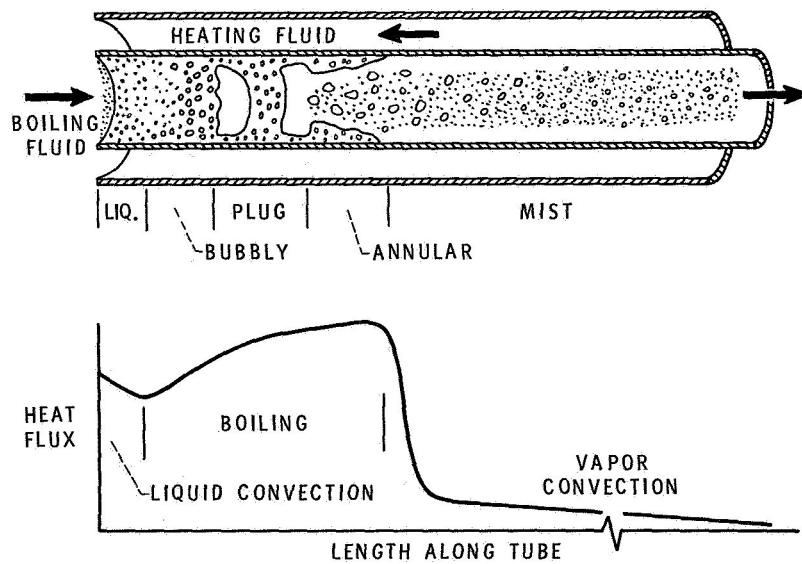
Figure 2-4. – Boiling flow regimes.

64

HEAT FLUX COMPARISON
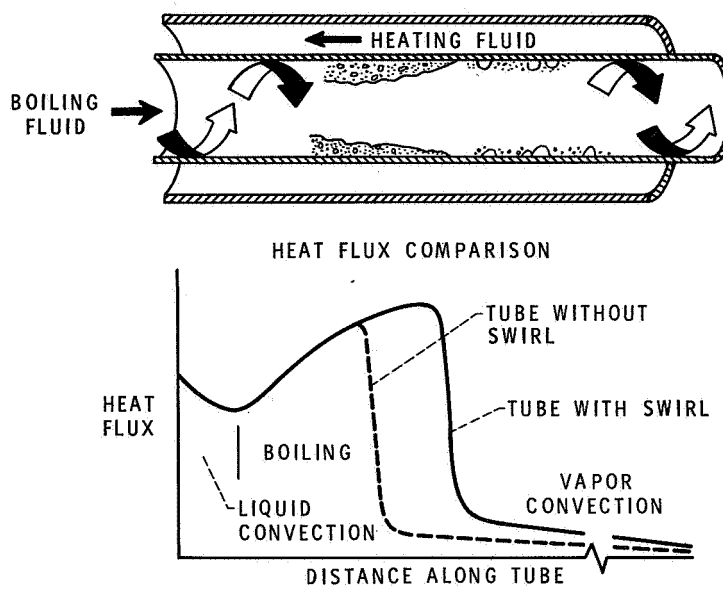
Figure 2-5. - Swirl-flow boiler concept.

TWISTED TAPE

HELICAL VANE ON CENTER ROD

HELICAL WIRE COIL

CENTER ROD IN HELICAL WIRE COIL
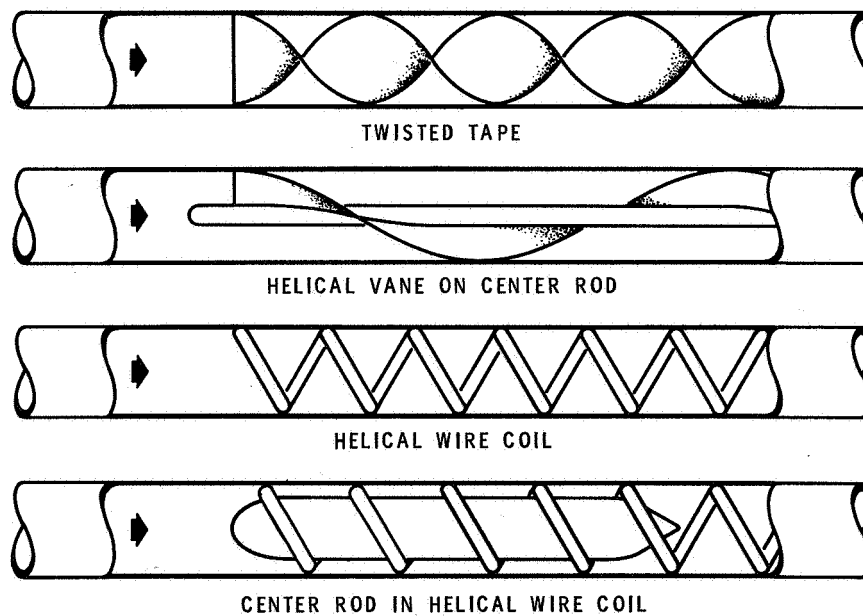
Figure 2-6. - Boiler tube inserts.
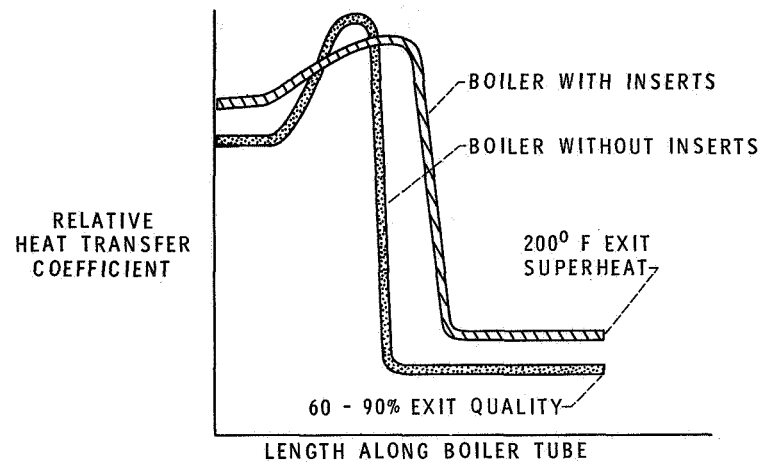
Figure 2-7. - Comparison of boiler performance.

Labels in figure: BOILER WITH INSERTS, BOILER WITHOUT INSERTS, 200° F EXIT SUPERHEAT, 60 - 90% EXIT QUALITY, RELATIVE HEAT TRANSFER COEFFICIENT, LENGTH ALONG BOILER TUBE
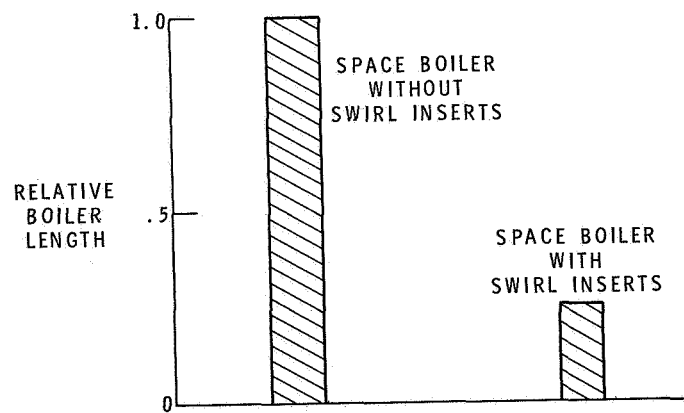
Figure 2-8. - Comparison of boiler lengths.

Labels in figure: SPACE BOILER WITHOUT SWIRL INSERTS, SPACE BOILER WITH SWIRL INSERTS, RELATIVE BOILER LENGTH, 1.0, .5, 0
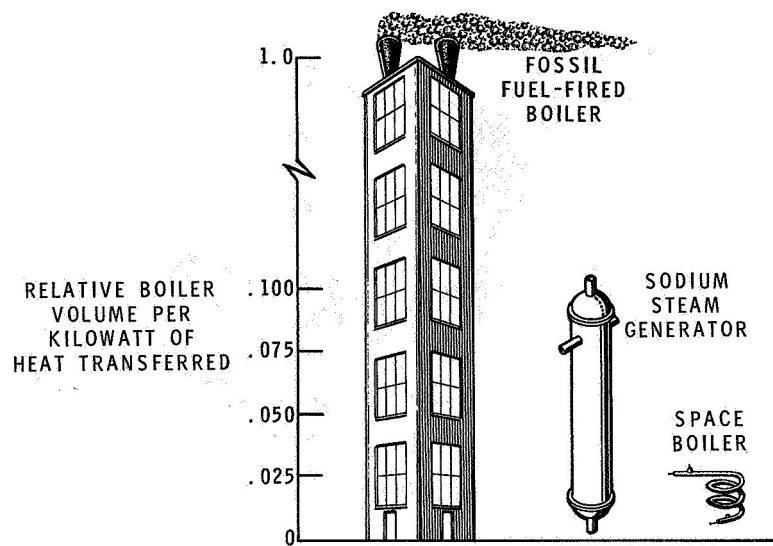
Figure 2-9. - Comparison of boiler sizes.

RELATIVE BOILER
VOLUME PER
KILOWATT OF
HEAT TRANSFERRED

FOSSIL
FUEL-FIRED
BOILER

SODIUM
STEAM
GENERATOR

SPACE
BOILER

1.0
.100
.075
.050
.025
0

36"

48"

CS-47796
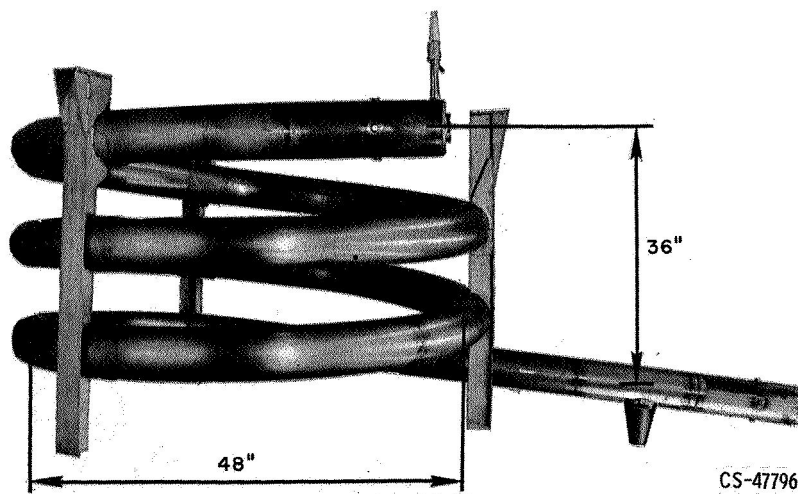
Figure 2-10. - SNAP-8 mercury boiler.
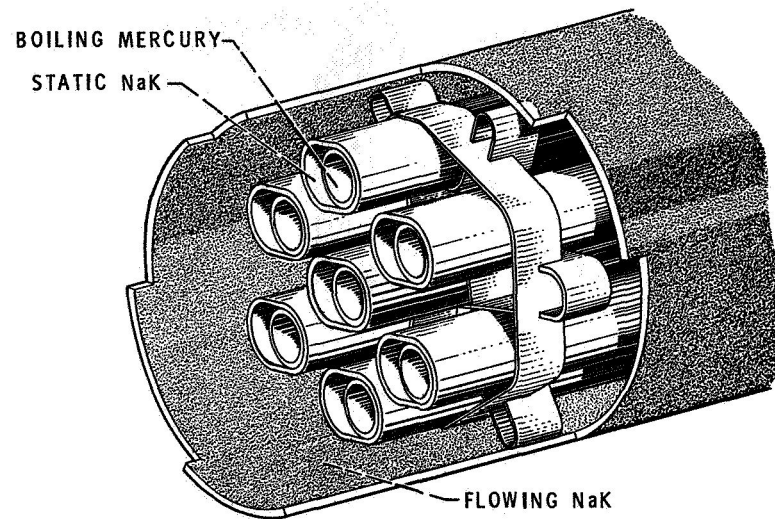
Figure 2-11. - SNAP-8 boiler tubes.
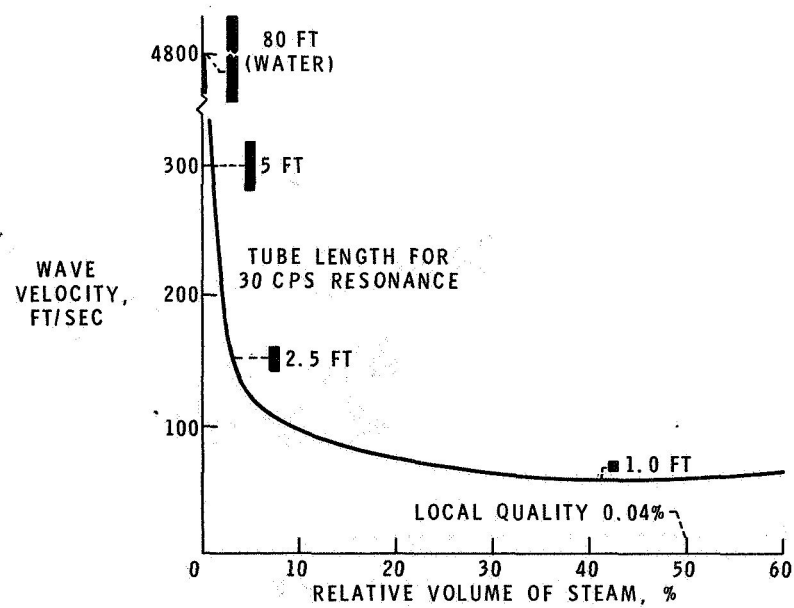
Figure 2-12. - Speed of sound for pressure of 1 atmosphere.

68
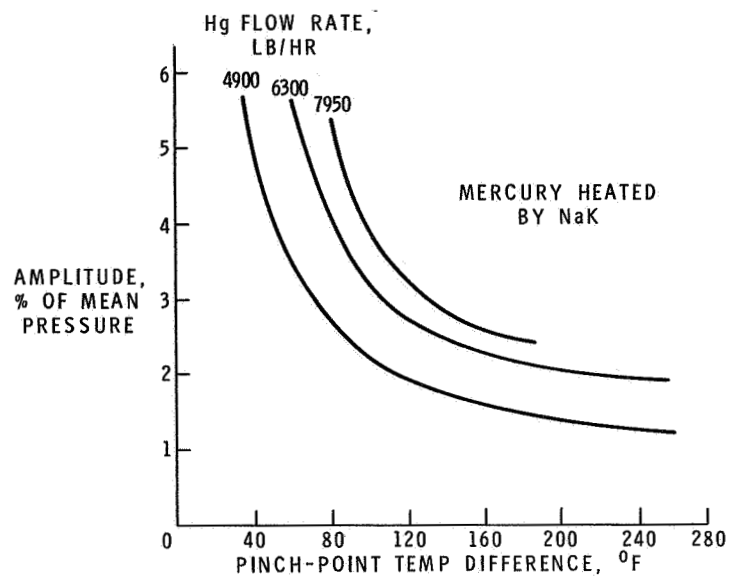
Figure 2-13. - Pinch-point effect on boiler-outlet pressure oscillations. (Mercury heated by NaK.)
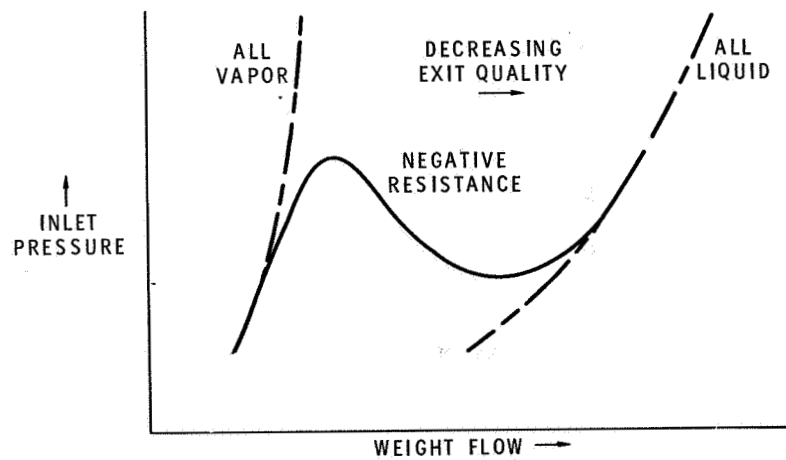
Figure 2-14. - Boiler pressure. Exit pressure constant.

PRESSURE

—————— BOILER INLET
— — — FEED SYSTEM EXIT

| POSITIVE | NEGATIVE | NEGATIVE |
| STABLE | UNSTABLE | STABLE |

PRESSURE

WEIGHT FLOW →
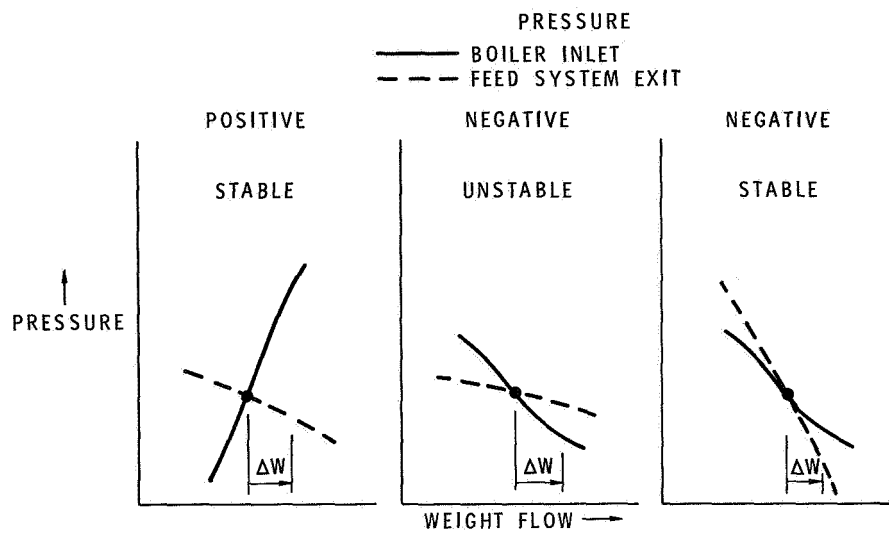
Figure 2-15. - Boiler resistance.
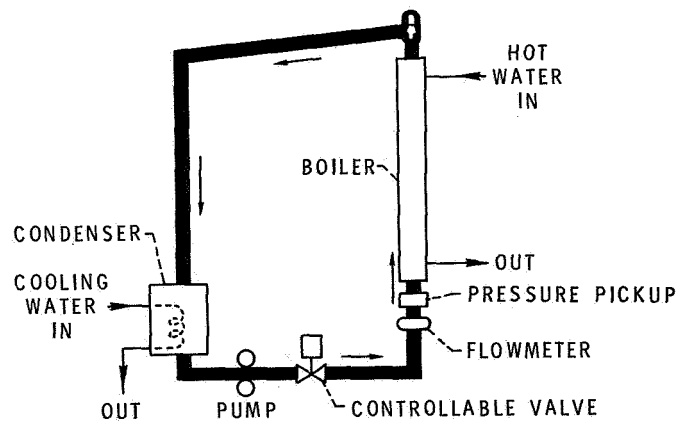
Figure 2-16. - Schematic diagram of boiling-Freon dynamics loop.
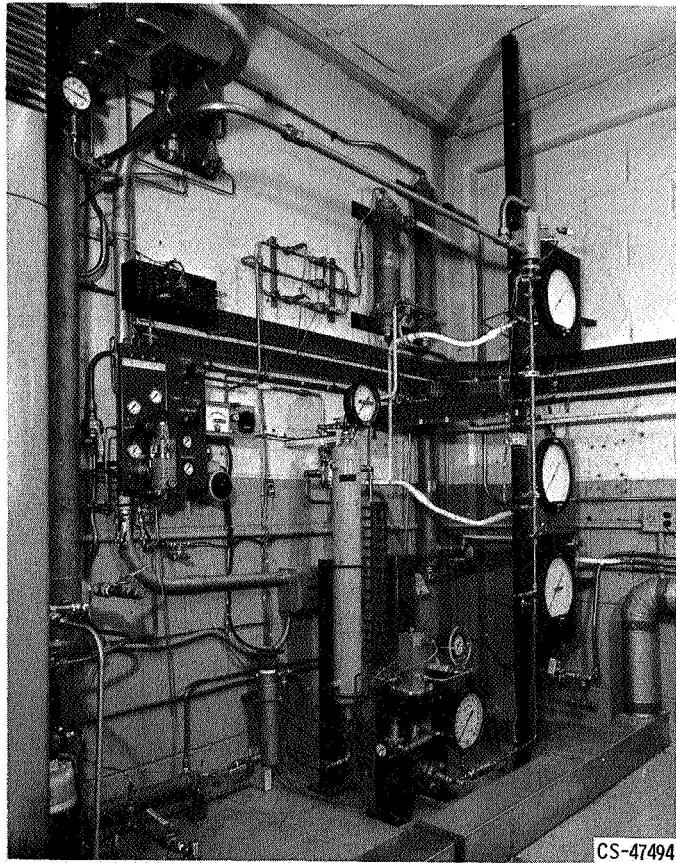
Figure 2-17. - Boiling-Freon dynamics loop.
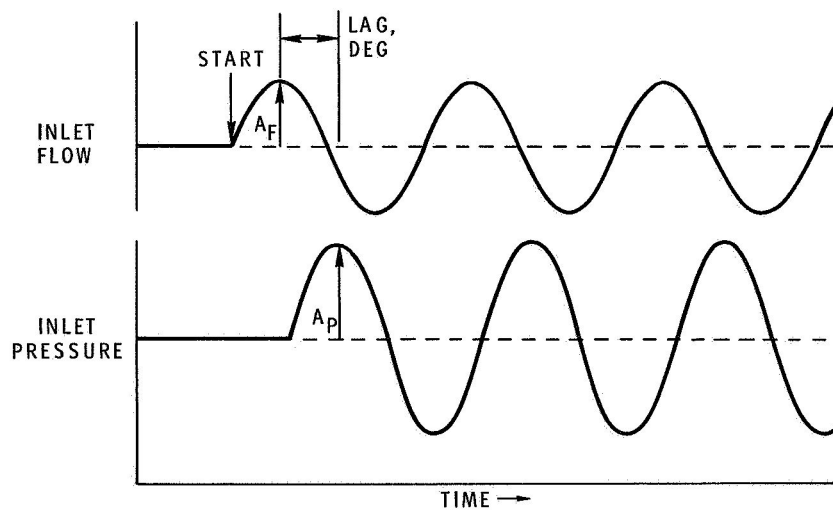
Figure 2-18. - Forced oscillations.
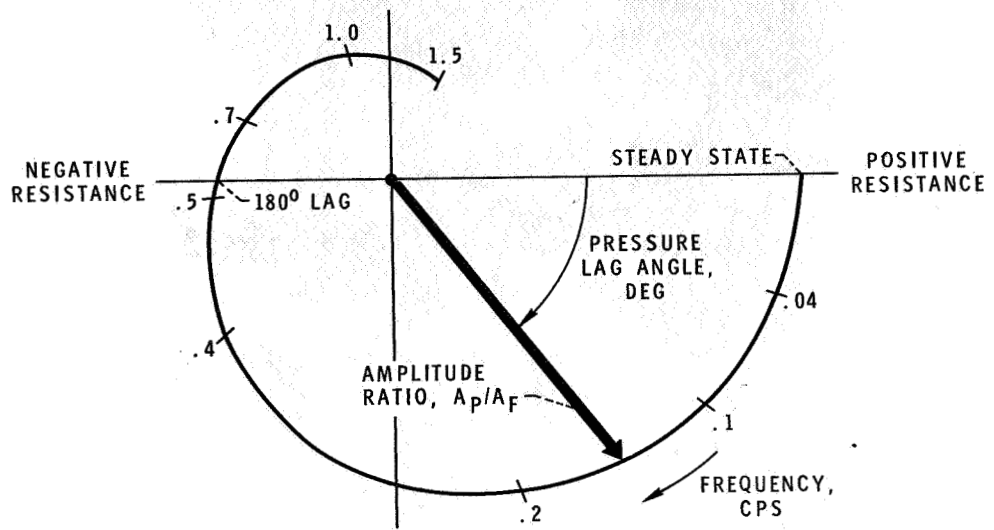
Figure 2-19. – Boiler inlet impedance in polar coordinates.
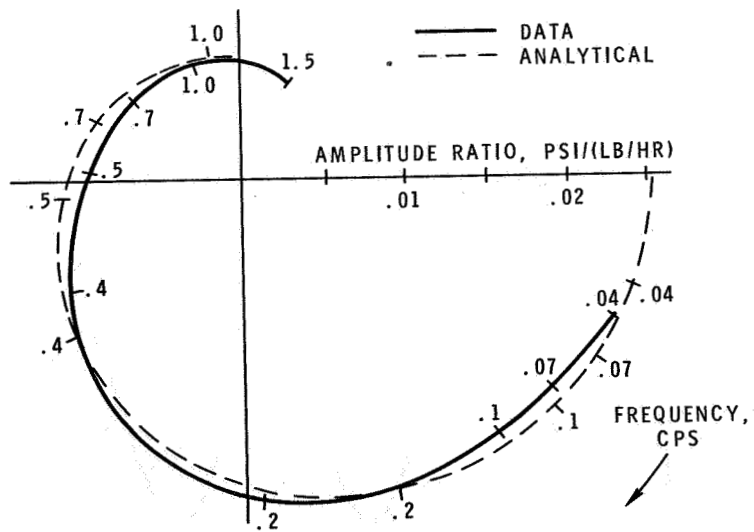
Figure 2-20. – Actual frequency response data for boiler inlet impedance.
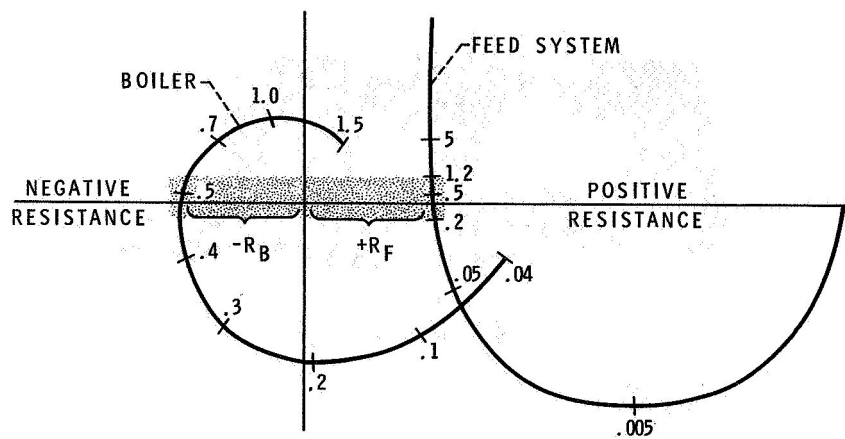
Figure 2-21. - Boiler inlet and feed-system impedances.
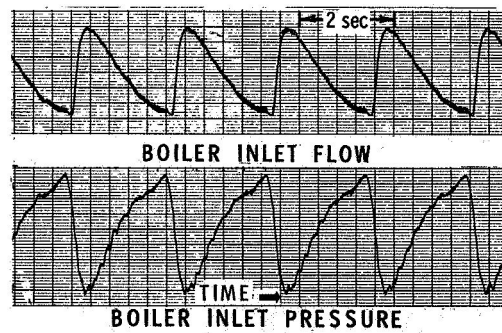
Figure 2-22. - Natural pressure and flow oscillations. Frequency, 0.48 cps; pressure lag, 180°.
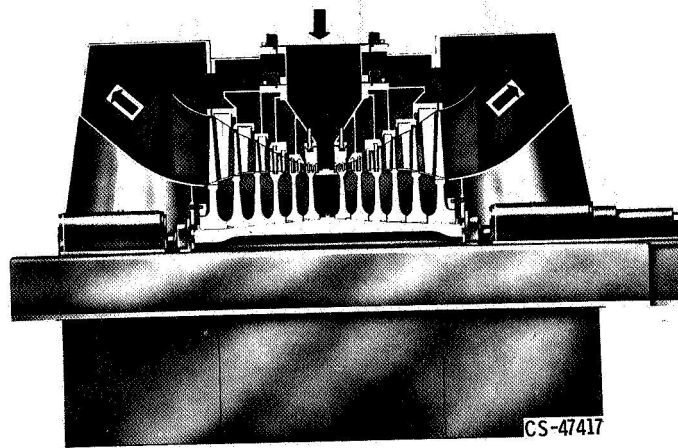
Figure 2-23. - Low-pressure turbine.
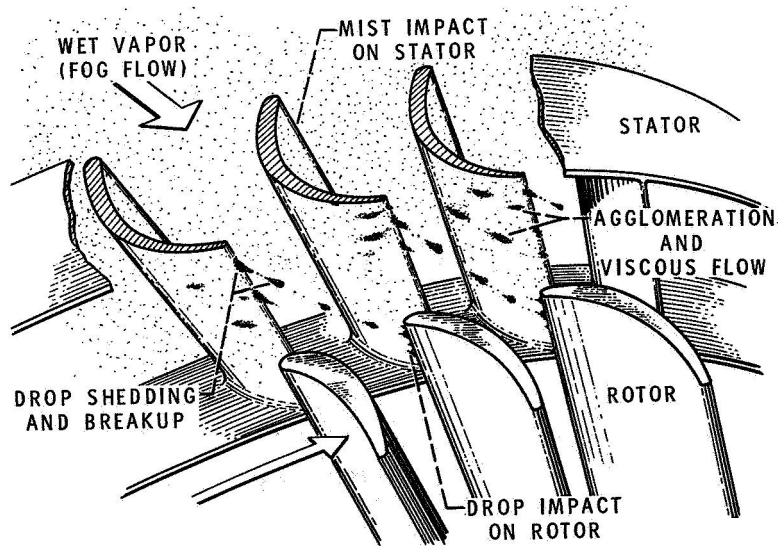
Figure 2-24. - Droplet growth and impact.
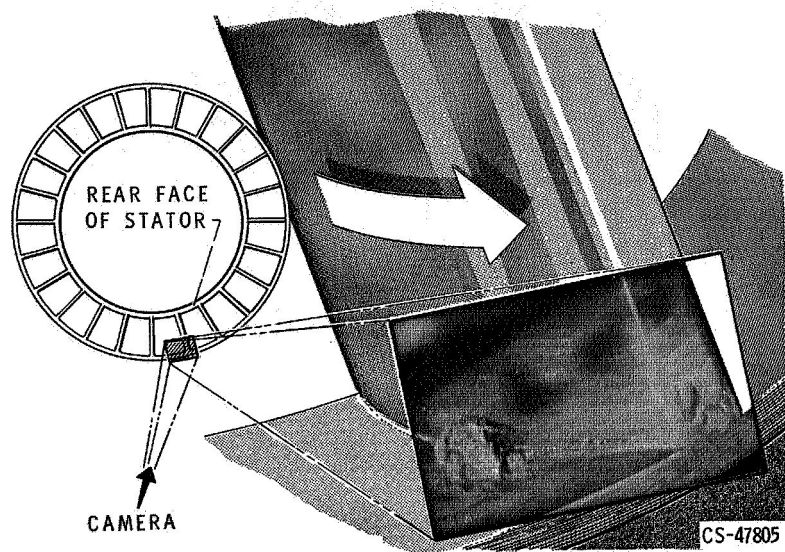
Figure 2-25. - Moisture flow visualization.
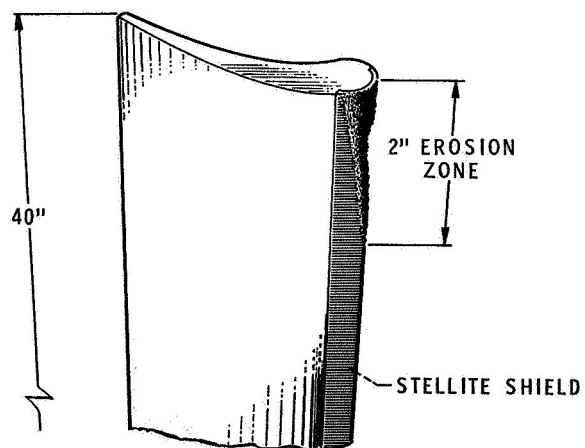
Figure 2-26. - Erosion damage of Yankee steam turbine. Ninth stage rotor after 13 000 hours; exit quality, 85 percent; temperature, 97° F.

U-700 (NICKEL BASE)

TZC (MOLY BASE)

NO IMPACT DAMAGE

0   INCHES   1

CS-47418
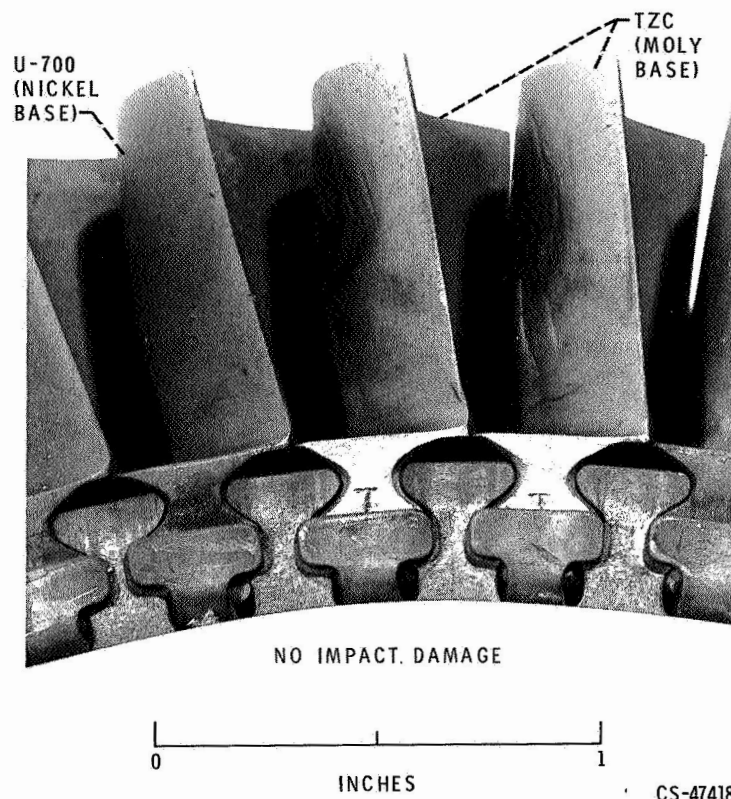
Figure 2-27. – Rotor-blade leading edge after 5000-hour test in potassium vapor. Exit quality, 92 percent.

CS-47584
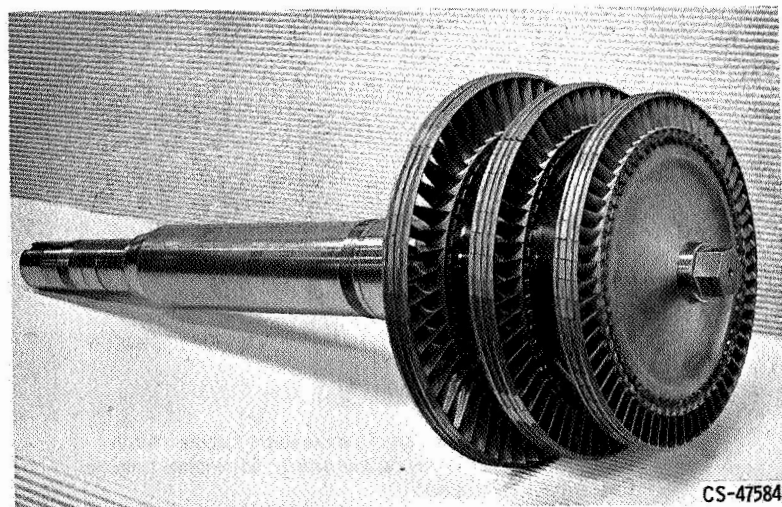
Figure 2-28. – Three-stage potassium vapor turbine rotor.
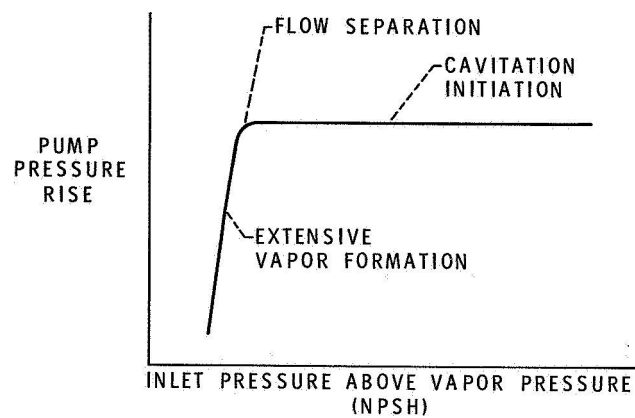
Figure 2-29. - Effect of cavitation on pump performance.
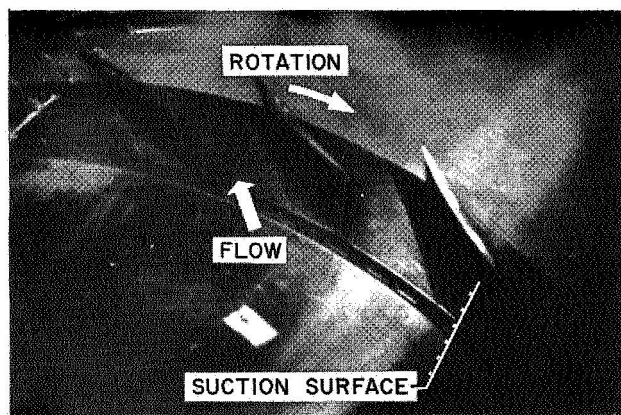
(a) No cavitation.
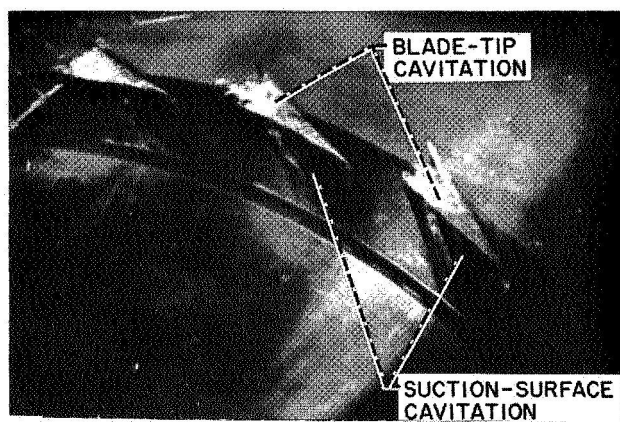
(b) Moderate cavitation.
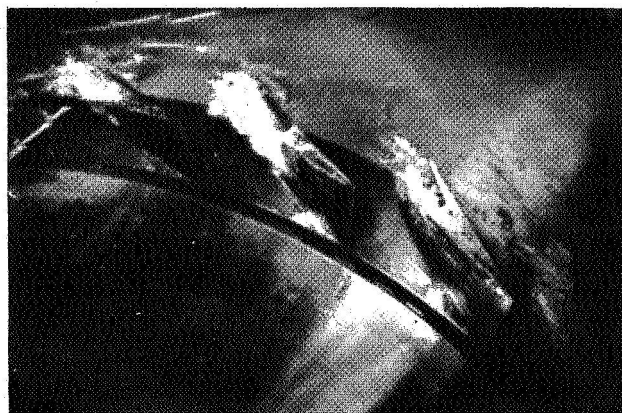
(c) Extensive cavitation.

Figure 2-30. - Axial flow pump rotor operating in water.

77

ROTATION

CS-47437
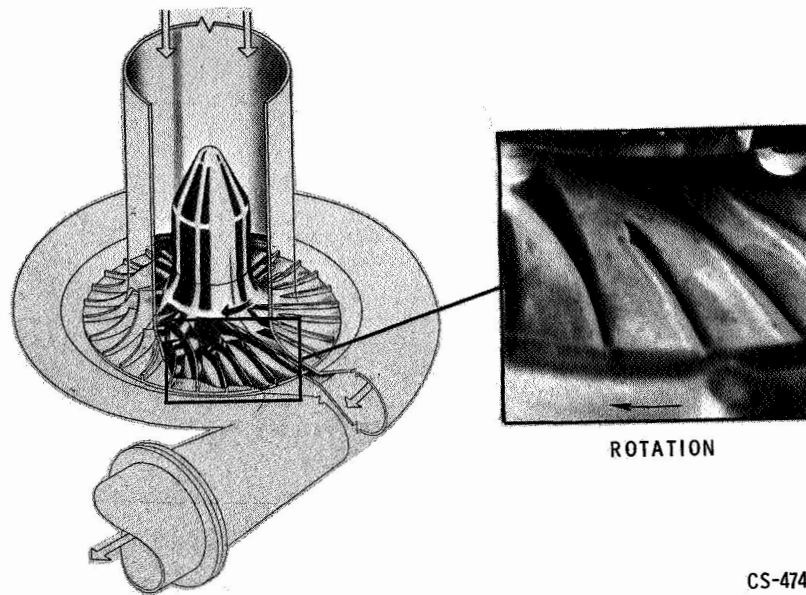
Figure 2-31. - Centrifugal pump.

ROTATION

BLADE
LEADING
EDGE

BLADE-SURFACE
CAVITATION

BLADE-TIP
CAVITATION
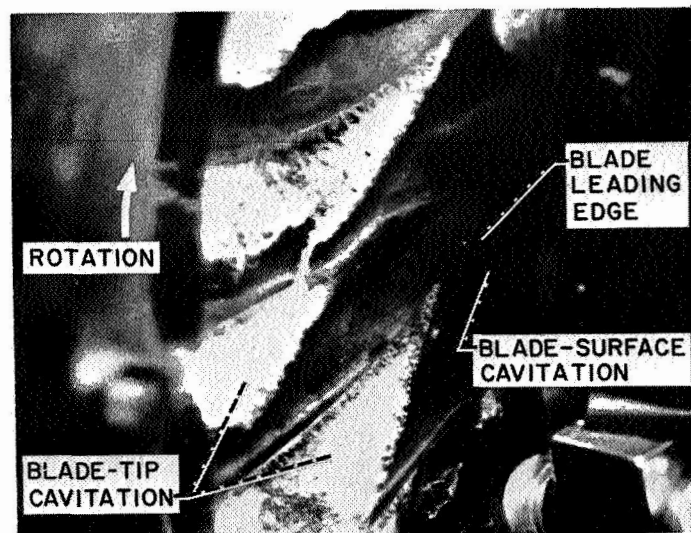
Figure 2-32. - Typical illustration of cavitation.
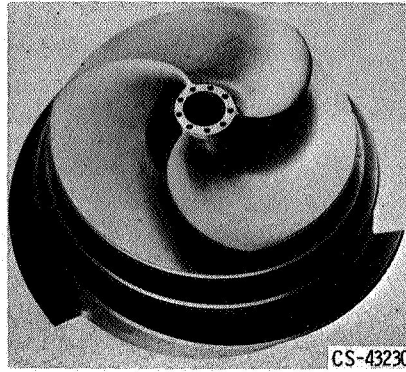
Figure 2-33. - Mixed-flow impeller for potassium tests.

Figure 2-34. - Rotor cavitation damage.

(a)   (b)

(c)   (d)   CS-38032
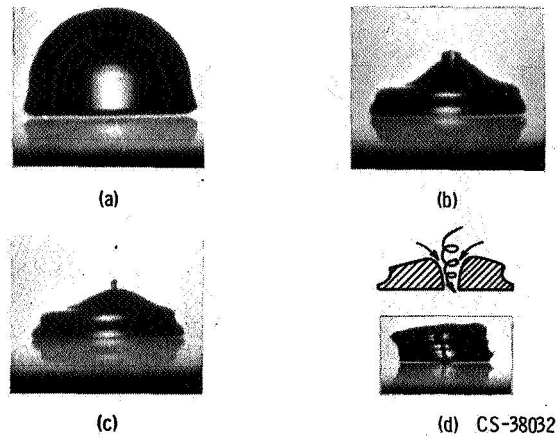
Figure 2-35. - Vapor bubble collapse mode. (Courtesy A. .T. Ellis, California Inst. of Tech., and T. B. Benjamin, Univ. of Cambridge.)

SPECIMEN SURFACE   CS-38033
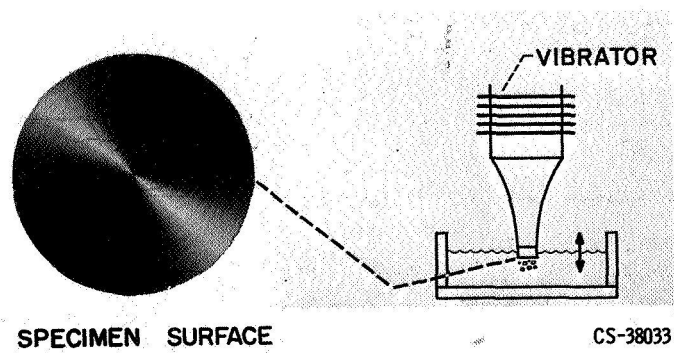
Figure 2-36. - Cavitation damage device.
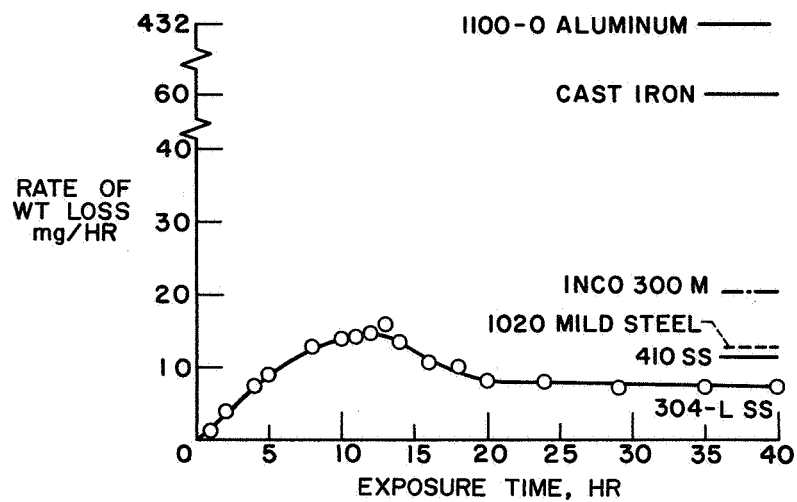
Figure 2-37. - Cavitation damage rate in 80° F water.
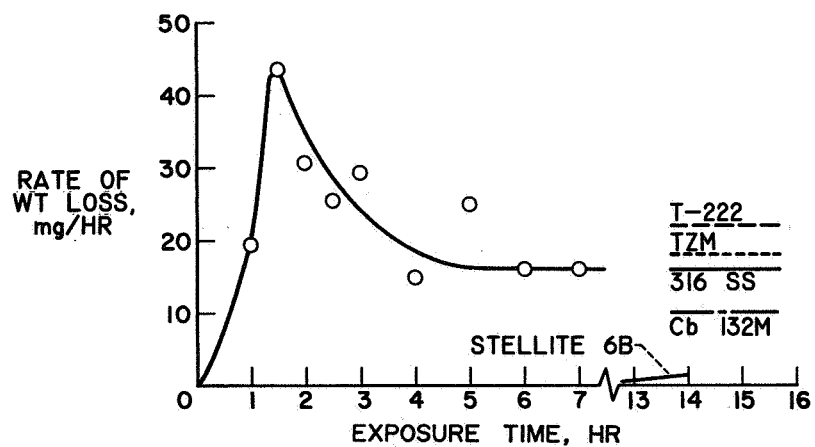
Figure 2-38. - Cavitation damage rate in 400° F liquid sodium.
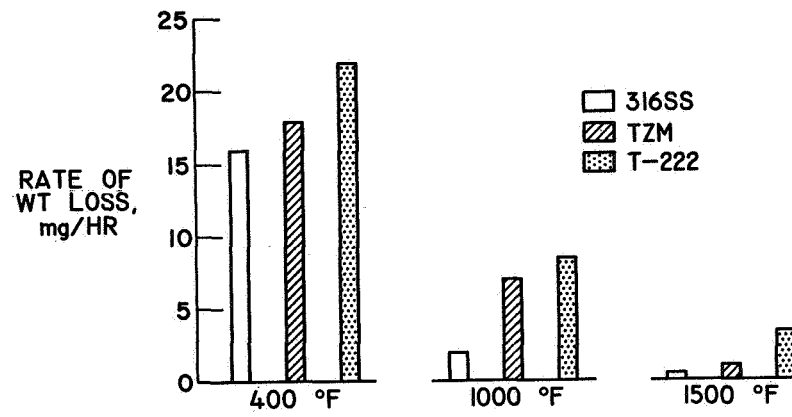
Figure 2-39. - Effect of temperature on cavitation damage rate in liquid sodium.
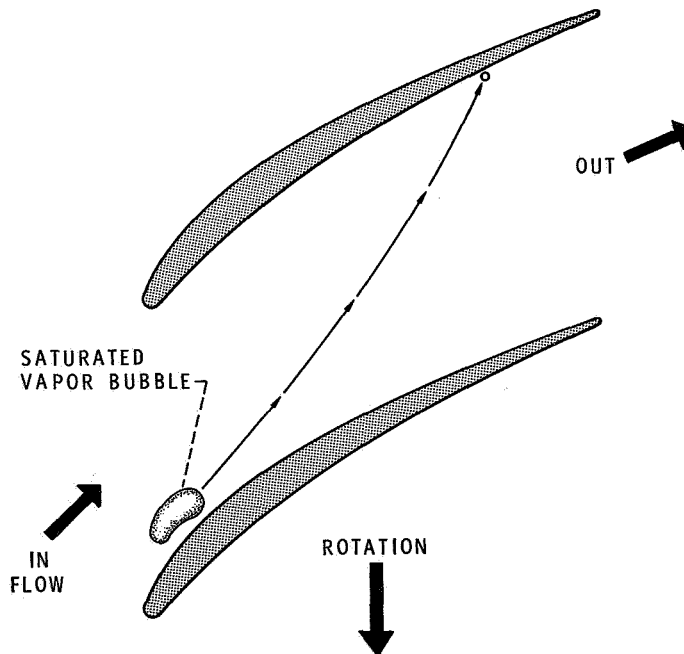
Figure 2-40. - Bubble collapse in pump.
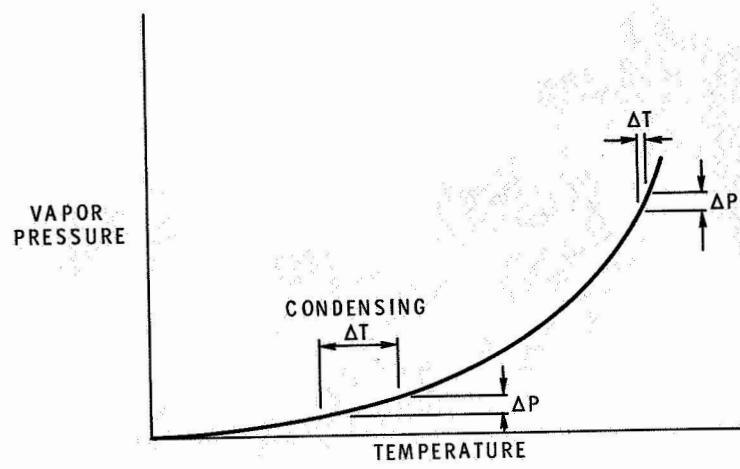
Figure 2-41. - Sodium vapor pressure.
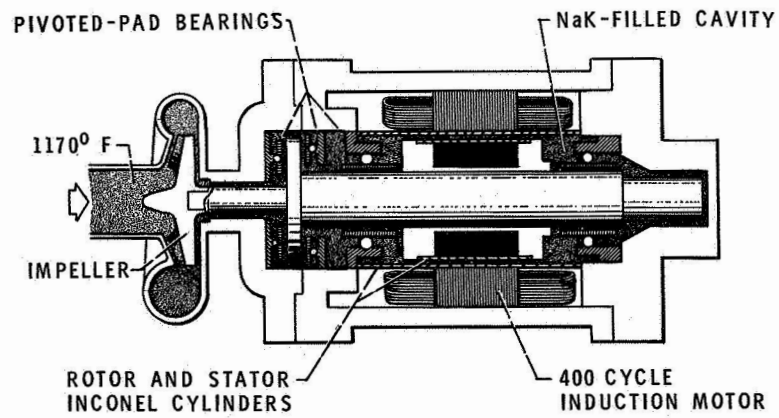
Figure 2-42. - SNAP-8 NaK pump-motor assembly.
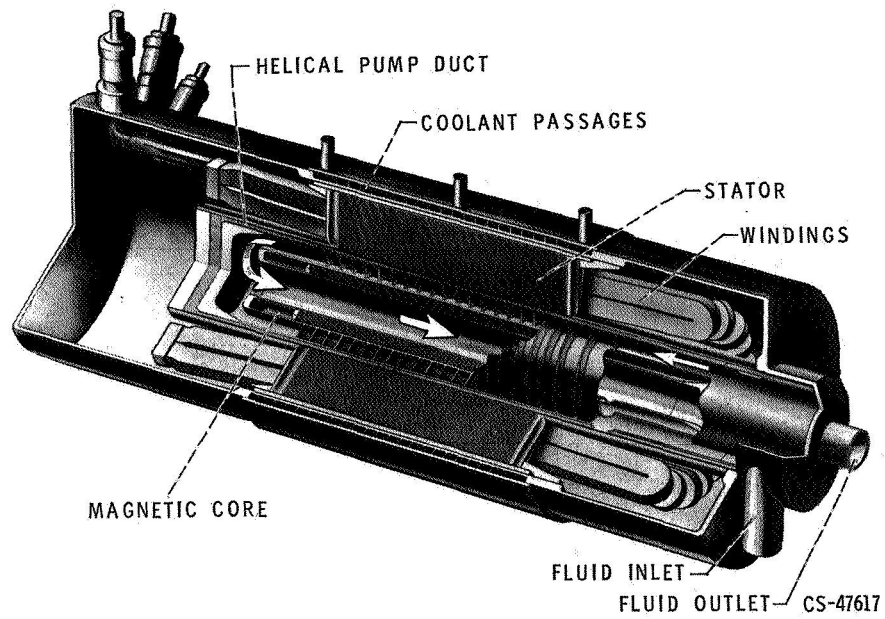
Figure 2-43. - Electromagnetic helical induction pump.
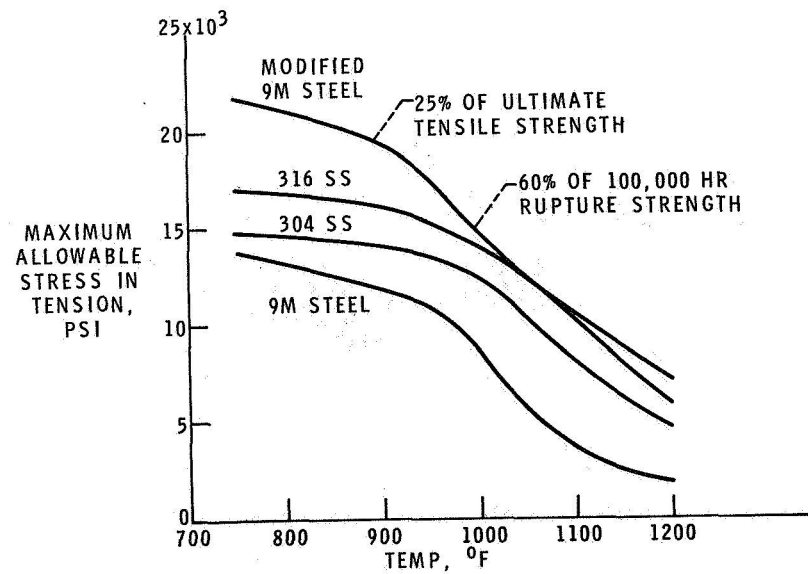
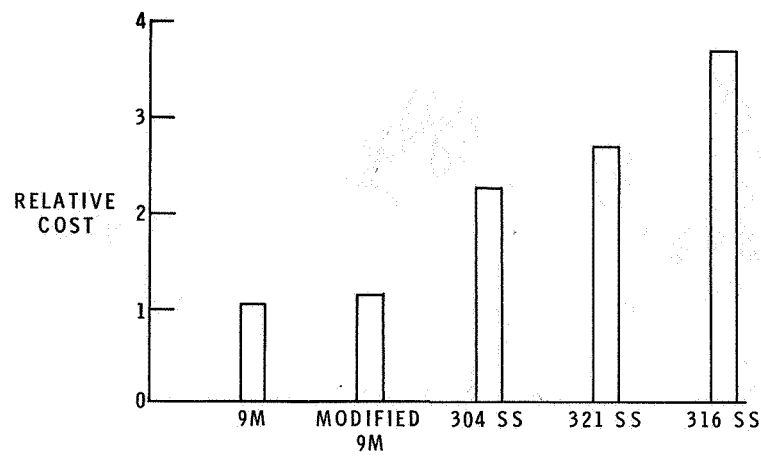Figure 2-44. - Strength of modified 9M steel. (ASME Boiler and Pressure Vessel Code.)

84

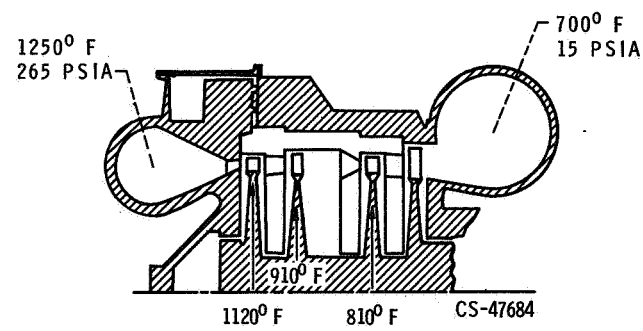Figure 2-45. – Relative cost of tubing. Tube, 2-inch outside diameter by 0.250-inch wall.
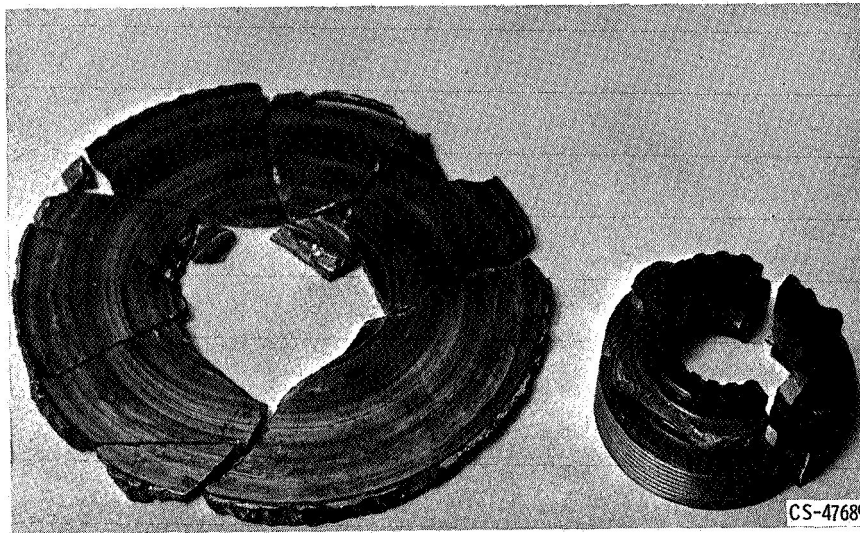

Figure 2-46. – SNAP-8 turbine.
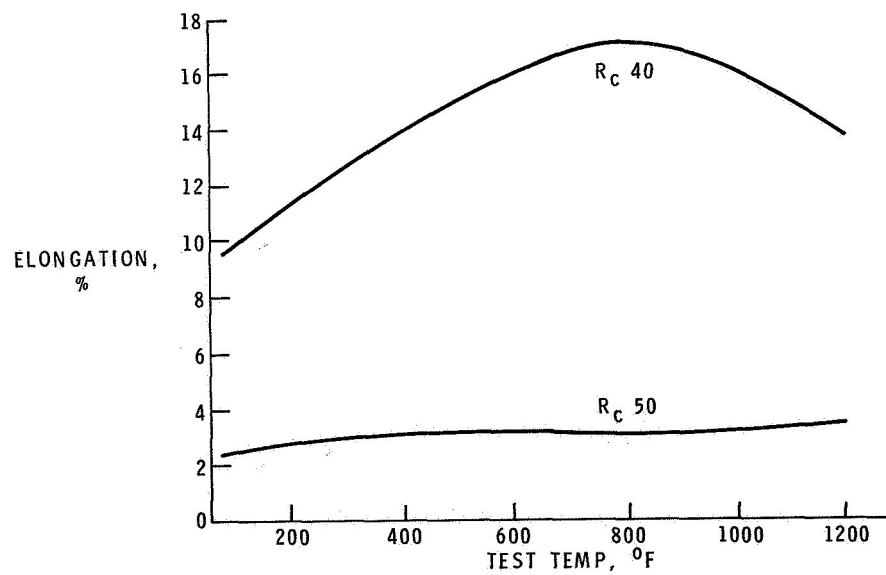
Figure 2-47. – First-stage turbine wheel.

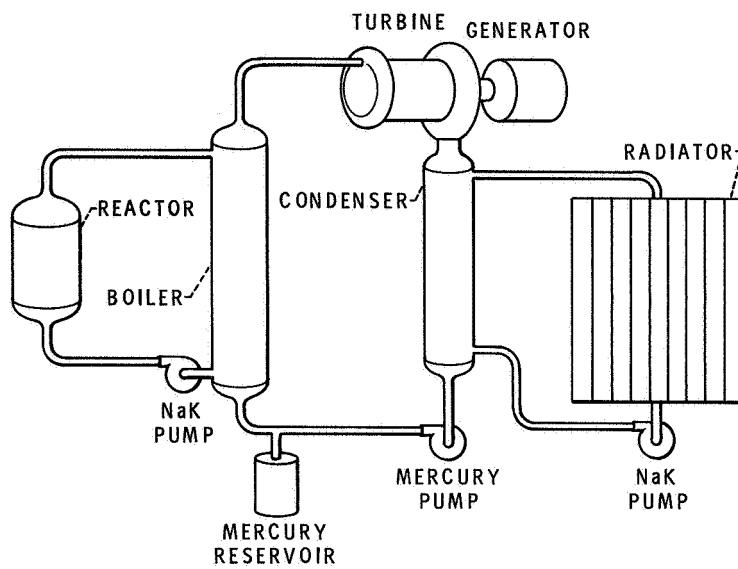Figure 2-48. – Effect of test temperature on ductility of Stellite 6B.

Figure 2-49. - Space nuclear powerplant (SNAP-8).

INPUT INFORMATION:
1. COMPONENT EQUATIONS
2. COMPUTING LOGIC
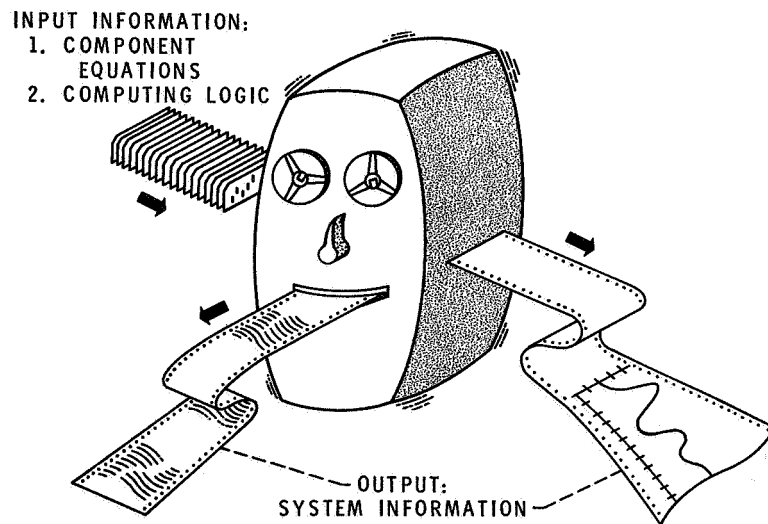
OUTPUT:
SYSTEM INFORMATION
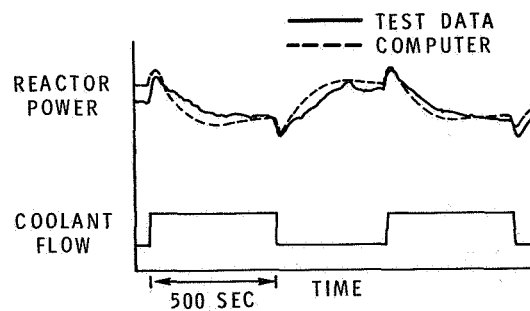
Figure 2-50. - Computer simulation.

Figure 2-51. - Comparison of reactor simulation with test results.
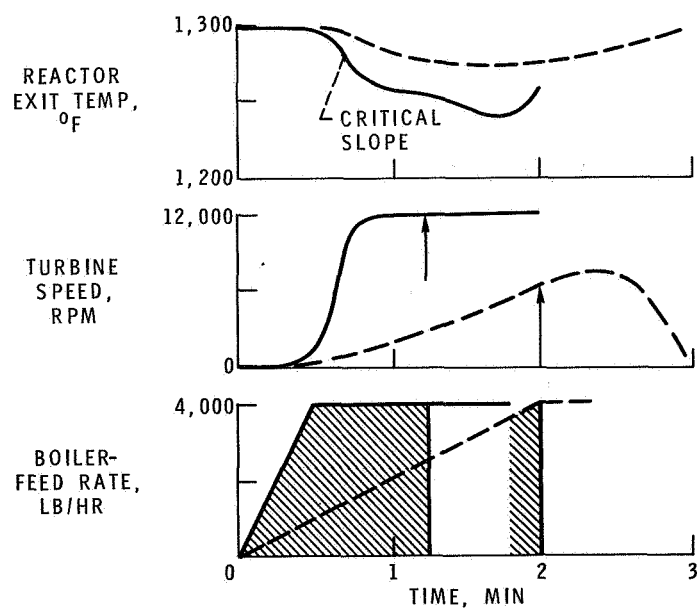

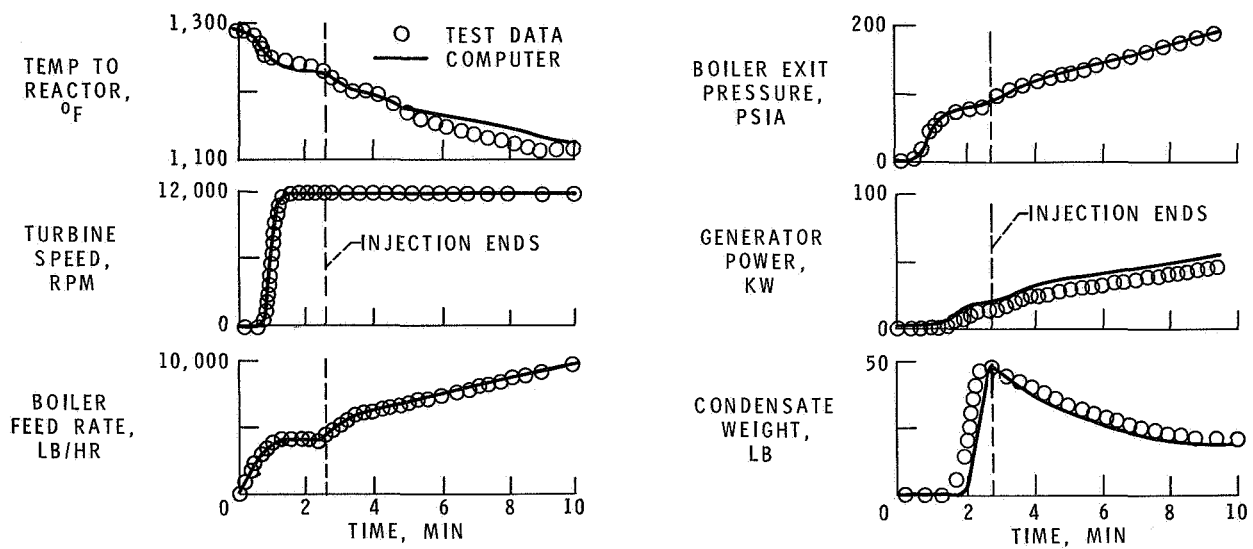Figure 2-52. - Typical startup problem.

88

Figure 2-53. – Comparison of test and computer results.

3. BRAYTON CYCLE SYSTEMS

Warner L. Stewart, William A. Benser, Arthur J. Glassman,
Donald C. Guentert, and Robert O. Hickel

This discussion is concerned with the Brayton or "gas turbine" powerplant, which does not currently represent a major contribution to the total world power output but is starting to find use in certain areas of applications and in the future could become a major power source. This type of engine has been developed in the last 30 years to a high degree of sophistication through its use in the aviation industry, and more recently it is being used for a myriad of applications covering a wide range of power levels.

The use of the "airbreathing" gas turbine in the utility industry began several years ago when such units were put on the line in a "peaking" capacity. Their features of low first cost and low maintenance made them ideal for this application, where plant efficiency and fuel cost were not dominant factors. Another use involves the combining of the gas turbine with a base-load steam system in order to increase the potential for achieving high cycle efficiency. A third use is that of the gas turbine in a more complicated fashion to increase its cycle performance and apply it as a straight base-load power source.

Still another area where the gas turbine is emerging as a power source is the closed loop configuration, where a gas such as helium is used as the working fluid. Such systems are in operation in Europe using a coal-fired heat source and are currently in the initial phases of being mated to a reactor heat source.

It is the intention of this discussion to review the principles of the gas turbine engine, with particular emphasis on the performance improvements made in the system through use of the advanced technology generated in the propulsion field. Special features of the cycle as applied to airbreathing power systems as well as closed loops, where gases other than air can be used, will be described.

OPEN CYCLES

SIMPLE CYCLE DESCRIPTION AND PERFORMANCE

A schematic representation of a simple open-cycle gas turbine system is shown

in figure 3-1. Air entering the system at atmospheric pressure is compressed, heated by means of combustion of a fuel, expanded through a turbine, and exhausted back to the atmosphere. The power produced by the turbine is used to drive the compressor and the generator. This open cycle is shown thermodynamically in figure 3-2 on a temperature-entropy diagram. The dashed line represents atmospheric pressure. The three steps in the process, compression, heat addition, and expansion back to atmospheric pressure, are indicated. Gas turbine peaking units, in general, use this simple process. Often, the turbine in a peaking system will be divided into two sections, one driving the compressor and one driving the generator.

Two major factors affecting the performance of the gas turbine system are compressor pressure ratio and turbine inlet temperature. The influence of these factors on open-cycle plant performance is shown in figure 3-3. This figure is based on the assumption of a compressor efficiency of 88 percent and a turbine efficiency of 90 percent. These are polytropic or, as sometimes called, small-stage efficiencies and would correspond to stage efficiency in machines having a very large number of stages. All turbomachinery efficiencies subsequently referred to in this discussion will be polytropic efficiencies. Plant cycle efficiency is plotted against pressure ratio for turbine inlet temperatures of 1500°, 2000°, and 2500° F. Plant cycle efficiency is defined as the net plant power output divided by the heat added by fuel combustion. Plant efficiency can also be expressed as a net plant heat rate. As a point of reference, a plant cycle efficiency of 40 percent corresponds to a heat rate of 8530 Btu per kilowatt-hour. This figure shows, first of all, the significant improvements in efficiency that can be achieved by increasing turbine inlet temperature. Maximum cycle efficiencies are seen to be about 31 percent at 1500° F, 39 percent at 2000° F, and 44 percent at 2500° F. Current peaking units of advanced design operate at turbine inlet temperatures of about 1500° F and yield cycle efficiencies of about 30 percent. Another point to note from this figure is the importance of selecting the proper pressure ratio that is required for obtaining maximum cycle efficiency. For the simple open-cycle system considered herein, the optimum pressure ratio is about 15 for a turbine inlet temperature of 1500° F and increases to about 50 at 2500° F.

Another important performance consideration is the required flow rate, as this reflects the sizes required for the components. The influence of turbine inlet temperature on specific flow, which is the flow rate in pounds per second per megawatt of electric power, is shown in figure 3-4. These flows are for optimum pressure ratio. At 1500° F, the required flow rate is about 15 pounds per second per megawatt. At 2500° F, the flow is less than half of that at 1500° F. Figures 3-3 and 3-4 indicate the reasons why there is a great desire for increasing turbine inlet temperature.

Another important factor affecting plant performance is the efficiency of the turbomachinery. This is illustrated in figure 3-5, where plant cycle efficiency is plotted against turbine efficiency for a constant compressor efficiency of 88 percent and a turbine inlet temperature of 2000° F. As turbine efficiency increases from 80 to 90 percent, there is nearly a ten-point increase in cycle efficiency. Thus, a one-point change in turbine efficiency results in about a one-point or about a 3 percent relative change in cycle efficiency. Variations in compressor efficiency have a slightly smaller effect on cycle efficiency.

These two aspects, high turbomachinery efficiency and high turbine inlet temperature, were actually the principal reasons why the gas turbine engine did not enter into the realm of practicality until the late 1930's when aerodynamic and mechanical know-how developed to a point where the gap between performance requirements and achievability was closed. Some of the results of the technology advancements made since that time will now be discussed.

TURBOMACHINERY TECHNOLOGY

Extensive research and development on compressors and turbines for aircraft propulsion have been carried on for the past 30 years. This extensive study has provided a large background of experience and data which form the basis of current design procedures. These procedures permit design of compressors and turbines which produce high levels of performance and require a minimum amount of development.

Efficiency

An example of a compressor based on current aircraft technology is shown in figure 3-6. This is an eight-stage research compressor. Because it is a research unit, it is not of flight weight construction; this is evident from the boiler-plate-type casing and heavy flanges. The aerodynamics, however, are typical of the current state of the art for jet engine compressors. The peak polytropic efficiency of this unit is 90.5 percent. This efficiency was obtained at a pressure ratio of 7.5, which corresponds to an average stage pressure ratio of 1.29.

Weight and operating range are extremely important in aircraft propulsion systems, and for an aircraft engine, this compressor would be operated at a higher speed and pressure ratio condition than discussed and would, therefore, operate at a somewhat lower efficiency.

In addition to aircraft-type compressors, there has been some experience here at Lewis with large compressors which are more representative of industrial units. Figure 3-7 is a picture of one such unit. This is the number one compressor from the 10- by 10-foot supersonic wind tunnel flow system. This unit is 20 feet in diameter. The man working on the blade fairing indicates the size of this machine.

This compressor also has eight stages. The peak efficiency of this machine is 91 percent and the pressure ratio at this operating point is 2.4. This is an average stage pressure ratio of about 1.12, as compared with a value of 1.29 for aircraft-type compressors. This 20-foot-diameter machine was designed with moderate blade loadings and low rotative speed, which results in this low level of stage pressure ratio. The high level of efficiency may be partly due to the large size of the unit and partly due to the conservative design. In general, big compressors are somewhat more efficient than small ones. The efficiency of a compressor of this size, 20 feet in diameter, will probably be 1 percent higher than a similar unit of conventional aircraft engine size, about 3 feet in diameter. The examples discussed indicate that compressor efficiencies on the order of 90 percent or higher are attainable with current state-of-the-art designs.

The turbine situation is parallel to that for the compressor, and the state of the art for turbines is just as advanced. An example turbine of the type encountered in modern aircraft engines is shown in figure 3-8. This is a $2\frac{1}{2}$-foot-diameter research turbine currently being studied at Lewis. The efficiency for this unit is 92 percent, which is slightly higher than the values quoted for compressors. Efficiencies for larger turbines might be slightly higher, perhaps 93 percent. The aforementioned compressor and turbine efficiencies indicate that the values assumed for the cycle analysis are reasonable.

Stage Loading

It is evident that rather high overall pressure ratios will be required for high plant efficiencies. The optimum pressure ratio for a peak cycle temperature of 2500° F is 50. Because of stage matching problems it is impractical to try to achieve this in a single compressor, and more than one compressor in series will be required. The first compressor, which would be the largest in diameter, is assumed to have a design pressure ratio of 5. Conservative compressors, such as the 20-foot-diameter compressor in the 10- by 10-foot wind tunnel, would require about 15 stages for a pressure ratio of 5. This would result in an extremely long unit and could result in mechanical problems as well as high cost of fabrication. The aircraft-type compressor discussed could achieve a pressure ratio of 5 in seven stages.

The levels of efficiency currently attained are very high, so compressor research efforts at Lewis are directed primarily at increasing stage pressure ratio without sacrificing efficiency. The principal factors affecting stage pressure ratio are shown in figure 3-9. Stage pressure ratio is plotted against rotor tip speed with loading as a parameter. This loading parameter is the ratio of work input per stage to a reference work expressed as a function of tip speed squared. The constants J and g are dimensional constants which relate the tip speed squared to units of work. Stage pressure ratio increases as the tip speed is increased at a constant value of loading parameter. Stage pressure ratio also increases as loading parameter is increased at a fixed value of top speed. The 10- by 10-foot wind tunnel compressor previously discussed is represented by the circle. The cross-hatched area represents the general range of present-day jet engine compressors.

There are research projects at Lewis directed toward achieving higher loadings at low tip speeds as well as high tip speeds. As tip speed is increased, the flow velocities relative to the blades increase to values above the sonic level, and shock losses are encountered. For example, at a tip speed of 1400 feet per second the velocity relative to the blade may be as high as 1.4 times the speed of sound. This is a relative Mach number of 1.4. Efficient compressors with relative Mach numbers of 1.1 to 1.2 have been operational for many years. Improved blade shapes have recently been developed which permit efficient operation at relative Mach numbers of 1.4.

Figure 3-10 shows a 20-inch-diameter rotor from the high tip speed program. This type of rotor is referred to as a high speed transonic rotor. It is designed for a tip speed of 1400 feet per second and a pressure ratio of 1.6 and is represented by the triangle on the loading curve in figure 3-9. As can be seen, the blades of this rotor are very thin and have very little curvature at the tip. The band at the midspan is for the purpose of damping blade vibrations.

The performance of one of these high speed transonic rotors is shown in figure 3-11. This is a typical compressor performance map and is a plot of pressure ratio against weight flow expressed as percent of design flow. The curves through the data points represent performance along lines of constant percent of design rotational speed. The heavy line is the stall limit. Operation to the left of this limit results in severe flow instabilities and deterioration in efficiency and pressure ratio. The dashed lines are contours of constant efficiency. At design flow, this rotor produced a pressure ratio of about 1.7 with an efficiency between 90 and 91 percent.

These data are for the rotor only. If a stator were to be added to make a complete stage, the efficiency would be decreased about $1\frac{1}{2}$ or 2 percentage points, but the effect on pressure ratio would be moderate. Tip speeds of 1400 feet per second

and greater are within current mechanical technology and are being used in fan stages of fan-jet engines and in the latter stages of high expansion ratio steam turbines. A multistage compressor utilizing stages of this type could achieve a pressure ratio of 5 in four stages. Current aircraft-type compressors employ about seven stages to achieve this pressure ratio. For open-cycle power generation, such stages would probably be designed for a somewhat lower speed in order to operate within the region of maximum efficiency. Under these conditions, an additional stage might be required.

To summarize this discussion, the techniques for design of the compressor and turbine components with high efficiency are in hand. Current research is directed to provide higher compressor stage pressure ratios at no sacrifice in efficiency.

Although, in general, the incentive to reduce the number of turbine stages has traditionally not been correspondingly great because of the relatively small number of stages involved, such is not the case now with high bypass ratio fan engines and would also not be the case for the power systems to be discussed. Therefore, there is other research, paralleling that of the compressor, being done to reduce the number of turbine stages while maintaining high efficiency. However, the major problem, by far, that has always confronted the turbine has been that of high inlet temperatures, and this will now be discussed.

HIGH TEMPERATURE TECHNOLOGY

The incentive to increase the turbine inlet temperature of aircraft gas turbine engines has existed for the same general reasons that were mentioned for the simple open-cycle gas turbine engine for electric power generation. Improvement in the overall performance of aircraft gas turbine engines results when higher turbine inlet temperatures are employed; as a consequence, in the development and application of gas turbine powerplants to airplanes, there has been a steady increase in turbine inlet temperature with time. An example of the increase in turbine inlet temperature for aircraft engines for the past 10 years is shown in figure 3-12. Turbine inlet temperature is plotted against time for both commercial and military engines. The band of temperatures represented by the double crosshatching indicates the range of cruise and takeoff turbine inlet temperatures for commercial engines. The double crosshatched band plus the single crosshatched band represents the range of cruise and takeoff turbine inlet temperatures for military engines. It can be seen that the military operate their engines at maximum temperatures that are about 100° F higher than that for commercial aircraft. This is done by the military to achieve higher engine performance during takeoff and certain maneuvers;

such high temperature operation, however, frequently results in reduced military engine life relative to that of a commercial engine. In this 10-year period, the turbine inlet temperature increased about 350° F for an average increase per year of about 35° F.

Materials

Part of the increase in turbine inlet temperature, but not all, has been permitted by improved turbine blade materials. An indication of the improvement in the elevated temperature capabilities of turbine blade materials in the past 10 years is shown in figure 3-13. In this figure, the 1000-hour stress to rupture strength has been plotted against metal temperature. It should be realized that for peaking and base powerplant operation of gas turbine engines, turbine blade life well in excess of 1000 hours will be required. As a consequence, actual blade design will be based on a criterion other than the 1000-hour stress-rupture properties of a material. It is common practice, however, to compare high temperature turbine blade materials on the basis of their 100- or 1000-hour stress-rupture properties. The stress-rupture properties of the materials shown in figure 3-13 are being used for comparison purposes only and are not intended for design use. All the materials represented in this figure are nickel-base alloys. Ten years ago, in 1958, one of the best turbine blade alloys was Udimet 600, represented by the lower curve. One of the best turbine blade alloys today is IN-100, represented by the upper curve. In the stress range of about 25 000 psi, which is typical for aircraft gas turbine blades, the 1958 material permitted a metal temperature of about 1600° F. For the same stress condition, the 1968 material permits a metal temperature of about 1700° F. From a metallurgical standpoint it becomes increasingly difficult to achieve ever-increasing high-temperature strength in metal alloys, particularly as the desired operating temperature approaches the melting point of the alloy. There is evidence, however, that further improvement in the high-temperature performance of nickel-base alloys can be achieved as evidenced in some initial results from an experimental alloy being developed and investigated by the Lewis Research Center. This material, known as NASA TRW 6A Alloy, is represented by a single data point. For a stress level of 15 000 psi, this experimental alloy has an allowable metal temperature of 1870° F, which is an improvement of about 80° F over that of the IN-100 material.

Figure 3-13 shows that, even for one of the best materials available today, the metal temperatures associated with turbine inlet temperatures of 2000° F or higher cannot be tolerated if reasonably long turbine blade life is desired. As a result,

the engine designer must resort to cooling of the turbine component so that reduced metal temperatures commensurate with the blade stress level and the desired blade life can be achieved.

Before getting into the details of turbine cooling, the effect of temperature on material life should be considered. Figure 3-14 shows the stress to rupture strength of the nickel-base alloy IN-100 for a range of material temperatures. Curves for 1000-, 10 000-, and 100 000-hour life are shown. The 1000-hour-life curve is based on experimental data, while the 10 000- and 100 000-hour curves are extrapolated from short duration test results.

In order to examine the effect of metal temperature on material life, assume a blade stress of 25 000 psi; if the metal temperature is 1700° F, a stress-rupture-type failure could be expected after about 1000 hours. If the metal temperature could be reduced about 270° F from about 1700° to 1430° F, the stress to rupture life would be increased by a factor of 100 to a 100 000-hour life.

Based on the curves shown, it is indicated that to achieve a blade life significantly greater than 100 000 hours, perhaps 175 000 hours, which is equivalent to about 20 years of operation, the blade metal temperature should be of the order of 1400° F for blade stresses on the order of 20 000 psi. For lower levels of stress, the metal temperatures could be somewhat higher.

In general, when high turbine inlet temperatures are desired, the engine designer is faced with the problem of employing sufficient turbine cooling to achieve blade metal temperatures that are capable of long operating life. The precise blade metal temperature requirements depend on the actual life desired and the turbine blade stress levels associated with a given engine design.

Turbine Cooling

Some of our latest aircraft engines for military aircraft already employ turbine cooling. The next generation of American commercial airplanes now in the development stage, such as the airbus and supersonic transport, will also use engines incorporating turbine cooling.

Air cooling. - Turbine cooling can be accomplished with coolants such as air, water, or liquid metals. To date, all production-type aircraft engines that are cooled use air as the cooling medium. An example of how an aircraft engine turbine is cooled with air can be seen in figure 3-15. Shown is a cross section of an aircraft engine with air flowing through the engine from left to right through the compressor, the burner or combustor, the turbine, and finally the exhaust duct. In this example, air for cooling the turbine is bled from the secondary air flowing

around the combustor. The stator vanes are cooled with air taken from the outer annulus, while the rotor cooling air is taken from the inner annulus. The details of the cooling air flow within the stator vanes and the rotor blades can be seen in the enlarged section. Here, stator cooling air is introduced at the base of the vanes, flows radially inward through small passages within the vanes, and is discharged at the ends of the vanes where it mixes with the combustion gas. The rotor cooling air is first ducted over the rotor disk before entering the rotor blade bases. It then flows radially outward through cooling passages within the blades and is discharged at the blade tips where it mixes with the combustion gas. In applying air cooling to an engine, care must be taken to make efficient use of the cooling air. Any air that is removed from the main combustion gas system and is not available to do work in the turbine penalizes the overall thermodynamic performance of the engine. It is therefore necessary to design cooled turbine vanes and blades that incorporate effective heat exchangers in the airfoil sections so that the cooling air requirements are kept at a reasonable minimum.

An example of an advanced air-cooled turbine blade for an aircraft engine is shown in figure 3-16. The full cross section shown in the center of the figure is discussed first. This is a cross section of a blade in which the cooling air enters a central cavity within the airfoil. The blade tip would be capped so that all the cooling air would flow out of the central cavity in a forward direction, as shown by the arrow. The air in the central cavity would be forced to flow through a series of orifices and cause high-velocity air jets to impinge upon the inside surface of the leading edge. These impingement jets result in high local coolant-side heat-transfer coefficients and provide excellent cooling of the leading edge. After cooling the leading-edge region, the cooling air enters a series of small finned passages which extend chordwise in the midchord region of the airfoil. A cross section of the finning and cooling air passages is shown in figure 3-16 (Section A-A). The cooling air flows through these passages at high velocity and cools the midchord region of the airfoil by forced convection. Near the trailing edge, the cooling-air streams from the finned passages adjacent to the suction and pressure surfaces join and flow through passages in the trailing edge region and is finally ejected from the extreme trailing edge into the gas stream.

When the combustion gas temperatures and pressures are high, the heat flux into the leading edge can cause high temperature rises in the cooling air during the impingement cooling process. In certain instances, the cooling air temperature after impingement may be so high that the air is no longer a suitable heat sink for the convection cooling process required in the midchord region of the airfoil. When this occurs, it may be necessary to remove the heated air from the blade. An example of how this might be done is shown in the lower cross section in figure 3-16, where only

the forward portion of the blade has been shown. The balance of the blade is the same as described previously. In this example, a portion of the cooling air in the central chamber is permitted to enter the chordwise passages in the midchord region of the blade before passing through the impingement orifices. The balance of the cooling air enters the impingement orifices and impingement cools the leading edge as in the previous blade. However, after the impingement process, the air is permitted to flow out into the gas stream through a series of slots or holes in the blade wall. With proper direction and velocity of this coolant, it can be placed on the gas-side surface of the blade so that a thin film of air, lower in temperature than that of the combustion gas, forms an insulating layer between the combustion gases and the blade metal. This is called film cooling and results in effective local cooling of the blade immediately aft of the film cooling slot.

Currently being fabricated at the Lewis Research Center are research types of vanes and blades incorporating the cooling systems shown in figure 3-16. Figure 3-17 illustrates a partly assembled vane incorporating impingement cooling, film cooling, and chordwise fins. The vane is made from several subassemblies (figs. 3-17(a) and (b)) that are brazed and electron-beam welded into a final airfoil assembly as seen in figure 3-17(c). The subassembly in figure 3-17(a) shows the chordwise fins adjacent to the pressure surface of the airfoil as well as the leading edge portion of the vane. The impingement orifices and the film cooling holes on the surface near the leading edge are also visible. The subassembly in figure 3-17(b) shows the finning adjacent to the suction surface of the airfoil. Before welding the two major subassemblies together, a thin sheet metal wall which forms the central cavity and confines the cooling air to the finned passages (see fig. 3-16) must be brazed to the fins. In the assembled view of the airfoil in figure 3-17(c), the film cooling holes on the pressure surface and the cooling air slots in the trailing edge are clearly visible. The performance of this vane will be experimentally evaluated at Lewis in a research-type engine capable of operating at turbine inlet temperatures up to 2500° F.

Air-cooled vanes and blades for either peaking or base-load gas turbine power-plants will have to be efficiently cooled so that long turbine life and minimum cooling penalties are realized. For a landbased power system, water-cooled heat exchangers could be used to reduce the temperature of the cooling air to 100° or 150° F as compared with 800° to 1200° F for aircraft applications. Lower temperature cooling air would permit the use of more simple blade configurations. Figure 3-18 shows a possible air-cooled blade or vane for a stationary gas turbine powerplant. This design is not quite as complex to fabricate as the vane shown previously for an advanced aircraft engine; in fact, it may be possible to cast this blade in one piece, except for the tip cap that would be required. In this design, a portion of the cooling air enter-

ing the blade base flows into a radial chamber near the leading edge; this air then passes through orifices to impingement-cool the leading edge. After the impingement process, the air is ducted rearward to enter the central cavity. The remaining portion of cooling air entering the blade base flows radially outward through the finned passages in the midchord region of the airfoil. Near the blade tip, this air is also ducted into this central chamber and mixes with the air used for impingement cooling. The air in the central chamber then leaves the blade through a series of slots in the trailing edge.

The calculated blade wall temperature distribution for this design is shown in figure 3-19, where the wall temperature is plotted against the percent chord from the leading edge. The vertical dashed line represents the leading edge of the blade. The portion of the curve designated as pressure surface is for the concave side of the blade section, and the portion designated as suction surface is for the convex side of the blade. The two extremes of the curve represent the trailing edge of the blade. The wall temperatures shown were calculated for a turbine inlet temperature of 2200° F and a cooling air temperature of 130° F. The ratio of cooling air flow to gas flow was 0.013 or 1.3 percent of the main flow and is considered a very acceptable value for this use. As shown here, the metal temperatures are about 700° to 800° F below the turbine inlet temperature. The minimum metal temperature is 1375° F and the maximum is 1500° F.

Based on the stress-rupture properties of available high-temperature materials, these blade temperatures should give acceptable blade life for a base power system. It should be realized that material properties other than stress-rupture ones must also be considered when designing turbine vanes or blades. Some of these factors are creep, low cycle fatigue, long term fatigue, material oxidation and sulfidation characteristics, and the change in material properties under long time exposure to elevated temperatures. It is beyond the scope of this discussion to consider each of these factors in detail. Some of them are discussed in the paper by G. Mervin Ault.

Liquid cooling. - It was indicated earlier that liquid-cooled turbines might also be used. To date, liquid cooling has not been used in production aircraft engines because it has not yet been necessary to take advantage of the higher coolant-side heat-transfer coefficients that result from the use of liquids. Liquid cooling schemes for turbines are more complex and difficult to employ than air cooling and probably will not be used until the demands of ever-increasing turbine inlet temperatures make it absolutely necessary.

When a liquid-cooled turbine system is considered, liquid water may intuitively appear to be a suitable coolant. Actually, liquid water results in overcooling of the turbine and causes an excessive amount of heat to be removed from the blades; this in turn results in undesirably large thermodynamic penalties for liquid-water cooling

systems. As a consequence, the use of liquid metal or superheated steam appears to be a more suitable approach to highly effective turbine blade cooling with a minimum of thermodynamic penalties.

An example of a liquid-cooled turbine scheme is shown in figure 3-20. This concept is being developed for a small gas turbine engine by the Continental Aviation and Engineering Company under an Army contract. The system actually employs two coolants, a primary coolant, which is permanently sealed within each individual blade, and a secondary coolant, which removes heat from the primary coolant in a heat exchanger built into the base of each blade. In this system, the primary coolant is a very small quantity of water which is placed in each blade during the fabrication process. The secondary coolant is kerosene-type fuel which is circulated through the heat exchanger built into the base of each blade.

When the engine is operating, the hot combustion gases passing over the blade airfoil section convert the liquid water to superheated steam. The steam is circulated within the blade by natural convection effects caused by the difference in density between the hot steam in the airfoil section and the relatively cool steam in the heat exchanger; the high rotative speed of the turbine rotor results in very high natural convection pumping effects. The fuel in the rotor is also pumped by natural convection effects caused by the combination of high rotative speeds and the difference in density between the fuel entering and leaving the rotor. In this concept, the heat removed from the blades is returned to the cycle when the fuel is burned in the combustor. Therefore, there are no significant thermodynamic losses chargeable to the cycle as a result of the turbine cooling process.

It is evident that high turbine inlet temperatures, in excess of 2000° F, are currently finding their way into advanced gas turbine engines, and high efficiencies are being achieved for the major rotating components. In the future, continued progress will be made in these areas with further improvements in the engine performance. In view of this, it could be expected that this type of engine could in the future have a rather dramatic impact on the utility field; that is, their role in this field could very well be extended from that of peaking service to that of a source of base-load power.

USE OF INTERCOOLING AND REHEATING

Since base-load units would have high plant cycle efficiency as their primary objective, not only would they utilize high temperatures with high efficiency components, but they would also include some additional components to achieve this goal. A system using additional components, an intercooler and a reheater in this case, is illustrated schematically in figure 3-21. Air enters the low pressure compressor

and is partially compressed. The air is then cooled within the intercooler. Since heat is generated during compression and compressor work is proportional to temperature, the use of intercooling serves to reduce the total compression work required for a given pressure ratio. The cooled air is then further compressed in the high pressure compressor and heated in the combustor by the burning of fuel. Partial expansion occurs in the high pressure turbine, which drives the high pressure compressor, and heating again occurs, this time in the reheater. Since turbine work is proportional to temperature, the use of reheating serves to increase the total work obtained for a given expansion. Final expansion to atmospheric pressure then occurs in the low pressure turbine, which drives both the low pressure compressor and the generator.

The flow process is shown thermodynamically on the temperature-entropy diagram in figure 3-22. This is similar to the one shown previously for the simple cycle except that two compression steps with intermediate intercooling are indicated at the bottom, and the two expansion steps with intermediate reheating are indicated at the top.

The improvements in plant efficiency resulting from intercooling and reheating are indicated on figure 3-23, where plant cycle efficiency is plotted against turbine inlet temperature for the simple cycle, a cycle with one intercooling, and a cycle with one intercooling ane one reheating. The values shown in this figure are based on the same turbomachinery efficiencies indicated previously, 88 percent for the compressor and 90 percent for the turbine. At a temperature of 2000° F, as an example, the use of one intercooling alone increases the efficiency from 39 to 43 percent and the addition of one reheating along with the intercooling increases efficiency up to 45 percent. For a plant of fixed power output, this corresponds to about a 10-percent reduction in fuel consumption with intercooling and about 5-percent additional reduction in fuel consumption with the reheating added. At other temperatures, the benefits are about the same magnitude with efficiency reaching about 50 percent at 2500° F. The reductions in fuel cost associated with such improvements in efficiency should more than pay for the additional capital cost of the plant. Additional intercoolings and reheatings can be used to yield further improvements in cycle efficiency. The incremental improvements, however, become smaller and smaller as additional intercool and reheat steps are added. The optimum number of intercoolers and reheaters to be used will depend on a detailed economic analysis for a given plant.

As mentioned previously, the airflow through the system is a prime determinant of the size required for the components. The use of one intercooling and one reheating results in about 40 percent less flow than for the simple cycle. Although the number of components is increased by using intercooling and reheating, the

sizes of the components are reduced as compared with the simple cycle.

In order to realize the benefits associated with the use of intercooling and reheating, the system must operate at increased pressure ratios as compared with the simple cycle. This is indicated in figure 3-24, where plant cycle efficiencies for the simple system and for a system with one intercooling and one reheating are plotted against pressure ratio at a turbine inlet temperature of 2000° F as an example. For the simple cycle, the optimum pressure ratio is 30, and efficiency decreases markedly if the pressure ratio is less than 20 or greater than 40. For the cycle with intercooling and reheating, the optimum pressure ratio is about 120. However, the curve is very flat in the region of maximum efficiency, and it is possible to operate at a pressure ratio of about 75 without a significant decrease in efficiency. This pressure ratio of 75 is still considerably higher than that for the simple cycle. Thus, with intercooling and reheating, nor only will additional heat exchangers be required, but also additional stages will be required for the turbomachinery.

EXAMPLE BASE-LOAD SYSTEM

In order to illustrate what the features of a base-load gas-turbine powerplant might be like, one example plant will be described. Some of the principal requirements selected for this plant are as follows:

Power level, mW_e. 1000
Generator speed, rpm 1800
Peak temperature, °F 2200
Compressor pressure ratio. . . . . . . : 75
Intercooler. . . . . One
Reheater . . . . One
Fuel . . . . Natural gas
Plant cycle efficiency, percent . . . . ~42

Power level was selected at 1000 megawatts, with a single generator operating at 1800 rpm. The reason for this speed being selected will be indicated later. The turbine inlet temperature was selected at 2200° F, with an overall compressor pressure ratio of 75. The plant utilized one intercooler as well as one reheat back up to 2200° F. Natural gas was selected as the fuel. A plant efficiency on the order of 42 percent was estimated. This efficiency is somewhat lower than indicated on figure 3-23. The reduction was made (1) to reflect consideration of work necessary to pump the natural gas to the high required pressures, and (2) to provide some allow-

ance for the thermodynamic penalties involved in cooling the high-temperature section of the engine.

Figure 3-25 shows a schematic of the major turbomachinery and heat exchanger components, with an indication of their size. This plant which uses two rotating spools, will be described by tracing through the airflow path. Approximately 4000 pounds of air per second are pulled into the low pressure compressor which is about 14 feet in diameter and develops a pressure ratio of 5. The flow then goes into the intercooler, which is of the crossflow finned tube type with the cooling water in the tubes. This heat exchanger is only moderate in size being about 26 feet in diameter and 4 feet long exclusive of the inlet and exit headers. The air then goes into the high pressure compressor, which is approximately 7 feet in diameter and develops a pressure ratio of 15. From the compressor, the air goes through the primary combustor and from there into the high pressure turbine. This turbine is split into two segments, with the single reheat located in between. After leaving the high pressure turbine, the flow is ducted into the low pressure turbine, which powers both the low compressor and the generator. This turbine is a multistage double-exit unit with a maximum diameter of about 14 feet. The use of a double-exit turbine and a rotative speed of 1800 rpm were required as a result of the very high volume flow exiting from the turbine. This very high volume flow is due to the high power level selected and the atmospheric exhaust pressure, which is obviously a requirement for an open-cycle plant.

This gives an idea what a high power, high performance base-load powerplant might look like. The system described is intended only to serve as an example. There are many configurations that might be evolved, including perhaps an additional spool with more intercooling and reheating. Also, the use of recuperation (transferring heat from the hot turbine exhaust to the cooler compressor exhaust) has not been examined for the open cycle. Recuperation was examined for the closed-cycle system to be subsequently discussed, and its effects are illustrated in that discussion. Such additions with possibly higher turbine temperature levels offer the possibility of achieving plant cycle efficiencies approaching 50 percent. Evolving such a plant would, however, have to be tempered by the additional complexity and associated plant cost.

FUELS

Before leaving the discussion of open-cycle gas turbine systems, a few comments relative to fuels are in order. Generally, three types of fuel can be considered for gas turbine peaking and base-load systems; these are natural gas, petroleum, and coal.

Natural Gas

Natural gas is a convenient, clean, easy-to-handle fuel for gas turbine power-plants and has been used successfully in peaking gas turbine applications for a number of years. In certain regions of the United States, which are close to natural gas sources, this fuel can be employed economically in either peaking or base-load powerplants. Use of gaseous fuels in a base powerplant having a pressure ratio of 75, such as the one just discussed, would, of course, necessitate pressurizing the gas to a high level so that it could be introduced into the combustor. Suitable methods for pressurizing the gas would have to be evolved. One approach would be to use compressors with intercooling. It is possible that liquefying the gas and then pumping it to high pressure in a cryogenic pump might be the best approach. In any event, methods for pressurizing natural gas to levels of the order of 1200 psi would have to be evolved, and the economics of the pumping systems would have to be considered in evaluating overall powerplant performance.

Combustors for natural gas should present no severe problems. In recent years the possibility of using liquefied natural gas in some aircraft applications has stimulated the research and development of natural gas combustors for advanced aircraft engines. Figure 3-26 shows a combustor that is currently under investigation at the Lewis Research Center. This is called a "swirl" can combustor, and it burns natural gas very efficiently with low pressure loss. The combustor shown is research-type hardware and incorporates a mounting flange which is excessively heavy for flight application. The horizontal tubes are fuel manifolds, and the daisy-shaped pieces are the swirl cans. Additional fuel manifolds are located at the top and bottom of the combustor for local fuel distribution control, and are strictly for research purposes. An enlarged view of one of the "swirl" cans is shown in figure 3-27. Natural gas enters the swirl can from two small orifices located in the manifold passing through the horizontal centerline of the can. The fuel is injected near each side of the swirl can at right angles to the main airflow and in a manner such that the flow is tangential to the inner wall of the swirl can. The fuel thus "swirls" and mixes with the combustion air. Efficient burning is obtained as the mixture moves downstream from the fuel manifold. For an actual engine application, the combustor would be curved into an annular shape rather than the rectangular cross section shown. This combustor is $2\frac{1}{2}$ feet wide and 1 foot high and represents the equivalent of a 90° sector of a combustor for an engine of the size required for the supersonic transport.

Petroleum

The second general category of fuel mentioned previously was petroleum. Generally, petroleum fuels are relatively expensive per unit of heat supplied and are therefore too costly for use in base power systems. For peaking systems, however, the petroleum-type fuels may be practical from the overall economic standpoint.

Coal

Coal has been considered for many years as a fuel for gas turbine engines that might be used in railroad locomotives or for stationary powerplants. Its major drawback, of course, is the problem of ash erosion of the turbine component. In the United States, the Locomotive Development Committee of Bituminous Coal Research, Inc. and the Bureau of Mines have investigated the use of coal in gas turbines quite extensively. Figure 3-28 shows the results of severe ash erosion on turbine blades that was observed in an investigation conducted by Bituminous Coal Research, Inc. In this investigation, the erosion was particularly severe along the blade trailing edge between the blade base and about the midspan region. The erosion is evidenced by the severe curve in the blade trailing edge; the trailing edge was originally a straight radial line. The damage shown in figure 3-28 resulted from about 750 hours of operation in a gas stream that had about 85 percent of the ash removed through the use of centrifugal separators. The Bureau of Mines has shown that, by careful aerodynamic redesign of the turbine and the use of titanium carbide protective devices near the root of the blade leading edge, the erosion problem on blades can be greatly reduced. From tests made on an improved turbine that has been operated by the Bureau of Mines for about 200 hours, it has been estimated that the turbine blade life in the modified turbine will be of the order of 30 000 hours before erosion becomes a degrading factor in turbine performance. Stator blade erosion for this turbine, however, remains a problem with stator life currently estimated at about 5000 hours. At this time it appears that considerable attention must still be given to the ash erosion problem before suitable life can be obtained in base-load coal-fired gas turbines.

An interesting powerplant concept in which coal is the primary fuel and in which both gas and steam powered turbines are used is shown schematically in figure 3-29. On the left side of the figure, coal is shown being heated. The volatiles are driven from the original coal and collected as a gas, which is used to drive a gas turbine shown in the right side of the figure. The nonvolatile portion of the coal is removed as a slurry of solids and liquid, which is called "char." The char is used to reheat

the gas turbine exhaust, which in turn fires a steam powerplant, as shown in the center portion of the figure. With such a system the gas may produce about 20 to 40 percent of the electrical energy while the char would produce about 60 to 80 percent of the electrical energy. Although the system is feasible from a technical standpoint, the overall economics of such a system are unknown at this time and require considerable study.

CLOSED CYCLES

Now the discussion will turn to the other type of gas turbine power system, that is, the closed cycle. This cycle is similar to the steam cycle, except that the working fluid remains a gas throughout the entire loop. Closed-loop gas systems have enjoyed considerable attention within NASA as a strong candidate as a source of power in such applications as space stations or lunar outposts. Also, as indicated earlier, such plants have been in operation in Europe with coal as the heat source and offer excellent prospects as part of a nuclear powerplant.

INERT GAS CYCLE

A closed-loop gas cycle power system is shown schematically in figure 3-30. The corresponding thermodynamic diagram is shown in figure 3-31. The closed cycle, in general, is similar to the open cycle except that the turbine exhaust gas is cooled and returned to the compressor inlet. The closed-cycle system illustrated has an intercooler but no reheater. A reheater was omitted on the basis that if the heater were a gas-cooled reactor, it might not be desirable to go through the reactor shield with two more gas ducts. If the gas heater shown here were only a heat exchanger forming part of a reactor coolant loop, then reheating could reasonably be included. The closed-cycle system includes a recuperator, which, as indicated by the arrow on the thermodynamic diagram (fig. 3-31), serves to transfer heat from the hot turbine exhaust gas to the cooler compressor exhaust gas.

The gas entering the low pressure compressor is partially compressed, intercooled, and then compressed further in the high pressure compressor. The compressor exhaust gas passes through the recuperator, where it is heated by the hot turbine exhaust gas. Final heating to turbine inlet temperature takes place in the gas heater. The hot gas is then expanded through the turbine, cooled in the recuperator, and further cooled back to compressor inlet temperature in the waste heat exchanger.

108

Performance

Plant performance for this system is presented in figure 3-32, where plant cycle efficiency is plotted against pressure ratio for turbine inlet temperatures of 1000°, 1500°, and 2000° F. The working fluid is assumed to be one of the inert gases such as helium or argon, and the assumed turbomachinery efficiencies are again 88 percent for the compressor and 90 percent for the turbine. The recuperator effectiveness assumed for this figure is 0.9. These curves are similar in trend to those discussed previously for the open cycle, with efficiency increasing with increasing temperature and maximizing at some optimum pressure ratio at each temperature. The maximum efficiencies are 25 percent for 1000° F, 39 percent for 1500° F, and 48 percent for 2000° F. One major point to note is the considerably lower values of pressure ratio for maximum efficiency for this closed-cycle system as compared with the previously shown open-cycle system; these pressure ratios are in the range of 2 to 4 for this system. This reduction in pressure ratio is principally due to the effect of recuperation, as will be shown subsequently. There is also an effect of the different working fluid. For given changes in temperature, pressure ratios are lower for monatomic gases such as helium than for diatomic gases such as air.

Pressure Level

The fact that the loop is closed allows additional design freedoms as compared with the open-loop system. There is the freedom to set system pressure level as desired. High pressure is desirable from the standpoint of reducing the sizes of the heat exchange equipment, but selection of a pressure level must be tempered by structural considerations as well as the achievement of satisfactory turbomachinery configurations.

Working Fluid

There is also the freedom to select any working fluid desired. The choice of a working fluid for a closed-cycle system has a major effect on the various components. For this discussion the working fluid is considered to be one of the inert gases, or a mixture of these gases, so as to permit a continuous variation of molecular weight. Figure 3-33 illustrates the effect of fluid molecular weight on the number of stages required for the turbine and the compressor. The left end of the

curve represents helium and the right end represents argon, both of which are available in sufficient quantities for use in large powerplants. The in between values of the molecular weight can be achieved with mixtures of these two gases. There are a relatively large number of stages required for use with helium, the example number shown being 22 for the compressor and 8 for the turbine. These numbers can be reduced significantly by increasing molecular weight, since the number of stages is inversely proportional to molecular weight.

The choice of fluid molecular weight also has a significant effect on the size of the heat-transfer components. This effect is illustrated in figure 3-34. The relative size of the recuperator, which is the largest heat exchanger in the system, is plotted against molecular weight. As molecular weight increases from that of helium to that of argon, the size of the recuperator increases by a factor of about $3\frac{1}{2}$. Since a recuperator for helium, based on an effectiveness of 0.9, would have a volume of about 15 000 cubic feet for a 1000-megawatt powerplant, any increases over this would be most significant in terms of size and cost. Figures 3-33 and 3-34 illustrate two major factors that must be considered when making a selection of working fluid.

Use of Recuperation

As previously indicated, a recuperator was included in the closed-cycle system. The use of recuperation serves to improve cycle efficiency by using some of the heat available in the turbine exhaust gas to heat the compressor discharge gas. In this way, the amount of heat that must be supplied by the heat source is reduced. The improvement in plant performance due to recuperation is shown in figure 3-35, where plant cycle efficiency is plotted against recuperator effectiveness. In discussing plant cycle efficiency, reference should be made to the curve with the arrow pointing to the scale on the left. Significant increases in plant efficiency are seen to result from increasing effectiveness, with these increases becoming more rapid as effectiveness approaches unity. At an effectiveness of 0.5, the curve indicates an efficiency of about 31 percent. At 0.8, the efficiency increases to about 36 percent, while at 1.0 there is an additional nine-point increase to about 45 percent.

Also plotted on figure 3-35 is optimum pressure ratio as a function of effectiveness. This is the curve with the arrow pointing to the scale on the right. Increasing effectiveness also serves to decrease pressure ratio and thus reduce the number of turbomachinery stages. For this system, pressure ratio decreases from 5 to 2 as effectiveness increases from 0.5 to 1. Therefore, from the cycle efficiency and pressure ratio standpoint, the effectiveness should be near 1.0.

Unfortunately, the attainable recuperator effectiveness is limited by the size of the recuperator. Figure 3-36 shows how this size changes with effectiveness. This is a plot of relative recuperator size against effectiveness. The size increases rapidly with increasing effectiveness and approaches infinity as effectiveness approaches 1. As effectiveness increases from 0.8 to 0.9, the size more than doubles. Going from 0.9 to 0.95 again more than doubles the size. As mentioned before, a recuperator designed for an effectiveness of 0.9 for a 1000-megawatt system would have a volume of about 15 000 cubic feet. Because of the rapid increase of recuperator size with effectiveness, recuperator effectiveness must be limited, probably to some value between 0.9 and 0.95.

Pressure Loss

Another important variable associated with both cycle efficiency and heat exchanger size is the pressure drop across the heat exchanger. This effect is illustrated with respect to the recuperator in figure 3-37. This plot of plant cycle efficiency against recuperator pressure loss shows a decrease in efficiency from 40 to 38 percent as recuperator pressure loss increases from 1 to 5 percent. This corresponds to a one-half-point decrease in cycle efficiency for each 1 percent increase in pressure loss. Figure 3-38 shows how the relative size of the recuperator varies with pressure loss. Since the heat transfer increases with increased pressure drop, increased pressure loss will result in a smaller heat exchanger. For the pressure loss range shown in figure 3-38, an increase of 1 percent in pressure loss can result in a 10 to 20 percent reduction in recuperator size. In view of the strong influence of recuperator effectiveness on the system both with regard to performance and hardware, it is obvious that extreme care must be exercised in the design of this component so that high levels of system performance can be obtained with a practical recuperator size.

Example Base-Load System

Now that some of the principal features of the closed-gas cycle have been discussed, it would be appropriate to describe one such example system in much the same way as was done for the open cycle. The following are the principal design requirements and features of one such unit:

Power level, mW$_e$ 1000

Generator speed, rpm 3600

Fluid . . . . Helium

Turbine inlet temperature, ^{o}F 1350

Compressor pressure ratio 2.5

Peak system pressure, psi 2500

Intercooler . . . . One

Recuperator effectiveness 0.925

Plant cycle efficiency, percent . . . . ~37

Consider it to be mated to a reactor, possibly a gas-cooled reactor. A 1000-megawatt system and a rotational speed of 3600 rpm are assumed. Helium was assumed to be the working fluid on the basis of its favorable heat transfer properties, as discussed previously.

A turbine inlet temperature of 1350° F is selected as a compromise between (1) a reasonable plant cycle efficiency, (2) reactor restrictions such as were described in the paper on nuclear reactors, and (3) the desire to use conventional superalloys in the turbine without cooling. A compressor pressure ratio of 2.5 is selected with a peak pressure level of 2500 psi. One stage of intercooling was assumed with no reheating, and the recuperator effectiveness was assumed to be 0.925. With these conditions, a plant cycle efficiency of approximately 37 percent was estimated.

Figure 3-39 shows a possible arrangement for this system. A single-shaft arrangement is indicated, with the generator located at one end and the reactor heat source at the other end. The turbine inlet is located at the reactor end in order to minimize high temperature ducting. The heat exchangers are split into two parts and are symmetrically located on each side of the turbomachinery shaft.

Helium at 4200 pounds per second and 1000 psi is drawn into the low pressure compressor, which is approximately $5\frac{1}{2}$ feet in diameter and develops a pressure ratio of 1.6 with 11 stages. From this compressor, the flow goes into the intercooler and then back into the high pressure compressor, where 11 stages are used to bring the pressure up to the peak value of 2500 psi. From there, the high pressure gas passes through the recuperator, where it is preheated by heat transfer from the turbine exhaust. The recuperator is the largest of the heat exchangers, and consists of two sets of four units in series, each unit being $9\frac{1}{2}$ feet in diameter and 63 feet long. The units would be of the multipass crossflow tube and shell type with the high density compressor exit gas going through the tubes.

From the recuperator, the gas goes into the reactor area where its temperature is raised to the peak value of 1350° F. It then passes through the eight-stage

$7\frac{1}{2}$-foot-diameter turbine, where a total of about 2500 megawatts of power is extracted, with approximately 40 percent of this power representing useful energy to power the generator. After the flow leaves the turbine, it passes through the recuperator and then through the heat rejection cooler where it returns to the compressor inlet. As in the case of the open cycle, this configuration serves only to illustrate how a high power closed-loop helium plant might be configured. Final determination of powerplant requirements and configuration would require considerable in-depth study involving both technical and economic aspects.

As indicated before, the selection of 1350° F turbine inlet temperature represents a compromise between desired cycle performance and restrictions from a reactor and materials standpoint. Boosting the turbine inlet temperature to 1500° F would result in a three-point improvement in plant cycle efficiency but at considerable expense of mechanical integrity. Since this plant assumes the use of a reactor heat source, possibly of the breeder type, the incentive to go to the high turbine inlet temperatures normally considered desirable for gas turbines is not nearly so great as it would be with a fossil-fueled plant.

CARBON DIOXIDE CYCLE

An example of a closed-cycle gas system using helium as the working fluid has just been discussed. Helium was selected as the working fluid because of its good heat-transfer properties and because it is chemically inert. As discussed previously, however, its low molecular weight results in a large number of turbomachinery stages. Another fluid of higher molecular weight that has been receiving considerable attention recently for application to closed-cycle gas systems is super-critical carbon dioxide. This fluid not only has a higher molecular weight, but also offers an advantage of reduced compressor work. This results because the compression process occurs in a region of the temperature-entropy diagram where the supercritical fluid properties are more like a liquid than a gas.

In figure 3-4C the temperature-entropy diagram for a simple form of this system is presented showing the location of the cycle relative to the saturation curve of the carbon dioxide working fluid. This cycle involves the same processes and equipment as the closed-cycle helium system. However, the compression process takes place in a region near the critical point of the carbon dioxide working fluid, which occurs at a temperature of about 88° F and a pressure of about 1070 psi. As in the closed-cycle helium plant, there are adiabatic compression and expansion processes and a recuperation process to transfer heat from the turbine exhaust to the compressor exhaust. Because of the 1070-psi critical pressure, the supercritical

113

carbon dioxide cycle is a high-pressure cycle operating with a compressor inlet pressure between 1500 and 2000 psi and a compressor discharge pressure of the order of 3000 to 3500 psi. By operating near the saturation curve, the compressor work, as shown by the compression line, becomes a much smaller fraction of the turbine work, represented by the expansion line, than in the closed-cycle helium system. As a result, the efficiency of the supercritical carbon dioxide plant is somewhat higher than the 37 percent plant efficiency mentioned for the example closed-cycle helium plant.

The primary advantage of the supercritical carbon dioxide cycle lies in the compactness of the turbomachinery. This is a result of the use of a high molecular weight gas as a working fluid at high pressure. The turbomachinery for the example 1000-megawatt closed-cycle helium plant utilized two 11-stage axial flow compressors and an 8-stage axial flow turbine. For a similar size plant using supercritical carbon dioxide, this multistage axial flow machinery could be replaced by a single-stage centrifugal compressor, or pump, about $2\frac{1}{2}$ feet in diameter and a single-stage radial inflow turbine about $5\frac{1}{2}$ feet in diameter.

The compactness of the turbomachinery for the supercritical carbon dioxide system, however, is accompanied by an increase in the required heat exchanger size. The supercritical carbon dioxide cycle is a highly recuperated cycle, and this coupled with the poorer heat transfer properties of carbon dioxide as compared with helium, result in a recuperator that may be of the order of two to three times the size of that required for the closed-cycle helium plant.

While on the subject of the carbon dioxide cycle, it should be mentioned that there are variations of this cycle that employ condensation. A temperature-entropy diagram for the condensing carbon dioxide cycle is shown in figure 3-41. In these cycles, the turbine expansion is continued to a pressure lower than the critical pressure, and the exhaust gases are cooled to a temperature lower than the critical temperature, so that condensation takes place. Some of these cycles result in higher efficiencies than the supercritical cycle; however, a heat sink is required with a temperature lower than the carbon dioxide critical temperature of 88° F.

Although the carbon dioxide cycle is of interest because of its good cycle efficiency and compact turbomachinery, there are some considerations that arise because of the properties of the working fluid, and these will require investigation. The chemically active nature of carbon dioxide, as compared with a gas such as helium, may present material compatibility problems, particularly at temperatures above 1300° to 1400° F. System dynamic studies will also be required because the rapidly changing properties of the carbon dioxide near the critical point raise a question concerning system stability.

CONCLUDING REMARKS

Some of the major thoughts brought out during the course of this discussion are as follows.

First, with regard to the open-cycle gas turbine, the technical advancements made in such areas as high component efficiencies and high turbine inlet temperatures have in the last three decades brought this type engine to a very high level of performance, and it would be expected that even further gains will be made in the future. As a result, not only will its use as a peaking device continue to expand in the utility industry, but also it could foreseeably become a major contender for base load. Fuel-type restrictions do currently represent an important factor such that potential use of this power source for base load will probably be limited to areas where natural gas is economically suitable.

Secondly, the gas turbine in the closed-loop form does represent an attractive candidate for base load in conjunction with a nuclear reactor. Helium is generally accepted as the desired working gas although others are being considered. It would also appear that moderate turbine inlet temperatures can be utilized with the small sacrifices in plant efficiency offset by the considerable reduction in the reactor and materials problem at the hot end.

In conclusion, although these systems appear technically attractive, the ultimate selection of a system for utility use must be based upon economic considerations. In-depth studies of these systems, therefore, must be made from both technical and economic standpoints in order that their competitive position be more firmly established.
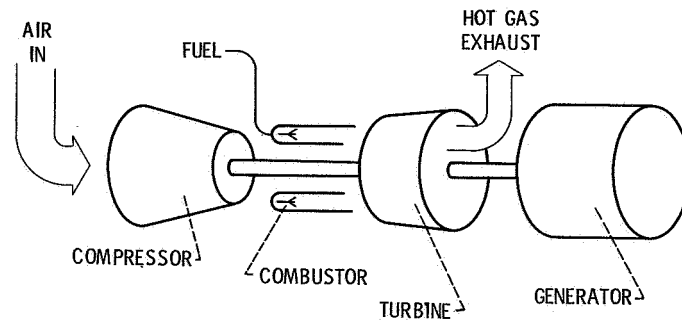
Figure 3-1. - Schematic of simple open-cycle gas turbine system.
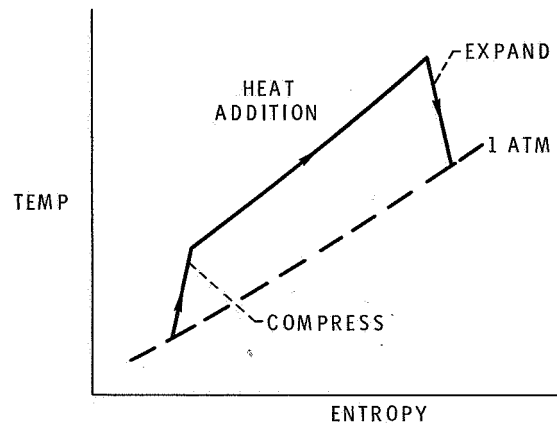
Figure 3-2. - Thermodynamic diagram for simple open-cycle system.
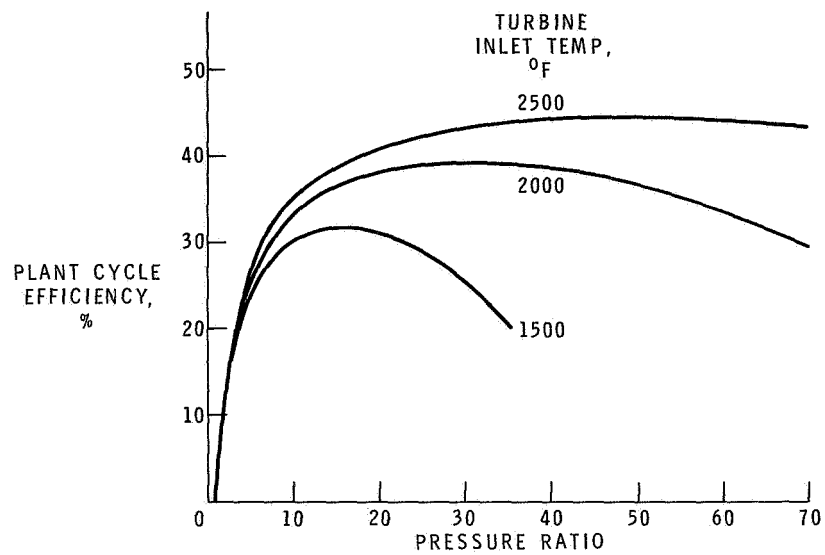
Figure 3-3. - Simple open-cycle plant performance. Compressor polytropic efficiency, 88 percent; turbine polytropic efficiency, 90 percent.
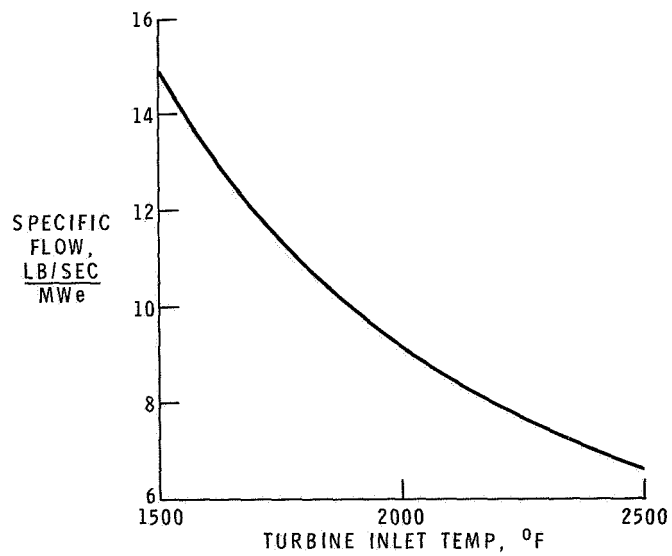
Figure 3-4. - Simple open-cycle airflow at optimum pressure ratio.
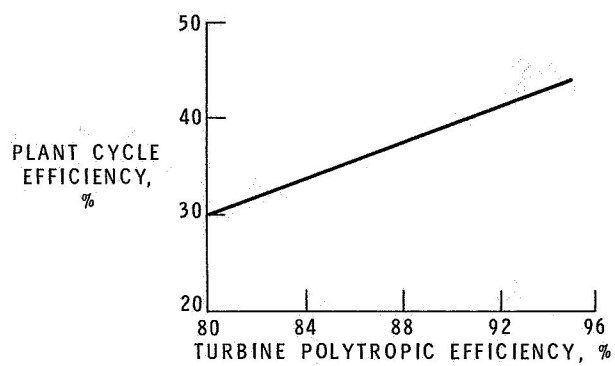
Figure 3-5. - Effect of turbine efficiency on plant cycle efficiency. Turbine inlet temperature, 2000° F; compressor polytropic efficiency, 88 percent.

CS-47561
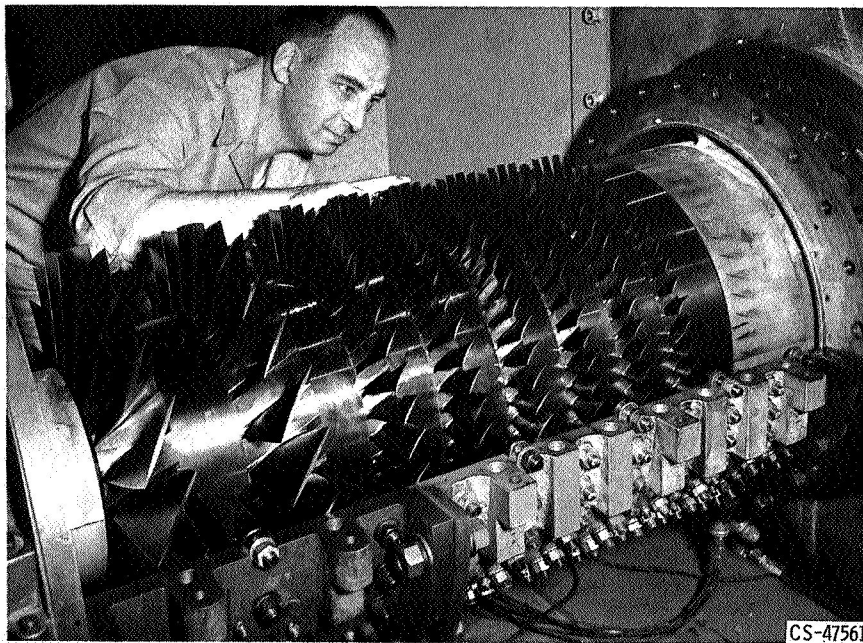
Figure 3-6. - Research compressor. Peak polytropic efficiency, 90.5 percent.
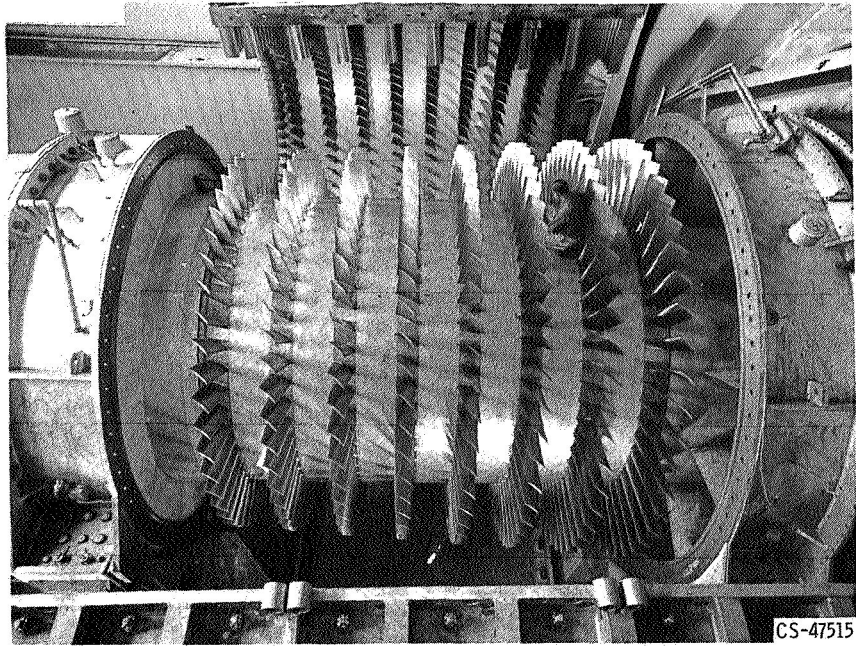
Figure 3-7. - 20-Foot-diameter compressor. Peak efficiency, 91 percent.
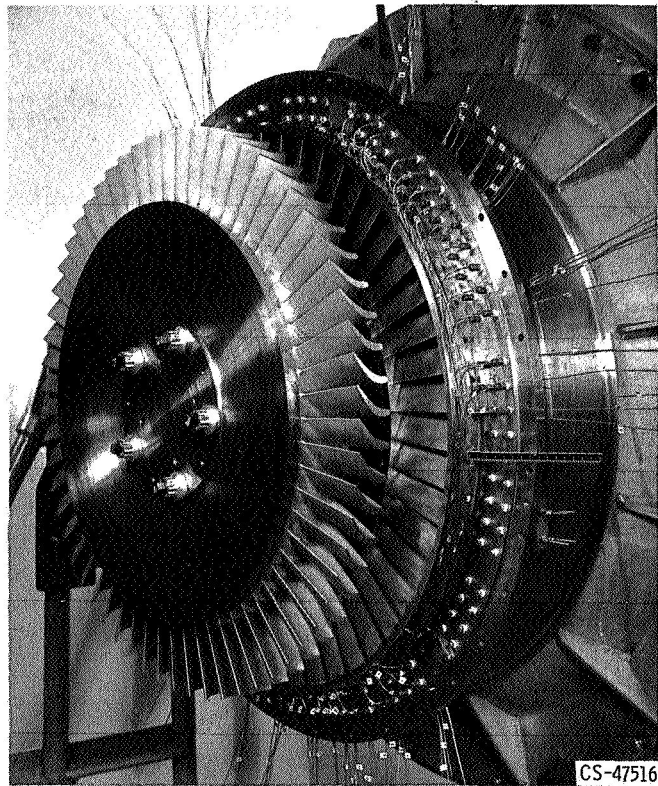
Figure 3-8. - $2\frac{1}{2}$-Foot-diameter research turbine. Efficiency, 92 percent.

120
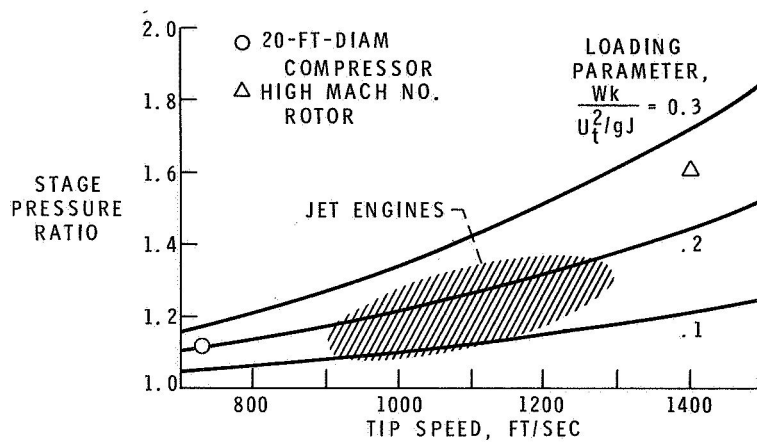
Figure 3-9. - Compressor loading.
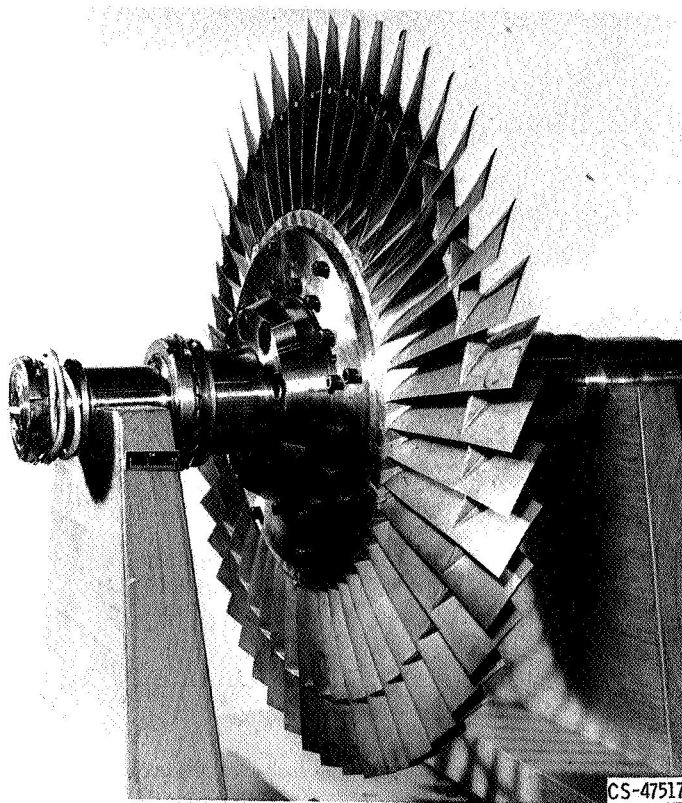
Figure 3-10. - High Mach number compressor rotor.

121
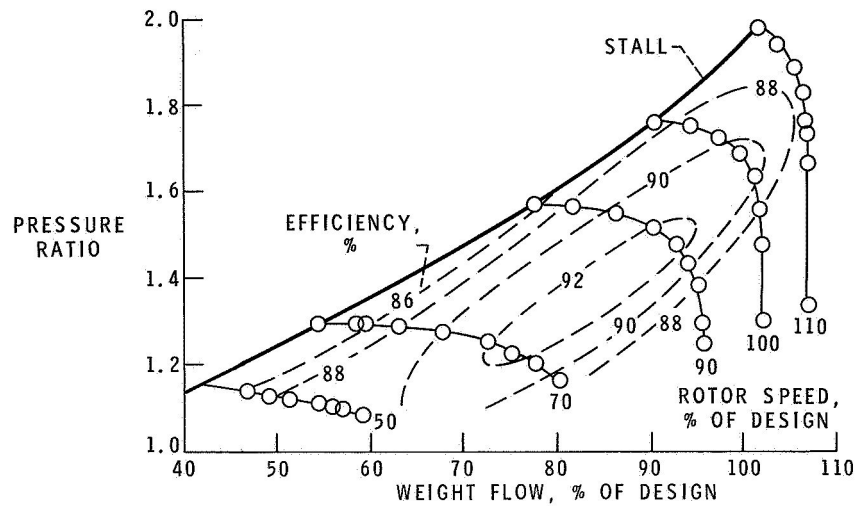
Figure 3-11. – High Mach number rotor performance.
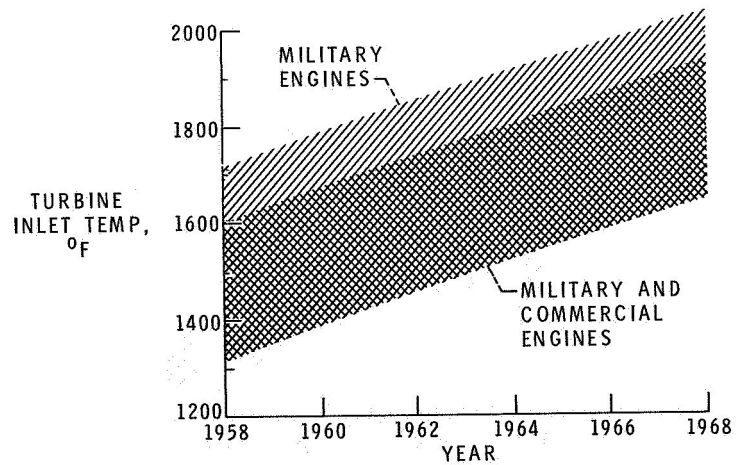
Figure 3-12. – Chronology of aircraft engine temperatures.

122
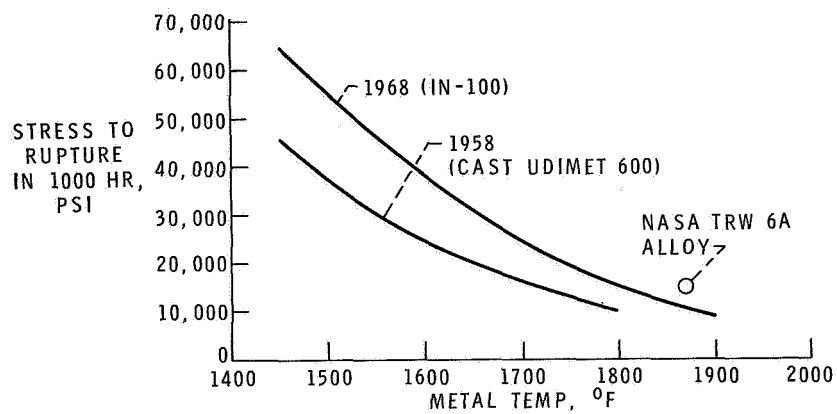
Figure 3-13. – Chronology of material strength.
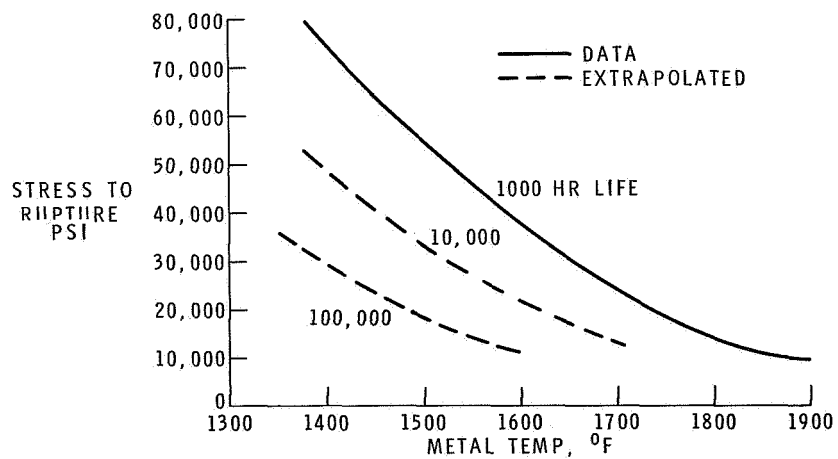
Figure 3-14. – Effect of temperature on life of IN-100.

STATOR COOLING AIR

STATOR VANE

COMBUSTION GAS

ROTOR BLADE

ROTOR COOLING AIR

TURBINE

COMPRESSOR

COMBUSTOR

EXHAUST
DUCT
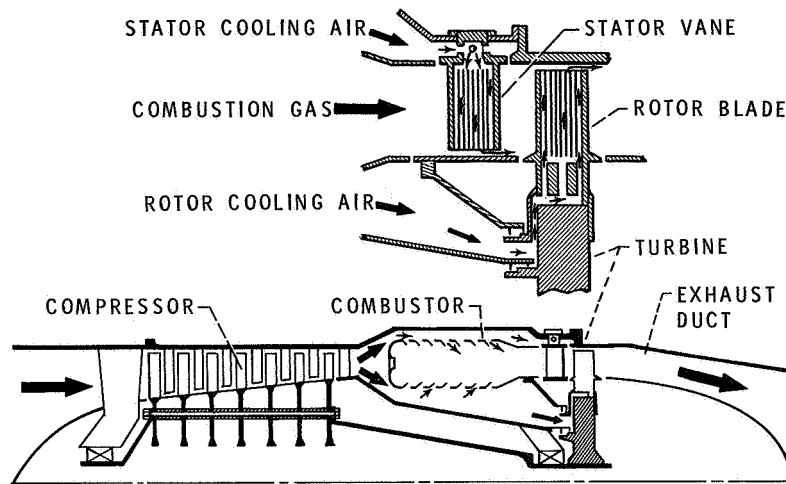
Figure 3-15. - Air-cooled aircraft engine.

SECTION A-A

A

A
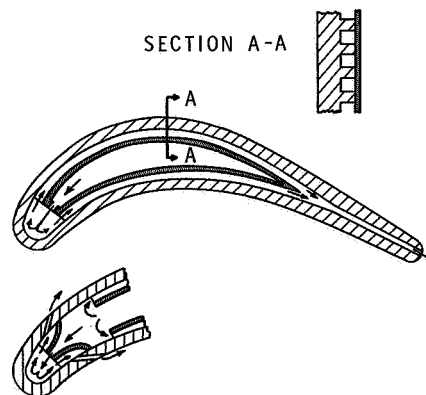
Figure 3-16. - Advanced air-cooled blade.
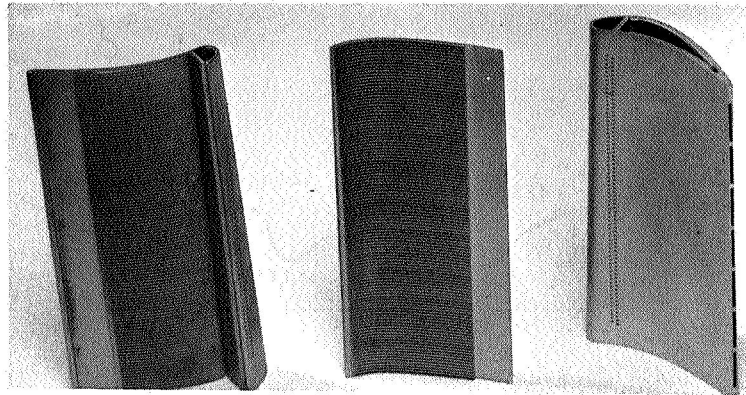
CS-47586

0   1
IN.

(a) Leading edge and pres-   (b) Suction surface.   (c) Assembled airfoil.
    sure surface.

Figure 3-17. - Advanced air-cooled vane components.
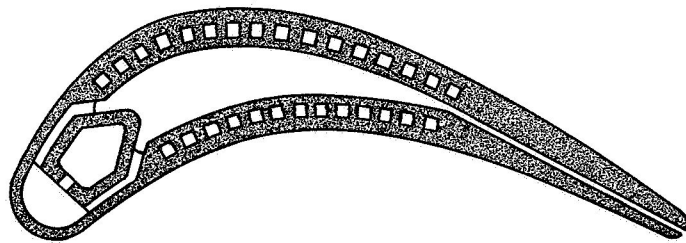
Figure 3-18. - Air-cooled blade for base-power turbine.
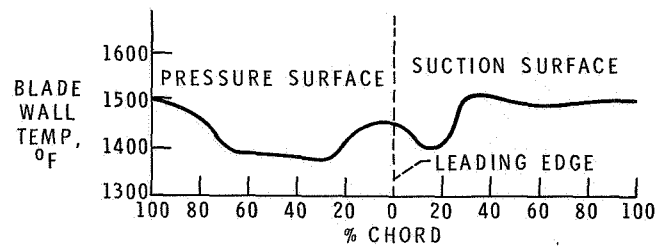
Figure 3-19. - Calculated blade metal temperature distribution. Turbine inlet temperature, 2200° F; cooling air temperature, 130° F; coolant flow/combustion gas flow, 0.013.
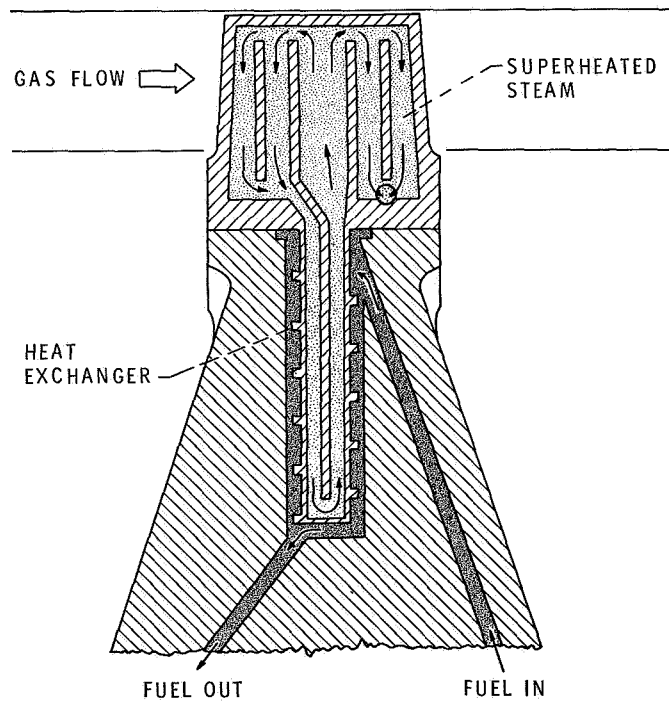
Figure 3-20. - Liquid-cooled turbine.
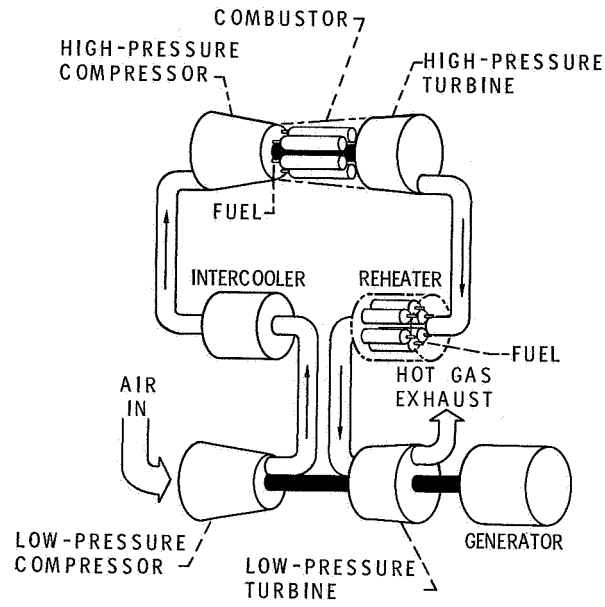
Figure 3-21. - Open-cycle system with intercooling and reheating.
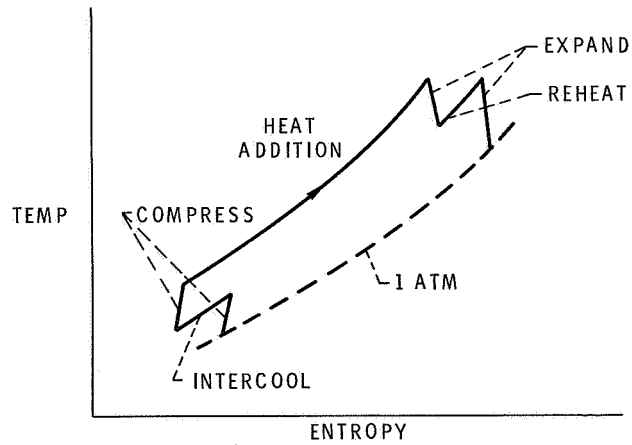
Figure 3-22. - Thermodynamic diagram for open-cycle system with inter-
cooling and reheating.
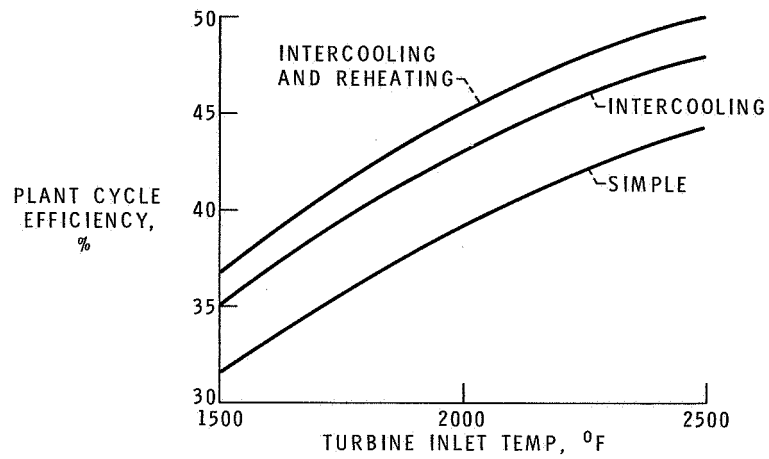
Figure 3-23. - Effect of intercooling and reheating on plant performance at optimum pressure ratio. Compressor polytropic efficiency, 88 percent; turbine polytropic efficiency, 90 percent.
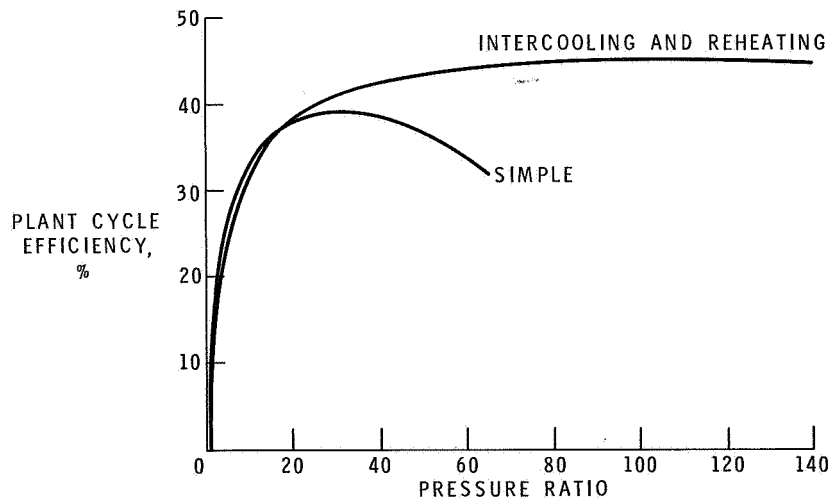
Figure 3-24. - Effect of intercooling and reheating on pressure ratio selection. Turbine inlet temperature, 2000° F.

128
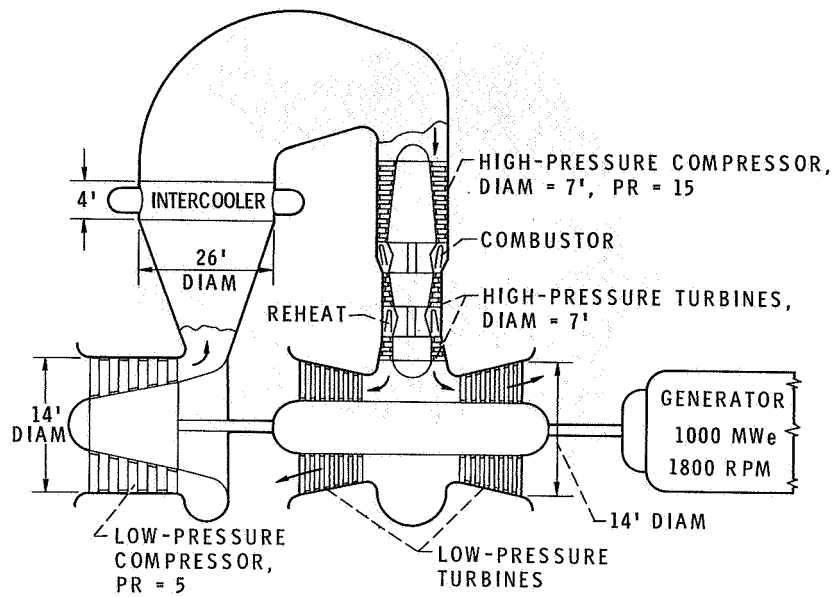
Figure 3-25. - Schematic of base-load open-cycle powerplant.
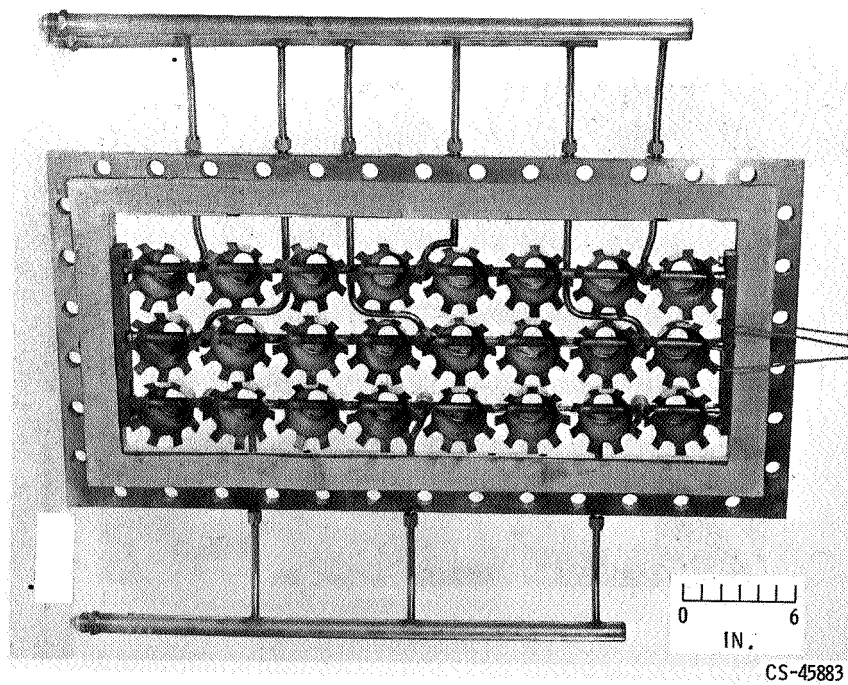
Figure 3-26. - Natural gas combustor.

CS-47585

0 |_____| 1

IN.
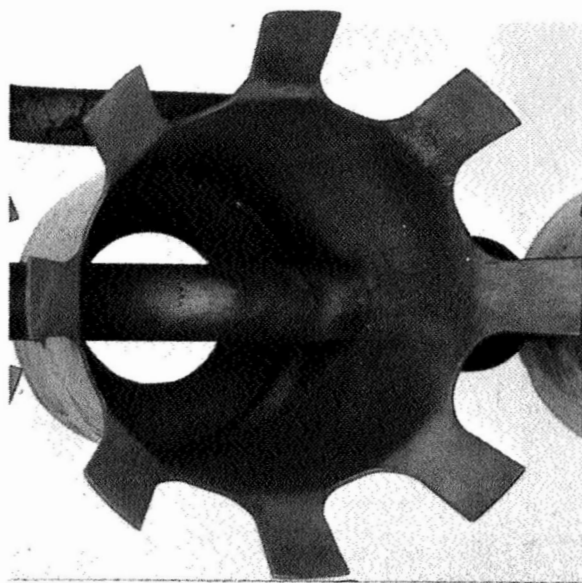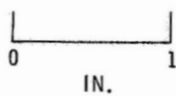
Figure 3-27. – Combustor swirl can.

CS-47514

Figure 3-28. – Turbine eroded by coal ash.
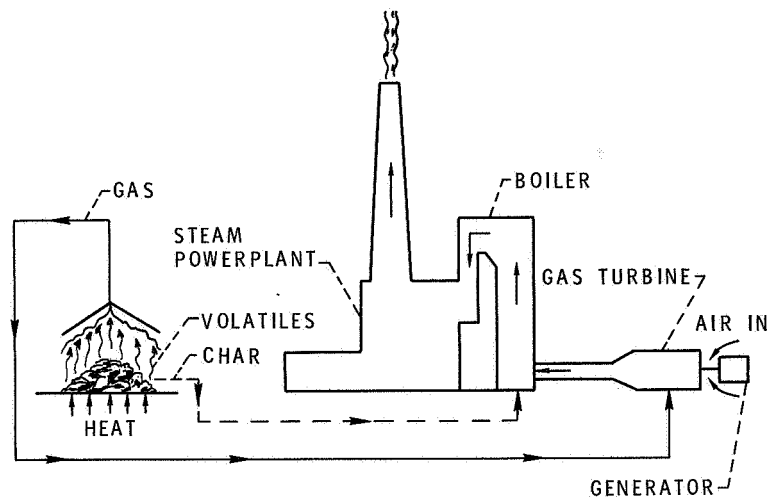
Figure 3-29. - Use of coal in combined cycle. Gas, 20 to 40 percent of energy; char, 60 to 80 percent of energy.
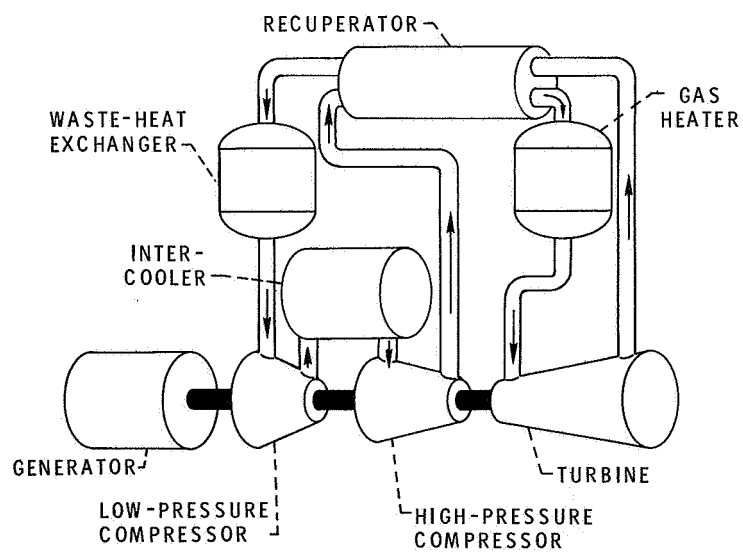
Figure 3-30. - Schematic of closed-cycle system.

131
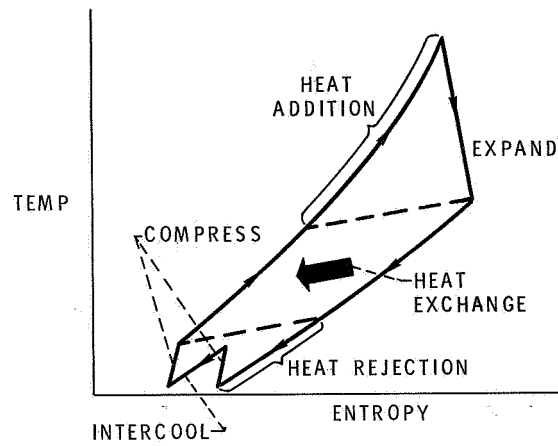
Figure 3-31. - Thermodynamic diagram for closed-cycle system.
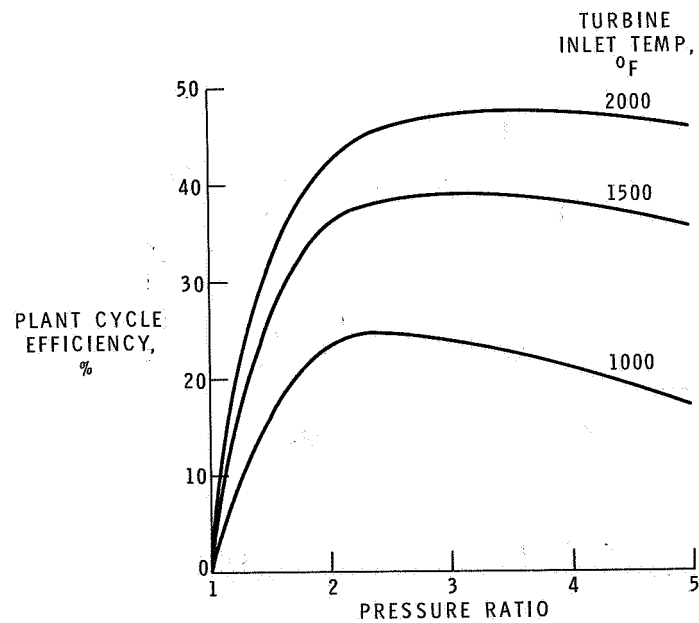
Figure 3-32. - Closed-cycle plant performance. Compressor polytropic efficiency, 88 percent; turbine polytropic efficiency, 90 percent; recuperator effectiveness, 0. 9.
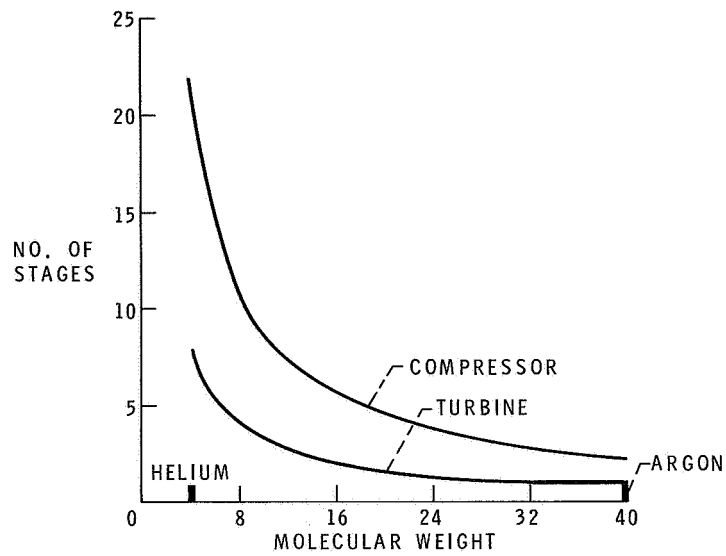
Figure 3-33. - Effect of working fluid on number of turbomachinery stages.
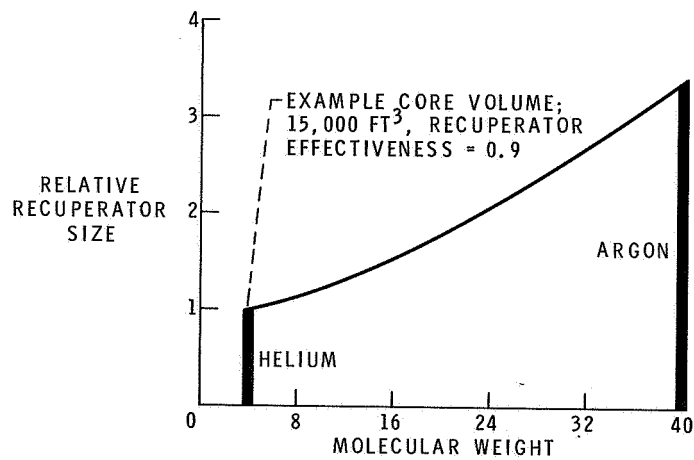
Figure 3-34. - Effect of working fluid on recuperator size.

133
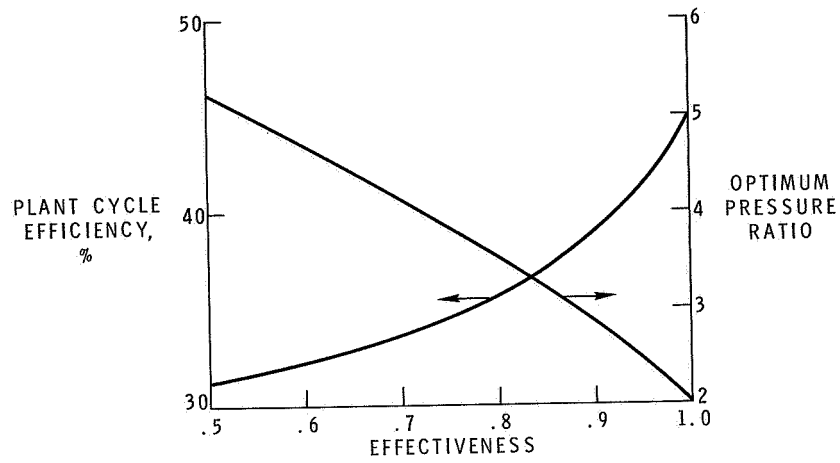
Figure 3-35. - Effect of recuperation on plant performance.
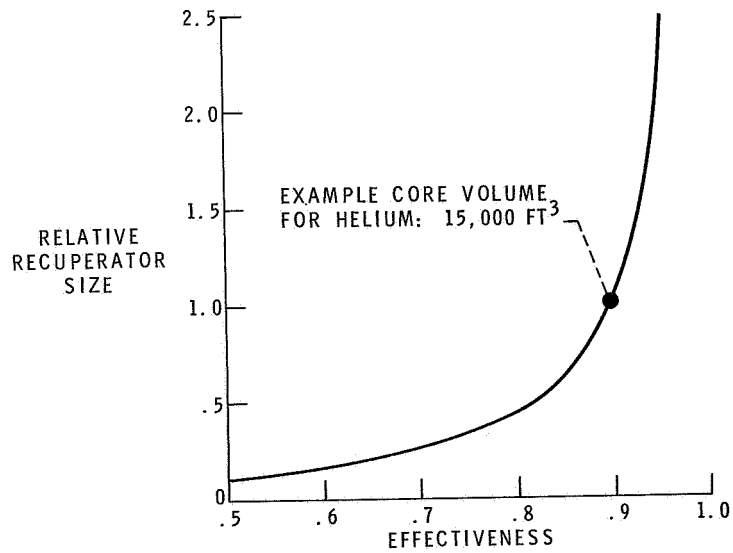
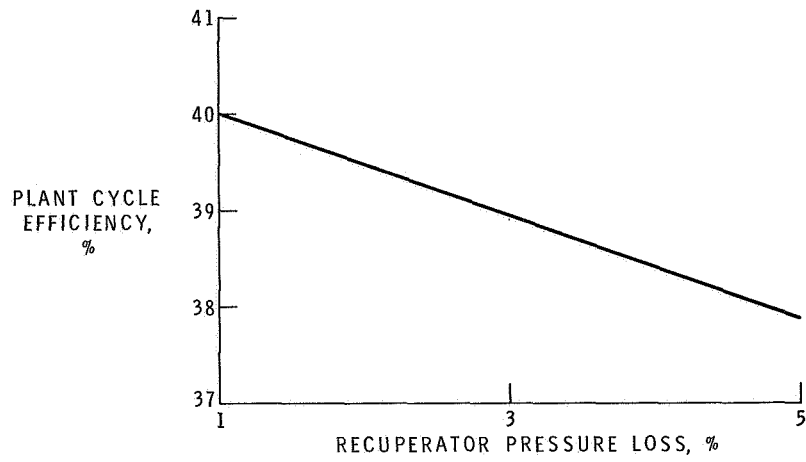Figure 3-36. - Influence of effectiveness on recuperator size.

134

Figure 3-37. - Effect of recuperator pressure loss on plant performance.
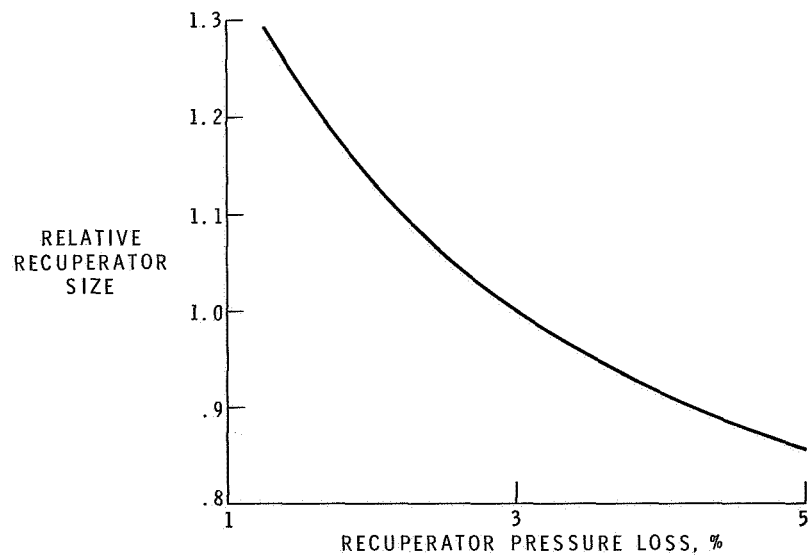

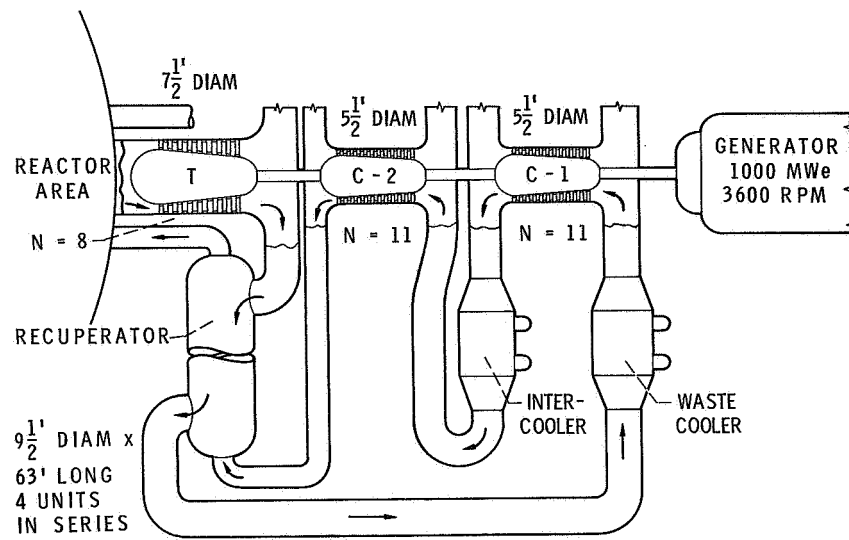Figure 3-38. - Effect of recuperator pressure loss on recuperator size.

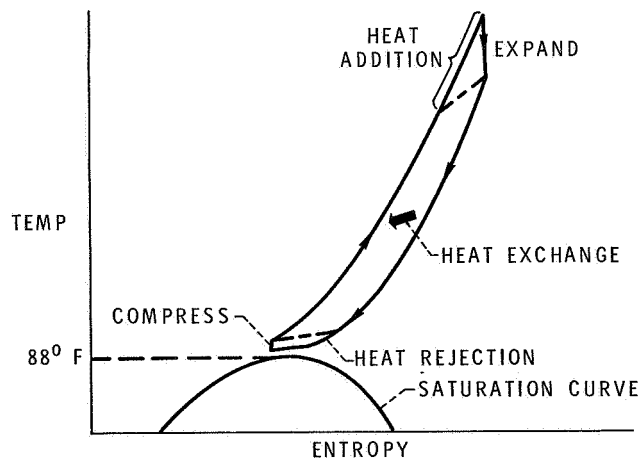Figure 3-39. - Schematic of helium closed-cycle powerplant.

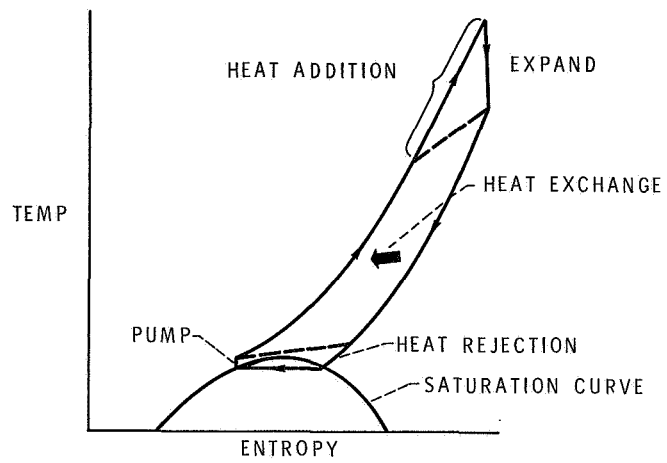Figure 3-40. - Thermodynamic diagram for supercritical carbon dioxide cycle.

Figure 3-41. - Thermodynamic diagram for condensing carbon dioxide cycle.

4. RELIABILITY

Seymour C. Himmel

Both NASA and the electric power industry are involved in the design, building, and operation of large and complex systems. These systems must operate efficiently and reliably. Failure can result in tremendous economic losses.

In the past, the electric power industry has been characterized by the application of modest incremental advances in technology as new plants were built. This relatively slow pace permitted careful and detailed investigation of the effects of the incorporation of these advances. In the process of preparing for this conference, it became evident that the electric power industry is on the threshold of the application of large advances in technology. This is quite similar to the situation in the late 1950's when, in order to undertake the space flight program, NASA had to take a large step in technology.

Such a step can, and in that case did, lead to difficulties. It is well known that in those days the space program was plagued by a lack of reliability in the systems being tried. To illustrate how bad the situation was, consider just the launch vehicles. In 1959, only 57 percent of the attempted launches succeeded. In 1960, only 59 percent met their flight objectives.

This was obviously a very unsatisfactory state of affairs. Upon close examination of the situation, it was found that the complexity of the systems, the new technology that was being used, and the rapid pace at which the systems were being developed all contributed to the poor performance obtained. Moreover, once the hardware was committed to flight, if something malfunctioned, it was not possible to get at it to find out what had happened - let alone to fix it. The electric power industry is fast approaching a similar situation. With some of the new reactors for power generation, one might as well be in space as it is frequently not possible to get at the hardware once a malfunction occurs.

In order to overcome the problems encountered, NASA developed a methodology for improving and maintaining the reliability and quality of the hardware. That the methodology is effective is illustrated by the fact that, in contrast to the less-than-60-percent success level previously noted, last year a 93-percent level was attained for the launching of twice as many vehicles. These vehicles, moreover, were of even larger size and greater complexity than those of 8 years ago.

The purpose of this paper is to acquaint you with this methodology. There are obviously many differences in our fields of endeavor, and all that is done to enhance the reliability of space systems may not be applicable or warranted in the power industry. But, it is believed that many of these techniques should be of value, and their application may permit the power industry to avoid some of the pitfalls encountered in the space program.

There are two basic parts to this methodology. The first is called reliability engineering and the second is called quality assurance. Where one ends and the other begins is a moot point. A somewhat arbitrary definition is used in this paper. What is important is that both are necessary.

In reliability engineering, it is established, by detailed examination and control of design, that a system is inherently reliable and, by test, that it can perform as desired. This process is called "qualifying" the system. In quality assurance, both inspection and testing are used to ensure that the system delivered by the manufacturer is as designed.

All of this sounds like an involved way of saying: "Use good engineering practice." In fact, that is all it is. It has been found, however, that today this is not the norm. Whether this results from the complexity of the systems, the rapid pace of development, the compartmentalization or specialization of engineers, or combinations thereof, is difficult to assess. The fact is that the problem does exist, and NASA has been forced to live with it.

RELIABILITY ENGINEERING

Reliability must be engineered into a system, it doesn't just happen. Reliability engineering consists of two basic parts, design and test. Some of the elements under these two major subdivisions are as follows:

(1) Design
    (a) Design criteria
    (b) Design practices
    (c) Design reviews
    (d) Reliability analyses
    (e) Failure mode analyses
(2) Testing
    (a) Breadboard
    (b) Prototype
    (c) Qualification of piece part, component, subsystem, system, and
        combined systems

140

Each of these elements plays an important role in the process of achieving a reliable system. All are required in order to attain a reliable system. Consider first the design of the system.

Design Criteria

After establishing what sort of system is required, that is, what it is to do and, conceptually, how it is to do it, the design criteria are established. Some of the criteria that must be established before undertaking a design are

(1) Structural factors of safety

(2) Electronic parts derating policy

(3) Codes or standards

(4) Functional specifications

(5) Environmental specifications

(6) Duty cycle

(7) Electromagnetic interference

Many of these criteria are self-explanatory. Others are a little more involved, for example, electronic parts derating. Such parts normally have a service voltage and power specified by the manufacturer. The basis for the rating is somewhat obscure, and the physics of failure is not well understood. It is known that in solid-state devices, for example, there is a premium on small size of the part and that the failure mechanism is somehow related to operating temperature. By test, it has been established that, if the power level at which a part is used is cut by half, the frequency of random failure is reduced by a factor of 5 or better. Therefore, as a design criterion, it is stipulated that all such parts be used at no more than about 0.7 the specified voltage and current level. (The actual numbers vary with the type of part under consideration.) When it is recognized that a typical launch vehicle contains about 300 000 parts, most of them electronic, the product of all those one-fifth's in failure rate has great significance.

Environment plays a major role in how a system will perform. Vibration, shock, and temperature are easily envisaged. Space systems must also contend with the salt-water atmosphere at the launch complex in Florida and the potential for growth of fungus in a hot and humid environment.

Considerations such as these lead to what may be termed a design margin of safety. It establishes the degree of conservatism built into the system. Among the duties of reliability engineers is that of providing the data on which to base the design criteria.

Design Practices

Once the criteria are established, the design process can proceed. The reliability engineer is an important participant in system design. During all phases of the design process, he has the responsibility for ensuring that proper design practices are employed. This involves more than assuring adherence to the design criteria, it also includes, among others: (1) making sure that as few different varieties of parts as possible are used; (2) recognition of critical functions that would benefit from provision of redundancy in the system; and (3) making sure that, when a new technique or component is applied, there is a real need for it and that it is not just a manifestation of the designer's normal desire to do something new. In addition, he conducts a reliability analysis of the system. This analysis takes the statistical information on the failure rates of piece parts and projects the probability of failure of the systems components. Although the answers are expressed in probabilities, with lots of nines following the decimal point, the absolute numbers are not that important. What is important is the relative standing of the elements of the design. If an element is calculated to be significantly less reliable than most others, it is a candidate for redesign and/or redundancy. Redundancy, although frequently desirable and useful, is not a cure-all. Sometimes addition of redundancy can cause more trouble than it cures. Recognition of this when it occurs is the province of the reliability engineer. Examination of the design for proper design practice is a continuous part of the design process.

Design Reviews

Another important element of the reliability engineering process is the design review. Design reviews are normally conducted at three points during the design process. The first one is the conceptual design review, which occurs relatively early in the cycle. At this point, the basic elements of the system are selected, and the mechanization schemes to satisfy the fundamental requirements are established. Preliminary design follows during which parts are selected, specifications are drafted, and preliminary drawings are made.

At this point, the intermediate design review takes place. During this process all the design data and schematics are reviewed to establish that the system can do the required job and that the components or parts selected satisfy the design criteria. When this has been established, a very important step begins. This is the failure mode and effects analysis of the proposed design. The design is examined to answer the following questions:

(1) How can a part or component fail?

(2) For each mode of failure - what effect does it have on system performance?

(3) How critical is this effect?

(4) Can the problem be obviated?

Basically, the failure mode analysis asks "what if?" and attempts to answer the question. To illustrate the sort of thinking involved, consider the schematic of a launch vehicle hydraulic system shown in figure 4-1. As can be seen, it is basically a simple system. A pump takes hydraulic fluid from a reservoir, raises its pressure, and passes it through a check valve to the engine gimbal actuator, whence it returns to the reservoir. The system pressures are measured by three transducers, two on the high-pressure side and the other on the return side. During the failure mode analysis, the question was asked: "What if a high-pressure transducer fails?" The transducer that had been selected was examined. It is shown in figure 4-2. It consists of a spirally wound Bourdon tube that moves a potentiometer. The working pressure of the system is 3000 psi; the gage was rated to 0 to 3500 psi. It seemed as if this was sufficient margin. The weakest point in the Bourdon tube is where it is brazed to the inlet fitting. If this were to break, the case of the transducer would be subjected to full line pressure and, for the instrument that had been selected, would fail because the electrical connector was merely soldered on to the case. In a short time all the supply of fluid would be exhausted overboard, and control of the vehicle would be lost. This possibility was, of course, totally unacceptable and was avoided by selecting a transducer case that could withstand full line pressure in the event of a failure of the sensing element. It was tolerable to lose a measurement, but not the whole vehicle.

This is not a hypothetical situation. It actually existed in a vehicle design and probably would have gone unnoticed if the design had not been subjected to a failure mode analysis.

As a result of such work at all levels of the design, the system design is modified to provide inherent reliability. One other important element is provided from the results of such analyses. That is, as each potential failure mode is identified, the test requirements for acceptance testing are established. These should be selected so that each of the modes can be detected. Thus, some of the instrumentation requirements for the system are established.

Following the detailed design of the system, everything is examined again in the final design review. This repetition is required because, at this juncture, the physical arrangement of the hardware has been established and this may have altered the intent of the design as established during the intermediate design review.

Figure 4-3 illustrates the sort of problem that can arise. Again, this actually occurred. It was decided to provide redundant gates in a particular circuit of an

autopilot because of its criticality. The schematic of the design is shown in the left of the figure. As can be seen, if one of the two gates fails, the signal can still get through - just what was wanted. When this was translated into a physical detailed design, however, the situation shown by the solid lines in the right sketch resulted. It looks, schematically, just like what was wanted - except that these gates are part of a single integrated circuit chip and are thus not truly independent. Were the chip to fail, both gates would most probably fail. The desired redundancy was there-fore not attained. The solution is shown by the dashed lines. In this case, the sec-ond gate was provided on another integrated circuit chip, and true redundancy was obtained. It is to uncover deficiencies like this that final design reviews are held.

As may be inferred from the examples given, it takes a special "breed of cat" to be a good reliability engineer. He must be a highly competent engineer, versed in design analysis, knowledgeable of how things are done in the "real world," and have the patience of Job. When such a paragon has been found, there is a most important thing that should not be done with him. That is, he must not be put to work for the project manager. He must not be subject to the pressures on the pro-ject to meet costs and schedules. He must be free to "nit pick" and to act as the conscience of the project. In NASA, the reliability engineer works with the project manager but out of an independent office that reports to the Center director.

Testing

After the final design review and the resultant design modifications, the first item can be built. Despite all the effort described, not a thing has been built; that is, nothing resembling the final design has been made. Frequently, as part of the design process, a breadboard setup is made. This is really a design tool - an ana-log simulation of the schematic to determine, for example, whether a complex cir-cuit will function as intended.

The first item that resembles the flight item is the engineering model or pro-rotype, this is normally built in an experimental shop. With it the first step in proving the reliability of the system is taken. The testing that is conducted is called design evaluation testing and is very similar to the formal qualification pro-gram. The nature of the testing is as follows:
(1) Functional tests
    (a) Design condition
    (b) Specification range, off standard
    (c) Tests for marginality

(2) Environmental tests

    (a) Pressure ⎫

    (b) Thermal   ⎬ combined where possible

    (c) Vibration ⎭

    (d) Shock

    (e) Atmosphere

    (f) Electromagnetic interference

    (g) Rain

    (h) Sand

    (i) Fungus, etc.

(3) Stress limit tests

(4) Life tests

    (a) Specified life

    (b) Extended life

It is important to note that the applicable portions of the tests listed are conducted at various levels of the hardware, that is, first on the piece parts, then on the components or modules, next on subsystems, and, finally, at the system level. Ultimately, if at all possible, similar tests are conducted at the combined systems level, that is, all-up with all systems interacting. The tests are described briefly in the following paragraphs.

First come the functional tests. These tests prove that the system can work as designed and are conducted at both nominal conditions and over the range of specified operating conditions, that is, over the range of inputs for which the system should perform properly. After this, the variables are permitted to exceed the specifications to determine whether a marginal condition exists; that is, whether an input slightly out of specification will cause the system to fail or malfunction.

When this series is completed, the environmental testing phase begins. The system is subjected, while operating, to the types of environments that it will experience in service. In qualification testing, the specimen is normally subjected to environmental conditions more severe than it would be expected to encounter in service. For example, in vibration testing it is normally required that the design be capable of surviving at least $1\frac{1}{2}$ times the expected flight vibration levels.

If it is at all possible, the environmental tests are conducted under combined environments such as the system will actually experience. On a launch vehicle, for example, a subsystem, or "black box," will be subjected simultaneously to vibration, thermal changes, and ambient pressure changes. The tests are designed so that these factors are applied as they would occur in flight.

If something fails during such tests, design changes are made to preclude such failure. Appropriate portions of the test program are repeated to prove the "fix"

before proceeding to other parts of the program.

When the environmental tests have been completed successfully, the subsystem enters the stress limit test. In this test, the input levels are incrementally increased. For example, the temperature level at which a "black box" is operated is extended on both high and low sides, to ascertain at what temperature it malfunctions. This type of test determines any critical weakness or marginality in the design and establishes the actually achieved design margins.

The last type of test listed, the life test, consists of repetitive cycles of operation at the anticipated environment. This is really a sort of fatigue test during which the time it takes for a system to "wear out" is ascertained.

When the prototype and all of its parts have successfully completed the tests with all the modifications incorporated, the next step can begin; that is, the drawings and process specifications are released to the production department for manufacture. The first few items produced in these shops are then subjected to the whole gamut of tests, this time for formal qualification. Recall that the prototype hardware was built in an experimental shop and that there is a vast difference between it and a production shop. This series of tests on the production hardware is viewed as qualifying both the hardware built in the production shop and the shop itself. When all these tests have been successfully completed, the design is considered to be qualified for flight.

QUALITY ASSURANCE

After all of the effort that went into the design and qualification process just described, it would seem that the problems are over and all that has to be done is to build or buy the product of all this work. Unfortunately, this is not the case. The system must be policed to ensure that the product will be precisely as designed. This is the function of the quality assurance program. The tools of this discipline include specifications, process control, inspection, acceptance testing at all levels, a closed-loop failure analysis and corrective-action system, and stock controls. In order to get a high-quality product each of these tools must be employed in a rigorous manner.

Specifications

First, consider the specifications that govern the items that are built or purchased. It is important that these be written as completely and precisely as pos-

sible. They should contain negative as well as positive statements. It must be remembered that you get only what you contract for.

The following example shows how an incomplete specification caused much trouble. In an autopilot, a large number of a particular type of transistor were employed. It had been a long, hard task to qualify a particular vendor's product for this application, and the systems were working wonderfully. Suddenly, the autopilot began to experience unexplainable functional failures during testing. Nothing had been changed; all parts were being purchased to the specifications always used, and the manufacturing processes employed in the electronics shop were the same and were being followed carefully. After extensive testing, all elements had been eliminated as the source of the problem, except this type of transistor. After some investigation it was found that, without notification, the vendor had "improved" his product. Figure 4-4 shows the gain characteristics of the transistor. The solid curve shows the gain as a function of the collector current of the original part. The dashed curve shows the characteristics after the improvement. The difference is apparent.

The purchase specification required that the gain at a specific current lie in the range enclosed by the circle. It did not say that the gain at lower currents should follow the solid curve. This had been considered an implicit characteristic of the device. Because many of the transistors in the autopilot actually operated at a much lower current (as shown by the dashed vertical line), the change of gain by a factor of 2 drew the circuits into instability. The new model transistor still met the specifications as written, and the vendor, who did not know the application, had no idea of the trouble a normal product improvement would cause. The specifications now state "No changes without telling us."

Inspection

Inspection is a vital element of quality assurance. In the qualification tests, not only is a design being qualified, but the manufacturer and the manufacturing process are also being qualified. The item must always be made in the same fashion in which the one that was qualified was made. This requires that inspection be thorough, that the most critical items are identified for special attention, and that strict adherence to all process specifications be maintained.

At one time, an inspector was a highly skilled, experienced, and capable craftsman who could perform all the tasks he was called on to inspect. Unfortunately, this is no longer generally true. Inspectors frequently do not understand what they are looking for. They merely follow instructions, and these, perforce, cannot completely describe what constitutes a good piece of work.

Testing

For this reason, reliance must be placed on the most powerful tool at our disposal - testing. Everything used is subjected to a rigorous acceptance test program at all hardware levels. The testing encompasses both functional and environmental tests. In fact, the tests are very similar to their counterparts during qualification testing. The principal difference is that the environmental levels are normally limited to what the expected service levels will be. The value of acceptance testing under appropriate environmental conditions cannot be overemphasized. Again, an example will illustrate the point.

During the acceptance flow response test, an hydraulic pump was rejected as being excessively noisy and exhibiting abnormal vibration. The pump is a conventional constant-pressure, positive-displacement, variable-flow device. A sample of hydraulic oil from the pump-case drain port contained a large number of bronze-colored particles and several pieces of broken ball-bearing retainer. Upon disassembly, it was found that the pump cylinder block bearing had been installed backward with the thrust face away from the bearing retainer. A sketch of the bearing is shown in the left of figure 4-5. Note the asymmetry of the bearing. The pump vendor's assembly instructions stated "Assemble with face marked THRUST next to bearing retainer." This marking is shown in the right of the figure. The outer race can support only minimal thrust in the reverse direction. When the pump was under test, the bearing broke. So much for the quality of the inspection. As this pump is not run until the rocket engine turbopump drives it at engine ignition and the pump does not fail immediately, it would have done so during flight and would have caused a mission failure. Only the acceptance tests prevented the improperly assembled pump from being installed on a vehicle.

Failure Analysis and Corrective Action

A necessary concomitant of any testing is a closed-loop failure analysis and corrective-action system. Unfortunately, design and manufacturing techniques are not infallible, and despite all the effort applied to preclude it, a subtle design deficiency may sneak through and cause trouble. When something malfunctions in a test, it is not enough to fix the one item and then proceed. It is vital that the cause of the failure be identified and corrective action be taken on all such devices. A subtle design deficiency and the failure analysis and corrective action taken are illustrated in figure 4-6.

This figure depicts an electrohydraulic servovalve that controls the engine

gimbal actuators. Basically, it is a differential electric motor driving a pilot valve that ports hydraulic oil to either side of a working cylinder to move the engine. The three leads shown carry the current for moving the electric motor in response to commands from the autopilot servoamplifier.

This valve had been subjected to a thorough qualification program and had come through with flying colors. During acceptance testing of a batch of these valves, one of them failed during the vibration test. The failure was a short circuit is one of the three wires to the motor. What had happened is shown in the photograph in figure 4-6. Notice how the three wires are pinched between the pole piece of the motor and the case. Upon investigation, it was found that the gap between the case and pole piece through which the wires from the armature had come was not quite big enough for a single wire. Thus, when the motor was assembled, the wires were slightly pinched. The amount of pinching involved was not enough to break through the insulation, however. The insulation is Teflon, and this material is subject to cold flow. When the valve was assembled at the vendor's plant, it sucessfully passed his tests. The pinched insulation, however, continued to flow. During the acceptance test, the added vibration (which is like that which would be encountered in flight) completed the insulation flow, and the short occurred. In flight, such a failure would have been catastrophic.

The failure analysis showed that, in the process of assembling the valve, the motor leads are soldered to a bulkhead connector and then the connector and wires are pushed into the case and the connector is screwed in place. Unless care is taken during this step, it is easy for the wires to slip out of the proper feedthrough area and be pinched over the sharp edge of the pole pieces. A number of steps were taken to correct this situation. First, the edge of the pole piece, which had been square and relatively sharp, was given a generous radius. And second, special assembly instructions and inspection callouts were implemented.

The most important aspect of this incident is the fact that a failure analysis was conducted. It would have been very easy to simply reject the valve and send it back to the manufacturer. Such action would, however, have left the valve with a large potential for catastrophic failure in a future flight.

Most of the preceding discussion and examples have been concerned with problems within a single component or "black box." Another important factor to consider is that of interactions or interfaces among systems. Whenever there is an interface, there is a potential for an incompatibility that can lead to trouble. Figure 4-7 illustrates a problem of this nature. This example demonstrates the importance of failure analysis as well as the pitfalls of an interface.

The figure shows a schematic of a portion of the propellant utilization system of a launch vehicle. The function of this system is to regulate the ratio of fuel and

oxidizer flows to the rocket engine so that the supply of both propellants is depleted at the same time. The portion of the system circuit shown is that between the error detector and the fuel valve controller. The solid lines are the original configuration. This is basically a very simple circuit. The information tap provided a means for measuring the output of the error detector. The signal went to both the telemetry system on the vehicle and through a landline to a recording instrument in the blockhouse. It was noticed during prelaunch testing that, when the umbilicals were ejected, a shift in the error signal was indicated by the telemetry signal. Although the shift was relatively minor, it should not have occurred. A failure analysis was instituted. A detailed analysis of the circuit at the launch site showed that, when the umbilicals were connected, the instrumentation in the blockhouse was loading the circuit and introducing a bias which evidenced itself when the umbilical connection was broken. As the vehicle was checked out in supposedly the same way in the factory, the obvious question was "Why didn't this show up then?" The answer was, quite simply, that the combined impedance of the blockhouse instrument and long line at the launch site was much different from that of the equipment used in the factory. The factory gear did not load the circuit. This is an almost classic example of the importance of using the same type of test gear in both the factory and field - an interface problem. Thus, the problem of the error signal shift was resolved.

While the problem was being investigated, it became obvious that, if there were a failure in the instrumentation system, it could cause a failure of the propellant utilization system. The original instrumentation line went directly to the telemetry set. If a short developed in the telemeter, the output of the error signal would be shorted, and control of the fuel valve would be lost. Thus, the desire or need for information of system performance parameters resulted in a design that introduced an unacceptable failure mode. Fortunately, the solution for both problems was straightforward and is shown by the small-dashed lines. The error signal was picked up as shown and fed through isolating resistors. The resistors serve two purposes. First, they provide a high impedance ratio so that the instruments can no longer load the circuit. Second, they isolate the instrumentation system from the propellant utilization system so that, if there is a short in the information system, it will not destroy the functional system.

This concludes our brief tour through a chamber of horrors. These are but a few examples of the sort of problems that the methodology NASA has evolved has helped prevent or catch. Although most of the examples have been of an electrical nature, a similar set concerned with purely mechanical components could have been used.

Operational Testing

The reliability and quality assurance program does not end with getting flight hardware through the acceptance test at the factory at the subsystem level. It continues all the way to launch and throughout the flight.

After the subsystems have been through their individual acceptance tests, they are assembled onto the vehicle in the factory and each system is tested. When the systems tests are completed satisfactorily, a combined systems test is conducted with all systems being required to operate while interacting with each other as they would in flight. (Ideally, this should be done in a simulated flight environment.) Only when this test has been passed is the vehicle ready to ship to the launch site.

At the launch site, the systems level tests are repeated to determine whether any damage or degradation has occurred during transportation and to prove that the airborne hardware is compatible with the ground-support equipment. Then a series of composite tests is undertaken to again demonstrate the integrity of the vehicle. Typically, there are three composite tests during which everything that will happen during launch and flight, short of actually igniting the engines, is checked out.

When all this testing is over, a data and readiness review is held. Each box, or major component, has a "history jacket" which documents its life story during manufacturing and testing. The data from all tests are now reviewed to ascertain whether each system is, and has been, performing within specifications and whether the data exhibit any trends indicative of deterioration - even if all readings are within specifications. Only when each system proves to be acceptable on the basis of all testing, is it considered ready for flight.

Subsequent to flight, all data from the flight are evaluated to ascertain whether the systems performed as predicted and whether any anomalies occurred.

CONCLUDING REMARKS

The reliability and quality assurance program described briefly herein is, however, no panacea. It can lead to a paper blizzard because all the things that are discovered must be documented and communicated in the hope of precluding a recurrence. This can lead to a reliance on paper rather than on sound engineering evaluation and judgement. The program does help to reduce the frequency of undetected human errors but, alas, does not eliminate them. Also, it takes money, sometimes a lot of it, but it can save much more - and that makes it worthwhile.

What has been learned in the struggle to achieve reliability?

First, testing is the most potent and least expensive aspect of the program

when measured against the cost of a flight failure. The equipment and facilities required to perform full-systems environmental tests are worth the cost. For a while, the ability to test the hardware of both spacecraft and launch vehicle systems was comparable. Now, spacecraft can be more effectively tested because their size is compatible with existing environmental facilities. It is now standard practice to put the whole spacecraft into an environmental chamber wherein almost the total flight environment can be simulated. We look forward to the day when the launch vehicles may be tested in the same manner.

Second, designs must possess adequate margins of safety. Getting such margins must be a conscious part of the design effort.

Third, testability must be designed into the hardware. Also, the test procedures and test equipment are part of the design process - they are just as important in achieving reliability as the functional design of the flight hardware.

Finally, it is essential to police the manufacturing and test processes. Close adherence to procedures is mandatory. Parts should be standardized as much as possible, and good housekeeping practices must be followed at all times and places.

As stated at the beginning, all that NASA does to achieve reliability may not be applicable to the electric power industry. However, the two fields have a basic similarity. Both are engaged in activities that are characterized by small build rates of the ultimate end item - be it a powerplant or a launch vehicle. But there are many components and subsystems that are common to many installations. Perhaps group action within the industry in the design and specifications of such common elements would be an effective way of reducing the cost to an individual company of implementing reliability and quality assurance requirements on purchased items.

High reliability has been difficult to attain, just as difficult to maintain, and even more difficult to improve. It is hoped that the experience of NASA will in some way be of value to the electric power industry.
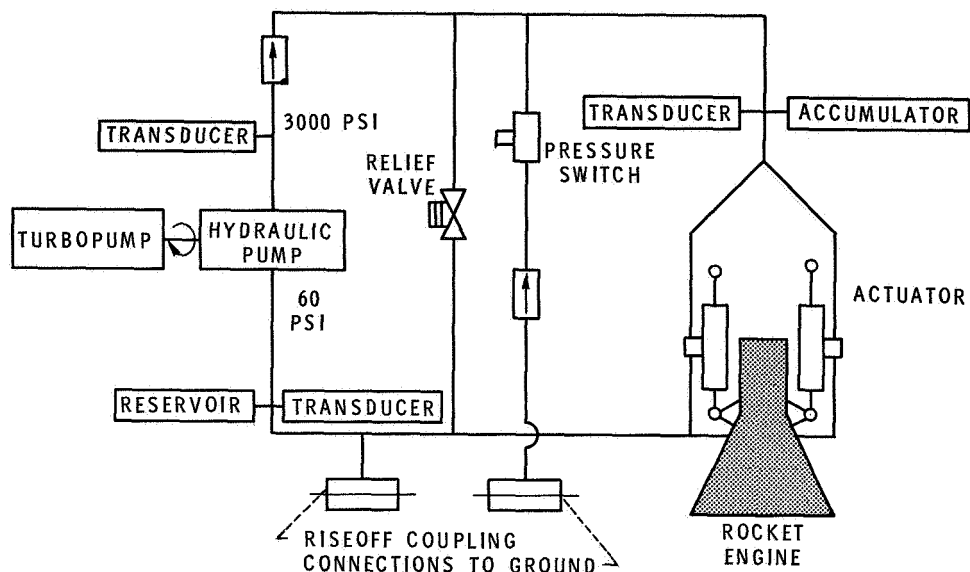
Figure 4-1. - Launch vehicle hydraulic system.
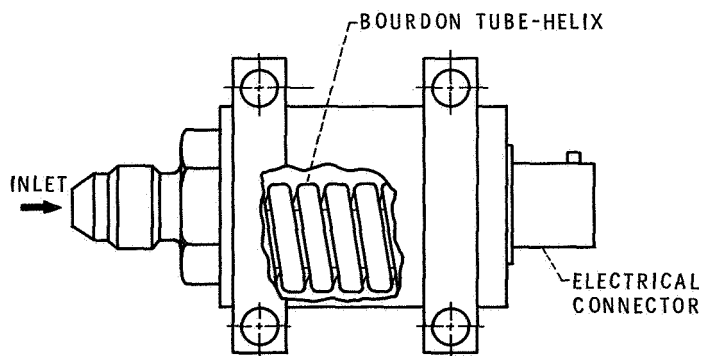
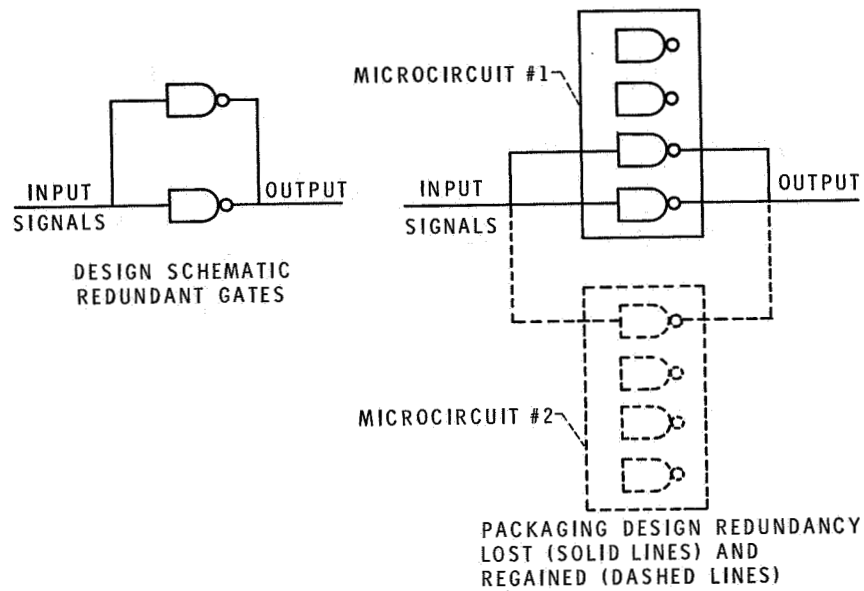Figure 4-2. - Pressure transducer, 0 to 3500 psia.

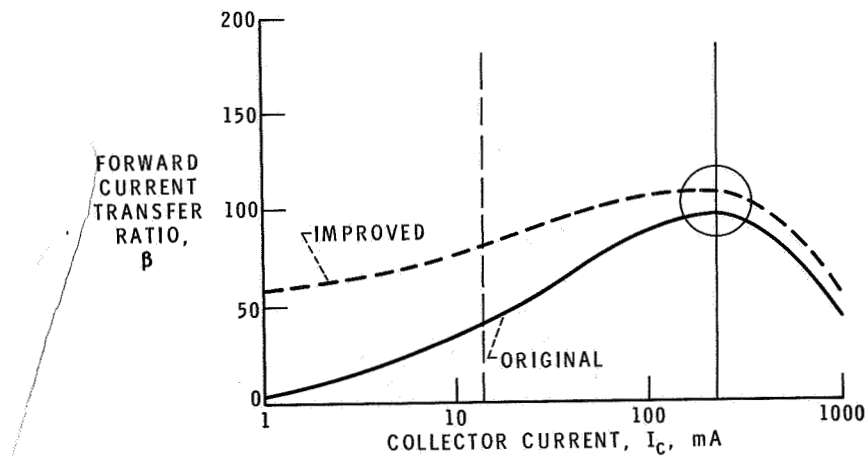Figure 4-3. – Schematic of autopilot circuit gating.
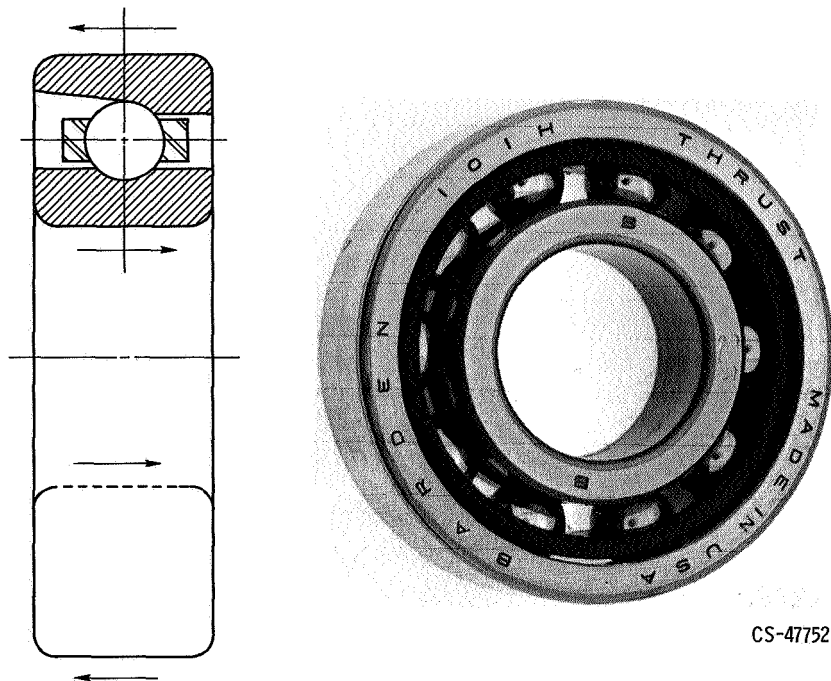

Figure 4-4. – Transistor characteristics.

CS-47752

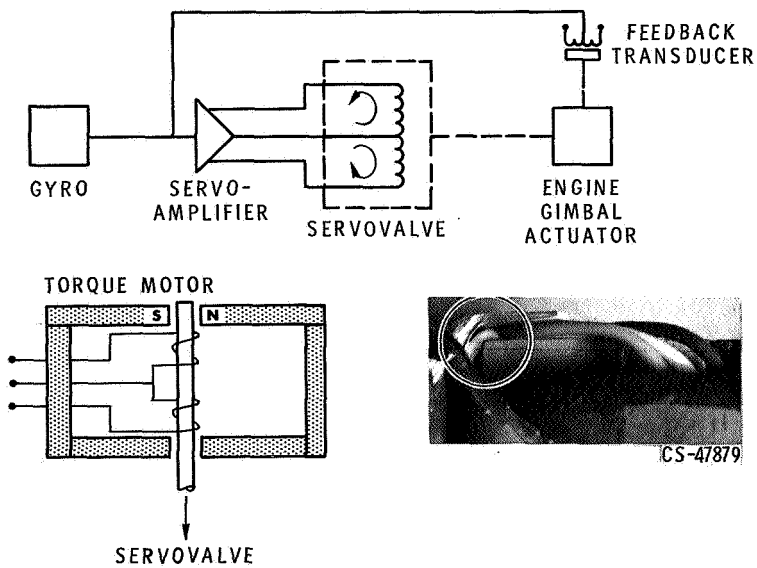Figure 4-5. - Hydraulic pump bearing. Arrows show correct direction for loading races.

FEEDBACK
TRANSDUCER

GYRO   SERVO-
        AMPLIFIER   SERVOVALVE

ENGINE
GIMBAL
ACTUATOR

TORQUE MOTOR

S   N

SERVOVALVE

CS-47879

Figure 4-6. - Electrohydraulic servovalve for engine gimbal control.

155
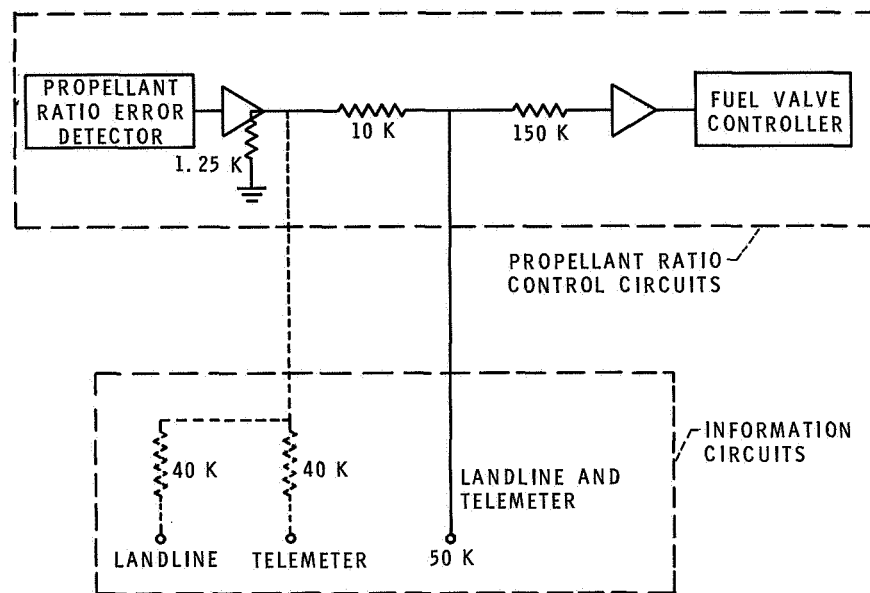
Figure 4-7. - Schematic of portion of launch vehicle propellant utilization system.

5. AUTOMATIC CHECKOUT AND CONTROL

Joseph N. Sivo

As explained in the paper by S. C. Himmel, careful testing and checkout of all vehicle systems are necessary to achieve success in the launch vehicle business. This testing procedure starts during the manufacture of parts and systems and it continues on the complete vehicle up to the moment of launch. Complete systems testing has contributed greatly to the success of the NASA space program. Although such a thorough checkout requires large expenditures of manpower and money, the end result - successful launches - justifies the approach.

Overall launch operations can be divided into three phases: prelaunch checkout, launch countdown or vehicle startup, and postlaunch control or steady-state operation. Experience has shown that the prelaunch phase is the most critical of the three and creates the greatest demand on manpower and equipment. If proper prelaunch checkout is provided, the startup phase, by comparison, becomes somewhat routine. This can, in most cases, also be said of the postlaunch or run phase. Therefore, most of the discussion herein is concerned with this prelaunch phase.

In the early days, rockets were relatively small single-stage vehicles. The Atlas booster (fig. 5-1) was used in the manned Mercury program and is somewhat typical of the smaller boosters. Checkout of all the vehicle systems was a manual operation, and launch crews were relatively small.

The Saturn V (fig. 5-2) is the three-stage vehicle soon to be used in the manned Apollo Moon program. It has eleven main engines - five in the first and second stages and one in the third stage - as compared to three main engines on the Atlas. The Saturn is quite large - standing some 350 feet high as compared to about 100 feet for the Atlas. The combination of multiple stages, their attendant interfaces, the need for in-flight stage separation, and the vehicle size combine to increase the number of system parameters to be checked a hundredfold over the Atlas.

A size comparison between the Mercury capsule and the Apollo spacecraft also serves to show the increased prelaunch checkout that is necessary. The Mercury capsule was a one-man single-stage device weighing about 3000 pounds used to orbit the Earth. The Apollo spacecraft, in contrast, is a four-stage system - a capsule to house three men on the trip from the Earth to the Moon and back, a stage to retro into and depart from a lunar orbit, and a two-stage two-man vehicle to land on and

launch from the Moon's surface. When fueled, the spacecraft weighs about 100 000 pounds. On the Mercury capsule, 88 system parameters were checked prior to launch. This number has increased to nearly 2600 checks on the Apollo system.

The change in vehicle and spacecraft size with the Apollo program reflected itself in the launch complex necessary to support them. Figure 5-3 shows the typical Atlas launch complex used for such programs as Mercury. The vehicle was assembled on the pad and checked out manually, and the launch was directed from a blockhouse only a few hundred yards away.

The Saturn complex shown in figure 5-4 is a different matter. The vehicle and spacecraft are assembled in the Vehicle Assembly Building, one of the largest buildings in the world, and they are then transported fully assembled to one of two launch pads - one is 3 miles distant, and the other is 5 miles. This entire launch complex covers over 30 square miles.

Experience had shown that the checkout of all systems prior to launch was mandatory if high reliability was to be achieved, but the vehicles have grown so in complexity and size that the proven manual checkout techniques were unable to cope with the increase in elements to be checked. The only recourse available was automation of checkout procedures wherever applicable. Automation in itself was no cure all, and it carried with it many new problems. However, the problems created by automatic or computer-controlled test and checkout are being resolved, and the ability to check out vehicles as complex as the Saturn V and its spacecraft has been demonstrated.

To give an idea of the complexity involved, table 5-I presents the number and type of measurements taken on the Saturn launch vehicle during checkout. Values of acceleration, vibration, temperature, pressure, etc. are taken throughout the testing and total some 2600 measurements including both analog and discrete.

The need for automation to conduct the tests that help to ensure reliability has been discussed, but questions such as the following must yet be answered: What is meant by the automatic checkout system? What are its major components? How does it work? What types of tests can be run?

Figure 5-5 shows a typical automatic checkout system that is currently in operation for the checkout of the Apollo spacecraft. This system is referred to as the Automated Checkout Equipment or ACE system and contains two main functional parts - a Command System and a Display System.

Test commands emanating from the test consoles are received and processed by the command computer which, in turn, sends appropriate commands through the transmission equipment to the vehicle under test.

The output of the instrumentation on the vehicle and the responses to the test stimuli are transmitted to the data receiving and recording equipment of the Display

System. Some of the data are routed through a data processing computer where they are made ready for display in engineering units on the test console cathode ray tube, sometimes referred to as a CRT. The data are also routed directly to the support consoles for presentation on conventional display devices.

A few examples of how to implement the testing with such a system help to explain how the system is utilized. Currently in the power industry, one of the procedures associated with startup of a turbogenerator unit is the gradual heating of certain parts of the turbine with steam to minimize thermal shock. This usually involves cracking the steam supply valve to allow steam to enter the turbine slowly. A somewhat similar procedure is used when cryogenic propellants are loaded. However, very low temperature thermal shock is the problem here.

Figure 5-7 shows a schematic of the hydrogen loading system of the Saturn V vehicle. The loading process is initiated by an engineer at the console pressing a start button. A vacuum-jacketed storage tank supplies hydrogen to the vehicle through either the chilldown valve, which controls the initial fill rate, or through the main fill valve to another pair of valves near the vehicle. Propellant normally flows through the fill valve into the tank. As the tank nears capacity, flow is metered through only the replenish valve at a low rate to complete the filling process. Propellant that is lost due to boiling in either the vehicle tanks or in the main storage tank is piped to a burn pond for disposal. The lost propellant in the vehicle tanks is replaced through the replenish valve. All the valves are operated electropneumatically. Level sensing probes of the continuous reading type are installed in each tank.

Previous calibration tests on similar vehicle tanks provided information on maximum allowable fill rates as a function of tank liquid level that avoid excessive thermal stresses due to cold shock. With these data, a propellant loading computer program was generated that applied all the limitations imposed on the filling process determined in the calibration tests. The program is a precisely organized sequence of events triggered by specific tank liquid levels.

In the actual tanking operation, outputs from the level sensors are sent to the computer and compared continuously with the reference standard stored in the computer memory. During the loading process, fill rates are changed depending on the liquid levels. For example, in the second-stage hydrogen tank, a small amount of hydrogen is introduced into the tank to cool the tank slowly to $-160°$ F, and then a low initial fill rate of 1000 gallons per minute is used up to the 5-percent level. Next, the rate increases to 10 000 gallons per minute until the 96-percent level is reached; then, it goes back to 1000 gallons per minute to the 99-percent level; and finally, it is topped at 500 gallons per minute. If a malfunction occurs, the filling process stops and manual valve control is possible from the control console. Propellant

loading is a precise and somewhat delicate process that has been found well suited to automated control.

On a vehicle like Saturn V, there are hundreds of specific events which must be checked as a function of time to assure that things are progressing in an orderly predetermined fashion. One of the specific event readout panels for the first stage is shown in figure 5-8, which is not meant to be read but only to illustrate how events are displayed in the control room. As each event occurs, for instance an oxygen purge valve opens, an appropriate light comes on and its companion light, the oxygen purge valve closed, goes off. When one considers that this purge valve may open and close several times during normal operation of the oxygen system, it is necessary to know not only whether the valve is open or closed, but also what should it be at the given point in time. This particular panel monitors 250 separate events and is only one of several like it. Although it does provide a real time presentation of all events as they occur, it is quite clear that an operator or many operators would be unable to visually keep tabs on all the events as they occur in real time.

The computer checkout system for the Saturn V has the capacity of scanning 4300 discrete events such as these every 2 milliseconds. As the scan progresses, the condition of each discrete signal is compared by the computer to the status it should have at the time of scan. If there is a disagreement in status, the test conductor is immediately notified of the anomaly. Depending on the anomaly, appropriate action is taken automatically by the computer if previously instructed to do so. Not only can the computer keep track of discrete signals as they occur, but it can conduct a test program that will exercise each discrete event to check if all are functioning properly.

Experience has shown that human error has a habit of being a rather unpredictable source of system failure. Although testing all parts of a complete system is of great value, the more testing that is done, the greater the chance of a human error causing failure.

The following example illustrates the type of error that can and does result from not following instructions exactly. Figure 5-9 shows an Atlas flight programmer that controls the sequence of events occurring on the booster after liftoff. The test that is run routinely on the programmer requires that both ac and dc power be connected to their respective input terminals at the start of the test.

Portions of the actual checkout sheet used while conducting the test are given in figure 5-10. The sheet specifies the order that the power leads are to be energized. The dc power must be energized before the ac power if load limits on components within the programmer are not to be exceeded. In other words, if the ac power is connected first, you overload the programmer. Certainly, sufficient instructions have been given to caution the checkout crews. Unfortunately, the programmer was

overloaded anyway. The cause was human error. Had this particular test been performed under automatic checkout, the failure would have been avoided. This is a typical case of a routine test that had been run a hundred times without any trouble suddenly causing a loss of both time and money. Once a routine test has been checked out using the computer and the computer test program verified, the test is always conducted in the same way no matter how many times it is run.

Another major problem in checking out complex systems becomes one of data handling. The more instruments that are used and the more tests that are run, the more that is learned about the systems. However, as usual, nothing is free. Instruments and tests generate data that must be analyzed if value is to be derived from the effort. This can become an overwhelming task using conventional techniques. However, having a computer available as part of the checkout system allows online data processing at extremely high rates.

For example, one of the critical decisions that must be made prior to launch is whether the winds aloft will cause structural damage to the vehicle due to vehicle bending. The question is handled in a very direct manner. Some time prior to launch, a wind sounding balloon, similar to the one shown in figure 5-11, is released at Cape Kennedy. Its motion is tracked by radar as it rises. Data from the radar are recorded on magnetic tape, which is fed to the computer. The computer converts the radar data to wind velocity and direction and then plots them as functions of altitude as shown in figure 5-12. The particular wind shown here reached a maximum speed of 250 feet per second or about 170 miles per hour at an altitude of 38 000 feet. The wind direction was nominally offshore.

The effect of wind loads on the vehicle is fairly straightforward. As the vehicle passes through the wind, the upper portion of the vehicle feels a higher wind force than the lower portion. This causes the vehicle to rotate in the direction of the wind. The vehicle attitude control system reacts to right the vehicle by gimbaling the engines so as to counter the rotation caused by the wind force. This action introduces a vehicle bending moment which, if high enough, could result in a vehicle structural failure.

In the past, wind data obtained from the balloon soundings were used in a manual calculation procedure to estimate if it was safe to launch. The process was rudimentary and time consuming. Wind data had to be taken 5 to 6 hours before launch to allow time for this manual operation. Since the winds can change significantly in a matter of an hour or so, this process was not entirely satisfactory.

Currently, this computation process has been automated and turnaround time greatly reduced. Now wind data obtained as little as 30 minutes prior to launch can be processed by the computer. A simulated flight of the vehicle through the winds is then made on the computer. Accurate estimates of the bending loads imposed on the

vehicle by the wind are thus obtained. In this way a higher confidence of launch safety is gained. It is also possible to have the computer determine a booster steering program that will minimize wind loads during the launch.

An example where online data processing as part of an automated checkout system could have avoided a costly delay, and perhaps in another situation a flight failure, is shown by an incident that occurred during checkout of the last Atlas-Centaur vehicle, which was launched in August 1968.

A complete systems test was conducted as part of the standard manual vehicle checkout procedure on the Atlas-Centaur. This test is a simulated flight sequence test where all events that will occur during actual flight are exercised with the exception of engine ignition. The vehicle is in the flight configuration with flight umbilicals connected and stage disconnects mated. As an example of the type of actions that occur during this test, the interstage electrical plug actuator is considered. For the test and for actual flight, the interstage electrical plug is mounted inside the actuator. At the time of stage separation, a signal is sent to the actuator which fires a powder charge that unlatches the springs in the actuator and pulls the plug apart. During the test, the telemetry data from the sensors on the vehicle are recorded on strip chart recorders. After the test, the traces are sent to a data analysis group for evaluation. Although visual monitoring of these recorders is possible in real time, the number of channels of data being recorded makes it difficult.

This particular test was completed at 6:00 a.m., and the data were immediately delivered to the analysis people. A comparison of each channel of data with a reference trace was made. At 3:00 p.m., an anomaly was noted in a trace of the yaw gyro responses. The problem was first thought to be a defective gyro, and the launch checkout crew was immediately notified of the anomaly. As already mentioned, the vehicle was undergoing a flight sequence test when the anomaly occurred. To rerun the test it was necessary to remate all the connections that had been broken as part of the test. This included the interstage electrical plug under consideration. After this was done, the test was rerun; however, this time no anomaly occurred. The temptation to ignore such an intermittent problem has been found to be wishful thinking. Consequently, the flight was canceled until whatever caused the anomaly could be found. The following week was spent trying to locate the cause of the trouble. After little success, laborious continuity checks were performed following many connects and disconnects of the various connectors in the faulty circuit. Finally, a pin in the flight interstage connector was found to be intermittently bad.

If automated checkout equipment had been in operation for this test, the anomaly would have been noted at the time of the failure and troubleshooting would have started before a change in configuration occurred. Then, the testing of only a small portion of the vehicle gyro circuits would have isolated the trouble. Although auto-

mated checkout has not been applied to a launch vehicle in the Atlas-Centaur class, incidents such as this have prompted its serious consideration.

One of the valuable byproducts of computer-controlled testing came about unexpectedly. Since testing procedure is relegated to a computer which relies strictly on input instructions, test engineers were required to describe in detail the test to be performed, the test stimuli, test limits, and possible failure modes and recovery routes prior to the start of testing. The result has been a reduction in hardware loss due to out-of-limit testing, poorly run tests, improper recovery action during a malfunction, etc.

Once the prelaunch phase is completed, a second and much shorter phase of the launch preparations begins. This is the launch countdown or perhaps better called the startup phase; for the Saturn V, this period begins 187 seconds prior to liftoff. The launch countdown differs from the prelaunch checkout in that the count is more a series of specific events programmed to occur during the count.

Figure 5-13 shows the launch director's countdown panel. Once the launch director initiates the count by pressing the start button, all events that occur are automatically controlled by the computer. The countdown starts with vent valve closure and tank pressurization, continues through power transfer and guidance alert, and ends with engine ignition and release of the vehicle. Throughout the count sequence, a constant comparison of what is occurring to what should occur is made by the computer. Any out-of-tolerance data results in a preprogrammed halt by the computer followed by a recycle to the beginning of the countdown. The many test points in the count allow rapid isolation of any malfunction. Recycle can occur at any time - even milliseconds prior to release of the vehicle. This is a completely automated portion of vehicle checkout and would be analogous to a startup of a boiler-turbine-generator unit.

The postlaunch phase starts once the booster has delivered its payload to its destination. After all the television coverage that was given to the Mercury and Gemini flights, most people are familiar with the checkout procedures followed in an orbiting manned spacecraft. This phase of the operation is similar to keeping tabs on a running system, and the main concern is watching for malfunctions. For unmanned payloads, the procedures are truly automated and operation times run into months and even years. Even for our manned spacecraft, much of the operation is automated.

In summary then, it can be concluded from the foregoing that automatic checkout of launch vehicles and spacecraft is not only desirable but essential as systems become larger and more complex. It not only reduces the time required for checkout but also increases reliability. Since these are two important factors, the automatic checkout of complex systems such as launch vehicles will continue to become more prevalent in the future.

TABLE 5-I. - SATURN V MEASUREMENTS SUMMARY

System	First stage	Second stage	Third stage	Guidance and control
Acceleration	3	11	0	4
Acoustics	4	5	0	1
Temperature	252	325	120	58
Pressure	234	198	88	13
Vibration	76	61	0	28
Flow	35	10	4	11
Position	1	44	8	21
Guidance and control	0	0	0	69
Radiofrequency and telemetering	0	0	0	26
Signals	133	223	74	112
Liquid level	22	6	7	0
Volts, amperes, and frequency	11	65	38	42
Miscellaneous	31	14	12	0
Angular velocity	3	3	0	33
Strain	71	27	0	32
Total	876	992	351	450
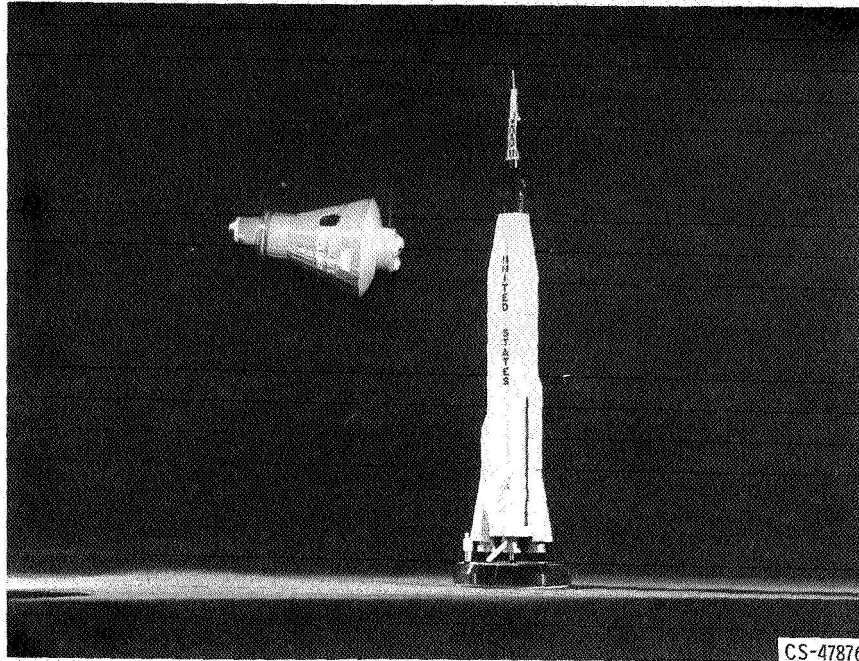
Figure 5-1. - Atlas booster and Mercury capsule.
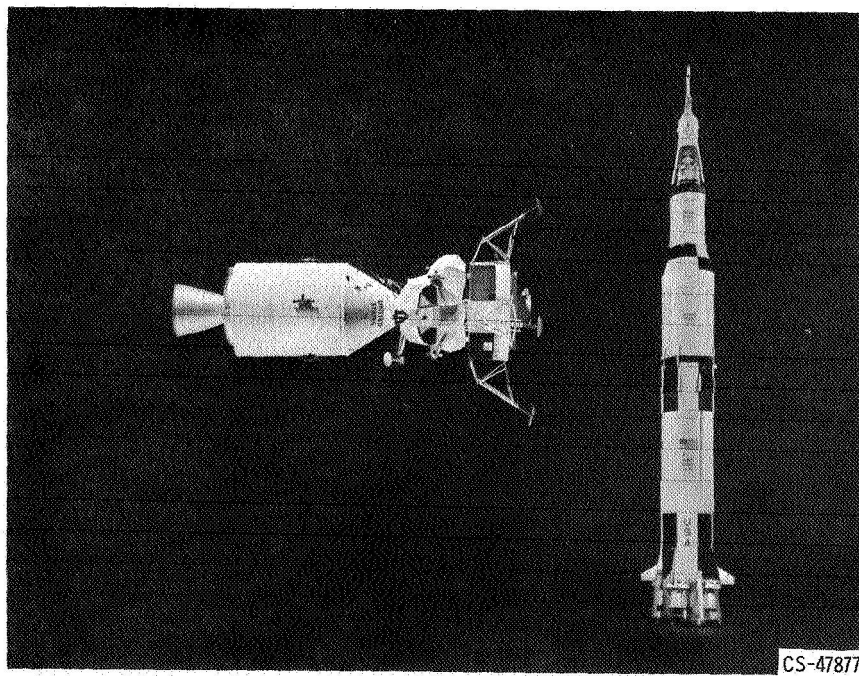
Figure 5-2. - Saturn V vehicle and Apollo spacecraft.
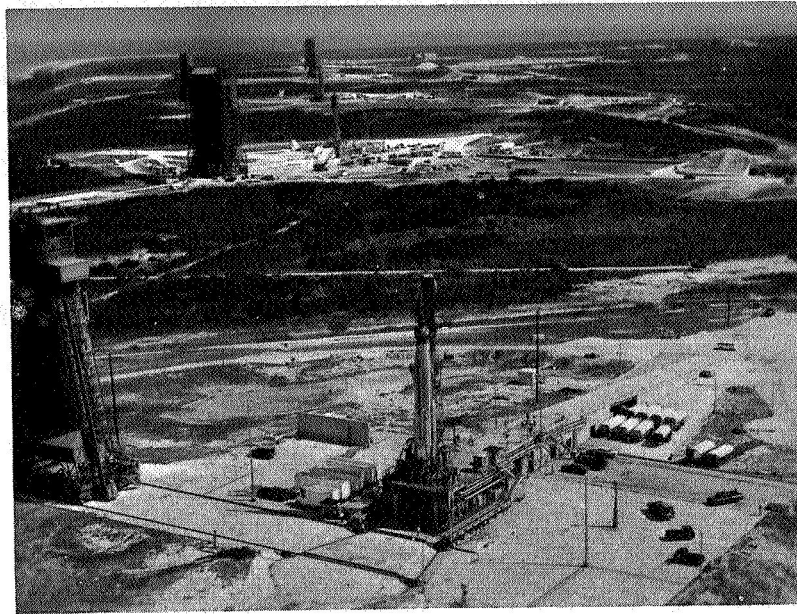
Figure 5-3. - Atlas launch complex.
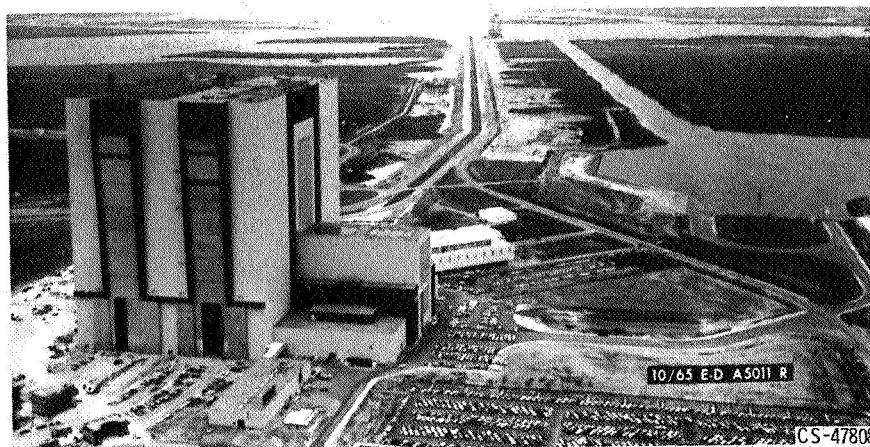
Figure 5-4. - Saturn launch complex.

166
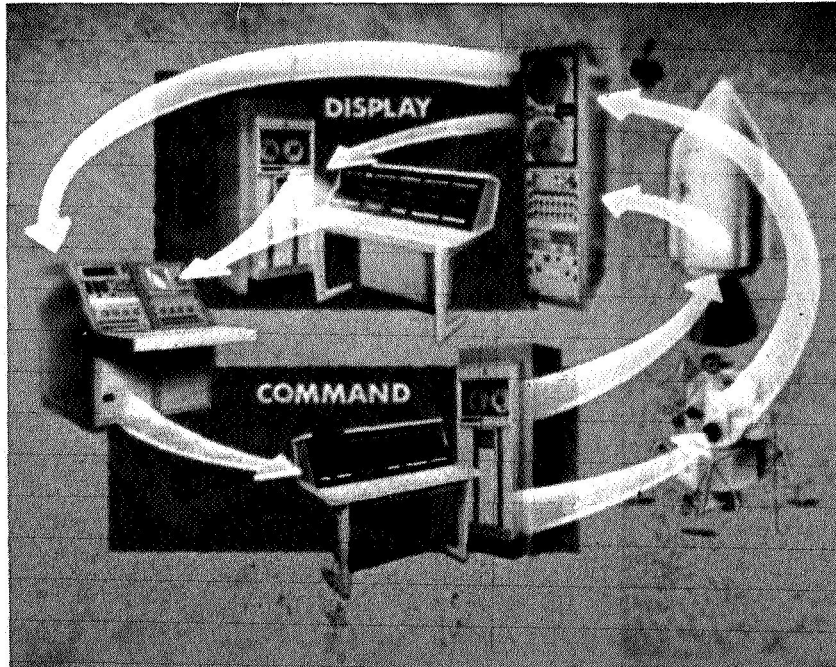
Figure 5-5. – Automated checkout equipment system.

Figure 5-6. – Cape Kennedy control room.

Figure 5-7. – Saturn V hydrogen loading system.

Figure 5-8. – Specific event readout panel.
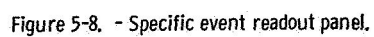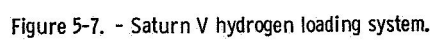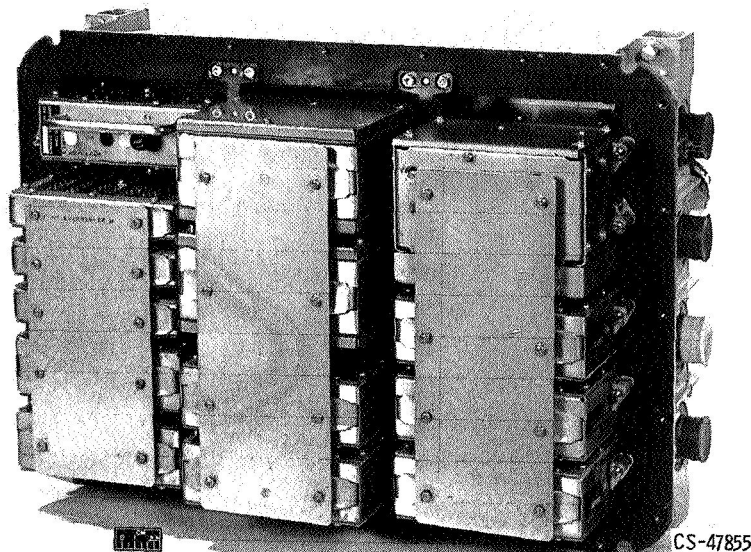
Figure 5-9. - Atlas flight programmer.

CS-47855

5.20.3 ... AT FIRST STAGE VEHICLE POWER PANEL.   E850

                    *****CAUTION*****   E860

                    DC POWER MUST BE APPLIED PRIOR TO AC   E870
                    POWER.   E880

        A. POSITION DC POWER SWITCH ON.   E890

            1. (DC POWER ON) INDICATOR ILLUM GREEN.   E900

            2. (DC POWER OFF) INDICATOR EXTINGUISHED.   E910

                                    CENTAUR TEST PROCEDURE

                                    AY66-0534-009-13D

                                    22 SEP 67   019

7.   POST TEST OPERATIONS   1270

7.1   --- SHUTDOWN   1280

7.1.1   /// PERFORM FIRST STAGE AIRBORNE POWER SHUTDOWN AS FOLLOWS: 1290

        ... A. TURN OFF GYRO POWER TEST BOX LOCATED IN THE BOOSTER   1300
               POD. RECORD TIME OF DAY ----------.   1310

                    *****CAUTION*****   1320

                    AC POWER MUST BE REMOVED PRIOR TO DC POWER.   1330

        ... B. TURN PROGRAMMER POWER TEST BOX SWITCH TO ''OFF''   1340
               (LOCATED IN BOOSTER POD) RECORD TIME OF DAY--------.   1350

        ... C. PLACE 400 CYCLE POWER SWITCH (S-4) TO THE OFF   1360
               POSITION (2072).   1370

Figure 5-10. - Sections of checkout sheet.
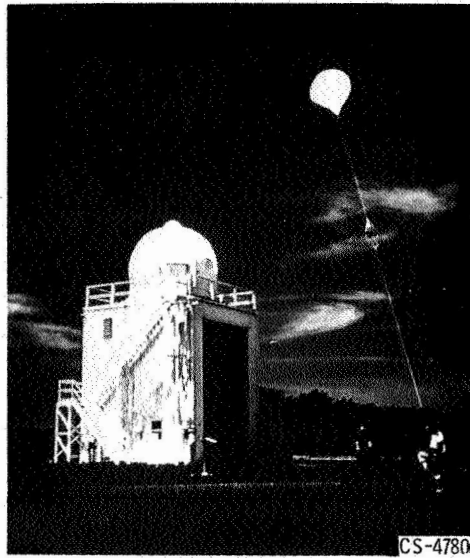
Figure 5-11. - Moment of release of radiosonde balloon.
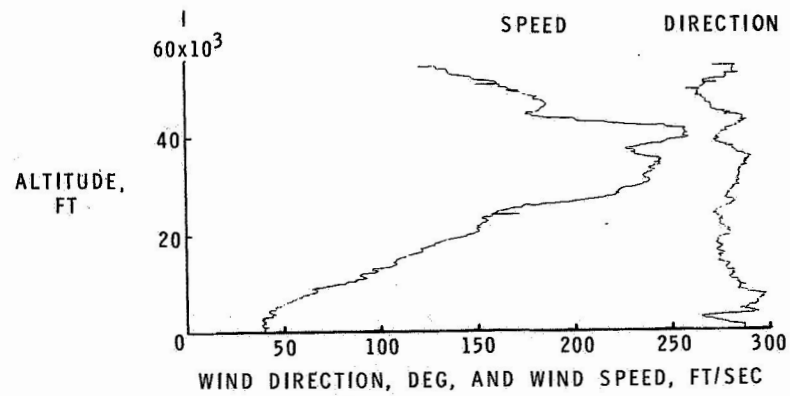
Figure 5-12. - Wind direction and speed as functions of altitude.

170
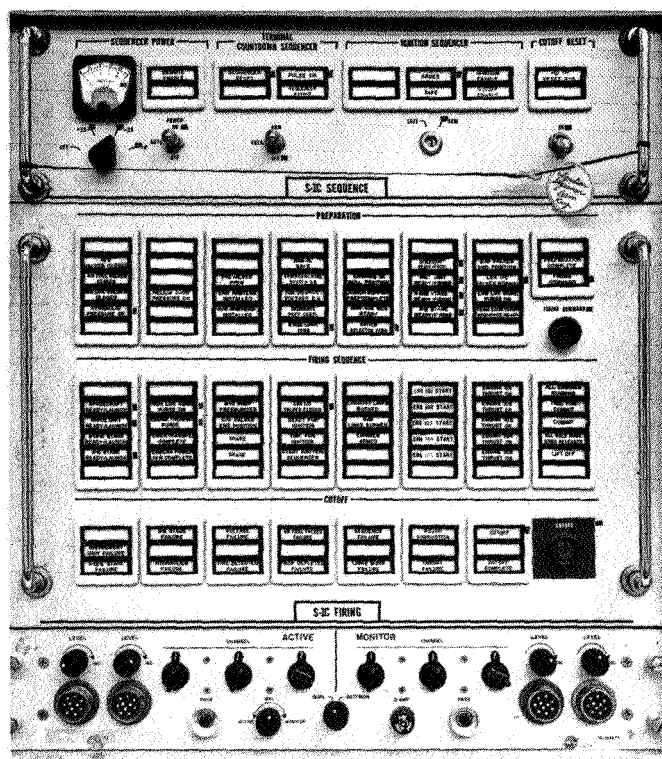
Figure 5-13. - Launch director's countdown panel.

6. INSTRUMENTATION

Isidore Warshawsky

An industrial power generating and transmitting system uses a variety of instrumentation to monitor and control the system. The principal demands made on the instrumentation system are that there exist a proper balance between accuracy and reliability and an adequate capacity for growth to accommodate future needs.

The means for meeting these demands are hardware, operational techniques, and the systems management that blends all ingredients into a consistent, effective instrumentation system. The hardware comprises tangible items like sensors, recorders, and intermediate components. The operational techniques include not only the installation and use of the hardware, but also the manipulation, analysis, and interpretation of the data.

A great amount and variety of instrument hardware already exists to form the building blocks of any instrumentation system. The Transducer Compendium published by the Instrument Society of America (ISA) lists over a thousand models of commercially available sensors. A commercial directory of electronic instruments lists over 10 000 models of instruments other than sensors. Consequently, modern industrial and aerospace instrumentation development is concerned even more with new techniques of using existing hardware - and of improving old techniques - than with hardware development. Nevertheless, both hardware and techniques are subjects of current research. This paper will give some specific examples of both. These examples are sometimes relevant to the advanced concepts presented in other papers of this conference and sometimes relevant to present-day systems. Some criteria for effective instrument systems management will also be discussed.

SENSORS, TECHNIQUES, AND THEIR COMBINATIONS

Liquid-Metal Pressure Measurement

A majority of the more than 300 pressure transducers listed in the ISA compendium are of the aerospace type. Some of the distinctive characteristics found in these are

(1) small size (e.g., 3- or 6-mm diameter cylinders; 1-mm thick disk)

(2) high output (e.g., 5 V because of built-in amplifiers or because of rheostat-potentiometer design)

(3) vibration resistance

(4) nuclear-radiation resistance

(5) 250° C ($\sim 500^{\circ}$ F) operation

Several of these characteristics may sometimes be found in the same sensor.

Some of the transducers capable of operating at 250° C may be used to measure gage, absolute, or differential pressure in a liquid-metal system. The manner in which one leg of such a transducer might be connected to a pipe containing liquid metal is shown in figure 6-1. Connecting tubes slope for drainage. Heaters are used to preheat the system in preparation for receiving the metal and for keeping it liquid thereafter.

When the liquid is sodium or a sodium alloy, the oxide of sodium tends to collect as a precipitate in the coolest part of the system. In order to prevent such precipitation from clogging the connecting tubing, a trap is provided and cooled as shown in the figure, so that the oxide will preferentially collect in the trap, where it may be drained off occasionally.

Transducers operating continuously at elevated temperature may suffer a zero shift of a few percent in a few months. If such shift exists and is intolerable and if periodic recheck of the zero is impossible, one of the arrangements shown in figure 6-2 may be preferred. Here, the transducer is at room temperature, and a slack diaphragm, operating at elevated temperature, isolates the liquid metal. The slack diaphragm transmits pressure or force with negligible resistance. In figure 6-2(a), pressure is transmitted through a NaK eutectic which remains liquid even at room temperature. This eutectic completely fills the volume between the slack diaphragm and the spring diaphragm of the transducer. Such a pressure-measuring assembly, although bulky and expensive, has proved accurate and reliable. In figure 6-2(b), force is transmitted to the tranducer spring through a long stainless-steel rod or tube, which is gas cooled to sustain the temperature gradient. Both of the arrangements shown in figure 6-2 are available commercially.

NASA-Lewis experience is now sufficient to ensure reliability of construction of systems like those shown in figures 6-1 and 6-2. This reliability derives from the ability to maintain adequate purity of the liquids, the containment material, and the purging and cover gases, and to make reliable welds without introducing oxygen contamination.

Electromagnetic Flow Metering

The electromagnetic flowmeter's advantages of obstructionless flow and negligible pressure loss favor it for liquid-metal flow measurement. The principle of the flowmeter (fig. 6-3(a)) is Faraday's Law, which states that, when a material flows at velocity V transverse to a magnetic field of flux density B, a potential gradient E/L is generated that is proportional to the vector cross product of B and V.

Flowmeters based on this principle have been used in oceanography, medicine, and rocket research. Flowmeters are currently available commercially, from many suppliers, for measuring the flow of weak or strong electrolytes. Pipe sizes range from 3 millimeters to over 1 meter. The standard units use a 60-hertz magnetic field in order to suppress polarization voltages at the electrodes. The conventional configuration is that of figure 6-3(c), wherein two metallic pins project through the wall of an insulating pipe to serve as electrodes; the leads from these pins must be dressed very carefully and symmetrically in order to prevent hum pickup that might otherwise obscure the Faraday effect signal.

In a liquid-metal application, there is no polarization; hence, a dc magnetic field may be used with a permanent magnet as a convenient source, and careful dressing of leads is not required. Figure 6-4 shows such a flowmeter. It is of 1/2-inch size, with a swaged guard heater to prepare it for accepting the metal and keeping it liquid thereafter. The large-diameter enclosures around the central tube are thermal insulation.

Two unusual consequences result from the high electrical conductivity of liquid sodium or potassium. First, the containment tube may be made of stainless steel, with electrode leads welded to the outside of the tube, thus maintaining high mechanical reliability (fig. 6-3(b)). The correction to the basic Faraday Law formula for the nonzero conductivity of the stainless steel is known accurately. Second, circulating fluid currents are induced, of the form shown in figure 6-3(b), that destroy the axial symmetry of velocity on which the basic formula is predicated. The resultant error may be as high as 4 percent, in a practical case; however, under a recent NASA-university contract, the error has been computed well enough so that resultant inaccuracy after the correction has been applied is less than 1 percent. After adding errors from other sources, the overall probable error of flow measurement may be no more than 2 percent.

The flowmeter may also be used with nonpolar, nonconducting fluids if the magnetic field is of relatively high frequency, say, 1 to 10 kilohertz, and the electrodes are capacitor plates (fig. 6-3(d)). The flow of lubricating and transformer oils has been measured successfully; commercial meters for this purpose may be available in another year. An NASA contract for developing a similar flowmeter for liquid

hydrogen has already produced a prototype that confirms the feasibility of such a measurement.

Temperature Measurement by Infrared Radiation

The development of infrared-sensitive devices, stimulated largely by military interest over the past 25 years, has resulted in many diverse applications of infrared photography and radiometry. Thus, infrared photographs from a satellite have distinguished over a dozen different types of vegetation and crops, and an aerial photograph of a citrus orchard can distinguish between healthy trees and those infected with insect scale, because the latter trees appear darker. In medicine, local regions of infection near the surface of the body are revealed by infrared photography because such infected regions are slightly warmer. The U. S. Air Force, in its research on arctic clothing, has taken time-lapse photographs of a man entering a refrigerated chamber, to observe the relative rates of cooling of different parts of the body. Such photographs confirm that skin areas of reduced circulation, like those covering most bony surfaces, are the first to feel the chill.

Boiler inspection. - Figure 6-5 shows the side of a boiler, including a door, as photographed by ordinary light and by infrared. A suspected heat leak around the edge of the door was confirmed by the infrared photograph, which showed a leak at the left edge of the door, but the photograph also revealed that the insulation behind an adjacent wall panel had failed. Such an advance finding reduced the subsequent downtime when the boiler was shut down for maintenance. Temperatures of some of the surfaces may be estimated by comparing image brightness in the infrared photograph with the brightness of the rectangles that appear in the strip at the top of that photograph. These rectangles represent strips of metal held at known temperature; in this photograph, the temperatures range between 60° and 250° C (140° and 500° F).

Jet-engine-turbine pyrometry. - Figure 6-6 shows a jet-engine turbine-rotor-blade pyrometer for flight use. This instrument, developed in England, uses a silicon photocell, may be fuel-cooled or air-cooled, is temperature compensated and vibration resistant, and has successfully undergone over 300 hours of actual engine operation.

The method of installation is shown in figure 6-7. The instrument sights between the stator blades, at an area on the rotor blade that is about 1 centimeter in diameter and about halfway between root and tip of the blade. Location and size of the area of view may be altered by changing the angle of sight or the viewing distance, respectively. However, the direction of sight is always controlled so that the

176

instrument may not see past the rotor. Thus, the photocell output represents some average temperature of the blade surfaces passing the line of sight. The photocell output more nearly represents actual blade temperature because (1) the space between adjacent stator blades resembles a blackbody cavity to a modest degree and (2) the spectral bandwidth of effective radiation is quite narrow because of the photocell's spectral characteristic; thereby, the dependence of radiant flux on blade-surface emittance is minimized.

The photocell can respond to radiation in only a few microseconds. Consequently, the passage of a single overheated blade is detectable, in laboratory tests, when photocell output is observed on a synchronized oscilloscope. This feature is useful in turbine-cooling research, where a rotor may contain only a few special test blades.

Mapping of blade temperature distribution. - At Lewis, NASA has used infrared to map temperature distribution on the surface of a stationary turbine blade under test in a high-temperature wind tunnel. As indicated in figure 6-8, the surface is photographed on infrared-sensitive film. Hotter areas produce brighter images, but the association of image brightness (more accurately, photographic-image density) with actual temperature requires several intermediate steps. Image density depends on the photographic-development process and on the intensity of radiation emitted by the surface. The latter quantity, for a surface of given temperature, depends on the emittance of the surface which, in turn, is determined by

(1) surface material

(2) surface roughness

(3) surface geometry

(The intensity of radiation also depends on the geometry and emittances of contiguous surfaces, but their effects can be made small in these controlled experiments.) Dependence on emittance may be minimized by using a narrow spectral bandwidth. The filter (fig. 6-8) and the spectral limitation of the infrared-sensitive film itself together define the upper and lower limits of the spectral band that provides the best compromise between sensitivity and emittance dependance. Thereby, a 10-percent uncertainty in emittance produces less than 1-percent uncertainty in temperature.

The more direct way to allow for the photographic development process is shown at the bottom of figure 6-8. A strip of turbine-blade material, of uniform cross section, is clamped between two massive blocks at known temperatures T_1 and T_2. Then, there is a linear temperature gradient in the strip. If photographs of this strip and of the blade under observation are taken on similar pieces of film, and both photographs are processed through the same developer at the same time, a match of optical densities on the two pieces of film will yield the corresponding temperatures.

A less direct, but more convenient and more accurate method of allowing for the photographic development process is shown in the middle view in figure 6-8. This method does not require the construction and maintenance of a heated temperature standard. In this alternative approach, a commercially available film strip, divided into areas of progressively higher transparency, is photographed while uniformly illuminated as shown in the figure. The relative transparencies of the areas are known accurately; hence, the relative intensities of radiation forming the photographic image are also known accurately. If photographs of the blade and the illuminated strip are taken on the same roll of film and then developed together, a match of densities on the two photographs yields the corresponding relative intensities of radiation emitted from various areas of the test blade. To obtain the final conversion to absolute temperature, a single thermocouple is installed at one point on the blade. The actual temperature corresponding to the photographic density at this point now being known, the temperatures corresponding to other densities also become known.

Figure 6-9 contains photographs of a typical heated blade and of a calibrating strip. The installed thermocouple may also be seen (there are several in the photograph, but only one is relevant to the present discussion). Since figure 6-9 represents a photographic negative, blacker areas represent hotter areas.

The corresponding contour lines of constant density are shown in figure 6-10, as well as the approximate values of corresponding temperature. The detailed interpretation of all that appears in figure 6-10 is beyond the scope of this paper; it suffices to note that, after the successive conversion from relative photographic density, to relative radiant intensity, to relative temperature (from Planck's radiation law), to absolute temperature, temperature differences of 10° F ($\sim 5^{\circ}$ C) are detectable.

To measure temperature of a moving rotor blade rather than of a stationary one, the camera of figure 6-9 is replaced by an image converter tube, as shown in figure 6-11. These tubes are similar to those used in military sniperscopes or snooperscopes. Since their operation depends on the presence of certain electrode voltages, the application of these voltages may be synchronized with the passage of a rotor blade past a fixed point on the turbine casing, to provide a stroboscopic effect. The image formed by the image converter tube may be photographed with an ordinary camera. The same image converter must be used to observe any calibration standards used. This technique is currently under development at Lewis and has not yet been proved to yield accuracies or sensitivities commensurate with those obtained by direct photography of stationary blades.

The problem of rotor-blade temperature measurement will be treated later, in the section Rotating-Shaft Data Transmission.

Potential Applications. - The availability of image converters suggests other applications of infrared. Observation with a snooperscope in the field might permit visual detection of overheated components of generating or distribution equipment. Figure 6-12, although taken directly with an infrared camera rather than through a snooperscope, illustrates such a potential application. Three distribution transformers on a utility pole are shown to be equally loaded. The low-voltage feeder from them is also noticeable. The utility pole also appears warm because it has been heated by sunlight and because its infrared emittance and absorptance are very high. Comparison with the reference scale at the top of the photograph would confirm that the transformers are operating within acceptable temperature limits. However, such a scale, calibrated to simulate metal objects, would ordinarily not be quantitatively correct for nonmetallic materials of considerably higher emittance.

Rotating-Shaft Torque Measurement

Research on high-speed pumps and turbines for cryogenic liquids has required the development of a shaft torquemeter capable of operating at shaft speeds up to 50 000 rpm. The optical torquemeter developed for this purpose obviously has wider application than this original use.

As shown in figure 6-13, a special torsional spring element is fabricated in the form of a shaft with polished reflecting surfaces at each end. An even number of surfaces is generally used at each end, to facilitate mechanical balance. A stationary optical unit measures twist of the shaft, independent of moderate translation between the stationary unit and the rotating shaft.

The optical system projects the illuminated image of a slit, by successive reflection from each of the reflecting surfaces on the shaft, on to two photocells separated by a hairline gap. Shaft twist produces unbalanced illumination on the two photocells. A servomechanism thereupon repositions the photocells to restore the null-balance condition. Photocell position is a measure of shaft twist.

If a laser is used as the slit illuminant, the resultant higher intrinsic slit brightness, with its consequent higher signal-to-noise ratio, yields higher accuracy.

Figure 6-14 shows torquemeter shafts having full-scale ranges of 2, 400, and 1200 foot-pounds, respectively. Inaccuracies of one percent or less have been obtained regularly.

When a very large shaft is involved, the manufacture of a special torsional element with its reflectors becomes very expensive. The alternative arrangement shown in figure 6-15 may then be usable. If a shaft is already available that is operating well within its proportional limit, so that it is a good spring, and if several

diameters of straight length of shaft are accessible, separate rings carrying mirrors may be clamped on to the shaft. Each ring is split and doweled to permit its installation without dismantling the machine. Diameters must be matched and concentricities maintained well enough to assure accurate balance. The distance between clamping planes constitutes the "gage length" of the spring. Calibration may be computed if shaft dimensions and shear modulus are known accurately enough. Otherwise, empirical calibration must be performed by clamping the shaft well outside the gage length and applying a known torque with hydraulic pistons; this torque need be only a small fraction of full-scale torque if the shaft is used well below its proportional limit and if there is adequate sensitivity.

Computations indicate that this sensitivity requirement can be met if a laser illuminant is used and if there is a multiplicity of mirrors, as shown in figure 6-15. A further advantage of using many mirrors is that standing torsional oscillations are averaged.

Bulk-Velocity Measurement with Pitot Tubes

This section will present a number of techniques associated with the application of the pitot tube to the measurement of bulk velocity in ducts or pipes. The techniques are not necessarily related; in fact, some are contradictory, but each is useful on some occasion.

Velocity measurement in smooth pipes. - The bulk velocity of a fluid flowing through a long, straight, round pipe with smooth walls may be deduced from a single measurement of linear velocity at the center of the pipe, as may be provided with the pitot tube shown in figure 6-16, because the velocity profile is well defined. The dependence on Reynolds number is no stronger than that of an orifice or venturi, but the pitot tube provides the advantages of smaller expense, negligible pressure loss, and freedom from the need for maintaining sharp edges or very clean surfaces. If line pressure is high, conventional engineering practice will lead to a correspondingly high differential pressure; then, if the fluid is primarily gaseous, even the presence of small amounts of liquid in the pressure line will not affect the differential-pressure measurement appreciably.

The static-pressure tap is a more likely source of error than the total-head tube. The tap in the side wall must be accurately flush and square, the wall itself must be smooth, and there must be no downstream obstruction nearby; the pitot tube is shown cantilevered for this last reason, although the supporting strut could have extended across the pipe if the wall tap had been located 90° away from the plane of section.

Velocity measurement in large ducts. - Bulk velocity in a duct so large that the velocity profile is uncertain and use of an orifice is uneconomical may be obtained by integration over the cross section. The pitot tube of figure 6-16 may be traversed continuously across the duct. Alternatively, a fixed rake of appropriately located pitot tubes may be installed, so that the sum of the total-head readings will yield the bulk velocity (fig. 6-17). In the latter case, the summation may be performed automatically if each total-head tube is connected through an identical flow impedance to a common plenum. The flow impedance, as shown in the detailed sketch of figure 6-17, might be a capillary 1/2 millimeter in diameter by 1/2 meter long. Identity of all impedances may be assured by cutting all the individual capillaries from the same piece of capillary tubing and locating all impedances at the same place so that they will all be at the same temperature. Danger of clogging the capillaries is minimized if the following conditions are met: (1) entrance ends of the capillaries are shaped to promote inertial separation of occasional droplets or solid particles, (2) capillaries are located at the common-plenum end of the connecting tubes, (3) these tubes are relatively long and of comparatively large diameter, (4) rates of increase of line pressure and velocity head are slow enough that entrainment velocities are low. Obviously, however, the capillaries cannot be used in an intrinsically dirty fluid.

The associated static-pressure measurement may use one of the techniques shown in figure 6-18. The more straightforward approach is to install a wall tap at 90° from the line of total-head tubes and in the plane of their mouths (fig. 6-18(b)). This approach may fail if the duct wall is so rough that one of the conditions for reliable static-pressure measurement is violated. Then, the necessary alternative is to mount a static-pressure measuring probe on the strut carrying the total-head probes (fig. 6-18(a)). This probe may be on the centerline of the duct, with static-pressure sensing holes on the side of the probe, in the plane of the mouths of the total-head tubes. The distance from this plane to the leading edge of the supporting strut should be greater, in this case, than would be necessary in the case of figure 6-18(b), in order to minimize the interfering effect of the strut. Nevertheless, this interference is appreciable and must be corrected for. The magnitude of the correction was determined at this Center many years ago and is known with sufficient accuracy to permit reliable bulk velocity measurement.

Inertial separation of droplets. - Figure 6-19(a) illustrates how total pressure may be measured in a gas stream containing entrained droplets of liquid and how clogging of the connecting tube may be avoided. This connecting tube extends downward into the pitot tube and is beveled to minimize droplet adhesion. The higher inertia of the droplets causes them to impinge on the rear surface where they are decelerated and drain through the bleed hole. This principle is used in all airspeed

heads for airplanes, which, of course, must fly through rain.

Figure 6-19(b) shows how placing the static-pressure-sensing holes behind a step may promote inertial separation of droplets. The presence of the step causes an appreciable error in static-pressure indication, but this error is reproducible, may be determined by calibration, and hence may be applied as a correction. This technique has been used in our icing-research measurements.

Measurement when particulate matter is present. - No always-reliable method exists for pressure measurement in a "dirty" gas stream. However, the following expedients have been helpful at one time or another.

(1) In applications where only an occasional measurement is required (e.g., a 10-sec reading every 10 min), a probe may be retracted for the time between readings, or else shielded against impact of the fluid.

(2) Using a probe of maximum tolerable diameter may reduce the frequency with which it must be cleaned.

(3) A flush-diaphragm miniature pickup may be mounted at the mouth of a total-head tube, or flush with the pipe wall to measure static pressure, provided ambient temperature conditions permit such installations. In total-head measurement, there should be sufficient overrange capability to handle an occasional particle of above-average kinetic energy. Build-up of dry particles at the nose ordinarily will not appreciably affect the integration of total pressure unless cementing occurs, so that diaphragm stiffness is altered.

(4) Reverse flushing with clean gas, often suggested, is ineffective unless the flushing gas is moving at high velocity. Elaborate precautions are required to prevent damaging the transducer during the flushing operation. This technique is applicable when sampling is acceptable, as in expedient (1).

Integration by Sampling

The technique to be discussed in this section is applicable to the integration of any physical quantity, such as pressure, temperature, flowrate, or composition, over an area of any shape. However, to simplify the discussion, it will be assumed specifically that the average pressure over a circular area is to be determined with an integrating rake like that in figure 6-17.

In order that the sum of the pressures measured by the individual tubes shall yield the average pressure, conventional mechanical engineering practice has been to divide the circular area into annuli of equal area and to locate a sampling probe at the center of gravity of each annulus (fig. 6-20(a)). If three stations are used on each side of the centerline, the error in average pressure yielded by summing the

individual readings will be from 1 to 3 percent, depending on the shape of the pressure profile.

The error would be reduced if the pressures were plotted against radius, a smooth curve drawn through the points, and the integral corresponding to this curve then determined (fig. 6-20(b)). This error would be smaller than that produced by the bar-graph summation of figure 6-20(a) because an additional item of intelligence is used: that the pressure distribution is smooth.

The operations of curve drawing and integration need not be performed literally, because a mathematically identical result can be performed by the mere addition of pressure readings, as in the original procedure, provided the measuring stations are at locations slightly different from those of figure 6-20(a). These revised locations are listed in table 6-I.

This integration technique is termed Chebyshev integration. It generally produces an error less than one tenth of the error obtained with the centroid-of-equal-areas method.

Rate Indication

In some engineering operations, knowledge of the rate of change of a physical quantity is even more important than knowledge of the absolute value of that quantity. Direct measurement and indication of this rate is then desirable. For specificity, assume that the rate of rise of turbine-nozzle-block temperature is to be monitored during turbine startup. If the temperature sensor is a thermocouple or resistance thermometer bulb, its output may be delivered to a resistance-capacitance differentiating network (fig. 6-21(a)) or to a resistance-inductance differentiating network. In the latter case, the inductor may be the primary of a step-up transformer, as in figure 6-21(b); the output voltage is thereby increased, but at the expense of a higher output impedance. Either circuit requires an amplifier of constant gain, because available output power is low. A further improvement is therefore achieved by using an operational amplifier, as in figure 6-21(c), so that amplifier gain stability is not required. The circuit of figure 6-21(c) uses the same differentiating components, R and C, as that of figure 6-21(a). However, if the rate of change of input voltage is very low, an additional resistor R' and capacitor C' must be included to inhibit the ability to differentiate higher-frequency components, such as powerline hum, whose derivative would otherwise mask the rate indication of interest.

Using resistors, capacitors, and an amplifier of sufficiently high quality, a rate of change of temperature of 200° C per hour may be measured reliably.

Time-Lag Compensation

The circuits of figure 6-21 are readily converted to lag-compensating circuits (fig. 6-22) by providing a dc path that adds the input signal to the derivative signal in appropriate proportions. Such lag compensation is particularly useful in control applications because it helps to avoid overshoot of the variable being controlled.

Time lag compensation concepts are illustrated in figure 6-23. Again, for specificity, the variable will be assumed to be temperature, because long time lag is most commonly associated with this variable.

If an abrupt, step-like change in temperature, shown by the heavy line, is imposed on a thermally massive object, the temperature of the object will rise slowly, as shown by the curve marked "original". A tangent to this curve at the origin will intersect the asymptote of the curve at a time termed the "thermal time constant" of the object.

Interposition of a lag-compensating circuit between sensor output and indicator will result in an indication that follows the curve marked "compensated", which has an equivalent time constant considerably shorter than that of the original object. Proper compensation is achieved when the electrical time constant of the basic differentiating network of figure 6-21, as used in figure 6-22, is equal to the thermal time constant of the object.

If electrical and thermal time constants are not matched, undercompensated or overcompensated responses are obtained, as shown by the dashed curves of figure 6-23. In either case, there is an improvement in response. However, in some control applications it may be necessary to avoid the overshoot associated with the overcompensated case.

Reductions in response time of 10 to 100 times have been obtained routinely. Principal applications have been in thermometry and hot-wire anemometry.

Rotating-Shaft Data Transmission

The transmission of electrical signals to and from rotating members has conventionally been performed through slip rings. This approach is troublesome where a high-speed system like a jet engine rotor is being studied, because considerable maintenance and careful manipulation are required to assure reliability. NASA-Lewis currently is developing an alternative telemetering approach; it is illustrated in figure 6-24.

Thermocouple leads from the turbine rotor are run radially to the center of the shaft, which is hollow, and then to the front end of the shaft. Pressure taps on the

compressor rotor are connected by radial tubes to miniature transducers mounted near the center of the shaft, and the electrical leads are also run to the front end of the shaft; the electrical-signal transmitting unit is mounted here because this region may be kept cool with relative ease.

Electrical signals are transmitted through a standard commercial rotating transformer. This unit has several pairs of stator and rotor windings that act like primary and secondary windings of a transformer. Each pair of windings is electrically and magnetically isolated from the others. Signals from 100 hertz to 1 megahertz can be transmitted with negligible modulation at the frequency of shaft rotation. The ball-bearing-supported rotor is coaxial with the main engine shaft and rigidly attached to it; only two semiflexible arms, attached to the engine nacelle and the stator casing, are needed to keep the latter from rotating.

An assembly of four printed-circuit boards, contained in a 10-centimeter-diameter by 10-centimeter-long can, is attached to the rotor and turns with it. This assembly contains solid-state circuitry for switching electrical signals, amplifying them, and converting them into digital form.

The block diagram of the system is shown in figure 6-25. Power enters through one channel of the rotating transformer in the form of 10-kilohertz square waves. This frequency is also used to define the clock frequency for the subsequent digitization. The incoming power is changed on a power converter board into dc power for operating the electronics and the pressure transducers. Outputs from the pressure transducers and thermocouples pass to a multiplexer board, which acts as a 2-pole, 36-position switch. Channel switching occurs 50 to 100 times per second. The multiplexer output is converted on a third board into a digitized, pulse-code-modulated form, leaving through a second channel of the rotating transformer as pulses of 5-volt amplitude. Effects of noise and hum at the output are therefore negligible.

Figure 6-26 shows the system hardware. The rotating transformer is at the center of the photograph. Clockwise from the upper left-hand corner are the power-converter, multiplexer, and digitizer boards, and a board containing amplifiers and other circuitry for controlling the sequence of electronic operations. Although individual components have been proved to operate satisfactorily at rotational speeds corresponding to 10 000 g at the rim of the boards, the assembly of the prototype has not yet been completed. If environmental tests are passed, an inaccuracy of less than 0. 5 percent of full scale should be attained.

SYSTEMS MANAGEMENT

Effective instrument systems management starts in the conceptual stage of a new plant design with a definition of the ultimate goals of the system. This first step is also the one step that transcends any mathematical or mechanistic analysis because it requires knowledge of engineering, economics, and public relations, and relies on experience, imagination, and vision. It must be performed at the highest level of management.

Subsequent management steps involve the translation of the basic goals into a system of hardware and defined operational procedures that will provide adaptability to changing needs, capacity for growth, and acceptable accuracy and reliability.

The advance specification and provision of features that have only a modest probability of subsequent use may constitute a sound insurance investment against the risk of having to add such features after a machine is built. Similarly, the cost of initial installation of features that may permit later automatization may be only a small fraction of the cost of their subsequent installation. Examples related to material presented in this and the preceding two papers of these proceedings are
(1) specifying a hollow shaft for possible later installation of data transmission leads,
(2) providing sufficient straight length of coupling shaft to allow subsequent torque measurement, (3) inclusion of ports for later insertion of probes, sighting tubes, or other diagnostic devices, (4) provision of checking terminals and pressure ports, and (5) addition of duplicate connections or ports for subsequent redundant connections that may improve reliability or expedite automation.

After full definition of the techniques of using the designated hardware and facilities, procurement of hardware may be initiated. Such procurement requires that the user, rather than the supplier, have the responsibility for correct specification.

At this Center, for each hardware item, such as a transducer, the following steps are taken.

(1) Every relevant performance item is specified, by stating, for each item, the acceptable limit of error, and the exact test method that will be used for checking that item. Construction features that affect reliability are also specified in concrete terms of performance. No performance item is specified that cannot be checked.

(2) The specification on each item is realistic. A common check is that the specification on each item is met by at least two manufacturers with their standard advertised equipment. Performance is specified (as the user requires it) rather than design, which is best left to the manufacturer.

(3) Specifications are rigorous; highest quality of performance is required. The premium paid for this quality is negligible compared with the cost of losing a single run because of inferior quality.

186

(4) Once specifications are established, award is made to the lowest bidder who meets all specifications.

(5) Each item is inspected and tested for each performance item specified, except where there is strong statistical evidence that some test need be performed only on samples.

The specific performance items characterizing a differential-pressure transducer of the type used to measure fluid velocity in a pipe are shown in the following list:

Sensitivity accuracy at standard conditions Sensitivity change with temperature Sensitivity change with time Hysteresis at midscale Repeatability for unidirectional approach Nonlinearity	Zero adjustment reproducibility Zero shift with line pressure Zero shift with mounting strain Zero shift with acceleration Zero shift with temperature
Full-scale-output change with supply pressure Full-scale-output change with line voltage Full-scale-output change with acceleration	Zero shift after overrange Hysteresis at zero Zero drift with time Zero shift after cycling
Range Sensitivity (transduction factor) Overrange protection Maximum line pressure Maximum ambient temperature Minimum ambient temperature Weather protection Power supply (line) voltage Line frequency Power supply (input) pressure Mounting	Source impedance Load impedance effect Line resistance effect Insulation resistance to ground Common mode rejection
	Chamber volumes Chamber volume change for full-scale ΔP Damping Natural frequency
	Pressure connections Vent or bleed connections Filter Zero adjustment accessibility

A more general list of items that might be associated with the installation of such a transducer is

Channel identification	Positioning
Electrical continuity	Alinement
Electrical polarity	Vibration isolation
Insulation resistance	Strain relief
Line and connector resistance	Weatherproofing
Cable dressing	Nonflamability
Grounding	Heat dissipation
Electrostatic shielding	Materials compatibility
Electromagnetic shielding	Lubrication
Transposition	Internal cleanliness
Crosstalk	Pressure tightness
Shunt capacitance	Vacuum tightness
Impedance balance	Thermal insulation
Checking terminals	Accessibility for maintenance
	Isolation for inspection

For every hardware component, subsystem, and system, the operations of qualification and checkout, as discussed in depth in papers 4 and 5 of this conference, are essential to ensure reliability. Nor can this reliability be maintained unless there is periodic maintenance and recheck of all system elements.

Finally, continued maintenance of operating economy and retention of competitive advantages requires periodic review and updating, to take advantage of modern developments.

TABLE 6-I. - STATION LOCATIONS FOR

SMOOTHED AREAL AVERAGING

IN CIRCULAR DUCT

Number of stations along one radius	Radial locations, fraction of duct radius
2	0.4597, 0.8881
3	0.3827, 0.7071, 0.9239
4	0.3203, 0.6382, 0.7699, 0.9473
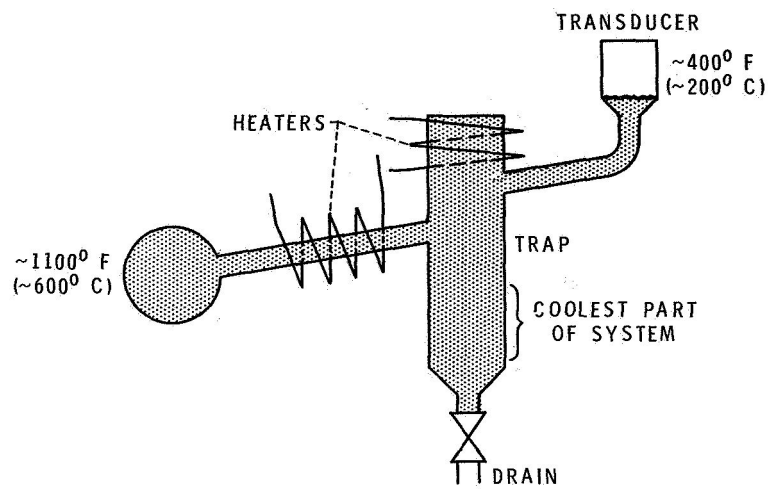
Figure 6-1. - Liquid-metal pressure measurement. Transducer at elevated temperature.
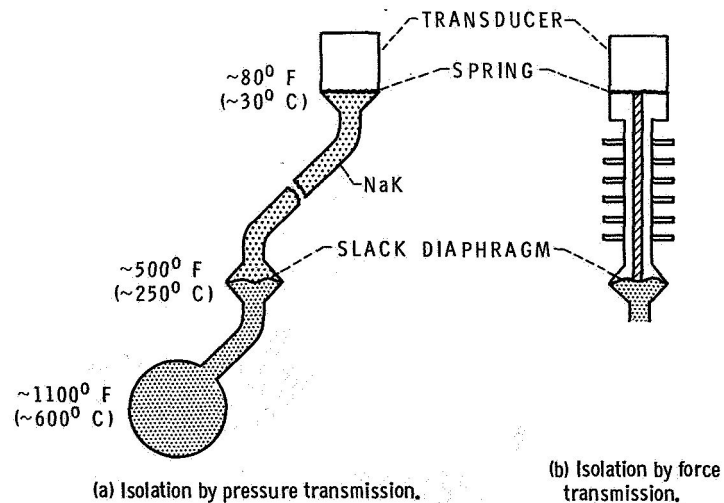
(a) Isolation by pressure transmission.

(b) Isolation by force transmission.

Figure 6-2. - Liquid-metal pressure measurement. Transducer at room temperature.

189

$$\frac{E}{L} \approx B \times V$$
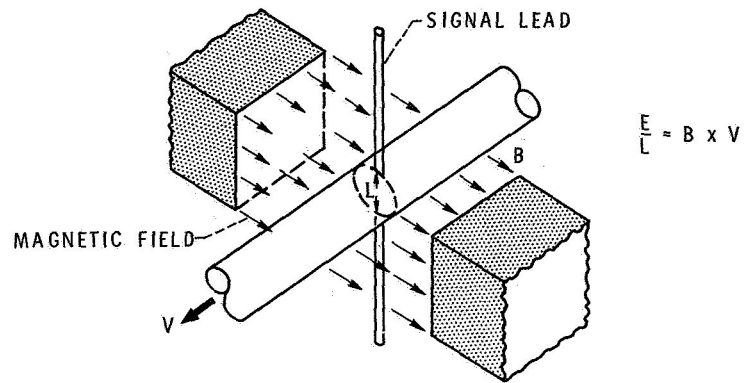
(a) Principle.
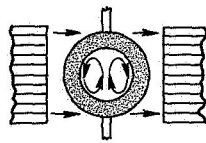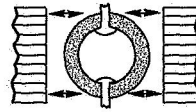
(b) Liquid metals.   (c) Electrolytes.   (d) Dielectric liquids.
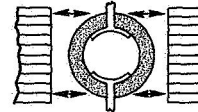
Figure 6-3. - Electromagnetic flowmeters.
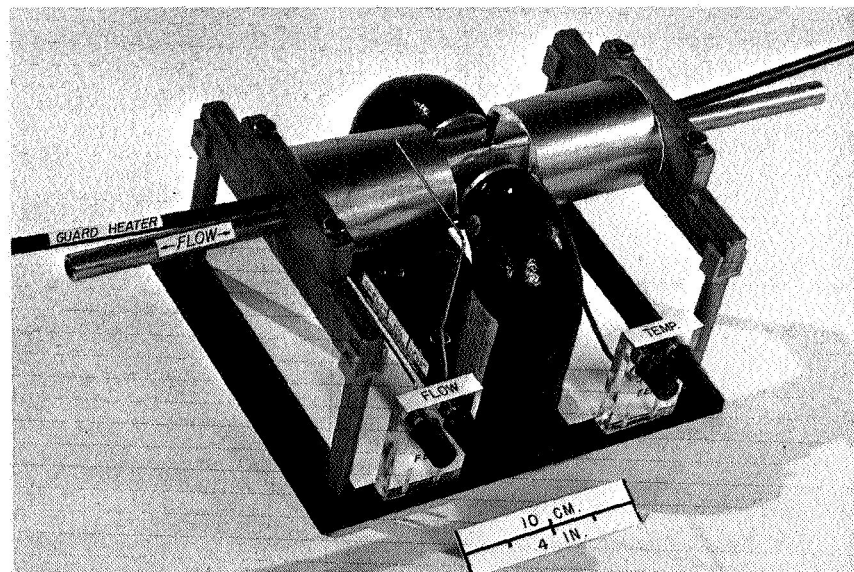
Figure 6-4. - Electromagnetic flowmeter for liquid metals.

CS-47662

190
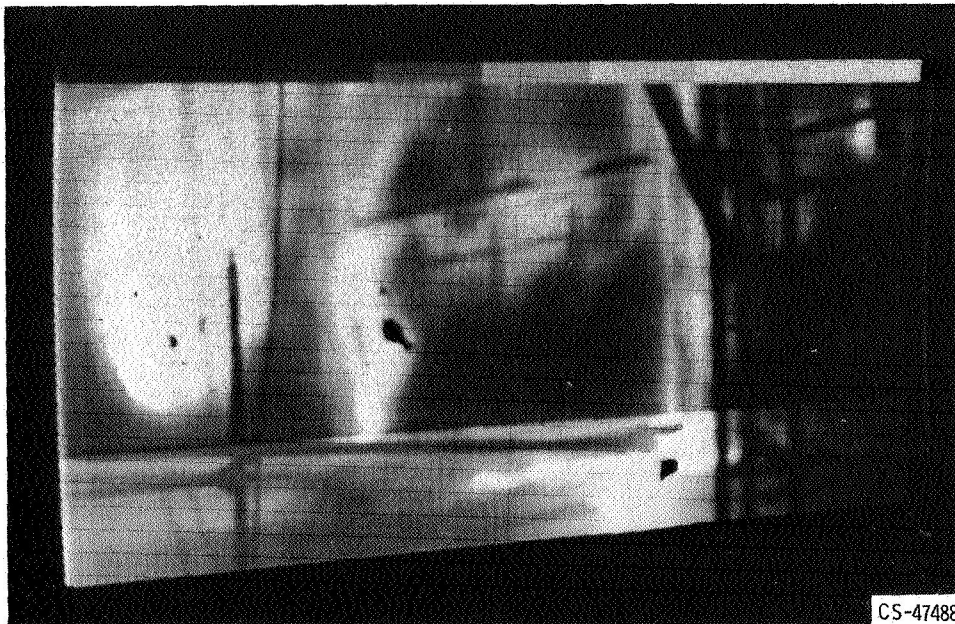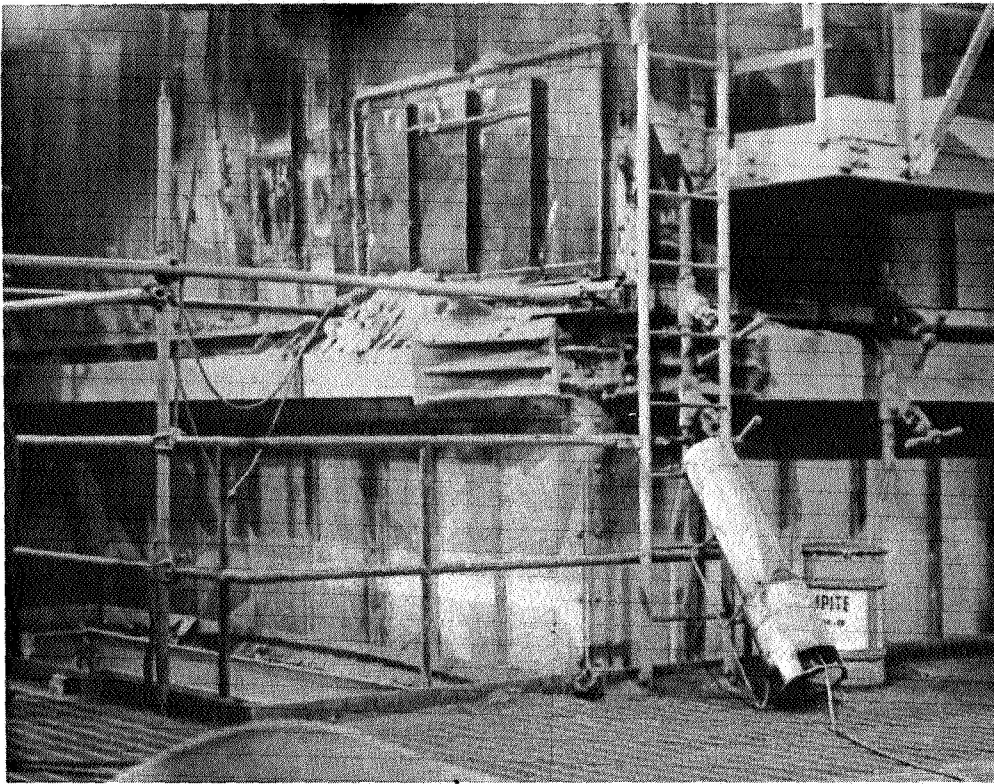
CS-47488

Figure 6-5. - Boiler door. Gray scale temperatures: 140^0, 160^0, 183^0, 214^0, 262^0, 300^0, 380^0, and 500^0 F. (Courtesy Barnes Engineering Co.)
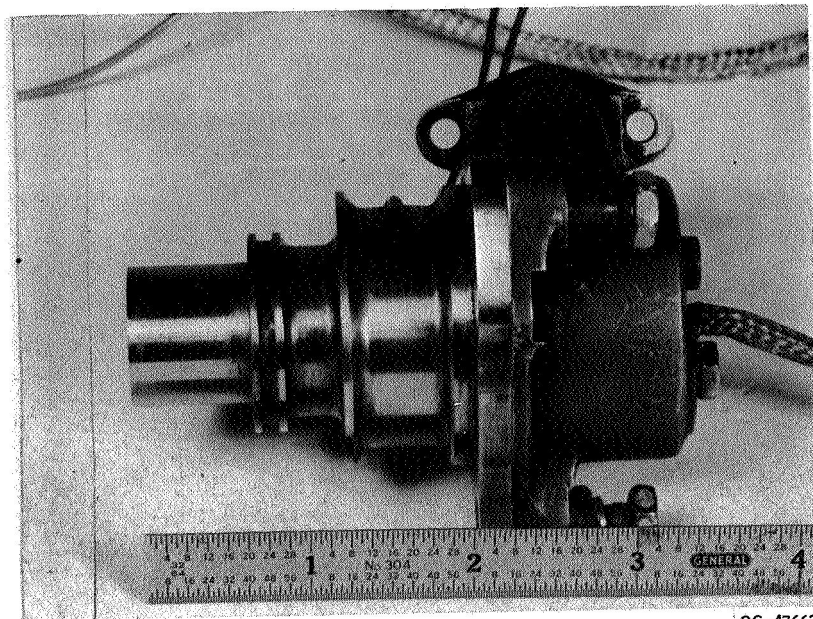
Figure 6-6. - Turbine-blade pyrometer for jet engine. (Courtesy Land/Electro-nite Co. and Rolls Royce, Ltd.)
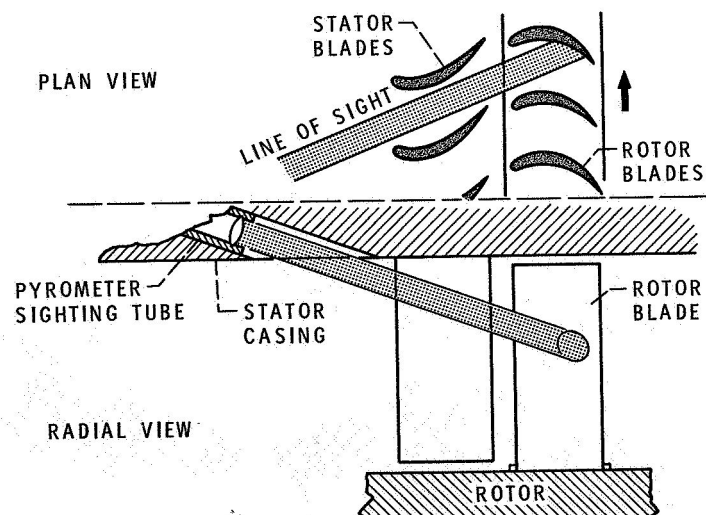
Figure 6-7. - Turbine-blade pyrometer installation.
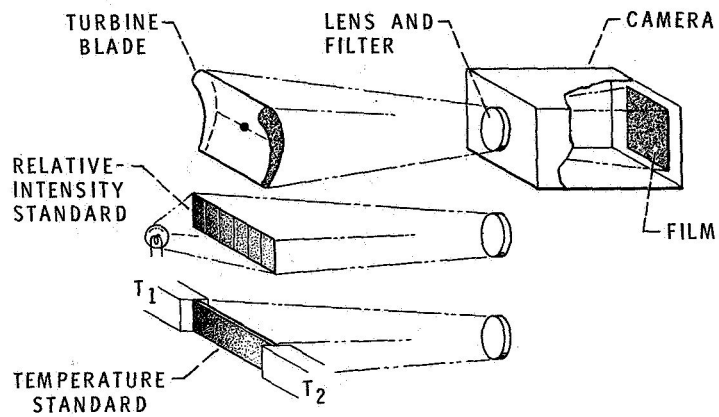
Figure 6-8. - Infrared temperature mapping. Stator blade.

CS-47393
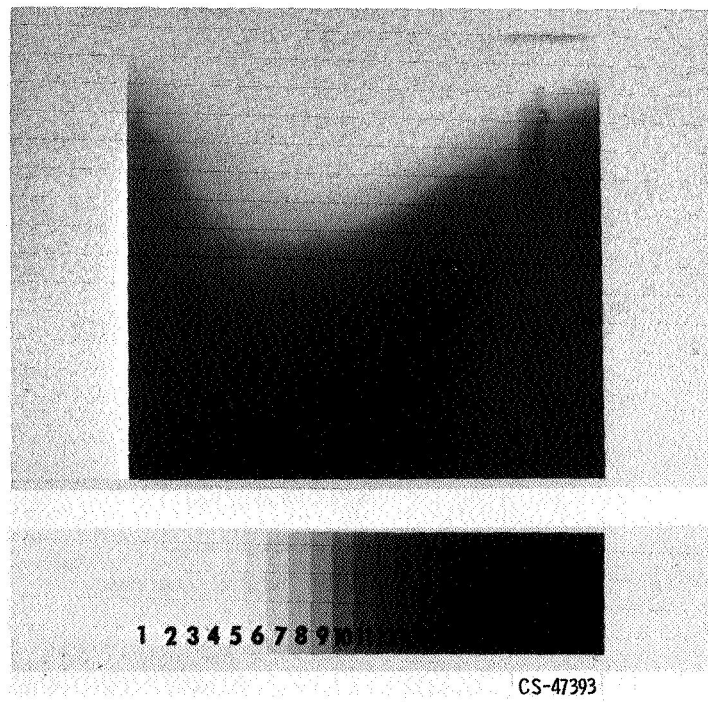
Figure 6-9. - Heated blade and relative intensity standard.
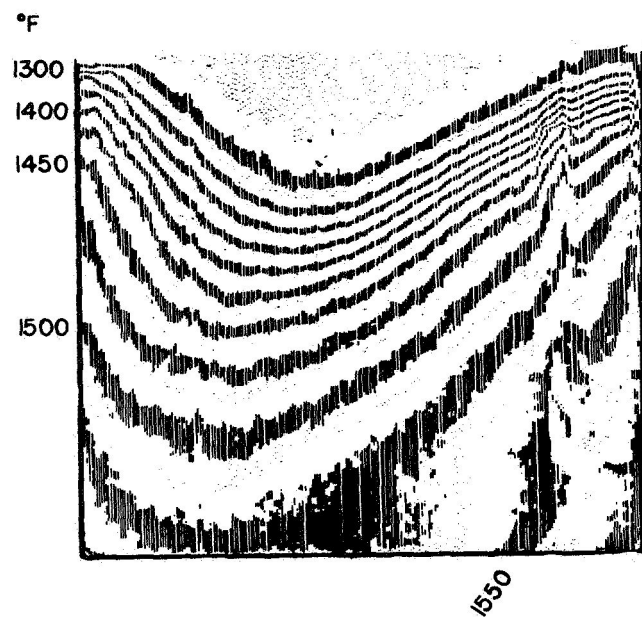
Figure 6-10. – Temperature contours on heated blade.
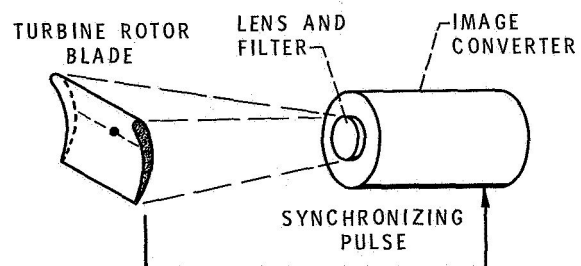
Figure 6-11. – Infrared temperature mapping. Rotor blade.
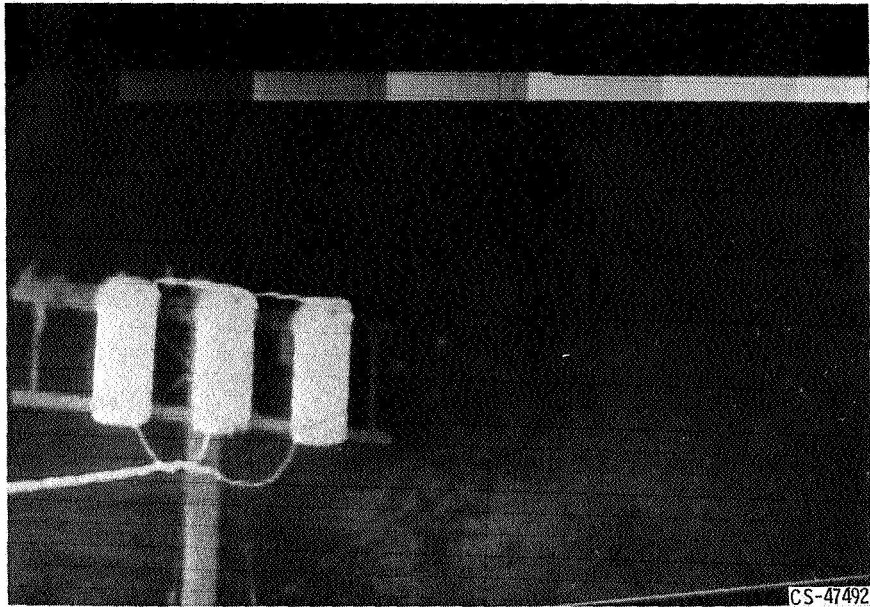
Figure 6-12. - Distribution transformers. (Courtesy Barnes Engineering Co.)
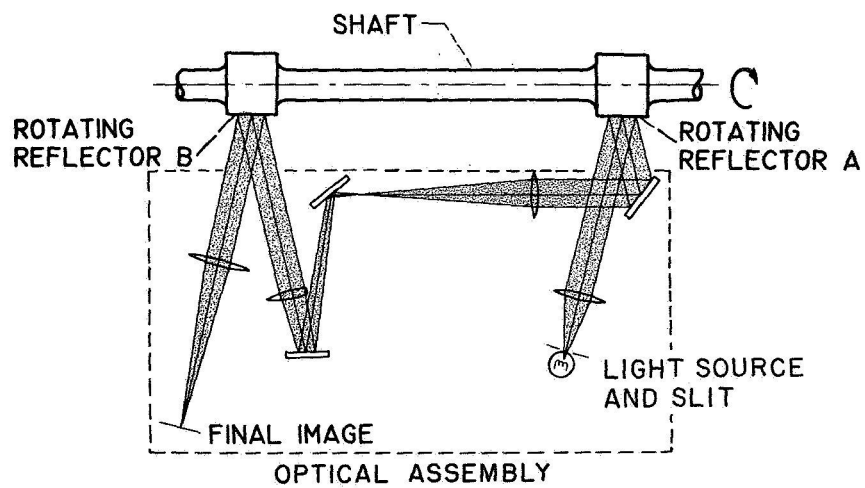
Figure 6-13. - Optical torquemeter.
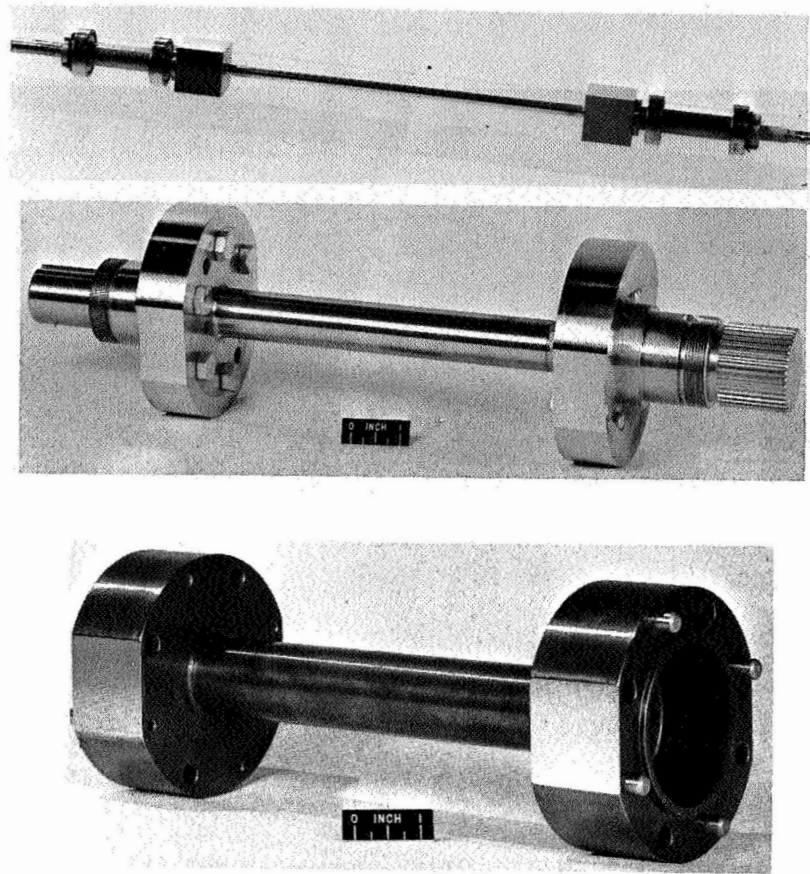
Figure 6-14. - Optical-torquemeter elements.
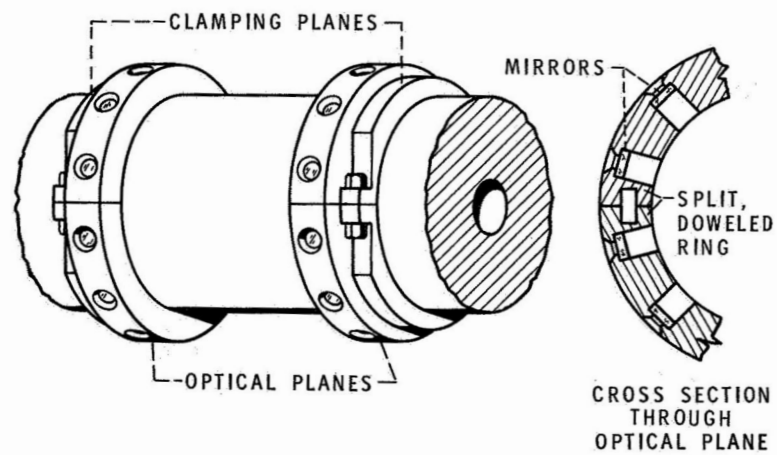
Figure 6-15. - Clamp-on optical-torquemeter element.
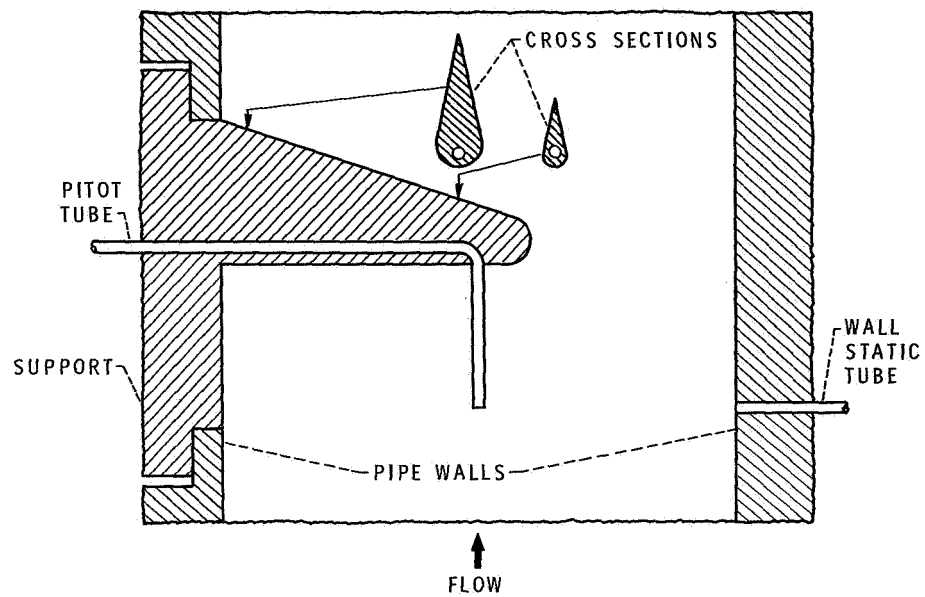
Figure 6-16. - Pitot tube.
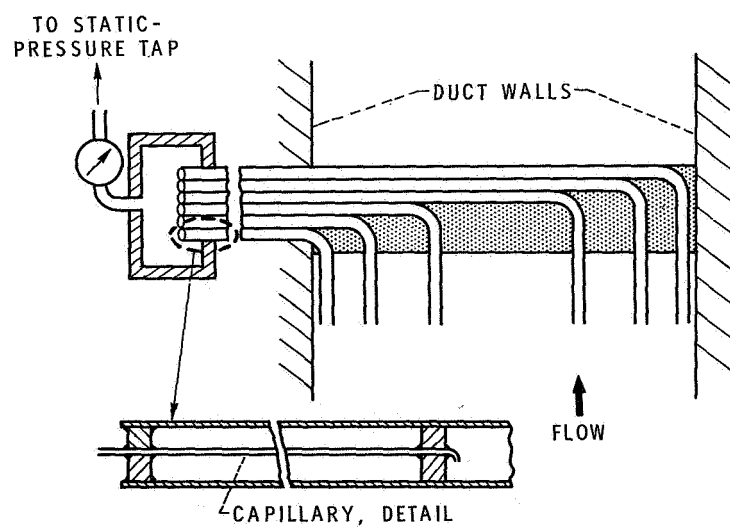
Figure 6-17. - Integrating rake.

(a) Strut-mounted probe. (b) Wall tap.
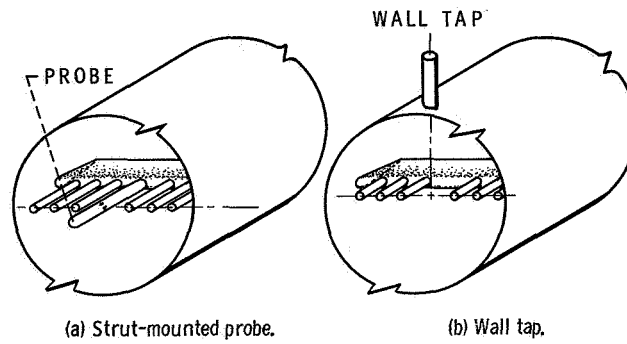
Figure 6-18. – Static-pressure measurement.

(a) Pitot probe.

(b) Static-pressure probe.
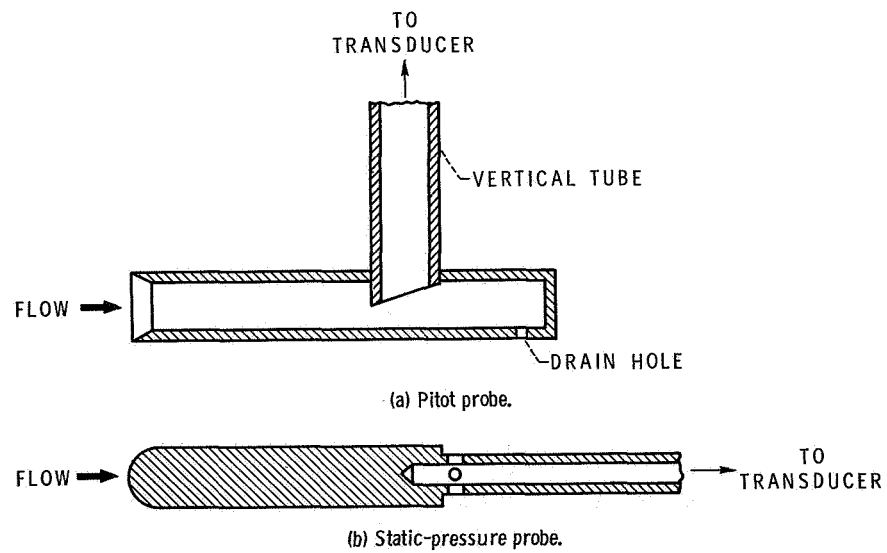
Figure 6-19. – Inertial separation of droplets.

(a) Summation of areas.

(b) Summation with smoothing
(Chebyshef integration).
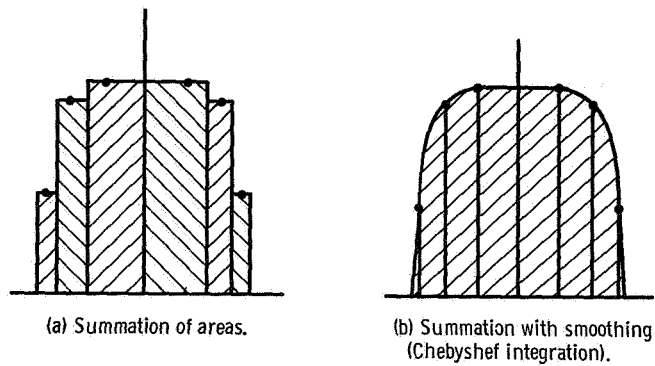
Figure 6-20. - Integration by sampling.

(a)

(b)

(c)

(a) Basic resistance-capacitance
network.

(b) Basic resistance-inductance
network with transformer.

(c) Practical resistance-capacitance network
with operational amplifier.
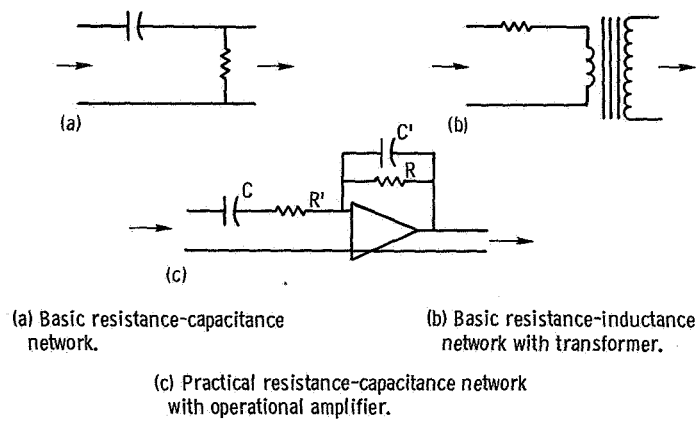
Figure 6-21. - Rate indicators.
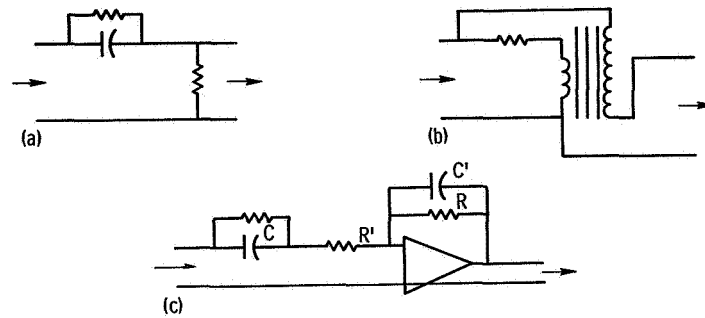
(a) Resistance-capacitance type.

(b) Transformer type.

(c) Practical resistance-capacitance type using operational amplifier.

Figure 6-22. - Time-lag compensators.
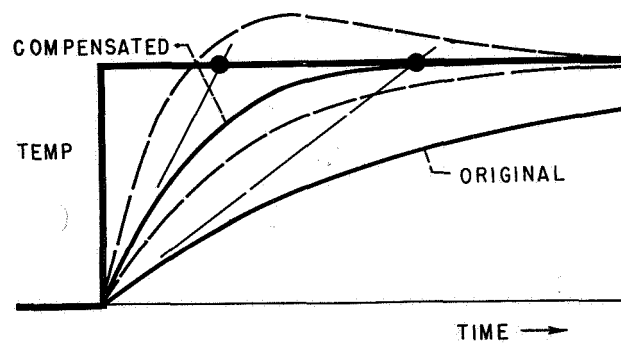
Figure 6-23. - Time-lag compensation.
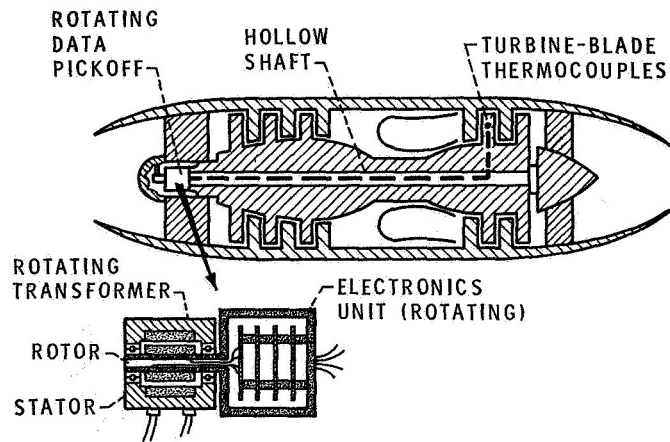
Figure 6-24. - Rotating-shaft data transmission.
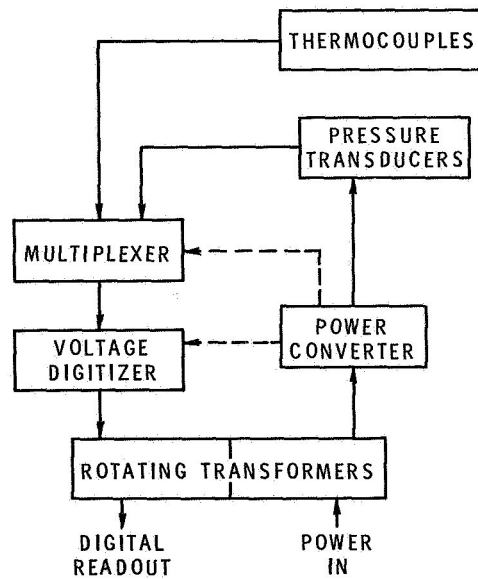
Figure 6-25. - Block diagram of rotating-shaft data transmission system.

201
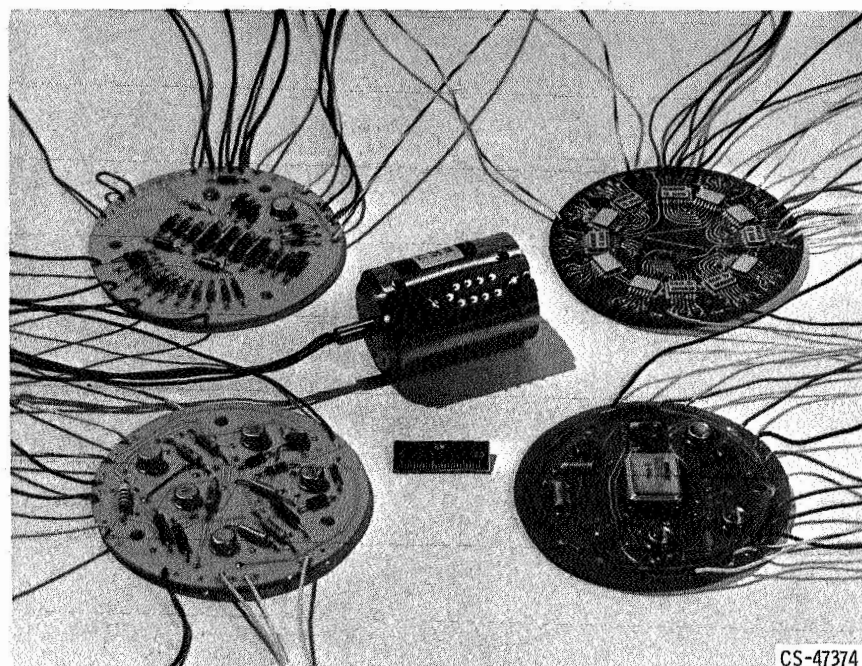
Figure 6-26. - Components of rotating-shaft data transmission system.

CS-47374

7. BEARING AND SEAL TECHNOLOGY

William J. Anderson and Lawrence P. Ludwig

Space-power systems and advanced aircraft gas turbines require bearings ranging in size up to approximately 6 inches in bore diameter and seals to about 7 inches in diameter. The application of our bearing and seal technology to power generating equipment would, therefore, represent a considerable extrapolation of size. Nevertheless, some of the improvements in bearings and seals, which have their roots in aerospace technology, may very well influence a change in the design philosophy used in generating equipment. Some development work would be required, of course, since the actual hardware was designed to meet different requirements.

BEARINGS

Bearing Power Loss

As generating systems get larger and larger, the power loss in the bearing and seal systems becomes a factor of greater economic importance. Larger units mean higher sliding speeds in the bearings and seals. Sliding speeds in bearings are now high enough so that the flow in the bearing film is no longer laminar but is at least partially turbulent. This has resulted in a sharp rise in bearing power loss.

An illustration of turbulence effects on power loss is given in figure 7-1. Since the degree of turbulence depends primarily on the Reynolds number in the bearing film, total power loss has been plotted against film Reynolds number. The Reynolds number in the film is a function of the sliding velocity V, the clearance C, and the kinematic viscosity γ, of the oil. As the machine size is increased, both the velocity V and the clearance C increase, resulting in a sharp increase in Reynolds number, turbulence, and total power loss. Two units of 240 and 600 megawatts, now in service, and a projected unit of 936 megawatts are spotted on the plot. The 600-megawatt unit has a total bearing power loss of 4000 kilowatts, while the projected total bearing power loss for the 936-megawatt unit is some 12 000 to 13 000 kilowatts. In this unit, the flow in the bearing film is fully turbulent.

The power loss of a rolling bearing system is shown in figure 7-2, plotted against shaft surface velocity. At low speeds, the power loss in a sliding bearing is comparable to that in a rolling bearing, but at high speeds it is considerably greater, especially when the flow in the bearing film becomes turbulent. Rolling bearings are inherently low power-loss bearings, especially at high speeds. For this reason, in part, they are used in space-power systems and in aircraft turbine engines, where power loss is critical.

In addition, rolling bearings perform well with lubrication techniques designed to minimize power losses. To illustrate, a typical lubrication system concept for minimizing power loss is shown in figure 7-3. Since very little oil is actually required to lubricate a rolling bearing, only a small quantity of oil is allowed to pass through the bearing. This keeps the losses due to churning and viscous shearing low. The major portion of the oil flow is bypassed around the bearing to provide cooling. It may be made to flow under the inner ring as shown, through the housing, or both. In large turbine engine ball bearings the inner ring is often split and provided with slots in the bearing center plane. A portion of the oil flowing underneath the inner ring passes radially out through the slots and through the bearing to both lubricate and cool. The concept shown in this figure was developed under contract for NASA by the Pratt & Whitney Division of United Aircraft Corporation.

As was stated previously, bearing power losses in large generating units now in service range up to 4000 kilowatts. This represents a loss of some $250 000 per year, based on a 6-mil per kilowatt-hour rate, and projected bearing power losses in units now being designed are several times as high because of turbulence effects. The use of rolling bearings would significantly reduce these losses, but these gains would have to be weighed against development costs and predicted reliability.

Rolling Element Bearing Reliability

Application severity. - The use of rolling bearings in generating equipment raises questions regarding their speed limitations, life, and reliability. Much progress has been made in these areas in the past decade, however, as a result of aerospace research. Any comparisons of bearing performance and reliability must be made on the basis of the severity of the application. Table 7-I illustrates the relative severity of bearing applications in industrial gas turbines and in a projected 1000-megawatt gas-turbine generating system. Two parameters are used. The parameter DN is the product of bearing bore in millimeters and shaft speed in rpm. It is the most widely used severity parameter, and is analogous to a peripheral speed. In comparing the performance of very high-speed bearings, however, DN

has distinct shortcomings. Limiting DN values do not remain constant for a range of bearing sizes. Data indicate that DN^2, which is analogous to a centrifugal force, may be a better parameter for gaging the severity of high-speed applications. This parameter provides an estimate of the loading between the rolling elements and the outer race. The ideal parameter may be DN^x where $1 < x < 2$, but a comprehensive program in this area has not been conducted.

As table 7-I indicates, the maximum continuous service DN value in industrial gas-turbine bearings now operating is about 1.32 million. This compares favorably with the 1.6 million value in a 1000-megawatt gas-turbine generating unit. On the basis of DN^2, the severity of bearing operation in industrial gas turbines greatly exceeds that in the 1000-megawatt projected gas-turbine generating unit. It, therefore, appears that bearings in present industrial gas turbines operate under conditions comparable to those in projected gas-turbine generating units.

Industrial gas turbines operate for periods of 16 000 hours without maintenance. The bearings and seals operate with high reliability for this time period, which is considerably greater than the longest overhaul time for aircraft turbine engines. However, aircraft engines must operate over a wide range of speeds, power ratings, and environmental pressures and temperatures, whereas industrial engines operate at a reasonably fixed set of conditions. Operation at a fixed condition improves the life of rolling bearings and especially of face seals.

Fatigue life. - The use of rolling bearings in applications where reliability is of paramount importance has usually been avoided because they are subject to fatigue failures. These failures can be predicted only on a statistical basis, so that failure by fatigue of an individual bearing cannot be predicted. It is highly improbable that rolling fatigue will ever be eliminated, but several developments of the past decade have significantly increased the fatigue life and reliability of rolling bearings. Three of these techniques are listed as follows:

(1) Consumable electrode vacuum melting
(2) Fiber control
(3) Hardness control

Since the origin of fatigue is in the material, attempts to improve fatigue life must deal with improvements in the raw material and its processing until the bearing is finished. Until recently, most quality bearing steels were melted in a ceramic crucible and in an air environment. Air-melted materials usually contain hard oxide inclusions that result from the reaction of the melt alloys and oxygen. In addition, ceramic contaminants from the crucible frequently go into the melt. These act as stress raisers which promote early fatigue cracking. The growing use of consumable-electrode vacuum-melted materials has resulted in more uniformly high-quality bearing materials and longer life bearings (fig. 7-4). In the consumable-electrode

vacuum-melting process, an arc is struck between the ingot, which serves as an electrode, and a water-cooled copper crucible. A vacuum is drawn to remove gases as the energy from the arc gradually melts the ingot. The vacuum environment prevents the formation of oxides, and the copper crucible eliminates the source of ceramic contaminants.

The effects of vacuum melting on bearing life are dramatic, as indicated by the bar graph. Each remelt results in improved life with a fourfold increase in life after five remelts. The actual life values shown are not important because these data were obtained in highly accelerated life tests.

A second way in which bearing fatigue life can be improved is through better manufacturing. Whenever a material is shaped by rolling, forging, or extrusion, the metal grains take on a stringlike pattern, resembling fibers - thus, the term fiber flow. The fiber flow in a bearing race that has been cut from tubing is illustrated in figure 7-5. Research conducted here at Lewis has shown that metals are weaker in fatigue when the ends of the fibers are exposed to the stressed surface than when the fibers are parallel to the surface. Note the fiber ends, which are exposed to the stressed region in the race cut from tubing.

If a special forging technique is used, a race with essentially parallel fibers in the highly stressed ball groove can be produced. The Fafnir Bearing Company has developed specially forged races based on the concepts developed at this Center. These indicate that a tenfold life improvement can be expected.

A third way in which bearing fatigue life can be improved is through hardness control. Research at this Center has indicated that resistance to rolling fatigue generally improves with increasing hardness. It would seem to follow from this that the rolling elements and races of a bearing should be heat treated for maximum hardness. Further research at this Center has indicated, however, that maximum fatigue life is achieved if the balls are made two points harder (as measured on the Rockwell C scale) than the races. These results are shown in figure 7-6 in which relative bearing life is plotted as a function of the difference in ball and race hardness ΔH. Each point represents a life determination for a group of 30 bearings. It is apparent that fatigue life can be reduced as much as 80 percent if ΔH varies much from 1 to 2. Normal manufacturing variations may result in bearings being assembled with ΔH values several points away from the optimum, with a consequent significant reduction in fatigue life. This illustrates the importance of specifying not only the proper ΔH but, also, of closely controlling component hardnesses so that the desired ΔH is actually achieved.

These are but some of the techniques that have been found to improve fatigue life. Others, including improved nondestructive inspection techniques for the location of minute flaws, are under development. Improvements in life of greater than

an order of magnitude have been demonstrated, and it is entirely possible that further improvements of a like order may be achieved.

SEALS

The performance and reliability of seals are also critical to the proper functioning of turbomachinery. Because of reliability considerations, buffer and labyrinth seals, rather than face seals, have generally been used throughout steam systems and, in some locations, in gas turbines. These noncontact seals are essentially reliable, but a significant loss in thermal efficiency is incurred because of seal leakage. In addition, these seals require a considerable axial length, and this has led to problems with critical speeds.

Face Seals

Leakage rates can be greatly reduced by using face seals (fig. 7-7), but there are problems that would have to be solved before their reliability could be considered satisfactory.

Figure 7-7 is a schematic of a conventional face seal used in many aircraft gas-turbine engines. It consists of a rotating seat attached to the shaft and a nonrotating nosepiece, which is held in sliding contact or close proximity to the rotating seal by a light spring force and by a force from the sealed gas pressure P_1 acting across the annular area behind the dam. For a typical 7-inch-diameter seal, sliding speeds to 300 feet per second are common.

A piston ring permits axial motion of the nose to accommodate for thermal expansions and to allow the nose to follow axial run-out movements of the seat face. The seal faces or dam (shown with an exaggerated leakage gap) restrict the leakage of the high-pressure hot gas into the sump for the oil lubricated roller bearing that supports the shaft. It is important to minimize leakage of hot gas through the seal because this degrades the lubricant and adds to the cooling requirements of the lube system.

Current pressure and speed limitations on the conventional face seal result from an inability to maintain a small net closing force on the nose, that is just large enough to make the nose follow the seat, yet not so large as to cause excessive wear. wear. To achieve long seal life, rubbing contact of the nose and seat must be prevented, but this must be accomplished with very small sealing gaps so that leakage rates are acceptable.

Deformation. - The problem is basically one of maintaining a proper balance between the closing and opening forces. The closing force is a function of the area over which the pressure P_1 acts and is readily controlled by the designer. The opening force is a function of the pressure in the gap. This is not easily controlled because it is greatly influenced by deformation of the sealing faces. This is shown in figure 7-8.

Portions of the nose and seat with greatly exaggerated sealing gap deformations are shown. Deformations of the seal faces can result in a sealing gap which is either convergent or divergent in the direction of gas leakage. If the deformation is convergent, seal operation is stable because, if a disturbance causes the nose to approach the seat, then a greater separating force is automatically generated in the gap. The equilibrium pressure profile is shown as the solid and the disturbed profile as the dashed line. Since the closing force (P_1 times its area) remains the same, the greater separating force opens the gap until equilibrium is again restored. Thus, a seal with a converging gap can run without rubbing contact.

In contrast, a divergent gap is unstable. A divergent deformation gap is more common and is usually caused by thermal gradients. If the nose is displaced to the dotted position, the leakage flow is effectively pinched off. This causes the average gap pressure (as shown by the dashed line) to decrease. Now the force tending to close the seal is greater than the separating force. This will cause the nose to slam down against the seat. At the high sliding speeds in advanced gas turbines, the resulting rubbing contact will generate more heat and make the divergence worse.

Face seals incorporating gas bearings. - In a development contract at Pratt & Whitney Aircraft, one of the approaches taken to solve the gap deformation problem was to add hydrodynamic or self-acting gas bearings to the sealing faces. These act to keep the faces separated even though divergence occurs. This seal is shown in figure 7-9.

The seal construction is similar to the conventional face seal shown previously. The only difference is that a self-acting gas bearing has been added under the sealing dam. This gas bearing consists of a series of shallow recesses arranged circumferentially around the seal face. Figure 7-10 is a view of the face of the nose, showing the sealing dam area and the gas bearing recesses. Each recess has a radial feed groove. An edge view shows the feed groove and recesses with the depth (typically 0.002 in.) greatly magnified.

The motion of the seat over these recesses drags or pumps the air from the feed groove into the recesses. This pumping action raises the gas pressure in the recesses creating a separating or lifting force. The closer the nose comes to the rotating seat, the greater is this force produced by the gas bearing (fig. 7-11).

The gas bearing lifting force for a typical seal is plotted as a function of the leakage gap height. When the gap is small (of the order of 0.2 mil), the recesses exert a large force to keep the faces separated. In this example, the lifting force generated is approximately 100 pounds. However, when the gap becomes large (1.0 mil) then only a small force of some 5 pounds is exerted. The self-acting gas bearing is inherently suited for seal operation because large forces are produced only when the faces are nearly touching. There is little tendency to produce a large gap that would result in high leakage rates.

Figure 7-12 shows a comparison of seal leakage in standard cubic feet per minute as a function of sealed pressure for labyrinth, conventional, and modified face seals. The leakage of a typical gas-turbine labyrinth seal is usually at least 10 times as great as that of a conventional face seal. The conventional seal works well at low pressure, but begins to fail at high pressures because divergent sealing faces cause heavy rubbing contact. The resulting vibration and wear lead to high-leakage rates. The leakage of a seal with a self-acting gas bearing is low over the entire range of pressures. Divergent surfaces have been created by thermal deformation, but the gas bearing generates enough force to keep the surfaces from rubbing. Inspection of this seal after test showed the surfaces to be in excellent condition.

The difference in leakage of this type seal as compared with a labyrinth seal, can be translated into efficiency gains, and for this reason, we are currently working on replacing certain compressor and turbine labyrinth seals with gas film seals of this type.

Visco Seals

In addition to noncontacting seals with a gas film between the sliding surfaces, studies have been made at Lewis and its contractors on noncontacting seals for liquids. The visco seal (fig. 7-13) is one such device and is used in the SNAP-8 space-power system to seal mercury. This seal consists of a rotor with a helical groove rotating within a close fitting housing containing the sealed liquid. The clearance between the shaft and the housing is dictated by mechanical considerations, vibration, and runout and is usually several mils. This type of seal is essentially a pump, which pumps the liquid back as fast as it tends to leak out, so that a liquid-to-gas interface is established within the seal length when the pumping effort of the grooves balances the pressure to be sealed. Thus, a pressure gradient is established from ambient at the interface, increasing across the seal, to the sealed pressure. For a given sealed pressure, the length of seal occupied by the

liquid depends on the peripheral speed of the rotor outside diameter, the liquid viscosity, and the clearance between the rotor and housing. If sealing is required at zero shaft speed, then a positive contact seal must be added to the system.

Models of visco seals have been constructed for the purpose of conducting visual studies of their performance. The model illustrated in figure 7-14 consists of a steel shaft in a clear plastic housing. The right portion of the shaft has helical grooves cut in its surface, and rotates in a smooth bore housing. The left portion of the shaft is smooth and rotates in a helically grooved housing. As can be seen, the stationary and rotating grooves are equally effective; for each seal the same wetted length is required to seal against the small head of the fluid in the reservoir above the shaft. Although the pressures developed in this model are quite low, significant pressures can be developed in a practical seal.

Figure 7-15 illustrates the sealing capability of a visco seal for two fluids: oil and water. Pressure in psi per inch of axial length is plotted as a function of rotor peripheral speed. The pressure that can be sealed increases with speed and also with fluid viscosity. The oil chosen has a viscosity some 50 times that of water and pressures developed are in that ratio. As an example, a 6-inch-diameter seal with a clearance of 4 mils running at 3600 rpm would produce about 20 psi per inch of seal length when sealing water.

There are a number of factors that must be considered in applying the visco seal, and one of these is the fluid film power loss which is comparable to that of a journal bearing of the same size, speed, and clearance. In dissipating this power loss, advantage can be taken of the seal pumping action, which induces a constant exchange of liquid from the film to the cavity and back. The film temperature tends to be uniformly low if sufficient cooling flow is provided through the cavity.

Since the visco seal operates with liquid, in case of a seal malfunction, the possibility of liquid entering the turbine areas must be eliminated through the use of some type of mechanical trap or slinger.

Spiral Seal

Another seal that works on the same pumping principle, is the spiral seal which is shown in figure 7-16. This is very similar in construction to the conventional face seal shown earlier except that the nonrotating nose has spiral grooves cut in its face. The motion of the seat across the grooves produces a pumping effort to seal the liquid. The seal is designed so that the spiral groove pumping effort develops a pressure greater than the sealed pressure, thus assuring sealing face separation and the formation of a liquid-to-gas interface within the seal. Orifices permit recircu-

lation of the sealed fluid to remove heat.

The spiral seal has two advantages over the helical-groove seal. It can be made smaller in size because smaller gap heights can be used. The gap magnitude is not dictated by shaft runout and vibration as for the helical groove seal. With smaller gaps, proportionally larger pumping pressures can be produced, and it will also seal at zero shaft speed because, when rotation stops, the seal closes.

CONCLUDING REMARKS

Although further development would be required to establish reliability and integration into present electric power generating systems, some bearing and sealing concepts discussed may have application in the system.

As pointed out, use of rolling bearings would significantly reduce the bearing power loss. The seal concepts could be used to achieve a marked reduction in leakage at the expense of some mechanical complexity. Incorporation of the seal types discussed would also make it possible to significantly reduce the axial length of machines. This would help to alleviate design problems associated with critical speeds.

The seal concepts discussed were derived from studies on seals in the 2- to 8-inch size range. However, the basic principles should be applicable to seal sizes found in large gas and steam turbine applications.

It has been shown that reliable bearing operation for periods of 2 years is being achieved at operating conditions at least as severe as those in projected industrial generating systems. Further improvements in bearing life and reliability can be expected over the next decade.

TABLE 7-I. - RELATIVE SEVERITY OF

BEARING OPERATION

Application	Severity parameter	
	DN	DN^2
Industrial gas turbine	1.32×10^6	12.4×10^9
1000-mW open-cycle gas-turbine system	1.6×10^6	4.8×10^9
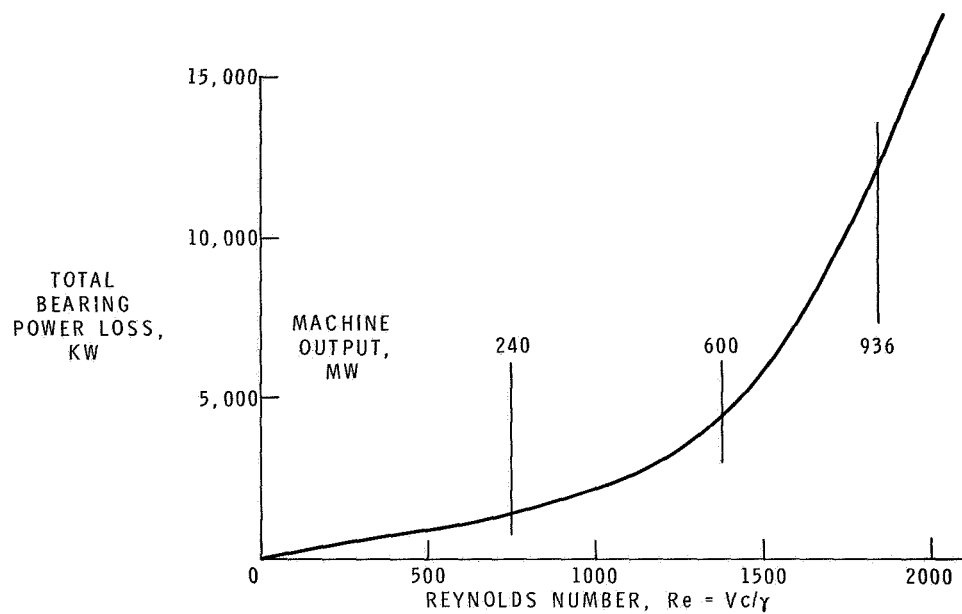
Figure 7-1. - Power loss in sliding bearings.
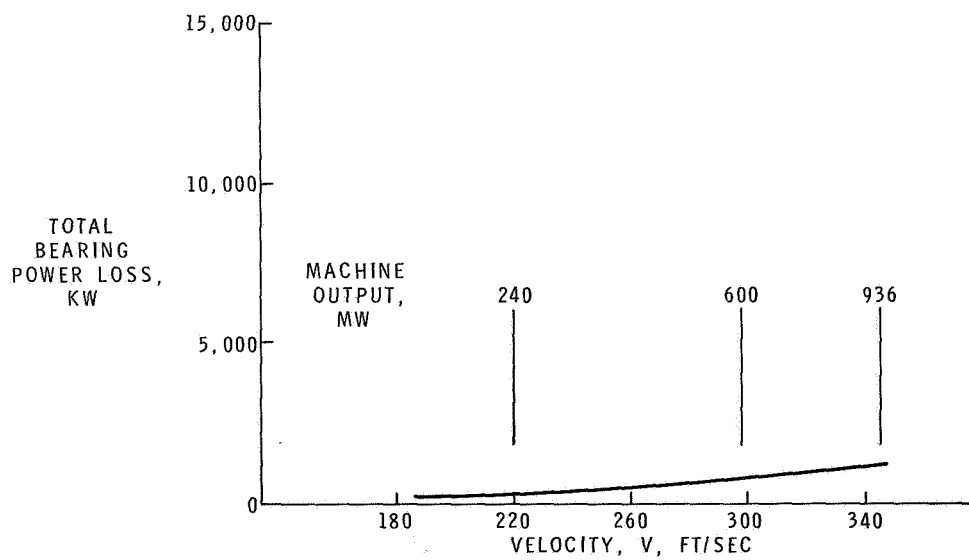
Figure 7-2. - Power loss in rolling bearings.
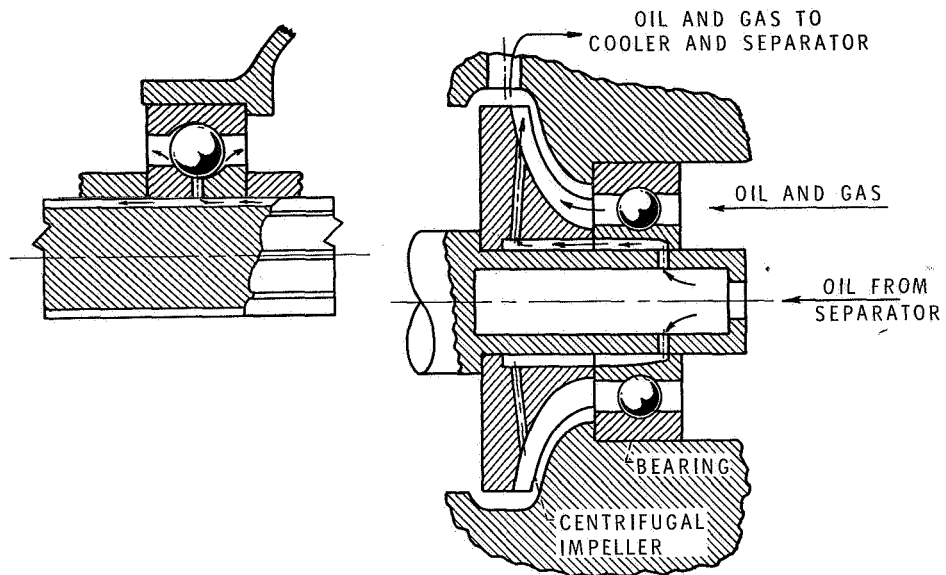
Figure 7-3. - Lubrication system concept.
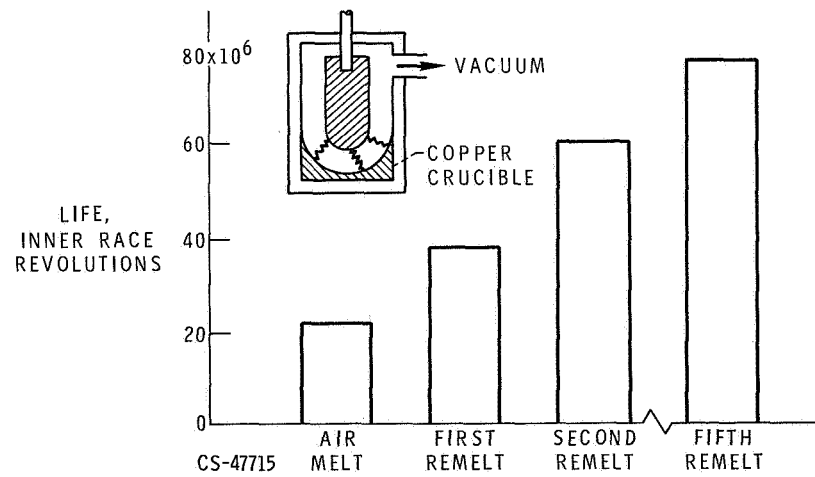
Figure 7-4. - Effect of successive consumable remelts on fatigue.

214
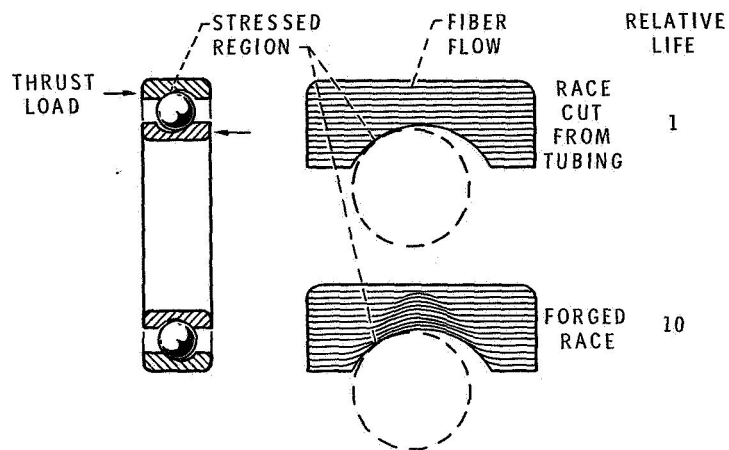
Figure 7-5. - Fiber flow in bearing races.
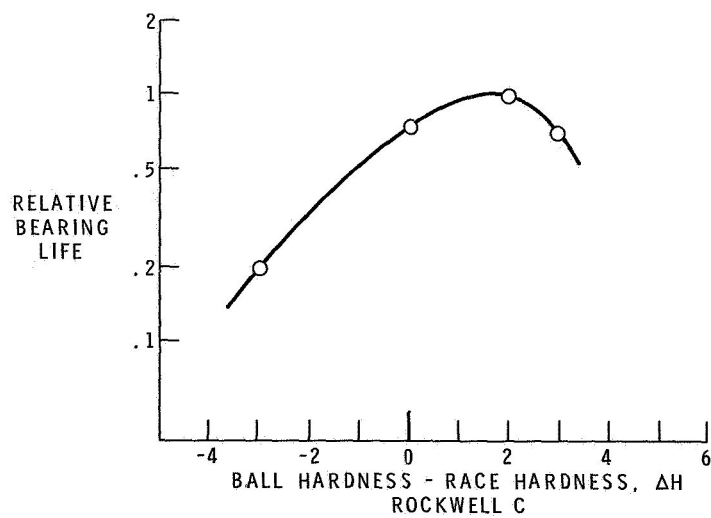
Figure 7-6. - Bearing life as function of component hardness.
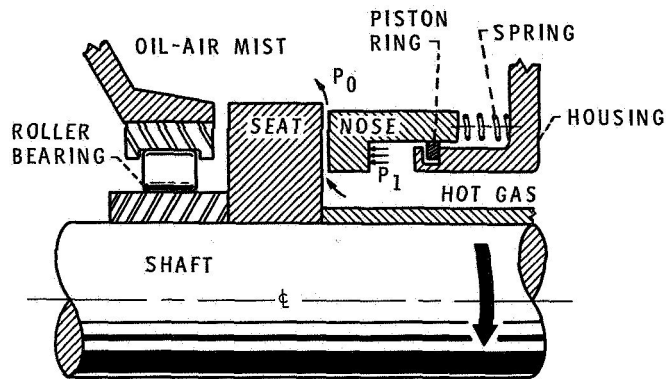
Figure 7-7. - Face seal.
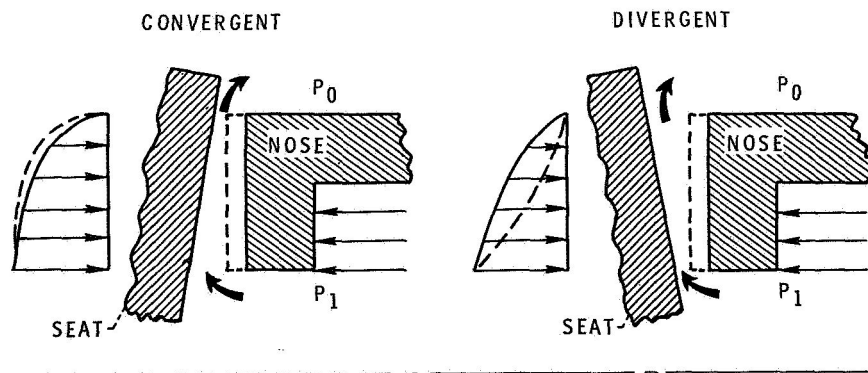
Figure 7-8. - Sealing face deformation.
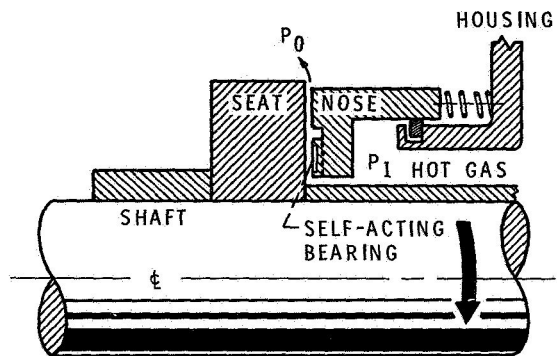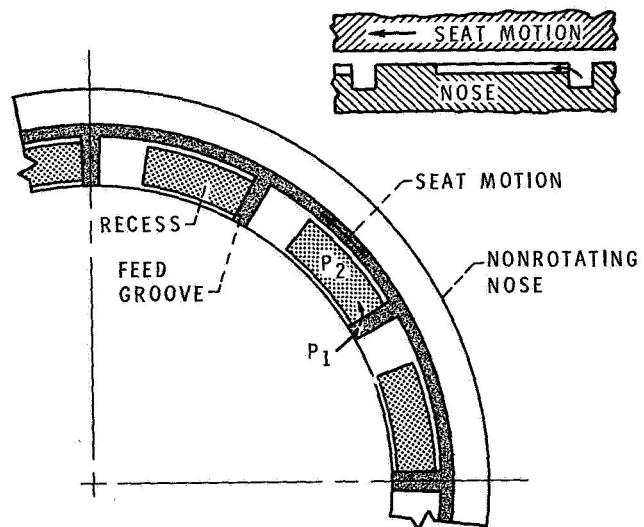
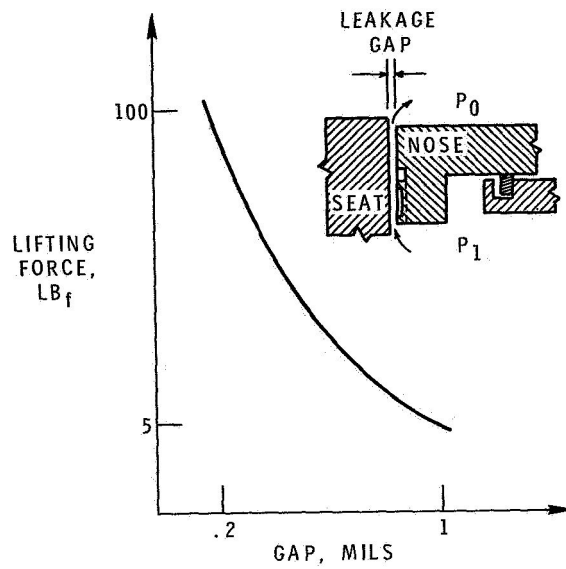Figure 7-9. - Face seal with self-acting bearing.

Figure 7-10. - Nose face with self-acting bearing.

Figure 7-11. – Gas bearing for seal support.
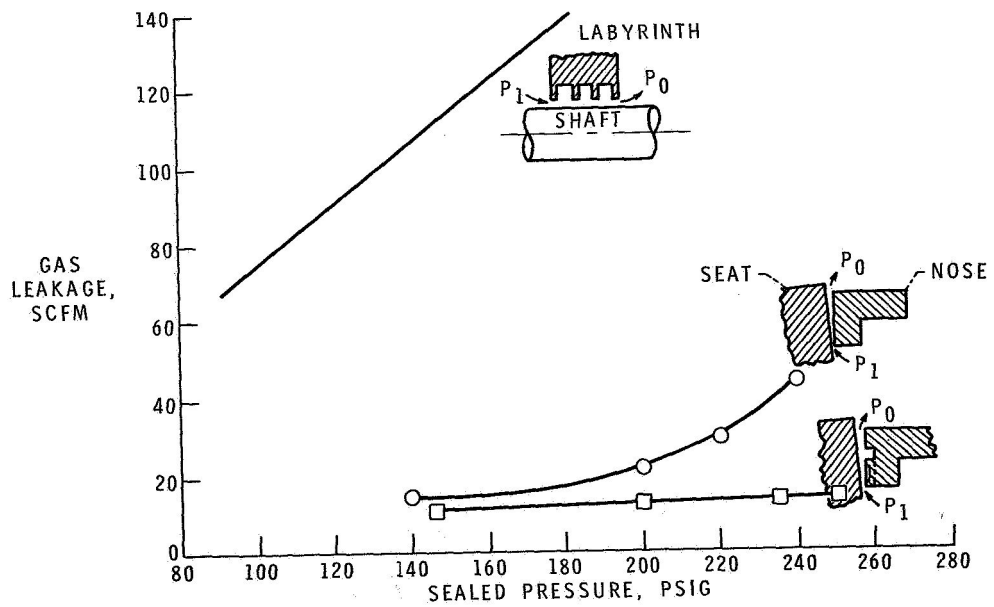
Figure 7-12. – Seal leakage.
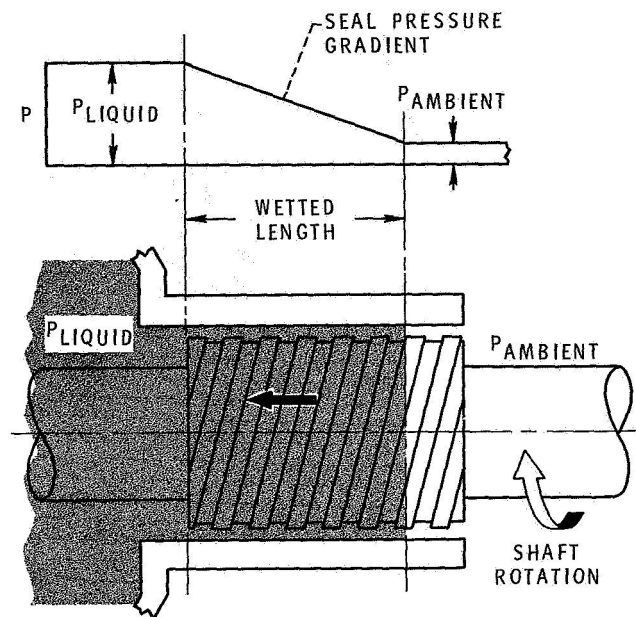
Figure 7-13. - Helical groove visco seal.

C-68-3267
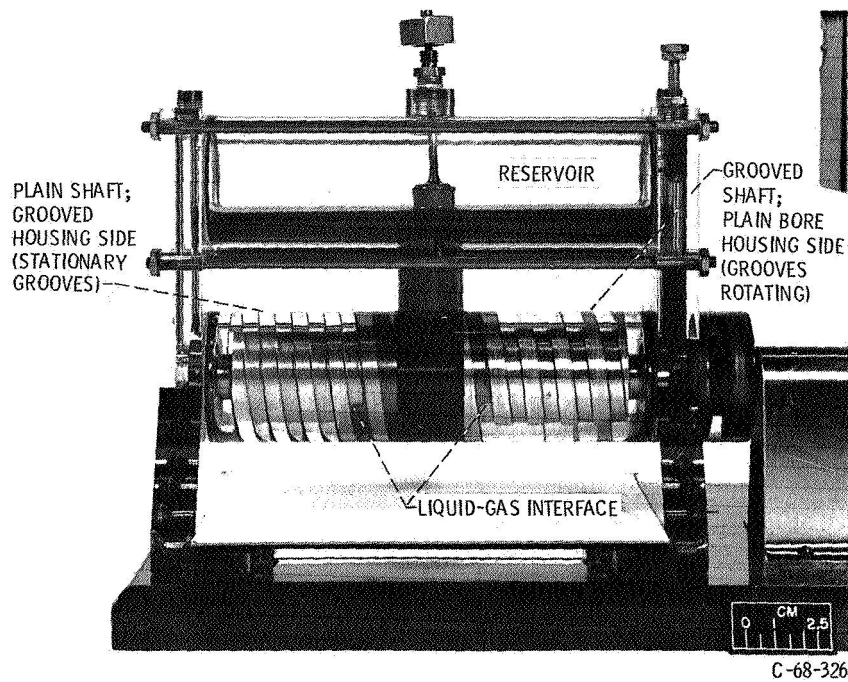
Figure 7-14. - Visco seal model.
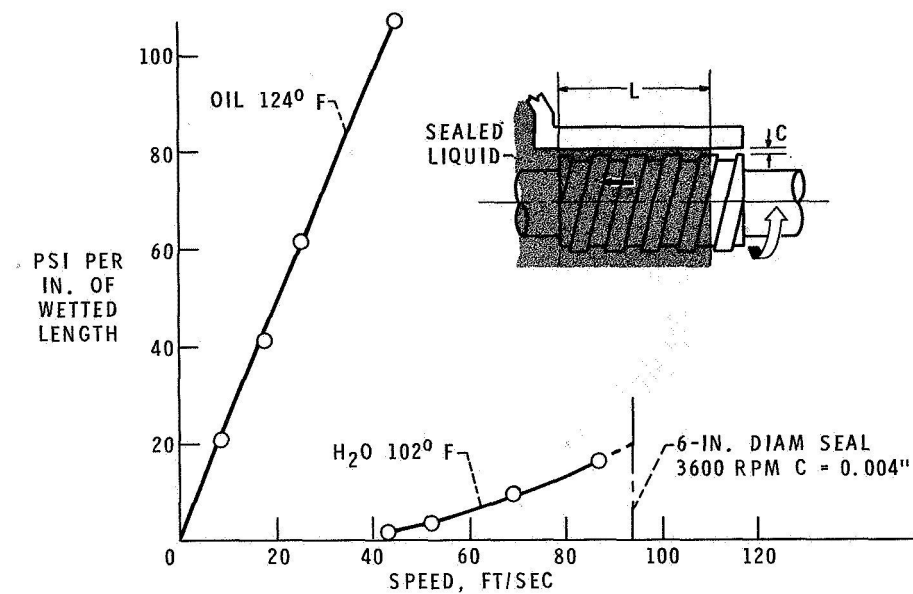
Figure 7-15. - Sealing pressures.
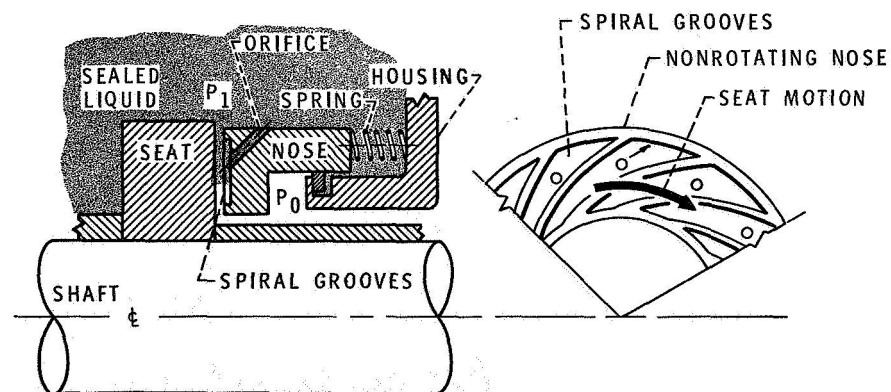
Figure 7-16. - Spiral seal.

8. ENGINEERING MECHANICS AND MATERIALS

G. Mervin Ault

A portion of the emerging technology in engineering mechanics and materials may be of interest to the power industry. Some aspects of NASA work in these areas has been described in other papers of this conference. The subjects to be reviewed herein are

(1) Engineering mechanics
    (a) Materials in long-time service: prediction of long-time properties; metallurgical embrittlement
    (b) Thermal fatigue and low-cycle fatigue
    (c) Brittle fracture of metals
(2) Materials
    (a) Materials strengthened by dispersed inert particles
    (b) Composite materials from fibers

PREDICTION OF LONG-TIME PROPERTIES

When materials are used at high temperatures, a common design criterion is "stress to rupture" (fig. 8-1). At elevated temperatures, when a load is applied to a metal specimen, the specimen may not fail immediately, but with sustained application of that load the specimen slowly elongates or "creeps" until finally it does fracture. Thus, for every stress at each temperature there is a finite time to fracture. To determine each data point used to define these curves, a specimen is loaded into a machine and left in the machine at temperature and under load until it fractures. If design data were needed for times of 100 000 hours ($11\frac{1}{2}$ yr), many machines would be in use for a long time.

In recent years, interest has increased in long-time properties. In aircraft jet engines operating lives as long as 15 000 to 30 000 hours (2 to 4 yr) are desired, and in space power systems operating lives of at least 5 years. For earth-bound power systems the need is for much longer operating lives of 20 to 40 years. Thus, there exists a common interest in drastically reducing the testing time to obtain design data. For example, if a device that will last 20 years is needed, a delay of

20 years to obtain design data before starting to build hardware is obviously unacceptable. It is thus desirable to have proven methods for extrapolating test data obtained in short times out to long times.

Several methods have been developed for this purpose. These methods generally depend on the substitution of temperature for time, as indicated on figure 8-2. (This figure is the same as fig. 8-1 except that the dashed lines have been added.) Suppose there is interest in the stress-rupture time for 40 000 psi and 1200° F. The figure shows that the rupture time is 10 000 hours. If the test could be made at the same stress, but at 100° F higher temperature, the test time would be cut by a factor of 10 to only 1000 hours. This transposing of temperature for time is possible if the mathematical relations among such data can be determined for a material. Methods for determining such relations have been developed, and they are generally known as "correlating methods," or "time-temperature parameters." Good success has been achieved with a parameter method developed at this Center, known as the Manson-Haferd parameter (ref. 1).

The Manson-Haferd parameter has been evaluated for a very large number of materials. An example of its use is illustrated in figure 8-3 for 17-22AS steel (ref. 2). In the upper right corner is shown the equation that describes the behavior of this material in terms of temperature T and time t. The constants are derived for each material by a prescribed systematic procedure (ref. 3) that uses a minimum of data. The correlating lines for the data are shown as solid lines, and the actual data as circular symbols. A good fit is indicated.

Once the parameter is determined, some interpolations and extrapolations of data are possible (i.e., if the designer wishes to know a reasonable approximation of the properties at another temperature, the parameter provides a rational basis for this interpolation as suggested in fig. 8-3 by the dashed line at 940° F).

Inadvertently, an opportunity arose to check a rather large extrapolation with this material. A specimen of 17-22AS steel was set up in the machine at 940° F with a stress intended to cause failure in much less than 1000 hours. The specimen was incorrectly loaded, however, and the stress was actually only one-half of that planned. After it had been in the machine for an appreciable length of time and had run well beyond the expected life, the mistake was discovered - it was found that the actual stress was only 40 000 psi. The specimen finally failed at 24 000 hours and was a good fit (fig. 8-3) to the line predicted by the parameter.

Although the parameter methods have been evaluated for a large number of materials in the 100- to 1000-hour time range, it is not often that data are available to much greater times, as was the case for the 17-22AS steel. An opportunity (ref. 4) to check the parameter methods to even longer times was provided through tests that were being run in Germany to evaluate several steels for steam turbine appli-

cations. The German investigators were running tests for 10 or 11 years, or nearly 100 000 hours. An example from the program is shown in figure 8-4. The NASA obtained material from these scientists and ran specimens over the time spectrum indicated on the figure (i.e., from 10 to about 3000 hr). From these relatively short-time tests the constants in the parameter were determined, and the predictions were made (solid curves in fig. 8-4). (The parameter here is a more general parameter than shown in the previous figure.) The data points are those obtained by the German investigators with their specimens in their test facilities. The general fit is quite good (e.g., the triangle on the right of the curve for 1202° F is at a time close to 100 000 hr, and it agrees quite well with the predicted line).

In general the so-called "time-temperature parameters" have proved very useful in minimizing testing and are now widely used.

A problem frequently encountered in long-time exposure of materials is metallurgical instability. An example is shown in figure 8-5 which illustrates the formation of a brittle phase known as "sigma phase" in the alloy IN-100, which is a commonly used bucket alloy. The two sets of stress-rupture data in the figure are for the alloy with only very slight differences in composition. The structure of the two compositions as revealed in the metallurgical microscope is shown in the two photographs, which differ in that the left one shows fine lines. These lines are the brittle sigma phase. As can be seen from the data plots, the one with sigma is weaker, and also there is a sharp break in the strength curve after a period of time. This is the time when sigma forms in the alloy. This formation of sigma in the alloy and the simultaneous break in the curve indicate instability. Unforeseen instabilities in alloys of this particular type would generally raise questions regarding extrapolations of data using time-temperature parameters. Currently, the problem of extrapolation of properties for such unstable materials is being examined.

It is even more important to learn how to design alloys so that such time-dependent instabilities do not occur. In addition to lowering high-temperature properties, the sigma phase may make the alloy brittle at room temperature.

Several General Electric Co. investigators (ref. 5) have developed a prediction method for avoiding sigma phase. The method involves using the alloy composition to calculate the electron vacancy concentration N_v of the residual matrix after other phases, such as γ' and the carbides, have precipitated. The electron vacancy concentration indicates the tendency for certain elements in the alloy to combine and form the undesirable phase, sigma. It has been found that as N_v goes above 2.48 (fig. 8-6) there is an increasing tendency to form sigma and as it goes below that value there is a lesser tendency. Many stainless steels are well into the sigma range and form the phase. The important high-temperature superalloys of

nickel base vary in their tendency, as indicated in the figure. Some important ones are on the border line, and slight changes in composition or processing can tip the balance. The superalloys of cobalt base do not form sigma, but they can form other embrittling phases. Studies of the embrittlement of HS-25 alloy are presented in references 6 to 8. This NASA laboratory is conducting studies to better define the parameters for avoidance of sigma phase in a sensitive nickel-base alloy (fig. 8-5), and to understand the embrittlement of cobalt alloys. Several other organizations are working on the development of high-temperature alloys for the power industry that are of a cost and strength more comparable to the stainless steels but entirely free of the embrittling sigma phase. Good progress has been reported.

THERMAL FATIGUE AND LOW-CYCLE FATIGUE (LCF)

A failure mechanism that is too often encountered in materials at high temperatures is thermal fatigue. Figure 8-7 shows an example of such failure for a steam power system component. The NASA has had considerable experience with such failures in gas turbines. Examples of thermal fatigue failures in turbine disks and buckets are shown in figure 8-8. Failures of this type may occur whenever materials operate with temperature gradients in a cyclic mode. The temperature gradients may occur either under steady-state operation or during starting and stopping. Basically the problem is that metals expand or contract when heated or cooled. If they are not permitted to expand or contract freely, something must give, and, thus, the metals flow plastically. The mechanism of thermal fatigue failure is illustrated in figure 8-9.

The turbine blade in figure 8-8 has a thin leading edge with a thicker adjacent section. Schematically, it is similar to the illustration in figure 8-9, where a thin section is attached rigidly to a thick section. If hot gases are passed across the structure, the thin section heats more rapidly than the thick section and tries to expand to a new length, as indicated by the dotted areas. Because it is rigidly attached to the thick section, however, it cannot expand as it desires. The free expansion is constrained by compressive forces from the attached heavy section. Because it cannot expand, something must give - the thin section flows plastically, as shown schematically in the right view of figure 8-9. This flow occurred during heating. If the structure is now cooled, the process is repeated, but in reverse; the thin section is pulled in tension and flows in tension. Upon repeated temperature cycles, the material goes through repeated compression and tension strain cycles until finally it cracks.

An objective of NASA research is to develop methods to predict, for any opera-

ting component, the cycles to failure in thermal fatigue. To achieve this the ability to compute certain factors is essential. From the environment the temperature gradients that will occur in the part and then the actual local strains must be computed. The strain calculation would not be too difficult if only elastic conditions were involved, but complex plastic strains must be included as well. If the plastic strains can be calculated, the relation between the cyclic strains and cycles to failure must be determined for any material.

Some years ago it was found, from simple laboratory tests, that there was a relation between the amount of plastic strain per cycle and the cycles to failure. This is the Manson-Coffin relation for plastic fatigue (refs. 9 and 10), which is shown in figure 8-10.

In recent years, Lewis has conducted more detailed studies to predict thermal fatigue failures of materials, starting with the relatively simple case of mechanical fatigue at constant temperature. Shown in figure 8-11 is a typical mechanical fatigue curve where cyclic stress is plotted against cycles to failure. These curves usually become horizontal beyond 10^6 to 10^8 cycles, and this is called the fatigue limit. With cyclic stresses below this line, the material should run forever. In mechanical fatigue attention has been directed toward factors affecting this fatigue limit. In thermal fatigue there is more interest in cycles to failure of much less than 10^5 - frequency 5000 and sometimes as few as 10 to 100. This is the range where for a particular cyclic stress there is a finite number of cycles to failure, which is the low-cycle fatigue (LCF) range. Thus, considerable attention is directed toward this portion of the fatigue curve. In thermal fatigue cyclic strains due to restraint of free thermal expansion are encountered, and thus laboratory tests are run with controlled cyclic strain rather than cyclic stress. (The shape of the curve is the same.)

In studying this region of the curve it has been found at Lewis that instead of having to run many fatigue specimens to define the LCF properties of a material, a reasonable approximation of the LCF properties can be achieved from a simple tensile test (ref. 11). A tensile test is run by taking a specimen and pulling it until it fractures. From the stress-strain curve (fig. 8-12) of the short-time tensile test three values are measured, the slope of the stress-strain curve (the modulus of elasticity E), the ultimate strength S_u, and a measure of the total strain of the material D (actually the reduction of area of the specimen cross section is used). By an empirical method developed at this laboratory and known as the method of universal slopes, the LCF curve can then be drawn (fig. 8-13). From the strength of the material and the modulus of elasticity, the elastic relation is drawn. From the ductility, that is, the plastic flow capability of the material, the plastic relation is drawn. The LCF strength curve is the sum of those lines. Of interest is that for

few cycles to failure, the LCF strength is controlled by the plastic properties of the material and for many cycles to failure the LCF strength is controlled by the elastic and strength properties of the material. For good LCF strength, materials are required to have good plastic flow capability and good strength.

The value of the universal slopes method for estimation of LCF from short-time tensile tests at room temperature is illustrated in figure 8-14 for four materials. The method has been tested on more than 60 materials with consistently good results. If precise LCF data are needed for design, the method of universal slopes can be used to provide guidance for planning the test program and to minimize the required testing.

Recently, efforts have been made to extend this prediction method from near room temperature to high temperatures within the creep range (ref. 12). At these high temperatures, the mechanism of material behavior is much different. The fact that the materials are in their creep range means that even under a constant load they will continue to flow plastically. Creep can cause the mechanism of cracking to change, too. As a result it has been necessary to modify the method of universal slopes for application at high temperatures in the creep range by the 10 percent rule. By a method described in reference 12 the 10 percent rule permits estimation of the average life in LCF at these high temperatures within the creep range (fig. 8-15). It has been found that the data show quite wide scatter about this predicted average at high temperatures, however. If a designer wished to draw a conservative lifeline to ensure, for example, only 1 percent failure probability, he would need to draw a new line (dashed line in fig. 8-15) about 1 order of magnitude of failure cycles below the derived line. This conclusion is based on the preliminary examination of 40 sets of high-temperature LCF data from many investigators.

A part of current NASA research in high-temperature LCF is directed toward understanding additional factors that must be taken into account to improve the estimation. For example, one factor is almost obvious. Creep occurs at high temperature. Thus, in addition to the magnitude of the cyclic strain, at high temperatures how fast that strain is applied (i.e., the strain rate) is of concern. An example (ref. 13) is shown in figure 8-16. The data points of figure 8-16 show the actual low-cycle-fatigue data. The lower curve is the estimated LCF from short-time tensile tests that were run at conventional strain rates, but those rates were far different from the strain rate of the LCF tests. When the strain rate of the short-time tensile test was rerun at strain rates that matched those of the LCF test, a much better estimation was obtained.

The material discussed herein has emphasized the studies undertaken at Lewis to estimate and understand LCF at constant temperatures. Thermal fatigue and

LCF are essentially the same except that in thermal fatigue the strain cycle occurs over a range of temperatures and thus the material properties change as the temperature changes. The process is, therefore, more complex than that for constant-temperature LCF. Significant knowledge has been gained on the more complex situation, and considerable effort has been directed against the total problem of prediction of cycles to failure of a component in a complex environment.

BRITTLE FRACTURE OF METALS

Another evolving technology of importance in the application of metals is fracture mechanics. It has been particularly important for NASA to contribute to this development because of the need to use very high-strength alloys of steel, aluminum, and titanium. Figure 8-17 shows the test firing of the world's largest solid rocket, commonly called the 260-inch rocket. This has been an outstandingly successful test program. Three test firings have been conducted, and in one firing a thrust of 5.6 million pounds was achieved from this single engine. The size of the case containing the propellant is indicated in figure 8-18. The diameter is 260 inches or about 22 feet, and the overall length is $62\frac{1}{2}$ feet. To save weight in such a large engine, high-strength steels with strengths perhaps five times those used in steam boilers and reactor pressure vessels must be used. In this particular case the metal is stressed to about 135 000 psi. The use of these high-strength steels operating at high-stress levels permits a wall thickness of about 0.6 inch in this application, and thus considerable weight is saved. (Wall thicknesses in boilers and reactor pressure vessels may be as great as 6 to 20 in.)

Unfortunately, there are occasions where large hardware fails. A failure of a large steam turbine is shown in figure 8-19. In the development phase of another version of the large solid rocket failure occurred, as shown in figure 8-20. This failure occurred during a water pressure test of a particular fabrication method for this propellant case. An important feature of this failure should be noted. When metals fail, they usually stretch and bend while tearing, and finally break into only two pieces. This propellant case looks very brittle - it has shattered in a manner more characteristic of an eggshell than a metal.

After some elaborate detective work, the origin of the failure was found in the area indicated by the arrows in figure 8-20. Figure 8-21 is an enlarged photograph of a small part of the tank wall at this point. The metal was 0.7 inch thick. In the center of the photograph is a small area that was a crack in the original hardware. This crack was only 1/8 inch in the vertical or thickness dimension and about $1\frac{1}{2}$ inches long. Actually, this is only a very small crack in a very large tank, and

the crack removed only 0.01 percent of the load-carrying area of the tank material. One thus might think it would be of little importance. In reality, although the total load-carrying area was reduced by only 0.01 percent, the effect of this crack was to cause the tank material to fail at only one-half of its strength as conventionally measured in the laboratory.

The phrase "strength as conventionally measured" is important because this introduces the concepts of fracture mechanics. Interest in fracture mechanics is based on the concept that when metals are fabricated into hardware or structures, it is axiomatic that they do contain flaws or will develop them within their service lifetime, and these flaws or cracks can drastically change metal behavior. As shown for this large rocket case, a relatively small crack cut the conventional strength in half and led to a catastrophic brittle-type failure.

This behavior is illustrated in figure 8-22. Shown schematically are two specimens, each with a crack, being loaded in tension. The specimen on the left represents a ductile metal, and the one on the right a brittle metal. Consider the ductile metal first. As the load is increased on the specimen, the crack moves across the specimen, and the metal stretches and tears. Just ahead of the crack tip, because of the stress concentration effect of the crack, a plastic zone develops where the metal is stretching and yielding. In the ductile metal this plastic zone is large, but in a brittle metal that has little capability to flow plastically, only a very small plastic zone develops. As the load is increased on the ductile metal and the crack moves through the metal, a large amount of stretching and tearing occurs, and a large amount of energy is consumed. In the brittle metal, on the other hand, very little energy is consumed in propagating the crack. Thus, in the ductile metal a high load to failure and slow crack propagation result; but in the brittle metal the failure load is low, and once the crack starts to move it may never stop. Catastrophic failure may result. The large rocket case was a typical example. Another way to understand this is to consider the stress state at the front of a crack, plotted in the lower portion of figure 8-22. In an ideal brittle material no plastic flow can occur, and as the tip of a sharp crack is approached the elastic stress rises to a very high value. In metals, plastic flow can occur, and the stress is reduced at the crack tip. Thus, "ductile" metals are less sensitive to cracks than "brittle" metals.

Not only is crack sensitivity a function of the material, but part geometry also has an effect, as illustrated in figure 8-23. Below the ductile metal another sketch of the same metal is shown, but in this case the specimen is much thicker. Now, in thicker cross section, as the metal is loaded, the metal surrounding the crack creates a triaxial stress state that inhibits the plastic flow within the specimen. This drastically reduces the plastic zone size or in other words raises the stress

concentration. (The difference in plastic zone size occurs only within the metal specimen, not on the surface. They are shown as different on the surface for convenience in illustration.) Now a "brittle condition" exists and the crack propagates easily. For a high-strength metal conventionally described as ductile there can be either "ductile behavior" or "brittle behavior," depending on part thickness, crack size, and geometry.

The discipline called fracture mechanics is developing methods whereby the strength of structures containing flaws can be related to measureable quantities of materials. (See refs. 14 and 15 for a general discussion.) For an important stress condition called plane strain which is characteristic of cracks in thick parts, test procedures have now been developed whereby a new material property of fracture toughness K_{Ic} can be measured. The new test method has been accepted as a standard by the American Society for Testing and Materials (ref. 15); NASA researchers have been major contributors in the development of this new material property measurement.

If conditions of plane strain are not met in the hardware, it is necessary to run simulated service tests wherein the conditions of the hardware are simulated in the laboratory, but with artificially produced cracks.

The importance of considering the existence of cracks in real hardware is illustrated in figures 8-24 and 8-25, which are based on an example developed during the selection of materials for a particular application.

Figure 8-24 shows the conventional approach to material selection. Here the operating stress was to be 150 000 psi. Material B was a candidate. Its yield strength was 200 000 psi; dividing the yield strength by the operating strength gave a safety factor of 1.3. Material A, however, had a yield strength of 285 000 psi, resulting in a safety factor of 1.9. Material A was the obvious choice.

But what if the hardware contains a small crack? Figure 8-25 shows the measured fracture strength as a function of crack size. Material A is very sensitive to cracks, and with cracks of only 0.050 inch or larger the material would fail at or below the desired operating stress. Material B, on the other hand, would tolerate cracks of at least three or four times the size tolerated by material A. If there were absolute certainty that the structure would be crack free or that the inspection method could positively identify every crack greater than 0.050 inch, material A would be a possible choice. This small crack size, however, is almost impossible to detect in large hardware. Also cracks may develop in service. Thus, the preferred material would almost certainly be material B. It is the better material at any crack size greater than 0.030 inch.

Again, the important concept is that most hardware will almost certainly contain small cracks when produced or develop such flaws during its service lifetime.

This should be considered in the evaluation and selection of materials. The evolving technology of fracture mechanics is providing the tools to handle this problem for the application of high-strength metals. (A portion of the Lewis Research Center work in this general area is presented in refs. 17 to 24.)

METALS STRENGTHENED BY DISPERSED INERT PARTICLES

Let us now consider dispersion-strengthened metals. The particular advantage of this method of strengthening is that, in concept, it provides a method for extending the use temperature of any particular metal (e. g., aluminum, nickel, or copper (ref. 25)).

The reason for dispersion strengthening can be understood from the following example of nickel-base alloys with which NASA has worked for many years. Figure 8-26 shows the microstructure of a high-strength nickel-base alloy as seen at an original magnification of ×750. The small particles shown tend to key the structure - to make it resist flowing or deforming under load and thus to make it strong. For highest strengths, it is important that these particles be very small and very close together. Generally, the closer the particles are to each other, the greater the strength. Particles about 1/2-millionth inch in diameter and 10-millionths inch apart are desired. The metallurgist can alter this structure by heat treatment. At very high temperatures, the particles will dissolve into the solid matrix, and at lower temperatures the particles will reprecipitate or reform. Unfortunately, as an effort is made to use the alloys at higher and higher temperatures, the temperature at which the alloy is to be used is the temperature at which the particles dissolve into the matrix, and thus the strength is lost.

To raise the use temperature of alloys, metallurgists are developing new materials called "dispersion-strengthened" metals. The concept is to distribute small particles that will strengthen, but not dissolve into, the metal. This is best accomplished by the methods of powder metallurgy. Figure 8-27 shows the structure of such a material that has been produced at Lewis (ref. 26). This material was made by dispersing 4 volume percent of ultrafine particles of thorium dioxide (ThO_2) into pure nickel. The structure looks so different from the microstructures in figure 8-26 because this structure has been magnified to about ×11 000 (using the electron microscope) to show the ultrafine particles of ThO_2 (the dots in the structure). These ceramic particles will not redissolve in the metal even at the melting point of nickel (2650° F). Thus, they continue to serve their strengthening function at temperatures approaching the melting point of nickel.

Available commercial materials made in this way are aluminum oxide (Al_2O_3)

distributed in aluminum, thorium oxide in nickel, and beryllium oxide (BeO) in copper. The strength of the dispersion-strengthened nickel is shown in figure 8-28, which is a plot of stress for rupture in 1000 hours against temperature in ^{O}F. Shown by the dashed curve is the strength of a typical conventional superalloy of the type discussed previously. The solid curve represents dispersion-strengthened nickel (ref. 27). Most impressive is the flat slope of the strength curve for the dispersion-strengthened nickel; it does not lose strength rapidly as temperature is increased. Although the conventional alloys are stronger at low temperatures, they rapidly lose strength as temperature is increased, particularly in the range of 0.6 to 0.7 of the melting point, in part because the particles that are largely responsible for strengthening are dissolving into the metal. The thorium oxide particle in the dispersion-strengthened nickel is stable, and the strength is retained.

Another advantage of dispersion-strengthened metals is the opportunity to create materials with physical properties that are not possible in conventional alloys. Alloying severely reduces thermal conductivity and electrical conductivity. For example, just 2 percent of aluminum added to copper reduces the thermal conductivity of copper by 75 percent. This fact can be shown also for the nickel-base materials just discussed. Figure 8-29 shows the thermal conductivity of nickel and the conductivity of a high-strength nickel alloy. The alloy has only 10 percent of the conductivity of pure nickel. The previously described dispersion-strengthened nickel, strengthened by the addition of 2 volume percent of discrete particles of thorium oxide, has 90 percent of the conductivity of nickel. This result is expected because much of the material is still the pure metal, not an alloy, and the only interferences to conduction in this pure metal are the isolated discrete particles of ThO_2. But there is a free path of pure metal all around these particles, which make up only 2 to 4 volume percent of the structure.

Examples of dispersion-strengthened conductors are BeO particles dispersed in copper and Al_2O_3 particles dispersed in copper. Data for BeO in copper (ref. 28) are shown in figure 8-30. The strength of the dispersion-strengthened copper compared with that of cold-worked pure copper (upper part of figure) shows that the dispersion-strengthened material holds its strength to high temperature and has a clear advantage.

A plot of the resistivity of these materials (lower part of figure) shows, as expected, that the resistivity of the dispersion-strengthened copper is only slightly higher than that of pure copper.

Another case where dispersion strengthening is being investigated to develop high-temperature materials of unique properties is for magnetic materials. If magnetic metal alloys are sought for use at high temperatures, the first objective is to achieve maximum Curie temperature. Next, alloying additions are considered that

will strengthen this good magnetic material. The NASA has developed a new cobalt-base alloy by conventional strengthening methods that look very attractive for this purpose (ref. 29). However, as the metallurgist seeks alloying additions to improve the strength of such alloys, he finds that the additions that improve strength unfortunately degrade magnetic properties. Thus, he again turns to the methods of powder metallurgy and dispersion strengthening to achieve an increase in use temperature with little degradation in magnetic properties. Such studies are being conducted under NASA contract (e.g., Westinghouse contract NAS 3-6465), and some materials of interest have been identified.

FIBER-REINFORCED MATERIALS

Whiskers (fig. 8-31) are nearly perfect single crystals of materials that have strengths of about 3 000 000 psi, approaching the theoretical strength of materials, whereas the materials in use today have strengths of only 5 percent of theoretical. Unfortunately, these near theoretical strengths are available only from these tiny, fragile whiskers, but other fiber materials in polycrystalline form are available in greater lengths and are less fragile. Typical strengths are shown in figure 8-32.

The whiskers of graphite and Al_2O_3 have strengths of about 3 000 000 psi (top of the figure). On the lowest portion of the figure are shown the useful strengths (yield strengths) of typical conventional bar materials. The most familiar of the polycrystal fibers is "E" glass. This fiber is used in most industrial applications of composites, such as fishing poles and boats. Even stronger fibers are being developed, for example, silicon dioxide (SiO_2) and a new glass fiber, "S" glass. These fibers have 2 to 4 times the strength of high-strength steels. Also shown are the strengths of two metal wires, steel rocket wire and tungsten. The strengths of boron and graphite are also included. There are, of course, many weaker fibers that have not been plotted.

For aerospace applications lightweight materials are of particular interest. Thus, if material density were factored in, the heavier metal wires of steel and tungsten would be lower in relative standing and the others, because of their low weight, would have even greater advantage. A great deal is heard about boron and graphite fibers, but this comparison suggests that at their present state of development, strength is not their greatest asset. These two materials are of interest because of their exceptionally high modulus of elasticity which is of prime importance in many structures, particularly for aerospace use, where stiffness and light weight are the prime design criteria.

To utilize the strengths of fibers they must be assembled into a composite with

232

either a metal or plastic matrix. Figure 8-33 shows a typical composite specimen made by assembling tungsten wires into a matrix of copper. The circles are the tungsten wires of 0.005 inch diameter, and the area between is copper. Fishing poles are often made by binding glass fibers together with a matrix of plastic. As a general rule in composites, the more fiber that is packed into the composite, the higher the strength.

Because good bonding is obtained with W-Cu and no damaging reactions occur between the two, NASA has used this combination as a model system for fundamental research into micromechanics of composites, and many publications are available to describe the work in this area (ref. 30).

As in the case of dispersion-strengthened metals, fiber-reinforced metals offer an opportunity to find new materials that will have a higher use temperature than conventional alloys. In an attempt to find better high-temperature materials for jet engine turbine buckets, new materials have recently been made by embedding tungsten wires in a superalloy matrix. Methods have been found for assembling these tungsten wire - superalloy composites such that in laboratory tests at 2000° F specimens have three times the 100-hour rupture strength of conventional nickel-base alloys used today. Although they are very heavy materials, even on a stress-density basis these composites have a significant strength advantage over conventional alloys (ref. 31).

With fiber composites as with dispersion-strengthened metals, there is an opportunity to tailormake materials with the specific properties needed. This applies particularly to physical properties, such as conductivity or resistivity. For example, in the W-Cu model system, the copper in the matrix provides high conductivity (or low resistivity), and the tungsten wires provide strength. The composite should have high strength and low resistivity, and a wide range of these properties is possible depending on the volume percent of tungsten wires in the composite.

Figure 8-34 shows some interesting data for this system (ref. 32). The parameter plotted is the ratio of strength to resistivity, and high values may be sought for some conductor applications. In the center portion of the figure is shown the range of values for W-Cu composites with the value depending on the volume percent of tungsten wire in the copper. For comparison, on the left is shown the strength-resistivity ratio for available electrical conductors, silver, aluminum, and copper. On the right are shown typical values for transmission cables, which are composite structures rather than composite materials. The W-Cu composites show a clear advantage. It should be pointed out, however, that on a cost basis this composite is not competitive with the standard conductors. Other combinations utilizing cheaper fibers with better conductivity than tungsten may prove to be of practical use. These W-Cu fiber composites, however, do have strength at temperatures where other

conductors are useless, and W-Cu might therefore have a use in some special applications at high temperatures.

Figure 8-35 shows the strength of some fiber composites that have been produced. Shown at the top of the figure are two conventional steel alloys for comparison, a structural steel and a high-strength alloy steel. Two classes of fiber composites are shown, fiber-reinforced metals and fiber-reinforced plastics. The volume percent of fiber in the composite is shown. Generally, if more fiber could be added, even better strengths would be achieved.

Composite data are shown for 25 percent steel wire in aluminum, 50 percent boron in aluminum, and the model system of tungsten in copper with 75 volume percent tungsten.

For plastics, NASA data (ref. 33) for filament-wound specimens of "S" glass and graphite and boron in epoxy plastic are tabulated, as well as data from other sources for glass fabric material. The strongest material is "S" glass in epoxy. All of these materials other than "E" glass are superior to structural steel in strength, but only "S" glass - epoxy has a large advantage over alloy steel. If more fiber could be added, however, all of the composite materials would show a significant advantage.

As mentioned earlier in this section, greater advantages are shown for fiber-reinforced materials if the comparisons are made on the basis of both strength and density. In figure 8-36 the same materials are shown, but because high strength and low weight are often required in aerospace applications, the comparisons are based on the strength-to-density ratio.

On the basis of that ratio many of the composites are far superior to the steels. The "S" glass epoxy has 13 times the strength-to-density ratio of structural steel and is five times better than the alloy steel. Even glass fabric material is superior to structural steel. The reason for aerospace interest in these materials is obvious. Often the strength-to-density advantage of fiberglass-reinforced plastics is of importance to nonaerospace applications. An example is the boom of the "cherry pickers" used by industry to lift and support men for work on power lines and transformers. If still another comparison were made on the basis of stiffness, the boron and graphite materials would be far superior to all other materials.

A final but important factor to consider in these materials is cost (table 8-I). Here the comparison has been made on the basis of the cost to do the job required of these materials - that is, to carry a load. Imagine that a 1-foot-long piece of material is required to carry a load of 100 000 pounds. If the material is strong, a small-diameter bar would do the job, but if it is weak, more material is required. The dollar values are the comparative numbers.

For the conventional materials the steel alloy is cheapest, costing only

28 cents for the material required. If the new high-strength maraging steels are used, the cost jumps to $1.92. An aluminum alloy is 96 cents, and titanium is $4.32. Other factors than strength alone, of course, dictate the use of higher cost materials. Aluminum is used in homes and cars, though steel would be cheaper. For aerospace applications, maraging steels, aluminum, and titanium are used because they save weight in space, and a pound saved in a vehicle headed for outer space can easily be worth $1000. Thus, initial material costs can be insignificant.

The cost shown for each fiber is that of the fiber alone, not of a fabricated composite. The cost of the glass fibers is competitive with the cheaper steels. When bar steel is converted into wire, the cost to carry a load goes up by a factor of 50, and graphite and boron are very expensive indeed. However, these latter fibers are newly developed materials, and their costs have already come down by factors of over 20 in the past 3 or 4 years. Both, but especially graphite, should decrease significantly as the market increases and production methods improve. Until then their use will be limited to aerospace.

There has already been great commercial interest in the application of glass fibers for reinforcing plastic, as would be expected from their low cost. Figure 8-37 shows a 10 000-gallon underground storage tank for gasoline. These tanks have become common at neighborhood filling stations. In addition to providing the necessary strength and light weight, glass-reinforced plastics are much cheaper than steel because of greatly superior corrosion resistance.

Figures 8-38 shows an auto trailer and a railroad tank car that have been fabricated by using the filament winding technique - exactly the technology developed for fabrication of rocket tanks. Use of fiberglass-reinforced plastic saves 9 tons of weight in a railroad car, which should mean cheaper transportation.

CONCLUDING REMARKS

In conclusion, five areas of emerging technology in engineering mechanics and materials have been summarized - areas that may be of interest to the power industry. Perhaps this presentation will stimulate more detailed discussions whereby NASA research efforts can be of further assistance on special problems of the power industry.

REFERENCES

1. Manson, S. S.; and Haferd, A. M.: A Linear Time-Temperature Relation for Extrapolation of Creep and Stress-Rupture Data. NACA TN 2890, 1953.

2. Manson, S. S.: Design Considerations for Long Life at Elevated Temperatures. Joint International Conference on Creep. Vol. II - Discussion. Institution of Mechanical Engrs., London, 1965, p. D-36.

3. Manson, S. S.: Succop, G.; and Brown, W. R., Jr.: The Application of Time Temperature Parameters to Accelerated Creep-Rupture Testing. Trans. ASM, vol. 51, 1959, pp. 911-934.

4. Mendelson, Alexander; Roberts, Ernest, Jr.; and Manson, S. S.: Optimization of Time-Temperature Parameters for Creep and Stress Rupture, with Application to Data from German Cooperative Long-Time Creep Program. NASA TN D-2975, 1965.

5. Woodyatt, L. R.; Sims, C. T.; and Beattie, H. J., Jr.: Prediction of Sigma-Type Phase Occurrence from Compositions in Austenitic Superalloys. Trans. AIME, vol. 236, no. 4, Apr. 1966, pp. 519-527.

6. Sandrock, Gary D.; Ashbrook, Richard L.; and Freche, John C.: Effect of Variations in Silicon and Iron Content on Embrittlement of a Cobalt-Base Alloy (L-605). NASA TN D-2989, 1965.

7. Sandrock, Gary D.; and Leonard, L.: Cold Reduction as a Means of Reducing Embrittlement of a Cobalt-Base Alloy (L-605). NASA TN D-3528, 1966.

8. Wolf, James S.; and Sandrock, Gary D.: Some Observations Concerning the Oxidation of the Cobalt-Base Superalloy L-605 (HS-25). NASA TN D-4715, 1968.

9. Coffin, L. F., Jr.: A Study of the Effects of Cyclic Thermal Stresses on a Ductile Metal. Trans. ASME, vol. 76, no. 6, Aug. 1954, pp. 931-950.

10. Manson, S. S.: Thermal Stress and Low-Cycle Fatigue. McGraw-Hill Book Co., Inc., 1966, p. 132.

11. Manson, S. S.: Fatigue: A Complex Subject - Some Simple Approximations. Exp. Mech., vol. 5, no. 7, July 1965, pp. 193-226.

12. Manson, S. S.; and Halford, G. R.: A Method of Estimating High-Temperature, Low-Cycle Fatigue Behavior of Metals. Presented at the International Conference on Thermal and High-Strain Fatigue, Institute of Metals, London, 1967.

13. Halford, G. R.; and Manson, S. S.: Application of a Method of Estimating High-Temperature, Low-Cycle Fatigue Behavior of Materials. Presented at the ASM National Metal Congress, Cleveland, Ohio, Oct. 19, 1967.

14. Shannon, John L., Jr.: Fracture Mechanics - Part 1. Machine Des., vol. 39, no. 23, Sept. 28, 1967, pp. 122-127.

15. Shannon, John L., Jr.: Fracture Mechanics - Part 2. Machine Des., vol. 39, no. 24, Oct. 12, 1967, pp. 188-194.

16. Anon.: Proposed Recommended Practice for Plane-Strain Fracture Toughness Testing of High-Strength Metallic Materials Using a Fatigue-Cracked Bend Specimen. ASTM Standards, Part 31, 1968, pp. 1018-1030.

17. Anon.: Fracture Toughness Testing and Its Applications. Spec. Tech. Publ. No. 381, ASTM, 1965, pp. 1-2, 133-196.

18. Fisher, Douglas M.; Bubsey, Raymond T.; and Srawley, John E.: Design and Use of Displacement Gage for Crack-Extension Measurements. NASA TN D-3724, 1966.

19. Brown, W. F., Jr.; and Srawley, J. E.: Plane Strain Crack Toughness Testing of High Strength Metallic Materials. Spec. Tech. Publ. No. 410, ASTM, 1967.

20. Srawley, J. E.; Jones, M. H.; and Brown, W. F., Jr.: Determination of Plane Strain Fracture Toughness. Mat. Res. & Standards, vol. 7, no. 6, June 1967, p. 262.

21. Pierce, William S.: Crack Growth in 2014-T6 Aluminum Tensile and Tank Specimens Cyclically Loaded at Cryogenic Temperatures. NASA TN D-4541, 1968.

22. Sullivan, Timothy L.: Uniaxial and Biaxial Fracture Toughness of Extra-Low Interstitial 5A1-2.5Sn Titanium Alloy Sheet at 20° K. NASA TN D-4016, 1967.

23. Sullivan, Timothy L.; and Orange, Thomas W.: Continuity Gage Measurement of Crack Growth on Flat and Curved Surfaces at Cryogenic Temperatures. NASA TN D-3747, 1966.

24. Orange, Thomas W.: Evaluation of Special 301-Type Stainless Steel for Improved Low Temperature Notch Toughness of Cryoformed Pressure Vessels. NASA TN D-3445, 1966.

25. Ault, G. Mervin; and Burte, H. M.: Technical Applications for Oxide-Dispersion Strengthened Materials. Presented at the AIME Conference on Oxide Dispersion Strengthening, Bolton Landing, N. Y., June 27, 1966.

26. Weeton, John W.; and Quatinetz, Max: Cleaning and Stabilization of Dispersion Strengthened Materials. Presented at the AIME Conference on Oxide Dispersion Strengthening, Bolton Landing, N. Y., June 27, 1966.

27. Anon.: TD Nickel Dispersion Strengthened Nickel. Rep. A-27045, Dupont Metal Products, New Product Information.

28. McDonald, Allen S.: A Dispersion Hardened Copper for Electrical Uses.
Metal Progress, vol. 89, no. 4, Apr. 1966, pp. 70-72.

29. Ashbrook, Richard L.; Hoffman, Anthony C.; Sandrock, Gary D.; and
Dreshfield, Robert L.: Development of a Cobalt-Tungsten Ferromagnetic,
High-Temperature, Structural Alloy. NASA TN D-4338, 1968.

30. Weeton, John W.; and Signorelli, Robert A.: Fiber-Metal Composite Mate-
rials. NASA TN D-3530, 1966.

31. Petrasek, Donald W.; Signorelli, Robert A.; and Weeton, John W.: Refractory
Metal Fiber Nickel Alloy Composites for Use at High Temperatures. Pre-
sented at the Society of Aerospace Material and Process Engineers 12th
National Symposium, Orange County, Calif., Oct. 10-12, 1967.

32. McDanels, David L.: Electrical Resistivity and Conductivity of Tungsten-
Fiber-Reinforced Copper Composites. NASA TN D-3590, 1966.

33. Hanson, Morgan P.: Glass-, Boron-, and Graphite-Filament-Wound Resin
Composites and Liners for Cryogenic Pressure Vessels. NASA TN D-4412,
1968.

TABLE 8-I. - COST OF FIBERS COMPARED

TO CONVENTIONAL MATERIALS

Materials	Cost of 1-ft-long bar to carry 100 000-lb load
Conventional:	
Steel (structural)	$ 0.28
(304 SS)	1.81
(maraging)	1.92
Aluminum (6061)	.96
Titanium (6Al-4V)	4.32
Fibers:	
"E" glass	0.12
"S" glass	.17
SiO_2 (quartz)	3.40
Steel (rocket wire)	8.40
Graphite (RAE)	62.00
Boron	115.00
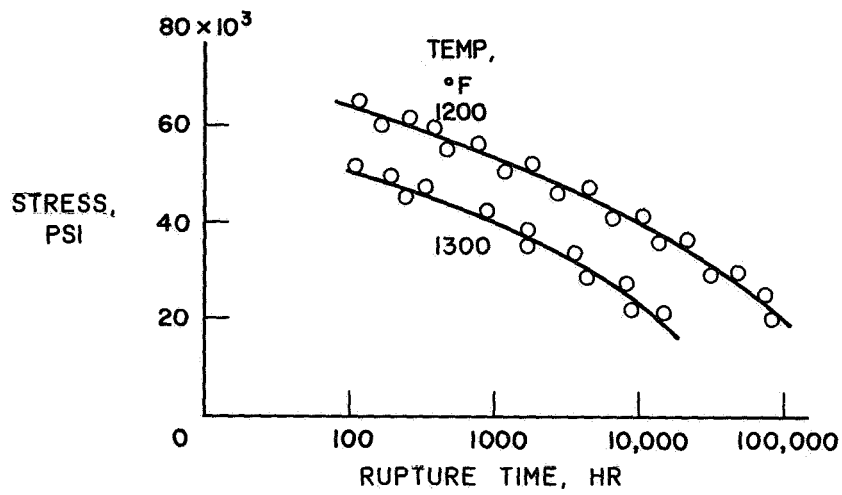
Figure 8-1. - Stress to rupture.
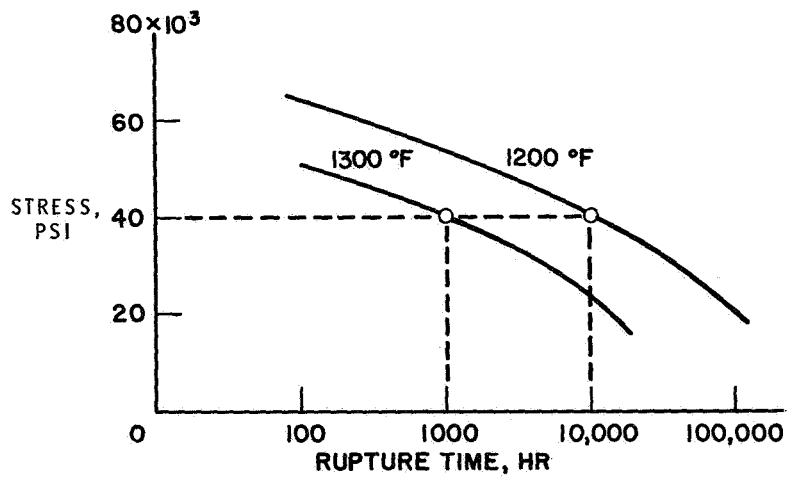
Figure 8-2. - Reduction of test time by increasing temperature.

$$P = \frac{T-660}{LOG\ t\ -\ 8.83}$$
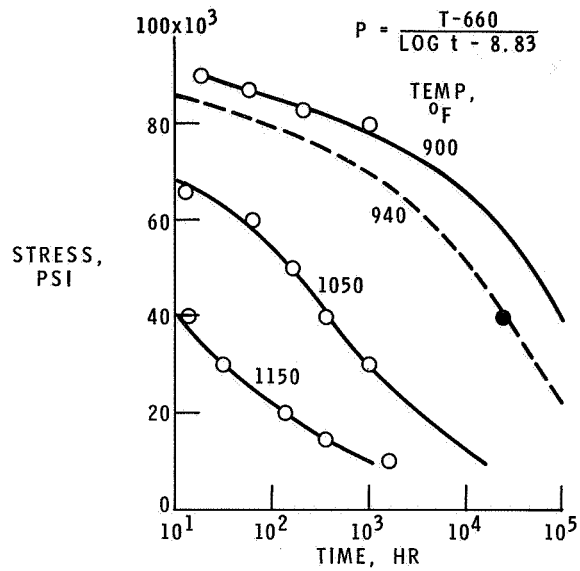
Figure 8-3. - Use of Manson-Haferd parameter to interpolate and extrapolate data.

$$P = \frac{LOG\ t\ -\ 8.87}{(T\ +\ 100)^{2.5}} \bullet$$
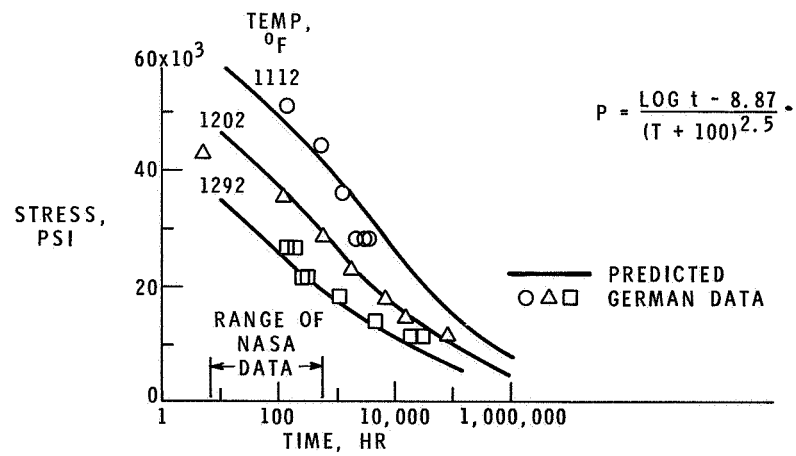
Figure 8-4. - Parameter extrapolations for German steel based on short-time NASA data.
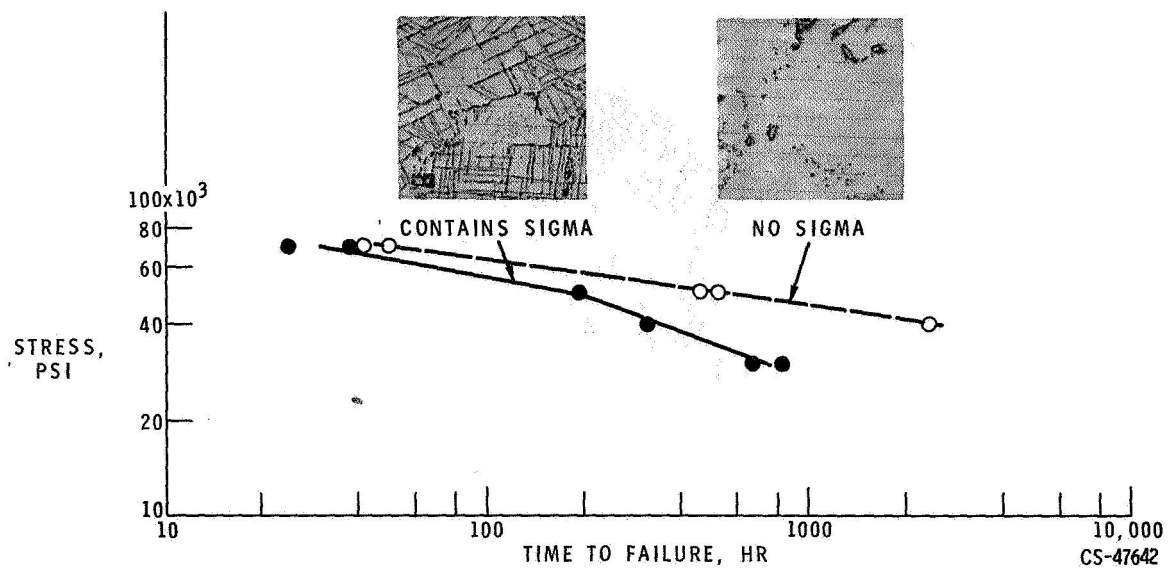
Figure 8-5. - Influence of metallurgical instability on long-time strength (1550° F).
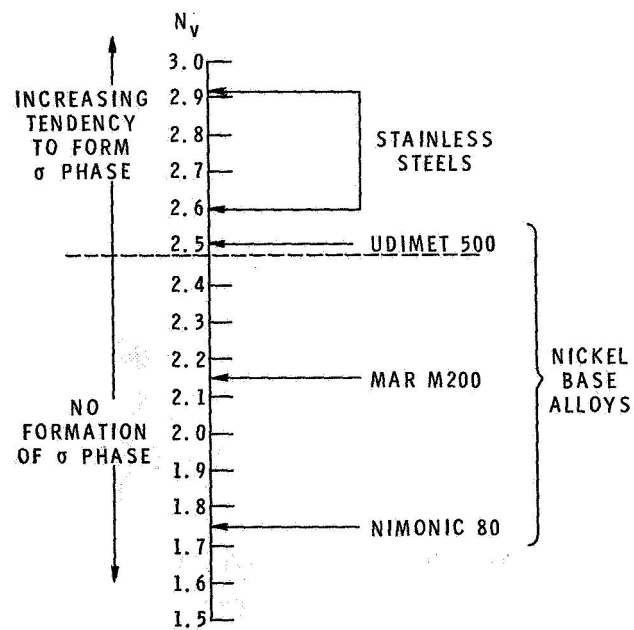
Figure 8-6. - Prediction of sigma formation from N_v calculation where N_v is function of elements in alloy and their electron vacancy.
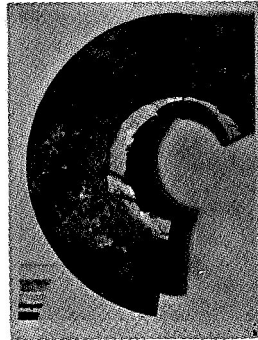
CS-47639

Figure 8-7. - Thermal fatigue failure of
superheater nozzle connection.
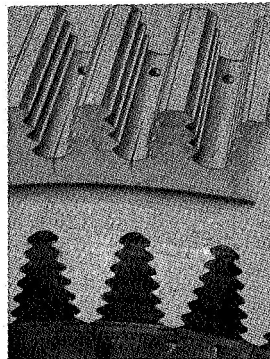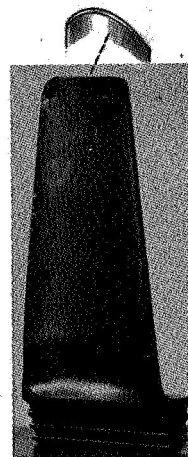
CS-47618

TURBINE DISK   TURBINE BUCKET

Figure 8-8. - Typical thermal fatigue failures.

242

CONSTRAINT
OF THERMAL   RESULTS   LOCAL
EXPANSION   IN   STRAINS

HEAT

EXPANSION   STRAIN
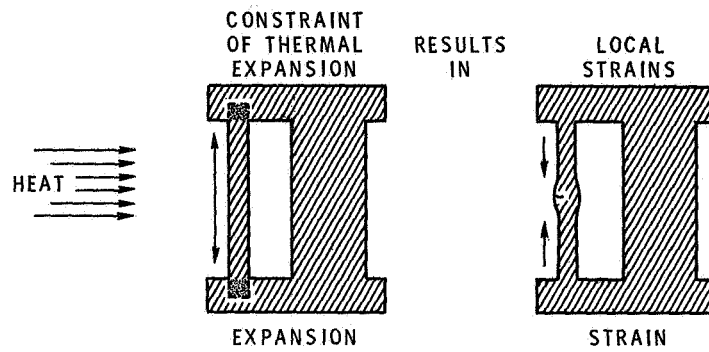
Figure 8-9. - Mechanism of thermal fatigue.

CYCLIC
PLASTIC
STRAIN,
$\Delta \epsilon_p$

$\Delta \epsilon_p = CN_f^Z$

CYCLES TO FAILURE, N_f
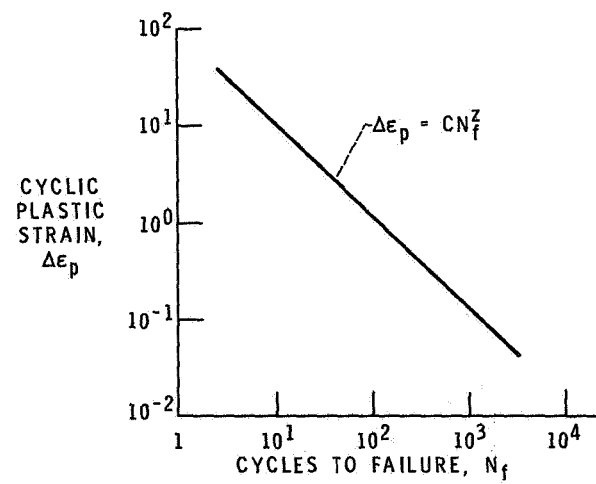
Figure 8-10. - Manson-Coffin rule for plastic fatigue.
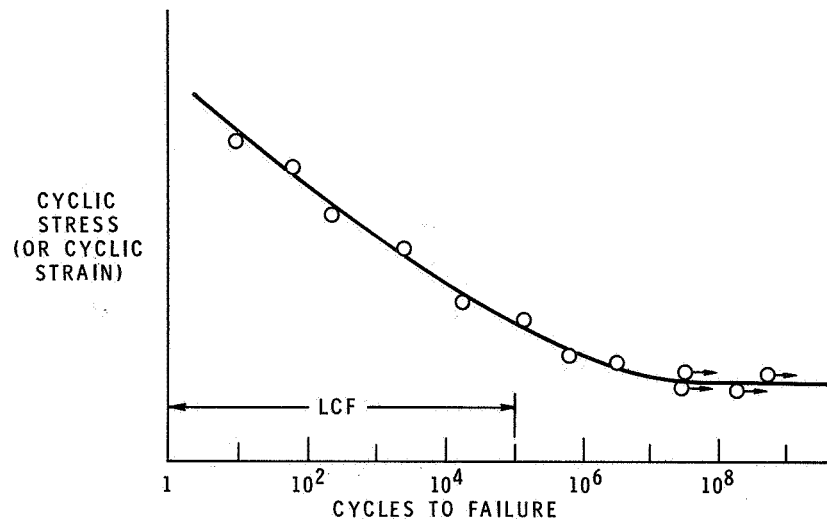
Figure 8-11. - Typical fatigue curve.
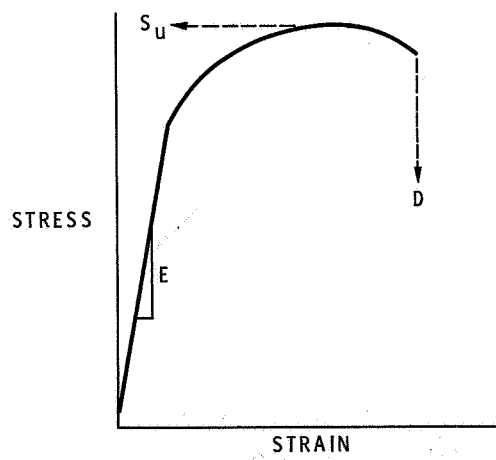
Figure 8-12. - Short-time tensile curve.

244
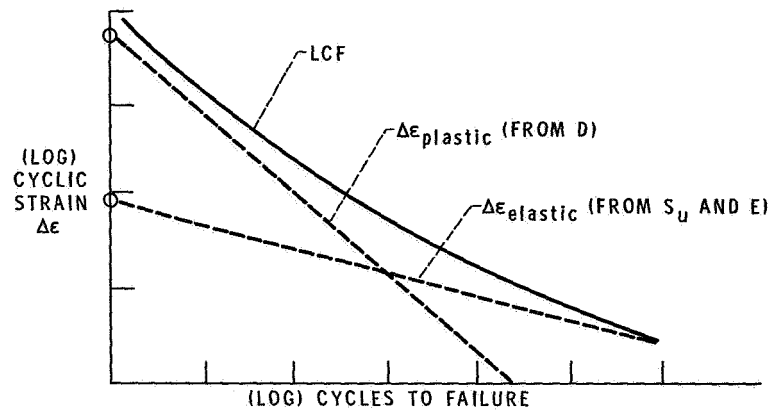
Figure 8-13. - Prediction of low-cycle fatigue from tensile test by method of universal slopes.
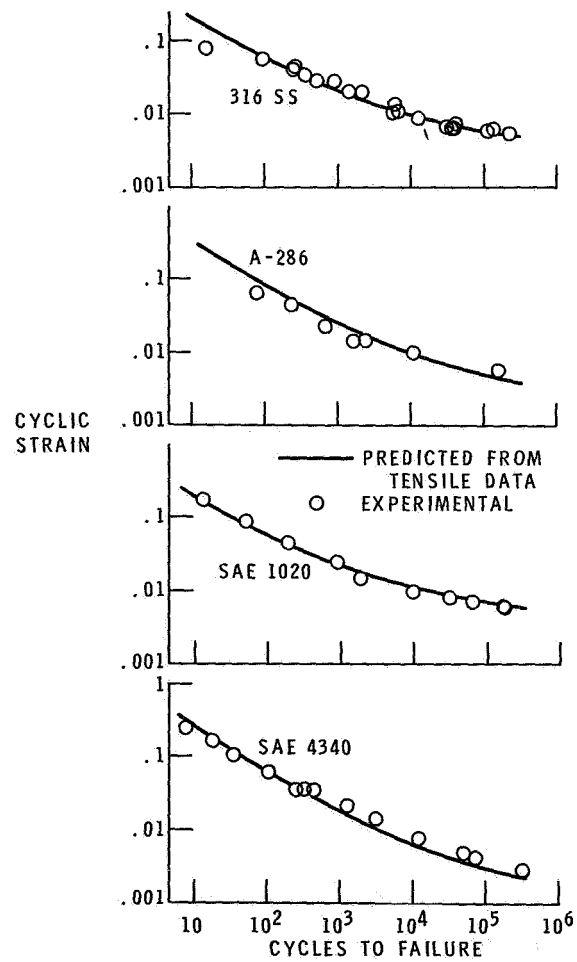
Figure 8-14. - Prediction of low-cycle fatigue from short-time tensile test.
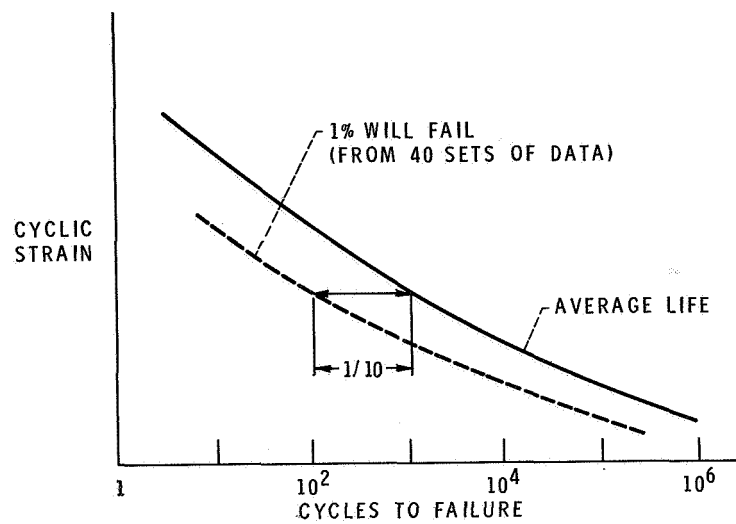
Figure 8-15. - Estimation of low-cycle fatigue at high temperature by universal slopes 10 percent rule.
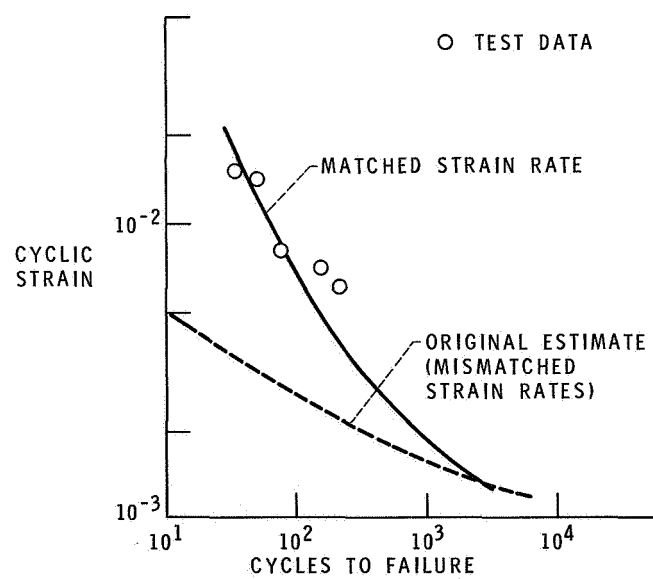
Figure 8-16. - Improved estimate of high-temperature low-cycle fatigue.

246
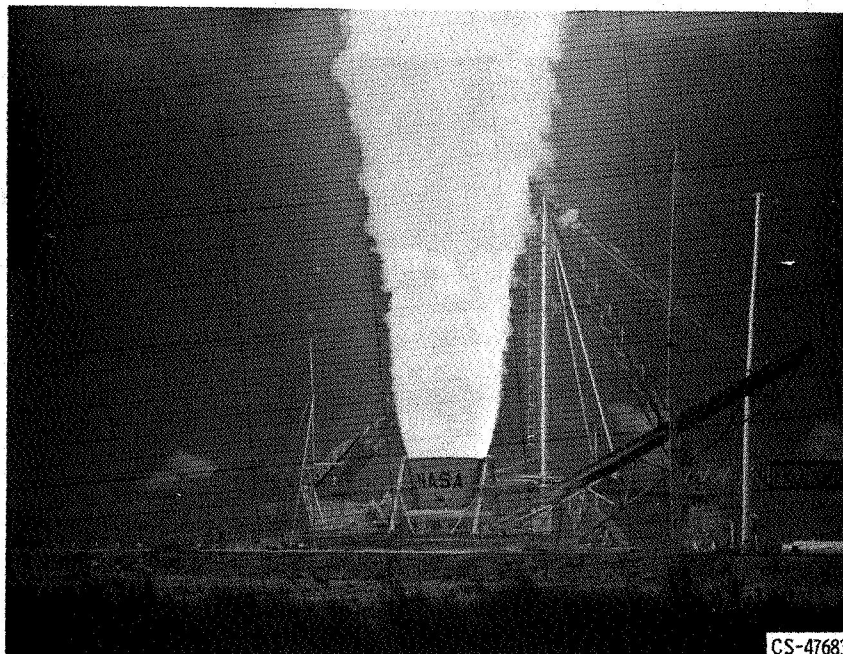
Figure 8-17. - Solid-propellant 260-inch-diameter rocket.

Figure 8-18. - Case for 260-inch solid rocket motor.

247
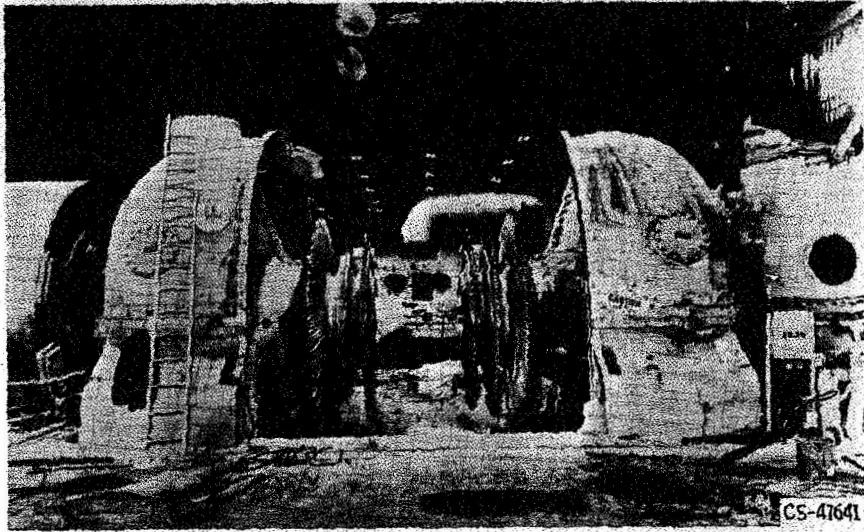
Figure 8-19. - Failure of steam turbine.
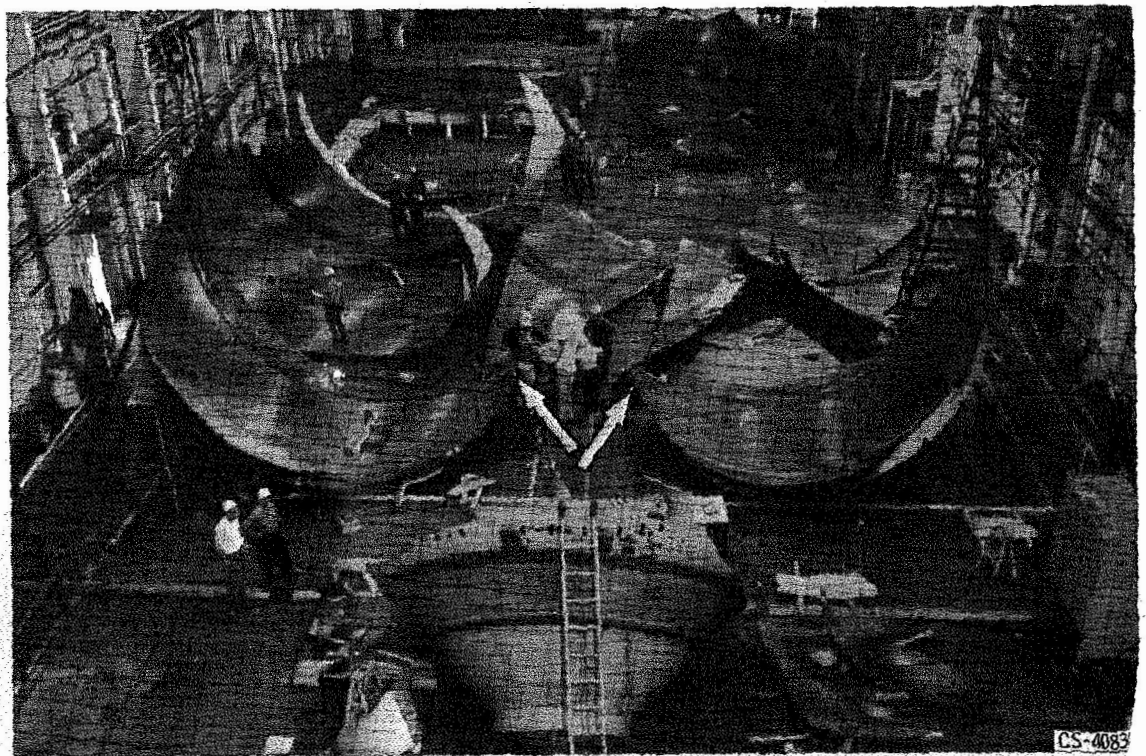
Figure 8-20. - Failed 260-inch rocket motor case.

0.7"

CS-47643
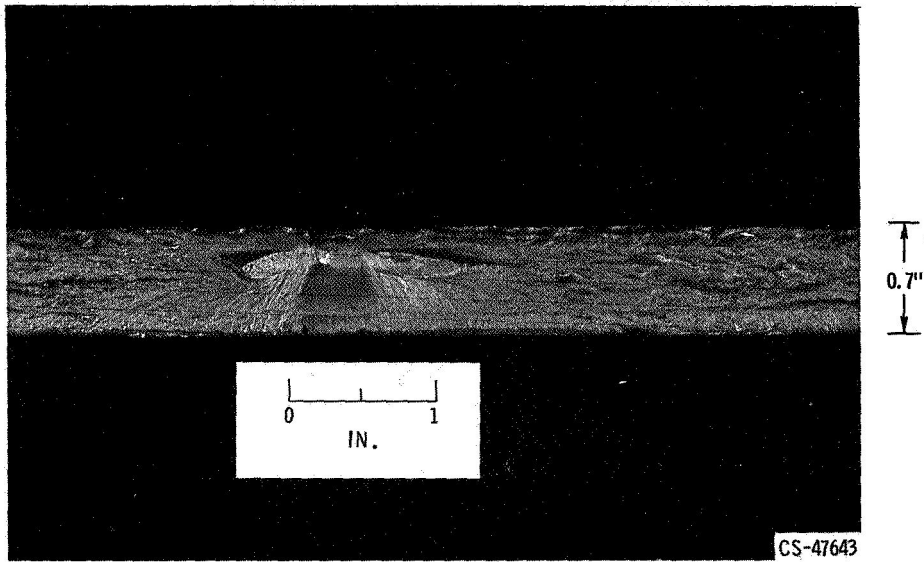
Figure 8-21. - Flaw at which fracture initiated.

"DUCTILE" METAL

PLASTIC ZONE

"BRITTLE" METAL

PLASTIC ZONE

ELASTIC

PLASTIC

STRESS
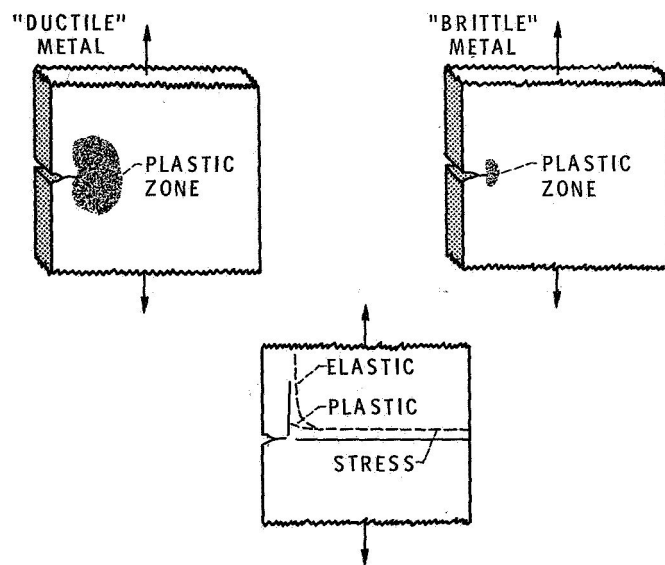
Figure 8-22. - Brittle fracture of metals.
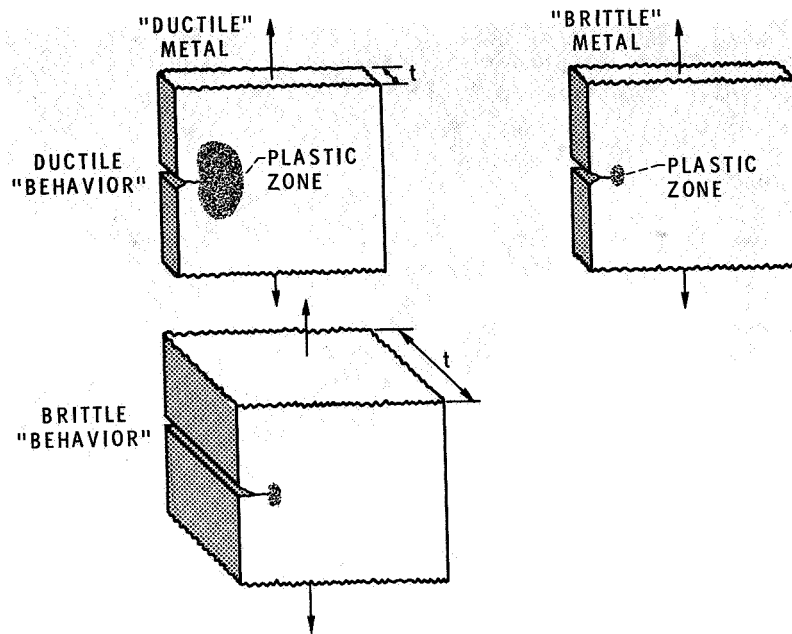
Figure 8-23. - Variation of fracture with part geometry.

	YIELD STRENGTH	SAFETY FACTOR	MATERIAL
	285,000	1.9 ←	A
	200,000	1.3 ←	B
	← OPERATING STRESS		
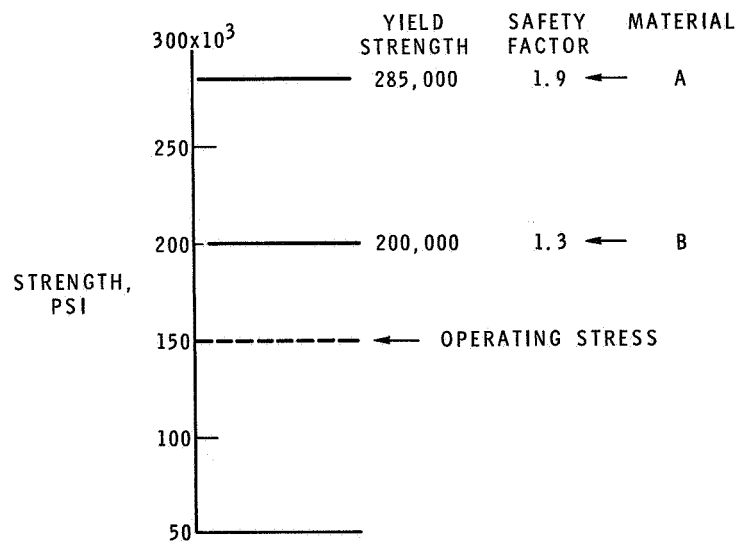
Figure 8-24. - Conventional comparison of materials based on safety factor.

250
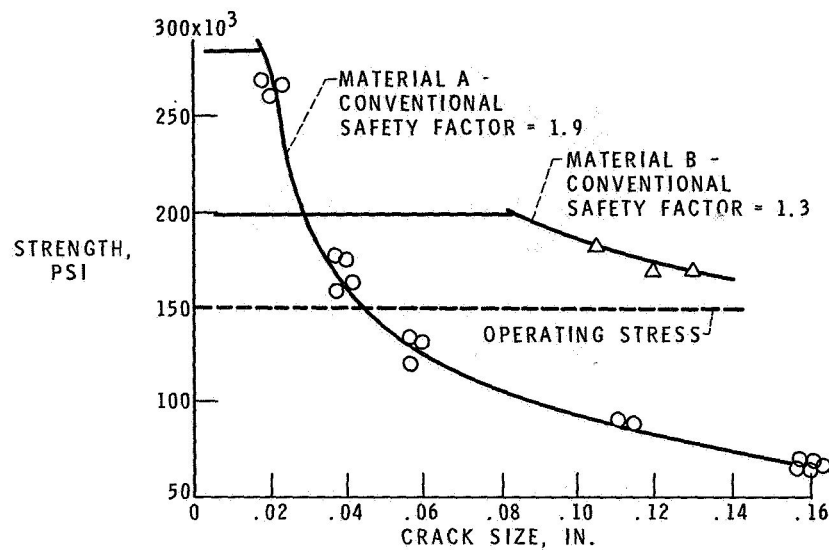
Figure 8-25. - Importance of considering material flaws or cracks in design.

STRONGEST CONDITION   AFTER HEATING TO 2175° F

├──┤
10 µ   CS-32042
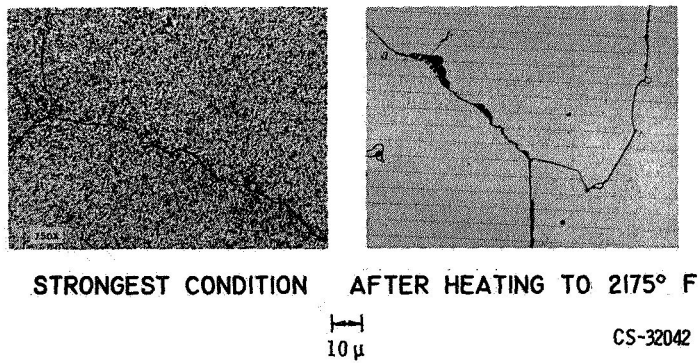
Figure 8-26. - Microstructure of typical high-temperature alloy.

CS-47640

1 μ

L___J
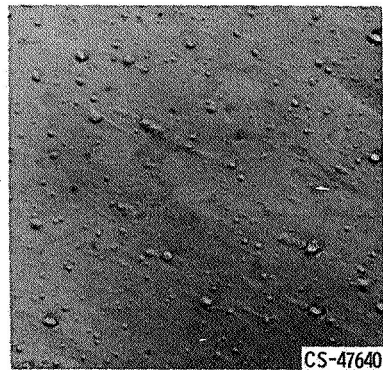
Figure 8-27. – Dispersion-strengthened super-
alloy (Ni + ThO$_2$).
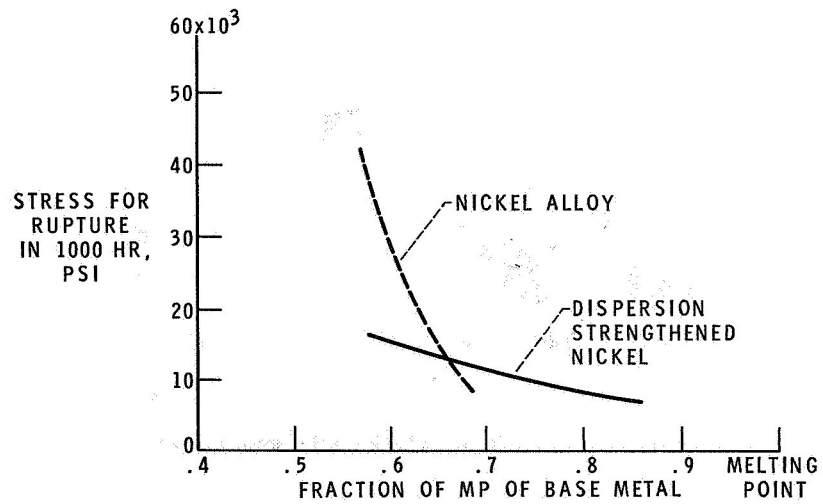
Figure 8-28. – Dispersion-strengthened metals retain strength to higher temperatures.
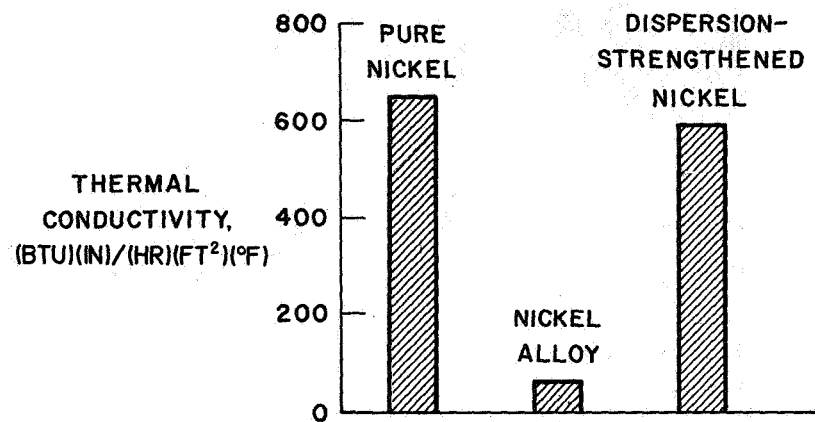
Figure 8-29. - Dispersion-strengthened pure metals maintain excellent conductivity.
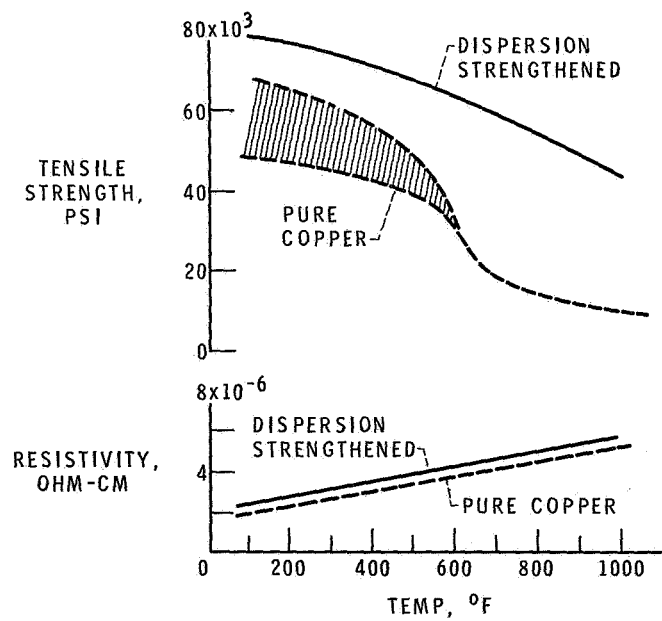
Figure 8-30. - High-temperature strength and low resistivity with dispersion strengthening.
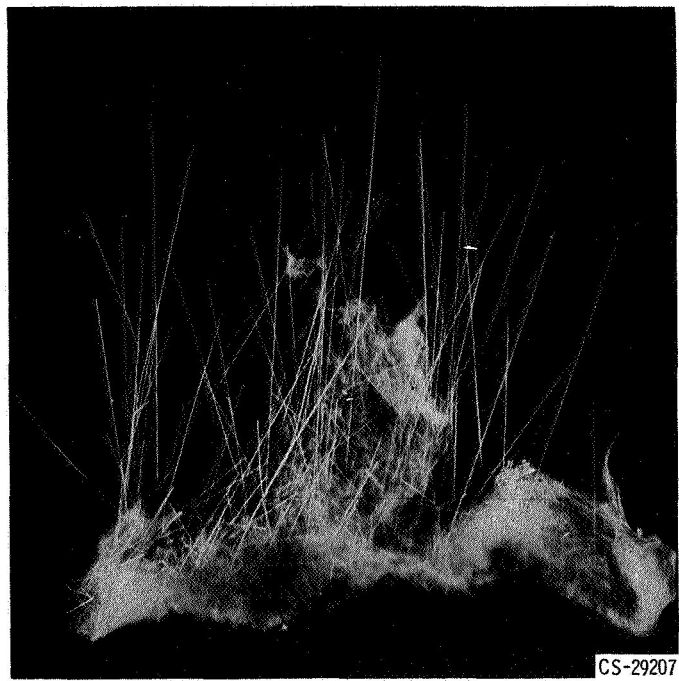
Figure 8-31. – Sapphire (Al$_2$O$_3$) whiskers.
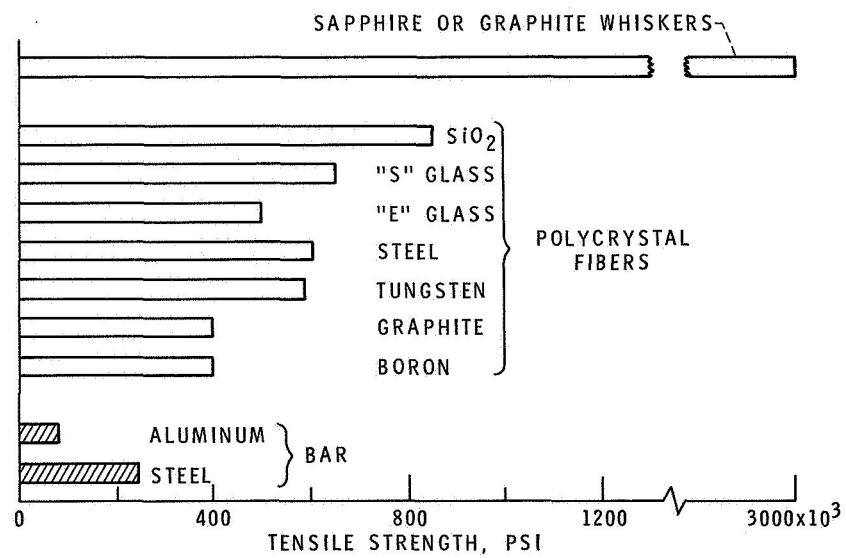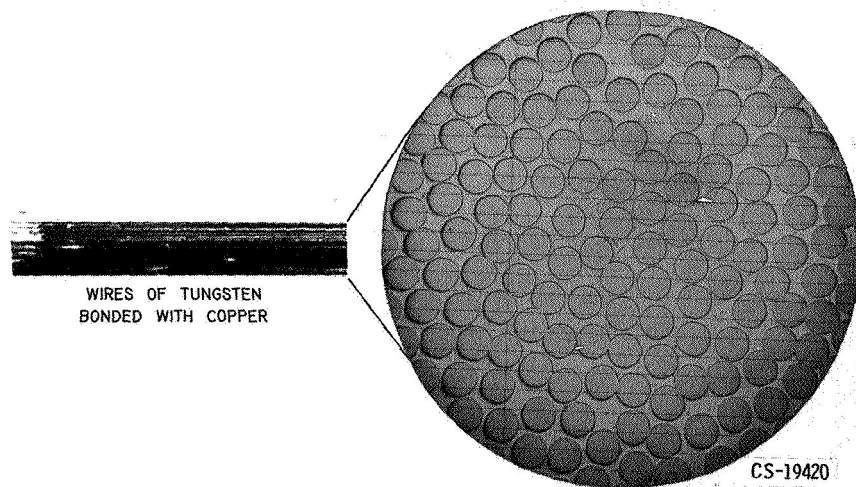

Figure 8-32. – Strength of fibers.

254

WIRES OF TUNGSTEN
BONDED WITH COPPER

CS-19420

Figure 8-33. - Composite materials from metal fibers.
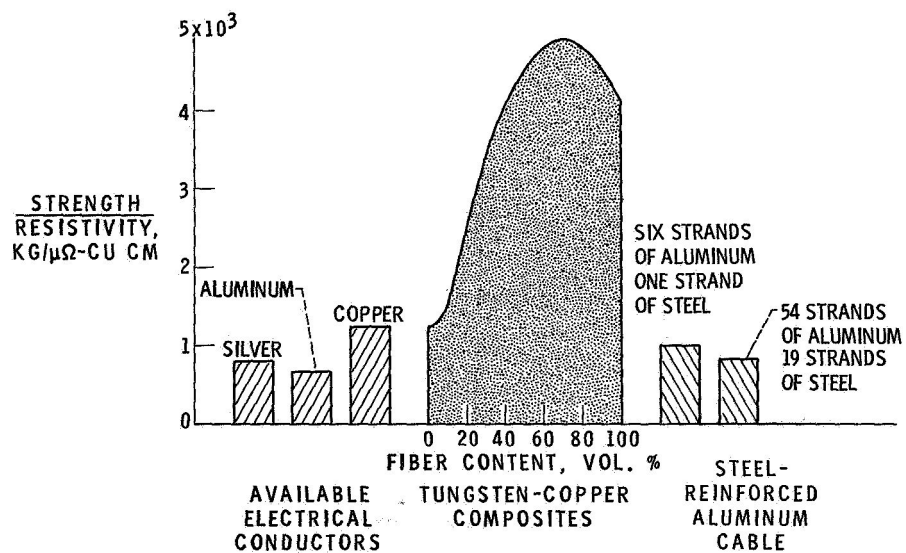
Figure 8-34. - Comparison of tungsten-fiber-reinforced copper composites with other electrical conductors.
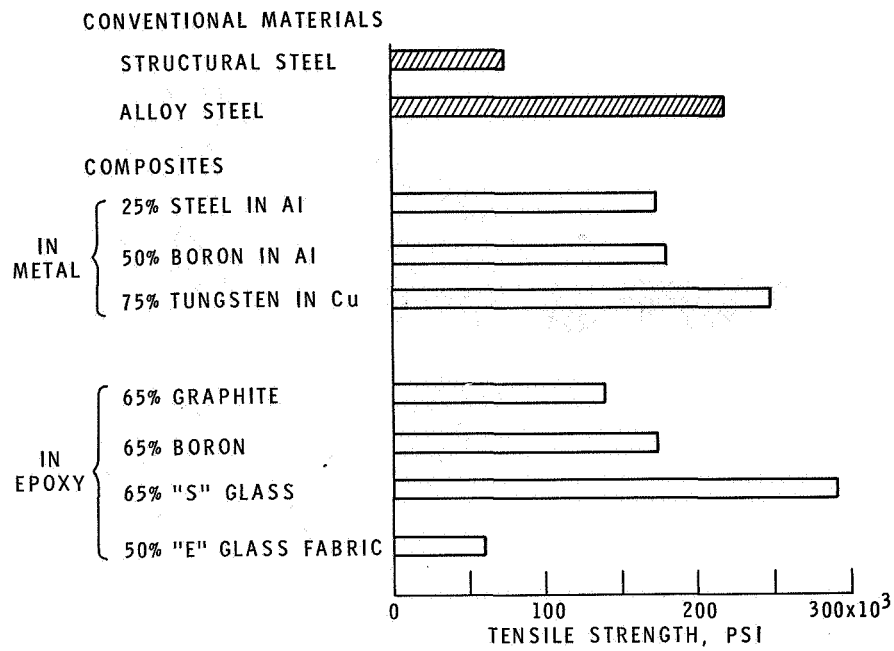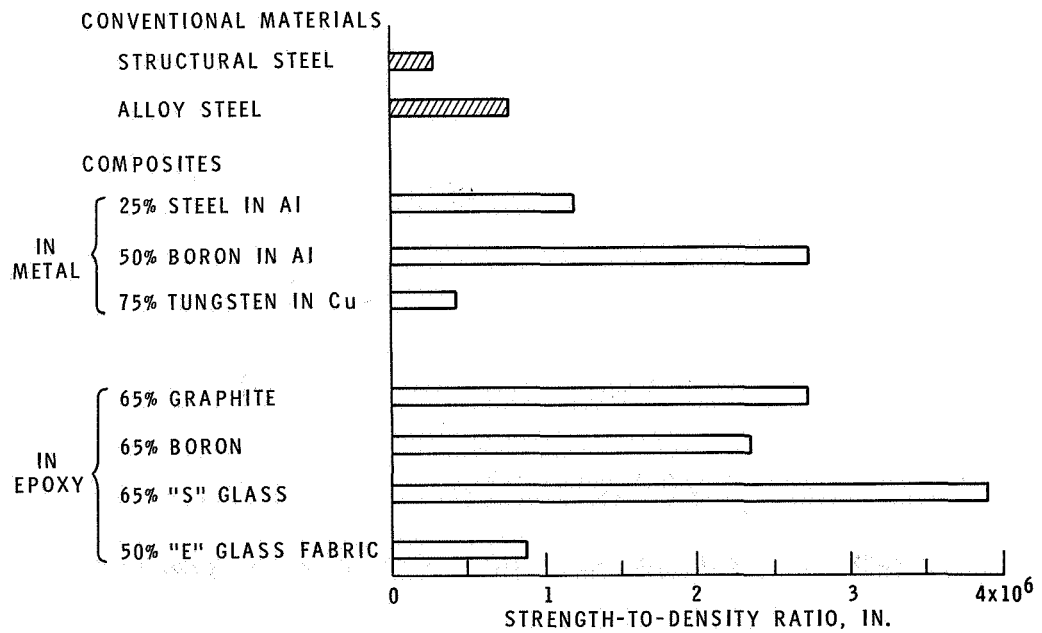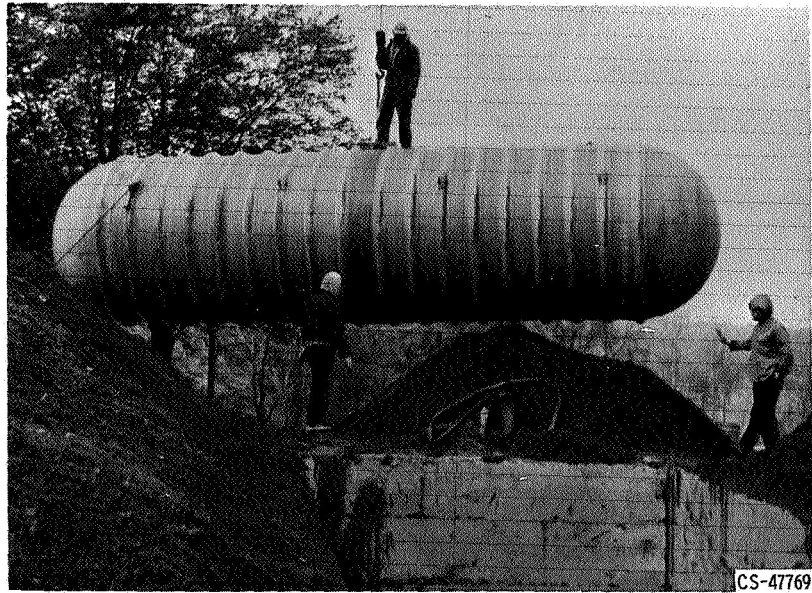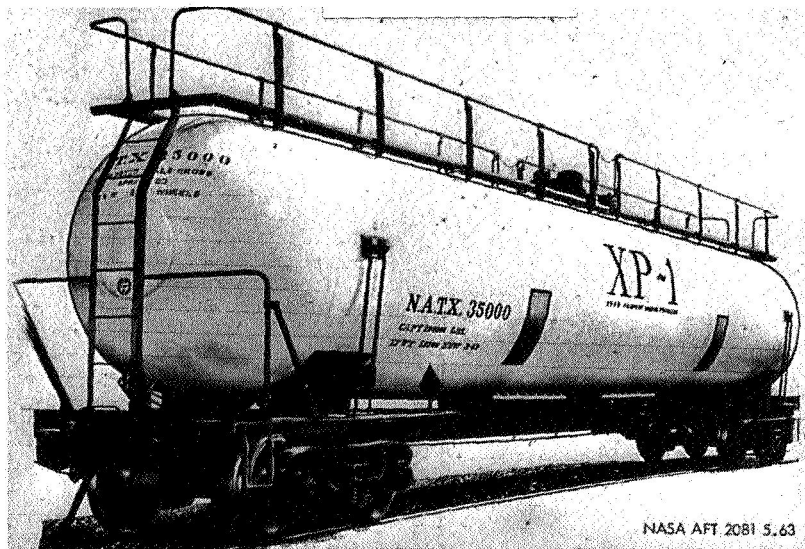
255

Figure 8-35. - Tensile strength of composites.

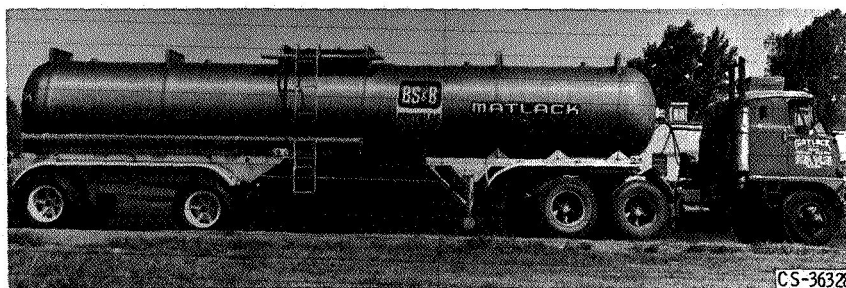Figure 8-36. - High strength-to-density ratios of composites.

256

Figure 8-37. - Fiberglass-reinforced 10,000-gallon plastic tank for underground storage.

Figure 8-38. - Filament-wound glass-reinforced plastic tanks.

9. CRYOGENICS AND SUPERCONDUCTIVITY

Donald L. Nored and James C. Laurence

Currently, the electrical industry is showing increasing interest in applications involving cryogenic temperatures. This interest is due to the decreasing electrical resistance of most conductors with decreasing temperature, which thus provides a considerable power savings. NASA is deeply involved in several areas of technology pertinent to this field. Conductors at low temperature, for example, are being used in high flux magnets. Storage and handling of cryogenic fluids required for such low temperatures are now routine. Information gained from the NASA efforts in these and other fields may be of future value to the electrical industry, such as in the design of low-temperature power transmission lines or other low-resistance devices.

An example of the effect of low temperatures on electrical resistance (in this case, for copper) is shown in figure 9-1. The electrical resistance ratio plotted is the ratio of the resistance of the conductor at any temperature to the resistance of the conductor at 492° R (i.e., the freezing point of water). The dashed curve is for common annealed copper, while the solid curve is for copper of 99.999-percent purity. For copper, as for most conductors, most of the change in resistance occurs at temperatures below about 150° R, with the resistance dropping rapidly before leveling off at some lower value. This final lower value of the resistance is called the residual resistance, and the more the material is refined, the lower the absolute value can be. All good conductors, such as copper or aluminum, show this decrease in electrical resistance of several orders of magnitude or more between room temperature and temperatures near absolute zero. Some materials, however, exhibit another phenomenon as absolute zero is approached, as illustrated in figure 9-2.

In this case, for tin of high purity, the resistance drops to zero at a certain critical temperature. This phenomenon is typical of many pure metals, alloys, and compounds, which as a class are called superconductors. Generally, the critical temperatures are close to absolute zero. There are a few superconductors, however, which have somewhat higher critical temperatures. Niobium, at about 16° R, is the best of the pure metals. Higher critical temperatures can be

achieved only by using an alloy or a compound. For example, Nb_3Sn becomes superconductive at about 33° R, a critical temperature twice as high as that of niobium.

Achieving the low temperatures of interest, for either normal conductors or superconductors, requires some type of refrigeration fluid. The liquid ranges of several fluids of interest are shown in figure 9-3.

Liquid methane and liquid nitrogen are common cryogens, used for a number of purposes. For example, they are useful as shield fluids; that is, they can be used to intercept heat and hence reduce the heat input to a colder fluid, with a resultant reduction in refrigeration requirements. As primary refrigerants, however, they provide only a small decrease in the resistance of conductors. The largest decrease in electrical resistance is obtained at temperatures below about 50° R; thus, neon and hydrogen are the cryogenic fluids usually considered for normal conductors. Currently, for the superconductors, a fluid with a liquid temperature range below 33° R is required, and, for all practical purposes, only helium can be considered. At Lewis, all these cryogenic fluids are in use today for a large variety of applications.

CRYOGENIC MAGNETS

One application, involving the use of liquid neon, is the large cryogenic magnet shown in figure 9-4. The coil section is shown in figure 9-5 in more detail. With a 1-foot-diameter bore, this magnet has a field of 160 000 gauss. With a bore of $4\frac{1}{2}$ inches, the field is 200 000 gauss.

High-purity aluminum (99.999 percent) is used in the magnet as the conductor. This purity was the highest that could be obtained without zone refining. The aluminum is made in the form of a long strip, rolled circumferentially around the bore. Each aluminum turn is reinforced with stainless steel to carry the load out to the external reinforcing ring. The loads can be quite high because of the high magnetic pressures. For example, a magnetic field of 150 000 gauss is equivalent to 14 000 pounds per square inch of gas pressure within the bore.

Between each turn are small channels to allow passage of liquid neon, and the cooling is accomplished by pool boiling. In practice, the whole core assembly is merely submerged into a bath of liquid neon, which is allowed to boil as necessary to dissipate the generated heat. The power consumption of this magnet is only about 1 megawatt at a current of 15 000 amperes. Operation of the magnet at liquid-neon temperature uses approximately one-twentieth as much power as

operation at room temperature. Because the current density in the conductor is 15 000 amperes per square centimeter, the device is also considerably smaller than a room-temperature magnet of the same field strength.

The neon-cooled cryogenic magnet was fabricated and installed in 1964. In 1967, the superconducting magnet, as shown in figure 9-6, was put into operation. The magnet itself is the cylinder at the bottom of the figure. The tube in the center is the support tube for the magnet, with the upper end being cooled by liquid nitrogen contained in the upper tank. This cooling reduces heat leak down the support tube. The entire magnet assembly is suspended inside a liquid helium tank for cooling of the superconductor. Electrical leads are cooled by helium boiloff gas before they pass through the nitrogen bath in the upper tank. This procedure is used to reduce heat leak to a minimum.

This magnet has a bore 6 inches in diameter by 15 inches in length and operates with a field of 140 000 gauss at a current of 90 amperes. Because the magnet is superconductive, the power is zero after the initial field is generated. A total of 55 miles of superconducting ribbon, 0.090 inch wide by 0.0003 inch thick, are used in this magnet. The superconductor itself is Nb_3Sn vapor deposited onto each side of a stainless-steel ribbon which is 0.0025 inch thick.

In operation, care must be taken to ensure that the superconductor does not become normal. In addition to a critical temperature, a superconductor also has a critical current and a critical magnetic field - either its own field or an external field, as shown in figure 9-7. Thus, there is a bounded region within which superconductivity exists. At the boundary, or surface, of this region, the material loses its superconductivity sharply, and outside the critical surface the material is a normal conductor. When a conductor is selected, all three variables must be considered. For example, in addition to the temperature, the current must be sized so that the generated magnetic field is less than the critical field. This problem, however, usually exists only for devices such as magnets.

In use, even though a superconductor is designed to operate within the critical region, there may be local fluctuations in current and magnetic field or variations in temperature at localized spots. The result will be that the superconductor becomes resistive (i.e., becomes normal) over a short length. To guard against this event, one approach is to have a copper backup of sufficient cross-sectional area to carry the current until conditions stabilize and the superconductive condition is regained.

Some examples of the techniques used for providing this copper backup are shown in figure 9-8. On the left is a typical superconducting ribbon; Nb_3Sn is vapor deposited over stainless steel, and copper is applied to both sides of the ribbon. On the right, NbTi superconductor wires are embedded in copper.

Fine wires are generally used to obtain as much surface contact with the copper as possible. The whole cable can be extruded to any desired size or shape. For example, a pipe for containing the liquid helium coolant might be made from the cable.

In addition to lowering resistive losses, the use of cryogenic temperatures also provides the advantage of extreme compactness. Figure 9-9 shows three conductors, each rated at 1500 amperes. In the case of the room-temperature copper conductor, seven cables of 0.75-inch diameter are necessary to achieve the current capability of 1500 amperes, while only one aluminum cryoconductor and one superconductor are required. A relative comparison of their total cross-sectional areas is shown in figure 9-10. The current density of the room-temperature cable is only 100 amperes per square centimeter, while the current density of the aluminum strip is approximately 15 000 amperes per square centimeter. The superconductor, however, has a current density of about one million amperes per square centimeter. As a result, superconductive devices are very compact in addition to having zero resistive power requirements.

However, although no heat is generated by the superconductive device itself, there will be heat leak into the system, and this leak will result in a small power requirement for replacement of the helium boiloff.

CRYOGENIC HANDLING AND STORAGE

To supply the liquid helium and the liquid neon used for the magnets, a liquefaction plant was built at Lewis. Figure 9-11 presents a sectional view of the plant showing the neon liquefier and the two helium liquefiers. The large storage bag outside the plant is used for conservation of the helium boiloff. The total helium liquefaction capacity is 250 liters per hour, and the neon liquefaction capacity is 60 liters per hour.

In addition to being used for the superconducting magnet, liquid helium is also used in the Centaur rocket vehicle to prechill the liquid-hydrogen pumps prior to launch. The liquid helium is air transported, as shown in figure 9-12, from Lewis to Cape Kennedy for this operation. This method of shipping liquid helium in a 5000-gallon Dewar has been in operation for several years and is an example of how such cryogenic fluids have progressed in only a short period of time from laboratory systems to operational use.

Indeed, contributing to such growth within the cryogenic industry has been the requirement by NASA for large quantities of liquid hydrogen as a rocket propellant. Only a few years ago, liquid hydrogen was not commercially available, nor were cryogenic components such as valves or instrumentation available. Today,

262

production capacity has grown to almost 200 tons per day, and components for both ground systems and flight systems are on the commercial market.

Figure 9-13 shows some typical components in a 2-inch liquid-hydrogen transfer line. This system is entirely vacuum jacketed, and conventional hand valves and vacuum-jacketed flexible hoses for attachment to trailers and rail cars are shown.

The sizes of the components for some of our testing can also become quite large, however. Figure 9-14 shows a 14-inch unjacketed liquid-hydrogen valve. This particular valve is rated for pressures up to 1800 pounds per square inch.

Components such as these are shown to indicate the extent to which technology in the field of cryogenics has advanced. Based on such liquid-hydrogen technology, liquid-helium handling problems have been remarkably few.

Another area in which technology has advanced rapidly has been that of cryogenic storage. Figure 9-15 shows a 200 000-gallon liquid-hydrogen storage tank at the Lewis Plum Brook facility. Alongside the building are two 34 000-gallon railroad cars. The fixed tank has a boiloff loss of only 0.05 percent per day; thus, almost 6 years would be required for the entire contents to boil away.

To achieve high efficiency, storage vessels such as these require the use of extremely good insulation. The type of insulation used is the so-called multilayer or superinsulation system, as shown in figure 9-16. This type of insulation has undergone extensive development by NASA as part of its liquid-hydrogen program. The system consists of alternate layers of highly reflective radiation shields and low-conductivity spacers. The spacers not only are made of low-thermal-conductivity material but also are selected to give many point contacts with the shields. Such point contacts provide high resistance to heat flow. To be effective, the system must also be evacuated to decrease the gas conduction. The net result is that radiation becomes the primary mode of heat transfer, and the highly reflective shields will minimize such radiation.

The effectiveness of evacuating the multilayer insulation is shown in figure 9-17. Thermal conductivity is plotted as a function of gas pressure within the insulation. Also shown are curves for three other families of cryogenic insulations. Multilayer insulation, when unevacuated, is not an efficient insulation. Glass fiber batting, foams (such as polystyrene), or fine powders are better; that is, they have lower values of thermal conductivity. When evacuated, however, multilayer insulation becomes better than its closest competitor (powder) by a factor of about 40.

Necessary to high efficiency of the multilayer insulation is the highly reflective, or low-emittance, shield. Some typical shields are shown in figure 9-18. Aluminum foil, in thicknesses from 1/4 to 5 mils, was first used as a shield, but the thin foils were fragile and easily torn, while the thick foils were heavy. An

improvement over aluminum foil was the development of aluminized Mylar - either coated on one side or on both sides. Commonly used is 1/4-mil Mylar with coatings of about 1000 Å thickness. These foils have a tear strength far superior to that of the aluminum foils, and they are also considerably lighter in weight. Current research is evaluating the desirability of using a gold coating in place of aluminum to obtain a lower emittance.

The other important element of multilayer insulation is the spacer. Some typical spacers are shown in figure 9-19. When Mylar (aluminized on only one side) is used as a shield, the Mylar can also serve as the spacer. This spacing can be accomplished by embossing or crinkling the single aluminized Mylar film to produce random small area contacts that create a high thermal resistance. This method of spacing can only be used with radiation shields of low conductivity (e.g., Mylar film) coated with reflective metal on only one side. This method also has the disadvantage of providing an insulation system that is sensitive to compressive loads.

The other two spacers in common use are glass paper and glass fabric in thicknesses of about 3 mils. The small fibers in these materials provide many point contacts and hence present a high resistance to heat flow. Under investigation are many other types of spacer, such as thin slices of foam or layers of silk netting. Weight, compressive load on the insulation, environment, cost, and method of installation must all, of course, be considered in the final selection.

These multilayer insulations can be applied in a number of ways. Figure 9-20 shows one method. In this commercial application, a large tank is being turned on a mandrel while the aluminum foil shields and glass-fiber spacers are fed from rolls arranged down the length of the tank. After wrapping is complete, the tank and its insulation will be placed into an outer metal shell to make a vacuum jacket. This type of application could also be used to insulate sections of pipe such as might be required for a helium pipe in a low-temperature power transmission line.

An alternative method of applying the multilayer insulation is to form it into blankets. In figure 9-21, extremely thick blankets are shown being installed in the vacuum space of the 200 000-gallon liquid-hydrogen tank shown in figure 9-15. Blankets are also used on flight-type tanks (fig. 9-22). In this case, nylon threads and Mylar tabs are used to form a quilted blanket of alternate layers of aluminized Mylar shields and glass paper spacers. The blankets are held to the tank surface by fasteners spaced at appropriate intervals and by an outer bag of Dacron netting. It has been calculated that this tank, when insulated and filled with liquid hydrogen, could go unvented for 200 days while in transit from Earth to Mars.

264

On a more down-to-earth application, multilayer insulation is currently being used on liquid-helium Dewars which are shipped, unvented, by boat from New York to Amsterdam and other European ports.

CRYOGENIC POWER TRANSMISSION LINES

Such remarkable effectiveness for multilayer insulation may lead to its use in low-temperature superconducting power transmission lines, such as shown conceptually in figure 9-23. The superconducting cable is shown in coaxial form, with the cable itself forming pipes for the helium coolant. Surrounding the pipe is the multilayer insulation. To reduce the heat load into the helium, a liquid-nitrogen-cooled heat shield is shown around the insulation. This procedure ensures that the helium insulation experiences a warm boundary temperature of only 140° R. Multi-layer insulation is also shown around the heat shield to reduce the nitrogen heat load. Finally, the outside pipe serves as the outer vacuum-tight jacket.

Vaporizing liquid helium is used in this conceptual model to keep the cable at approximately 8° R, with the vapor returning back to the refrigeration plant in the gaseous-helium line. The use of vaporizing liquid helium will probably present some problems with two-phase flow in the pipe, and liquid-vapor separators will probably be required periodically down the line. An attractive alternative concept that avoids these problems would be the use of supercritical helium for cooling instead of vaporizing liquid helium.

If liquid helium were to be used, the initial quantity required for just filling the line might be somewhat large. As an example, a pipe 2 inches in diameter and 1000 miles in length would use approximately one-tenth of the 1967 annual helium production. The cost, however, would be only about four million dollars, based on estimates for future liquid-helium costs. This amount would probably be very small compared with the overall cost of the line.

The heat shield, or radiation shield, is cooled by vaporizing liquid nitrogen, and it intercepts the radiant heat from the external shell, which would be at Earth ambient temperature. The heat intercepted by the metal shield would be conducted to the nitrogen pipes; thus, the nitrogen would not have to be placed in large, expensive, annular pipes.

Again, several alternatives to this shield design could be considered. Two possibilities are all-gas cooling or all-liquid cooling with no vaporization. Another possibility would be to use liquefied natural gas in place of liquid nitrogen. Current studies are evaluating the economics of building pipelines for liquefied natural gas. The equipment, techniques, refrigeration plants, and pumping stations developed

for such pipelines could be used for low-temperature power lines. An intermediate shield cooled by liquid hydrogen could also be considered.

The outer vacuum shell surrounding the whole cable system could merely be a concentric pipe, as shown, or it could have flanges down the side to permit easier cable installation and maintenance. The vacuum itself could be obtained by using mechanical roughing pumps for start-up and then using cryopumping after chilldown. The cold helium pipe will make an excellent cryopumping surface and would freeze out all gas constituents with the exception of helium. To remove the helium molecules, either left from the initial gas or from small leaks, ion pumps or cryosorption pumps could be used. Since both annular spaces require evacuation, the radiation shield must be perforated, as indicated, to allow passage of gases.

The multilayer insulation is conceptually shown as being wrapped around the pipes. In any final design, however, this method of applying multilayer insulation would have to be evaluated against alternative concepts, such as the use of blankets. Equally important would be the evaluation of field or factory application. Cost and ease of maintenance or repairs would be important considerations in the final evaluation.

The effectiveness of multilayer insulation for this conceptual design can be illustrated by figure 9-24. For a 2-inch-diameter helium pipe, total refrigeration power for both helium and nitrogen is shown as a function of insulation thickness. In this example, conservative values of the many variables, such as the insulation performance, are assumed. Several different configurations of the model are considered, as shown by the curves.

The dashed curve is for the special case of no nitrogen shield, with the outer vacuum jacket being spaced from the helium pipe by a distance equal to the thickness of the insulation on the helium pipe. As can be seen from the curve, small amounts of helium insulation are quite effective in lowering the power requirements from the large zero insulation value.

The particular condition of using only a nitrogen shield spaced 2 inches from the helium pipe (with the outer jacket spaced 3 in. from the nitrogen shield and with no helium or nitrogen insulation in the system) is shown by the circled point indicated on the ordinate. Comparing that value of power with the dashed curve shows that only about 2 inches of helium insulation would be required to be equal to a single nitrogen shield. The complexities of two separate refrigeration systems would thus be avoided.

However, as shown by the two lower curves, using insulation on the nitrogen shield appears to offer the most potential for reducing refrigeration power to a minimum. The amount of insulation required is not large; for example, 1 inch of insulation between the nitrogen shield and the outer jacket would lower total power

requirements by a factor of about 6. If in addition to insulation over the nitrogen shield, insulation between the helium pipe and the nitrogen shield were also to be used, the total power requirements could be lowered even more - but only to a small extent, as shown by the two curves. Even 2 inches of helium insulation would only lower the power by approximately 3 kilowatts per mile of transmission line as compared with the condition of using only an insulated nitrogen shield with no helium insulation.

Obviously, final determination of the amount of insulation desirable and its location in the system would depend on economic trade-offs between overall initial costs and refrigeration plant operating costs, with such trade-offs being made for much more detailed designs than the simple conceptual model shown. Indeed, many detailed engineering design optimizations and cost studies would be necessary for all elements of the transmission line system to attain the final line design. No attempt has been made herein to do such detailed design and evaluation. Only one area, that of multilayer insulation, has been examined. These brief calculations do tend to indicate, however, that multilayer insulation, as available today, is worthy of consideration in the design of a superconducting power transmission line. Even if a normal conducting line operated at liquid-hydrogen temperature were desired, many of the same considerations as brought out by this conceptual model would still apply.

SUMMARY

NASA is involved in several areas of cryogenic technology which may be of potential interest to the electrical industry. Magnets built of superconducting materials are in routine operation. Cryogenic fluids, including liquid helium, are being produced and handled on a large-scale commercial basis. Cryogenic insulation technology is well advanced. Information from all these areas may be useful in making cryogenic power lines or other low-temperature electrical equipment a ' future economic possibility.
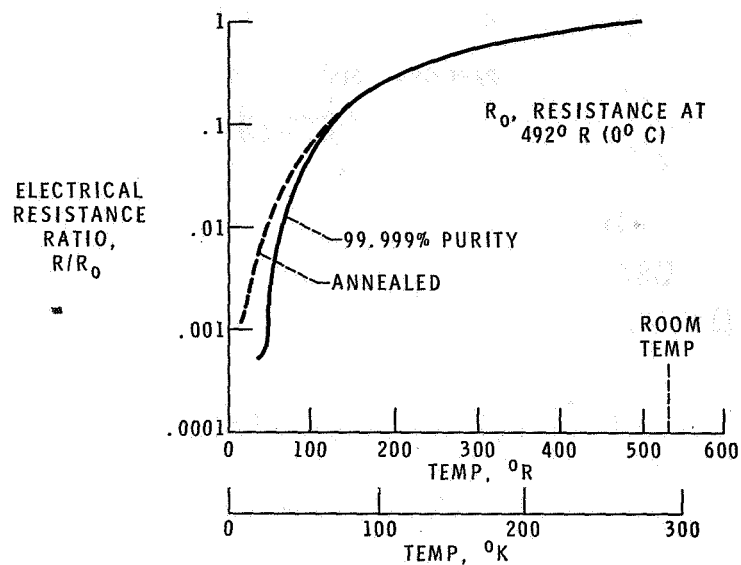
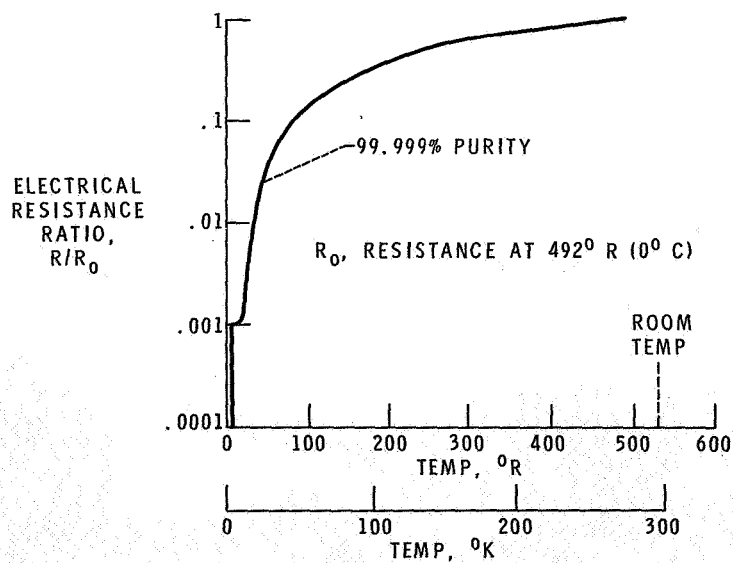Figure 9-1. - Electrical resistance of copper.

Figure 9-2. - Electrical resistance of tin.

FREEZING POINT   BOILING POINT (1 ATM)

METHANE

NITROGEN

NEON

HYDROGEN

HELIUM

TEMP, °R
0   50   100   150   200   250   300

TEMP, °K
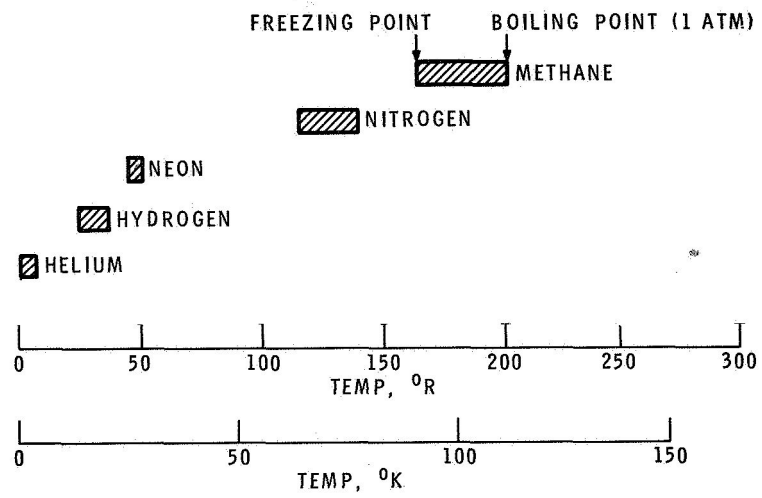0   50   100   150
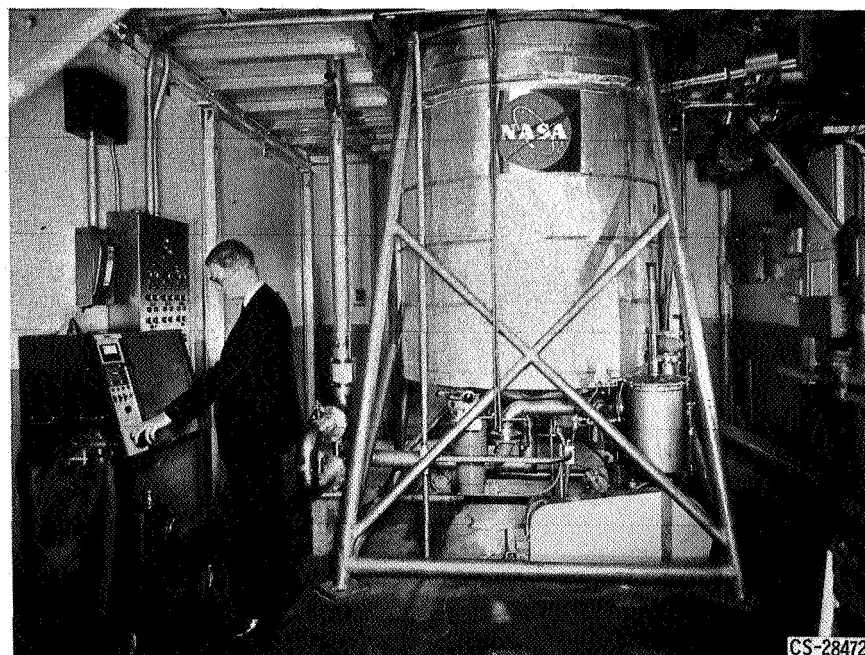
Figure 9-3. - Liquid temperature range of cryogenic fluids.

Figure 9-4. - Neon-cooled cryogenic magnet.
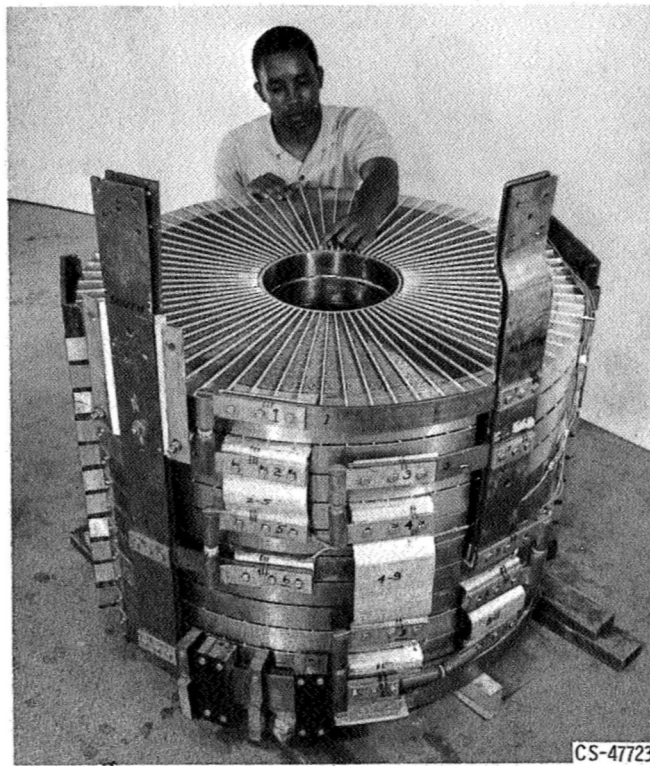
Figure 9-5. - Neon-cooled electromagnet coil assembly.
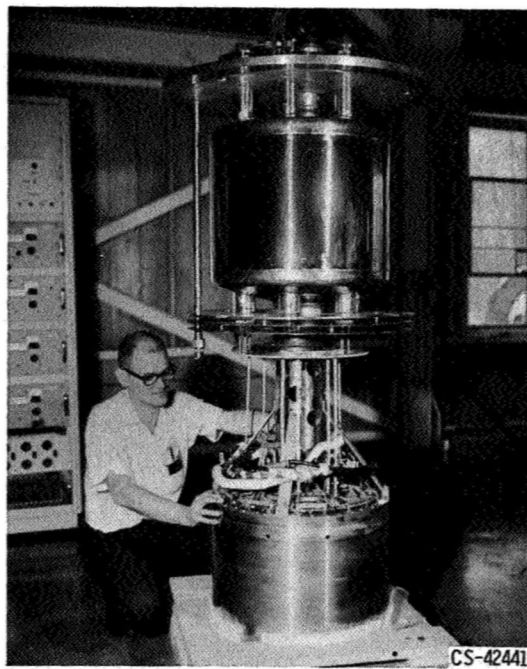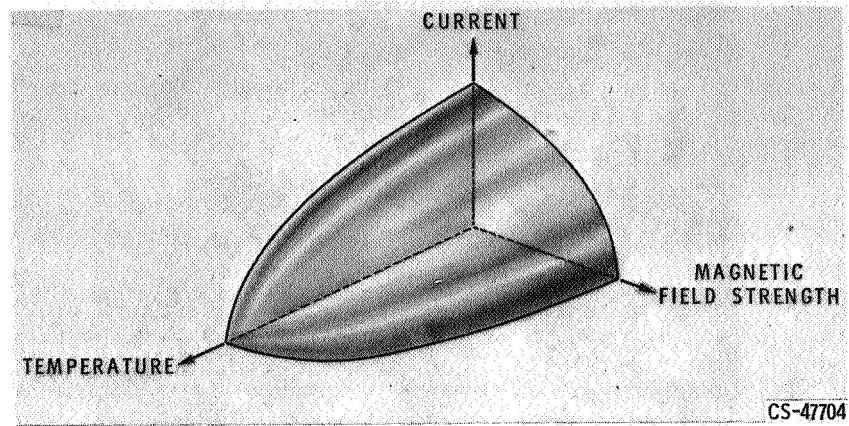

Figure 9-6. - Superconducting magnet.
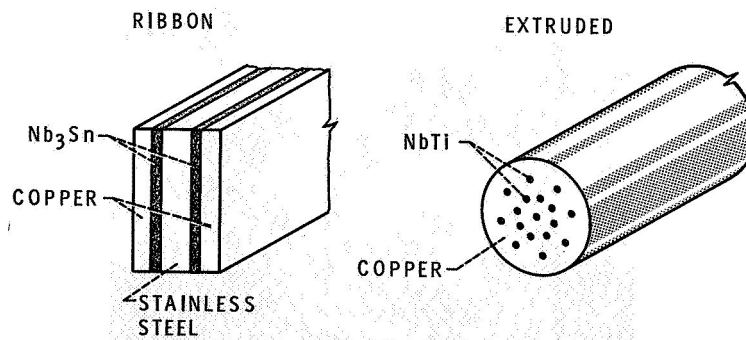
Figure 9-7. - Critical surface of superconductor.

RIBBON

EXTRUDED

Nb₃Sn

COPPER

STAINLESS
STEEL

NbTi

COPPER
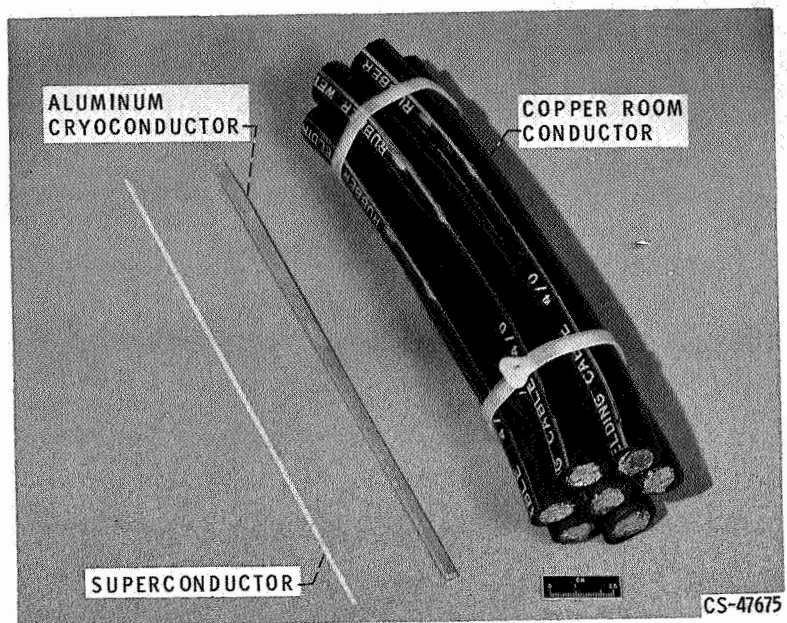
Figure 9-8. - Typical cross sections of superconducting cables.

272

Figure 9-9. - 1500-Ampere conductors.
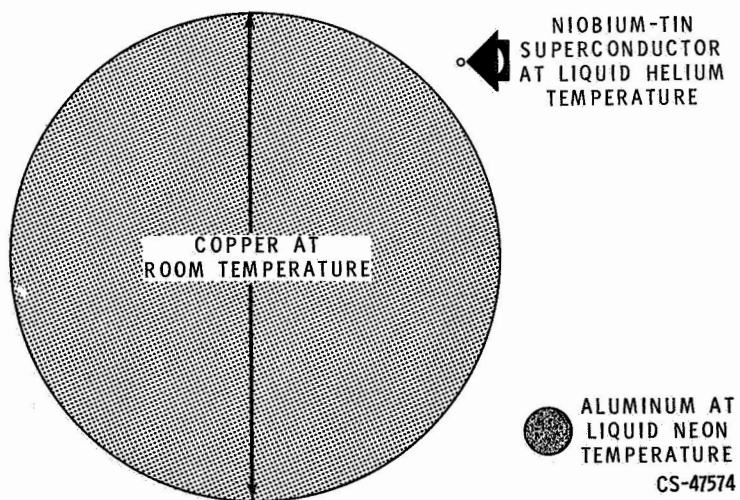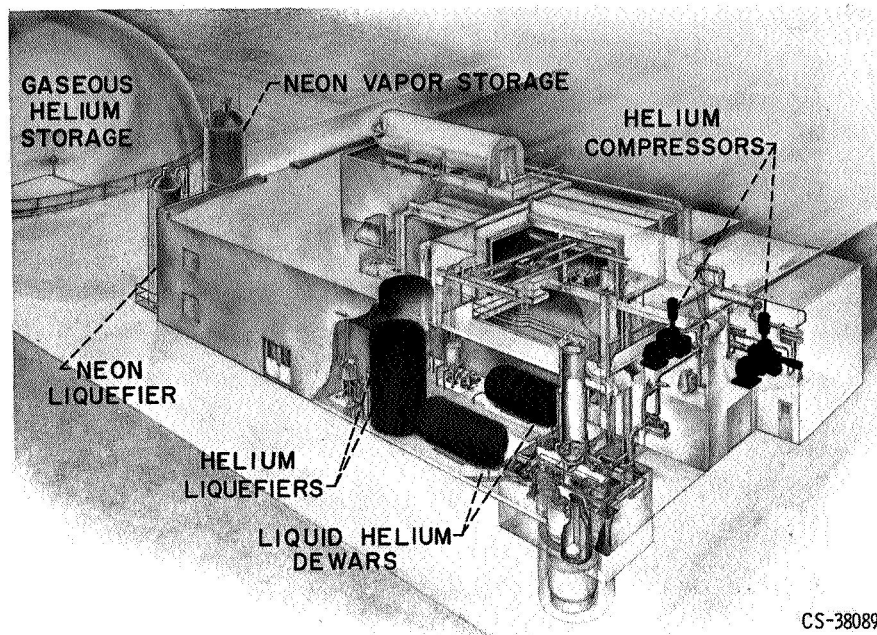

Figure 9-10. - Comparison of conductor areas.

Figure 9-11. - Helium liquefier.

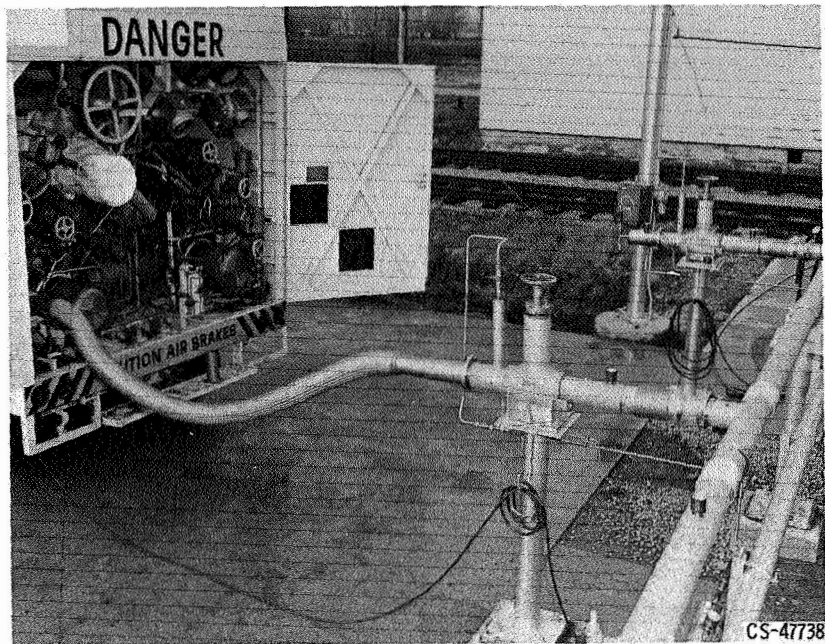Figure 9-12. - Air transport of liquid helium.
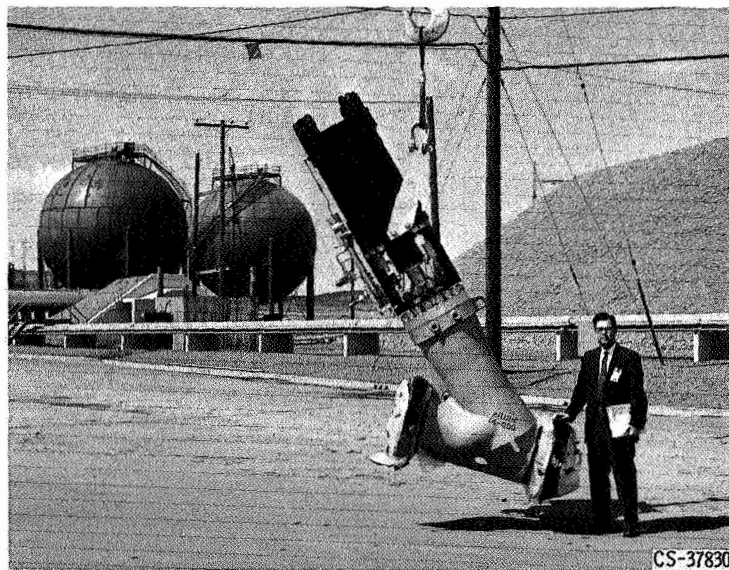
274

Figure 9-13. - Flow-line components.

Figure 9-14. - 14-Inch plug valve.

275
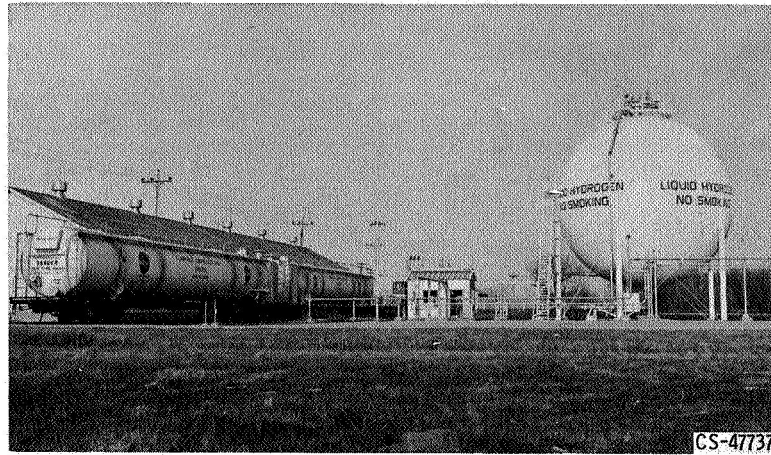
Figure 9-15. - Plum Brook liquid-hydrogen storage facility.

MULTILAYER (ALTERNATE
LAYERS OF REFLECTIVE
SHIELDS AND SPACERS)

LIQUID

TANK WALL

OUTER WALL

VACUUM   CS-38088
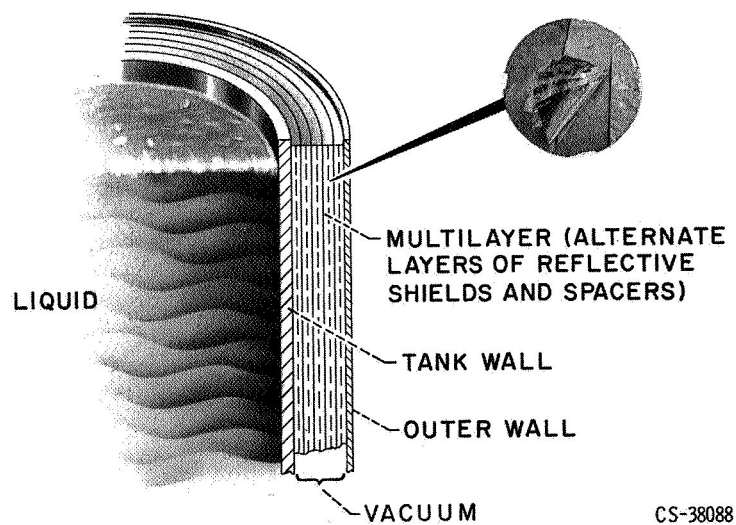
Figure 9-16. - Multilayer insulation.

276
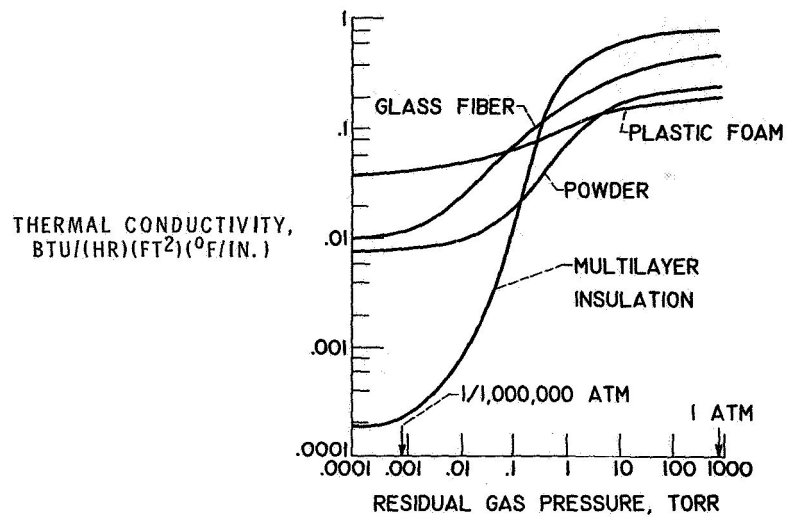
Figure 9-17. – Effect of residual gas pressure.
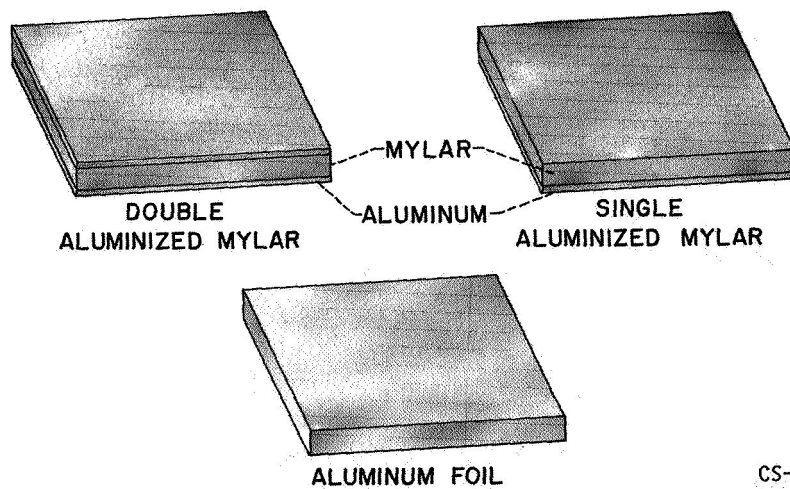
Figure 9-18. – Multilayer insulation reflective shields.
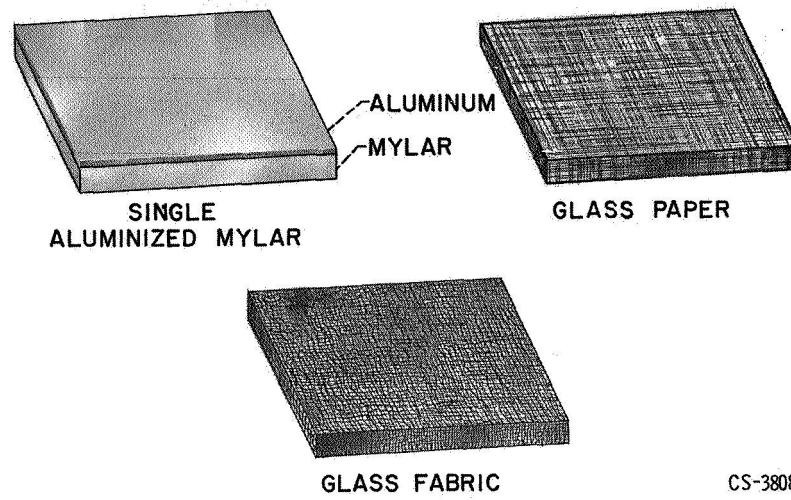
Figure 9-19. - Spacer materials in current use.
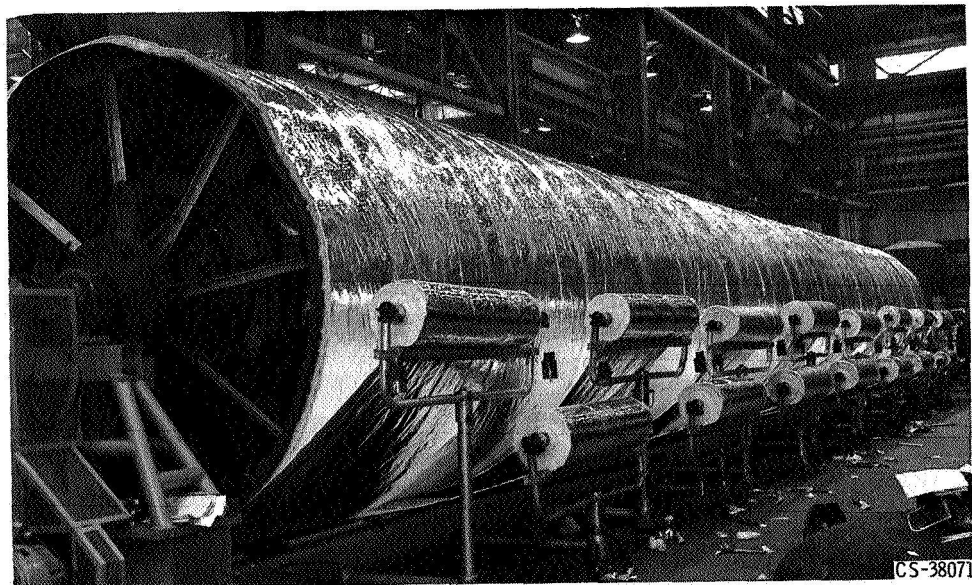
Figure 9-20. - Machine winding of multilayer insulation. (Courtesy Linde Div., Union Carbide Corp.)
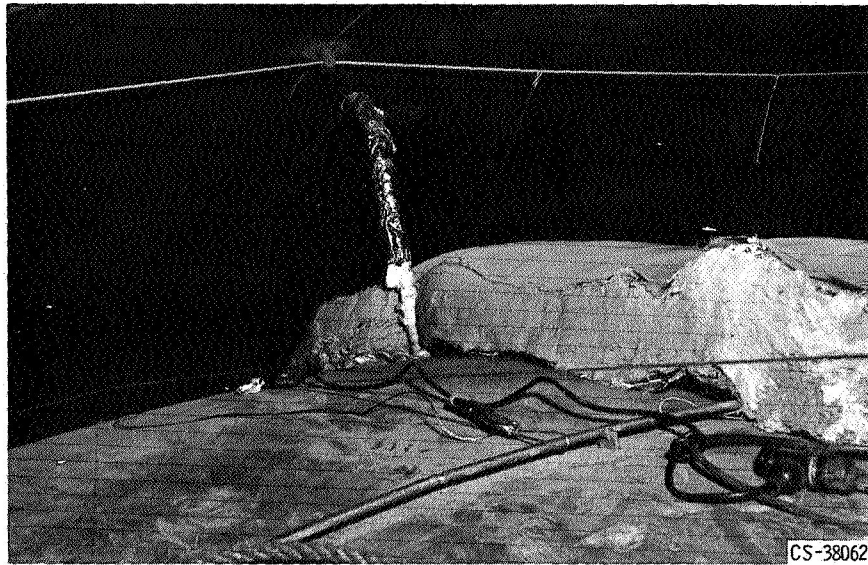
Figure 9-21. - Application of multilayer insulation to ground storage tank.
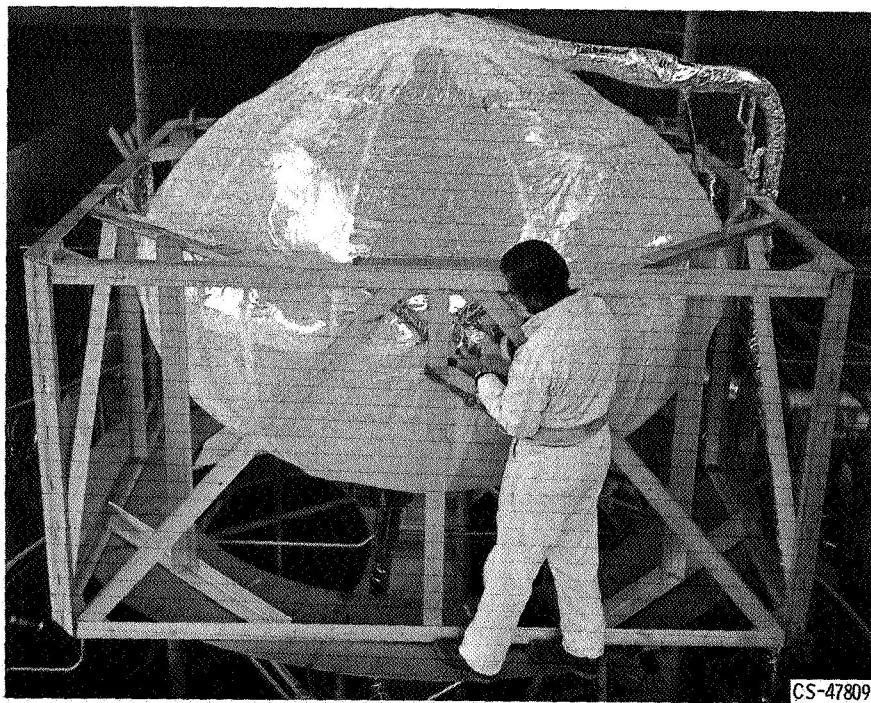
Figure 9-22. - Insulation of 9-foot-diameter liquid-hydrogen tank. (Courtesy Lockheed Missiles & Space Co.)

279

Figure 9-23. – Conceptual model of superconducting power transmission line.

Figure 9-24. – Effect of insulation on refrigeration power for 2-inch liquid-helium line.

10. DIRECT ENERGY CONVERSION

Harvey J. Schwartz and James J. Ward

In NASA space-power-generation work, considerable emphasis has been placed on direct energy conversion. This is an advanced technology which is of interest though not necessarily of immediate usefulness to industry. Direct-energy-conversion methods are those methods by which energy from the sun, a n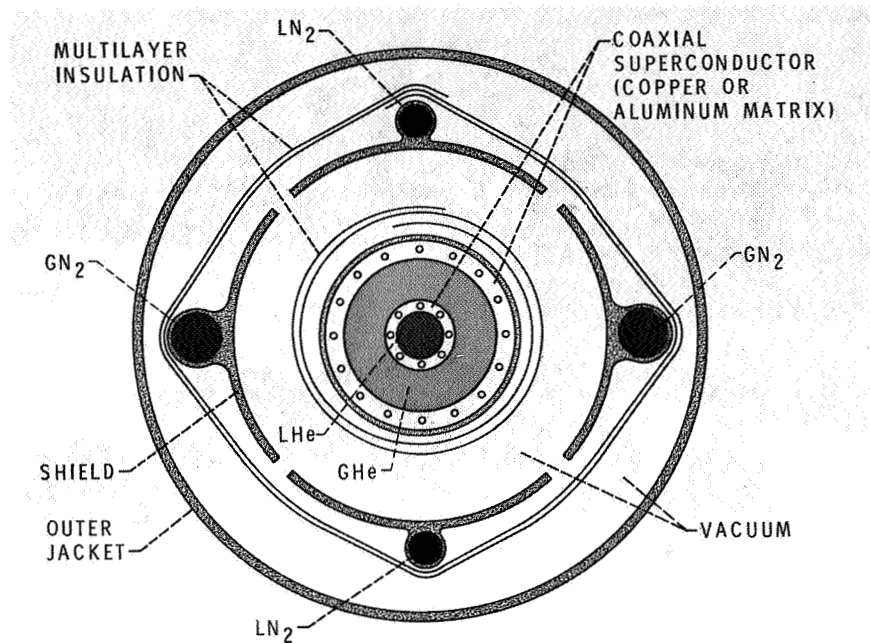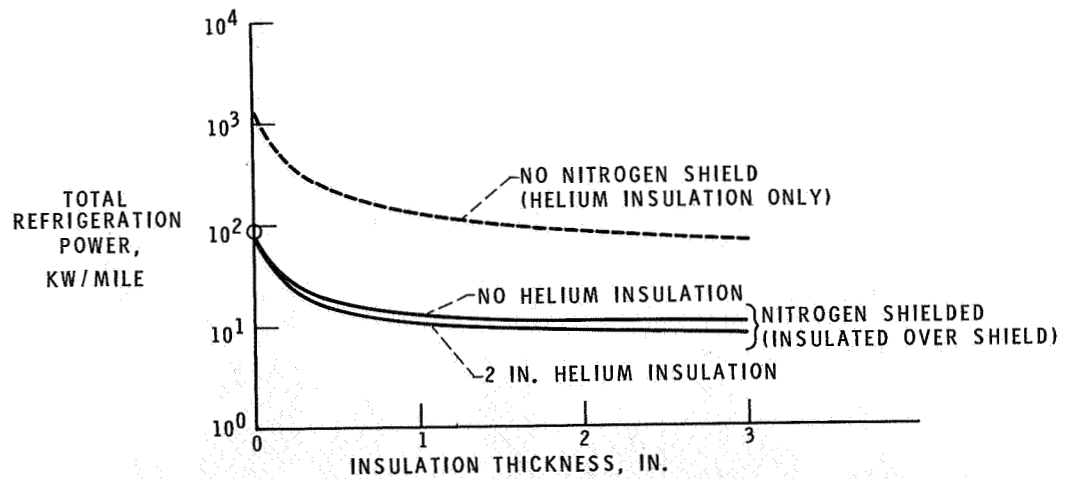uclear reactor, or a chemical reaction can be converted directly to electricity. Four types of direct-conversion processes are discussed: electrochemistry, thermoelectrics, thermionics, and magnetohydrodynamics, more commonly called MHD.

ELECTROCHEMISTRY

Traditionally, the energy in coal and petroleum fuels is released as heat by burning the fuel. This heat is then used to power a mechanical generating system. In an electrochemical process, this heat-production step is avoided, and a large part of the energy in the fuel appears directly as electricity.

There are two types of electrochemical energy converters: the familiar storage battery and the fuel cell. In a battery, the reacting chemicals, one a fuel and the other an oxidizer, form the negative and positive electrodes within the case. These electrodes participate in the energy-producing reaction. The products formed by the reaction are likewise stored within the battery, so that the composition of the active materials within the container changes as energy is generated. A battery continues to operate until all the reactants contained on the electrodes are used up, after which it must be recharged or discarded.

A fuel cell differs in that the reacting chemicals are stored outside the case and are fed to the electrodes when energy is to be produced. The electrodes serve only as reaction sites and current carriers. The products of the reaction are removed as rapidly as they are formed so that there is no net change in the composition of the material within the case. As a result, energy can be generated as long as reactants are supplied and products are removed.

Batteries are well known for their ability to store energy. Energy storage is particularly important in space, since virtually every function performed by a spacecraft is initiated or controlled by electricity which must be generated or stored onboard. Ideally then, batteries for space must be light, have long service lives, be sealed to operate in vacuum, and in some cases, must withstand rapid recharging.

At present, most spacecraft energy storage needs are met by rechargeable batteries. Battery performance characteristics are shown in table 1-I. The available theoretical and actual energy densities are listed as well as the battery life in terms of the number of charge-discharge cycles delivered when 25 percent of the rated output is used during each discharge. The nickel-cadmium battery, while lowest in both theoretical and actual energy density, and therefore the heaviest of the space batteries shown, can deliver well over 10 000 cycles in low-altitude earth orbit. While only slightly better on a theoretical basis, the more favorable design features of the silver-cadmium system allow a significant increase in energy density but only about one-third the life. The silver-zinc battery offers major improvements in both theoretical and actual outputs. However, problems discussed later presently limit the life to 400 cycles. For comparison, the lead-acid traction battery is shown. While it is comparable to nickel-cadmium on a weight basis, it has the life characteristics of the silver-zinc system for this type of service.

NASA battery technology programs seek to improve each of these three space battery types. In addition, new kinds of batteries are being developed for service under extremes of temperature and to produce much higher energy outputs per pound.

This discussion is confined to work on zinc-electrode batteries because they have been prominently mentioned for electric vehicle use, and electric vehicles are a potentially interesting market area for the utilities industry.

Zinc-battery research is being performed by NASA in the following areas: silver-zinc cell development, zinc electrode structure, organic electrolyte, and the zinc-oxygen cell.

For the past 3 years, NASA has supported the development of a long-life rechargeable silver-zinc cell which makes use of a novel inorganic separator material to hold the electrolyte between the electrodes. The performance characteristics of this cell are shown in figure 10-1. Cycle life at 25 percent depth of discharge is shown as a function of operating temperature. The new cell delivers 5 to 7 times the life of the standard cell at room temperature and can operate over a much broader temperature range. The life of this cell is now limited by zinc-electrode problems, rather than separator-related failures. Testing is presently

underway on new zinc-electrode compositions and structures which have given as much as twice the life of the zinc electrodes used in the experimental cells (fig. 10-1).

Major increases in energy density are possible through the use of highly energetic reactants. These require stable organic liquids for electrolytes in contact with highly reactive electrodes. The most common fuel electrode in use is lithium metal, while zinc is one of several elements whose compounds look interesting as oxidizers. A nonrechargeable lithium - copper-fluoride cell which performs well over a limited range of temperatures and discharge rates has proved successful. However, the development of a rechargeable organic electrolyte battery is a much more difficult technical problem, and at present no organic electrolyte battery exists which is suitable for either space or electric vehicle use.

A sealed zinc-oxygen battery presently under development could be attractive for ground as well as space use because it solves one of the major problems of the zinc-air combination, namely the need to purify the incoming air by removing carbon dioxide and other harmful contaminants. This is a new program in which know-how obtained while developing a rechargeable hydrogen-oxygen battery is combined with the zinc electrode and cell work described earlier.

It is appropriate at this point to direct a few specific remarks to the subject of batteries for electric vehicles, since this is a potentially significant application for advanced battery technology work. Many studies have been made to decide what kind of battery is best suited for this application. As is the case for space batteries, it must be light, compact, and efficient, and in addition, must be inexpensive. Specific comparisons have been drawn in a number of ways. Figure 10-2, taken from the 1967 Department of Commerce study entitled "The Automobile and Air Pollution," shows the specific power produced by the battery as a function of the energy density obtained for a particular set of vehicle specifications and operating conditions. In general, the usefulness of a battery for vehicle propulsion increases as both of these values increase. While other studies use different assumptions regarding vehicle size and performance, the relative positions of the various systems shown do not change significantly.

However, performance is not the only criterion for judging vehicle batteries. Because the installed power supply may reach 50 kilowatts and 50 to 100 kilowatt-hours, considerable quantities of materials are involved, and cost and availability are important. Table 10-II shows raw material and availability data for classes I, II, and III of systems shown in figure 10-2.

Despite its poor performance, the lead-acid battery offers acceptable costs and fair availability of raw materials. These features make it suitable for some

limited motive power uses such as golf carts and forklift trucks. Nickel-cadmium and nickel-zinc batteries have performance characteristics that look adequate for the delivery-van type of vehicle. Unfortunately, raw materials for the nickel-cadmium battery cost twice as much as those for the lead-acid battery, and the supply of cadmium is poor in terms of large-scale vehicle use. On the other hand, the raw material costs for the nickel-zinc battery are comparable to those for the lead-acid battery, and a distinct performance advantage has been demonstrated. These factors coupled with the availability of raw materials have led to renewed interest in the nickel-zinc battery in recent years.

The silver-zinc and zinc-air batteries seem suitable for some specific-purpose passenger cars, although the range, speed, and acceleration may be somewhat less than desired. Silver-zinc can readily be dismissed on the basis of the price and the limited supply of silver available. The zinc-air combination is the one receiving major attention today. The cost of zinc and its availability, coupled with the anticipated performance, make this battery look very attractive. However, in assessing this system, one cannot overlook the need for a precious-metal catalyst for the air electrode. Based on current technology, a figure of $500 per kilowatt for the catalyst alone is not unreasonable. Earlier it was stated that a vehicle battery may require 50 kilowatts of installed power. Clearly, such electrodes are economically unattractive, and a successful low-cost air electrode will be required before this system can be a serious contender for vehicle propulsion.

Much better performance would be possible with development of the class IV systems, shown in table 10-II, namely, sodium-sulfur, lithium-chlorine, and organic-electrolyte batteries. These couples offer the greatest promise for electric vehicles. The raw materials are inexpensive and available. However, these are advanced systems, all of which have difficult technical problems still to be solved. These kinds of technologies will not be easy to develop, but they are the ones that seem to offer the greatest promise for a publically acceptable, wholly battery-powered car.

While batteries are of interest as a means for storing energy, fuel cells hold a different attraction. Conversion efficiencies of 45 to 65 percent make the fuel cell, in theory, a contender for a central station power. This application, in fact, spurred fuel-cell research at the turn of the century, but the successful development of the steam turbine power cycle greatly reduced that research effort. Interest was rekindled by the work of Bacon in England in the 1930's and increased in the 1950's under both Government and private support of research. It is the space program, however, which produced the first real application of a fuel cell wherein its uniquely high efficiency was a key factor in its selection. The most

284

advanced fuel cells and fuel-cell systems that exist today are those built for the space program.

Figure 10-3 shows the assembly of a Gemini fuel-cell power system. This system, built by the General Electric Company, was used on seven Gemini flights. The three 24-volt fuel-cell stacks which make up one power system are shown just prior to being assembled into their container. Two complete power systems were carried on the spacecraft, each delivering 120 to 640 watts.

The Apollo fuel-cell system, shown in figure 10-4, delivers 600 to 1400 watts from a single 28-volt fuel-cell stack. Three powerplants of this type built by Pratt & Whitney Aircraft will be carried aboard the Apollo spacecraft. To date, the system has been flight qualified and was flown during unmanned tests. A third system, designed and built by the Allis-Chalmers Manufacturing Company, has been developed to the point where it is ready for flight qualification testing.

Each of these systems is different in terms of the cell design, electrolyte, operating temperature and pressure. However, as these systems exist today, their characteristics can be summarized as follows: Hydrogen-oxygen fuel-cell systems have an overall efficiency of 50 to 60 percent. While single cells have run for a year or more, the expected life of a complete system is only 1000 to 3000 hours. Costs are high, with $25 000 to $50 000 per kilowatt typical today. Obviously, for a commercial fuel cell, this lifetime is too short, costs are too high, and the attractive efficiency is only available when hydrogen is used as the fuel. Basically, three problems confront the development of a commercial fuel cell. Lifetimes of 20 to 40 years are desired, as are low capital costs, and efficiencies of 50 percent or more must be obtained from inexpensive fuels. The problems of life, efficiency, and cost can all be related to the existing requirement to use precious metals such as platinum, silver, gold, or palladium in the fuel-cell electrode, structure, or system. The major cost elements for several commercial fuel cells, capable of operating over a number of temperature ranges, are shown in table 10-III along with remarks pertaining to significant problems of each type. For all low-temperature fuel cells in use today, platinum or silver must be used to catalyze the air-electrode reaction. Platinum has also been the most effective fuel-electrode catalyst. As a result, catalyst costs are very high, and the supply of platinum is so limited that even if it were feasible to use catalyst loadings of only 10 percent of the currently effective quantities, the large-scale use of fuel cells would still be impossible.

The electrochemists offer a seemingly simple solution to this problem, namely, to raise the operating temperature to the point where expensive catalysts

are no longer required. Indeed, higher temperature cells are being operated without the presence of precious metal catalysts. However, these expensive materials do not really disappear as expected but appear in other forms in the fuel cell or system. For example, moderate-temperature fuel cells can be catalyzed by nickel and nickel oxide but require pure hydrogen to maintain their efficiency. The purifier, made of a palladium-silver alloy is either made a part of the electrode or appears as a separate system component. This purifier may cost as much as the fuel cell itself. For intermediate- or high-temperature cells, expensive materials appear in electrode structures or cell components, not for their catalytic properties, but because of their inherent corrosion resistance and electrical conductivity. As a result of using these materials and the specialized construction methods required for elevated-temperature devices, costs are expected to be very high. Demonstrated efficiencies have been below those of lower temperature cells, and the maximum attainable may be only 40 percent from inexpensive fuels.

The conclusion is that new catalyst technology, in terms of finding less expensive materials and making more effective use of the present expensive ones, is required. Toward this end, NASA-sponsored research is being conducted on the nature and site of the key reaction processes within the electrodes, on improvement of the electrode structures themselves, and on the synthesis and testing of entirely new materials as catalysts. It is clear that the fuel cell cannot be competitive without a new technological invention. Should such an invention come into being, however, the fuel cell could be a serious candidate almost overnight. There is no way of predicting when this may occur, but there is likewise no reason to think that it is impossible.

THERMOELECTRICS

Like the battery and the fuel cell, the origins of thermoelectricity date back to the early 1800's. In 1820, Seebeck was working with an electrical circuit made of dissimilar materials and found that a voltage was developed in the circuit when one of the junctions was heated. Attempts were made to generate electrical power using this effect shortly after its discovery. With the materials available at that time, the conversion efficiency was less than 1 percent. Relatively little progress was made in thermoelectricity during the following century. Finally, in the mid-1950's, when an understanding of the behavior of semiconductor materials was acquired, interest was focused on generator development.

As shown in figure 10-5, thermoelectric couples now make use of a negative or N-type and a positive or P-type semiconductor element. The elements are

connected at one end through what is called a hot shoe. The point of contact between each element and the hot shoe is called the hot junction. The open end of the couple is called the cold junction, and the elements are connected through the electrical load at the cold end. Heat is applied to the hot shoe and flows through the elements. A fraction of this heat is converted directly into electricity. The unconverted, or waste, heat is rejected at the cold junction.

Semiconductors are used for energy conversion because they offer the best compromise between the voltage that can be developed in the current and the temperature difference that can be maintained across the elements.

A couple fabricated by RCA and being used in a program at Lewis is presented in figure 10-6. Silicon-germanium (Si-Ge) elements are used in the form of half cylinders. The hot shoe is a silicon-molybdenum alloy. Electrical leads are bonded to the elements and a stud is provided for mounting the couple on a support plate. The hot shoe measures 1.1 inches on a side and the elements are 0.4 inch long.

The couple was designed to operate at a hot-junction temperature of 1500° F and a cold-junction temperature of 800° F. The conversion efficiency is 3.5 percent and the power output is 0.3 watt. The high cold-junction temperature was selected so that waste heat could be rejected to space by radiation.

The performance could be improved by reducing the cold-junction temperature, as illustrated in table 10-IV, where the maximum useful temperature and the efficiency which can now be realized in ground applications are listed for the three most commonly used materials, bismuth telluride (BiTe), lead telluride (PbTe), and Si-Ge. The efficiency is based on the hot junction being at the maximum useful temperature and a cold-junction temperature of 100° F.

Bismuth telluride can be operated at a maximum hot-junction temperature of 500° F, resulting in an efficiency of 6 percent. Lead telluride, which has seen the most use to date in this country, can be operated at a temperature of 1000° F with a corresponding efficiency of 10 percent. The third material, Si-Ge, is not as efficient as the tellurides when operating over the same temperature range, but can be used at much higher temperatures (1800° F), also resulting in an efficiency of 10 percent.

These efficiencies are quite low, but the important point is that the efficiency is independent of power output. These values can be achieved at a power output of a fraction of a watt, and thermoelectrics have been used at low power levels in space and on the ground.

Five radioisotope-heated generators have been operated in space at power levels up to 25 watts, and several, more advanced generators will be used in future missions. For example, the SNAP-27 generator, shown in figure 10-7, is to

be used in the Apollo program for powering experiments on the lunar surface. The generator produces 56 watts of electrical power. The cylindrical radioisotope heat source contains plutonium fuel. Lead telluride couples, about the same size as the Si-Ge couple shown in figure 10-6, are arranged around the heat source. Waste heat is conducted from the couple cold junctions to the outer shell of the generator and is radiated to space from a series of metal fins. The generator weighs 46 pounds and, like its predecessors, is quite compact, measuring 18 inches long and 15 inches across the fins.

In addition to the isotope-heated generators, there has also been one nuclear-reactor thermoelectric system operated in space, the SNAP-10A, which used Si-Ge couples and produced a power output of 500 watts.

On the ground, thermoelectrics have been used only in special applications. As an example, PbTe couples have been used for many years as sensors in the safety control system in gas furnaces.

Radioisotope and propane-heated generators have been used at power levels of 100 watts or less in a number of applications, including powering automatic weather stations in remote areas, powering deep ocean navigational aids, etc. In all these applications, thermoelectric generators proved to be very reliable.

Whether or not thermoelectrics will eventually be used at much higher power levels depends entirely on improvements in efficiency. The three main technology areas being pursued with the objective of improving efficiency are materials research, materials optimization, and cascaded materials. Programs in these areas are supported principally by the Atomic Energy Commission and by NASA.

Research programs directed toward the development of improved thermoelectric materials have been in progress for several decades. This activity led to the discovery of the telluride class of materials in the mid-1950's and Si-Ge in 1960. No better materials have been found since 1960 and the lack of positive experimental results is now being supported by theoretical arguments. Of course, it is impossible to predict what might happen in a research area, but there may be no better materials than the ones now in use.

An effort is being made to improve the efficiency of existing materials by optimizing their composition and improving the techniques used for bonding the elements to hot- and cold-junction materials. Only modest improvements in efficiency are expected from these efforts.

The cascaded materials program is directed toward improving generator efficiencies by using two or possibly all three available materials in a single generator with each material operating over the temperature range in which it is most efficient. With the development of cascaded generators, the maximum thermoelectric efficiency for ground applications should approach 15 percent. At this level, ther-

moelectrics will not be a major power system. But, the couples are simple and very reliable and will certainly continue to be used in applications where small amounts of power are required for moderately long periods of time.

THERMIONICS

In contrast to thermoelectrics, thermionics is of principal interest at power levels ranging from tens of kilowatts to tens of megawatts. Thermionic conversion is based on the fact that electrons are emitted from a hot metal surface. As shown in figure 10-8, a thermionic converter consists basically of two electrodes separated by a small gap. One electrode, the emitter, is maintained at a high temperature. The second electrode, the collector, is maintained at a lower temperature. When heat is added to the emitter, electrons escape and move across the gap to the collector. Part of their energy is given up at the collector in the form of heat which must be rejected. The remainder of their energy is available to do work in the external load as they return to the emitter.

In all practical converters, cesium vapor is introduced into the space between the electrodes. The addition of cesium increases the current flow and also allows the electrons to move across a much wider gap than would be possible if the space were evacuated.

An actual converter is quite a bit more complicated than might be first envisioned for several reasons: (1) even with cesium addition, the interelectrode spacing is limited to values of the order of 0.010 inch; (2) in order to contain the cesium vapor, the electrode system must be surrounded by a leak-tight envelope; (3) a way must be provided to control the cesium vapor pressure, which is critical to the operation of the converter.

A cutaway view of a laboratory test device is presented in figure 10-9. The emitter is the circular disk at the top. The collector is located below the emitter. The cesium vapor pressure is controlled by adjusting the temperature of a pool of liquid cesium located in the reservoir. Cesium vapor occupies the space between the emitter and collector and the space enclosed by the outer envelope. The emitter and collector structures must be electrically isolated, and this is accomplished with an insulating metal-to-ceramic seal.

The high operating temperatures necessary for thermionic conversion require that the emitter and the part of the outer envelope in contact with the emitter be made of refractory metal. In most cases, the remainder of the outer envelope, as well as the collector and the collector support structure, are also made of refrac-

tory metal. Laboratory test devices are typically 1/2 inch in diameter and produce up to 40 watts of electrical power.

The efficiency which is presently being achieved in the laboratory is presented as a function of emitter temperature in figure 10-10. The band shown results from the use of different combinations of electrode materials. The minimum acceptable temperature is 2500° F for which the efficiency is 7 to 10 percent. Increasing the emitter temperature to 3000° F increases the efficiency to 14 to 17 percent. These are not particularly high efficiencies. An interesting point about thermionic conversion is that the efficiency does not increase continuously as the collector temperature, which for this range of emitter temperature is 1400° F. It is the combination of an acceptable efficiency and high heat-rejection temperatures that makes thermionics attractive for high-power space applications. It is quite possible that this same combination may make thermionics of future interest for ground applications as a topping cycle in which the heat rejected by the thermionic system would be transferred to a conventional steam plant.

Considering heat sources, temperatures of 3000° F can easily be achieved by burning a fossil fuel and air. However, refractory metals cannot be exposed to the products of combustion. Some work has been directed toward the use of protective coatings around the converter, but the results to date have not been very encouraging.

Currently, the most interesting heat source for thermionic conversion is a nuclear reactor. Technology programs, directed toward this application, have been supported by NASA, AEC, and other government agencies since the early 1960's. The major technology areas are as follows: converter performance, converter life, and high-temperature fuel.

The objective of the converter-performance program is to reduce the emitter temperature. Encouraging results have been achieved, particularly over the past 2 years, in developing techniques for orienting the crystal axes of tungsten in a particular way. Preliminary data indicate that, for a given efficiency, a reduction in emitter temperature of 200° to 300° F should be possible with these new techniques. This activity is continuing but there are no prospects at present for reducing the required temperature below about 2200° F.

Several converters have been operated continuously for periods of 1 to $1\frac{1}{2}$ years at emitter temperatures of 3000° F. However, these lifetimes are not being consistently achieved. The major cause of converter failure has been loss of cesium through leaks in the outer envelope. Work in this area is directed toward improving metal-to-metal joining techniques and metal-to-ceramic seal structures.

In addition to converter improvements, a nuclear fuel with high-temperature capability is required for the thermionic reactor. The problems involved in this

290

area were discussed in the paper on nuclear reactors.

In perspective, steady progress is being made in thermionic technology. However, the technology is difficult because of the high temperatures involved and it will be some time before a high performance nuclear thermionic system can be designed with real confidence.

MAGNETOHYDRODYNAMICS

Magnetohydrodynamic (MHD) power generation is quite different from direct-conversion techniques. The MHD generator is, in fact, identical in operating principle to a conventional generator. Instead of a solid conductor, a conducting fluid is used. As shown in figure 10-11, as the fluid flows through a channel at right angles to an applied magnetic field, a voltage is developed across the channel. The fluid may be a liquid metal, a liquid-metal vapor, or a gas.

The highest generator efficiency demonstrated has been 56 percent, which was achieved with a small liquid-metal unit. However, efficiency estimates for very large generators producing hundreds of megawatts of electrical power are 70 to 75 percent. These are efficiencies for the generator only and are not overall system efficiencies.

The performance of an MHD generator depends on three factors: the electrical conductivity of the fluid, the velocity of the fluid, and the strength of the magnetic field. In table 10-V, typical values of the electrical conductivity in mhos per meter, the velocity in feet per second, and the magnetic field strength in kilogauss are presented for a liquid metal and two high-temperature gas systems.

A liquid metal has an electrical conductivity of 10^6 mhos per meter. This value is only 1 percent of the conductivity of copper but is quite adequate for power generation in combination with a velocity of 300 feet per second and a magnetic field strength of 10 kilogauss. A magnetic field strength of 10 kilogauss is within the capability of conventional magnets. The problem with this system is to find an efficient way of accelerating the liquid. Most approaches involve mixing the liquid with a vapor and accelerating this two-phase fluid through a nozzle. Before entering the generator, the vapor is either condensed or removed from the liquid in a separator. Considerable component technology has been developed for liquid-metal systems. With presently available components, the overall efficiency of a liquid system would be less than 10 percent at a peak temperature of 2000° F. Work is continuing on the development of components in which fluid friction effects are less significant and modest efficiency improvements are expected.

In gas MHD systems, the principal problem is achieving acceptable electrical conductivity. Consider first an open-cycle combustion-fired generator. The flame temperature when hydrocarbon and pure oxygen are burned can reach 5000° F. If the products of combustion are seeded, that is, if an easily ionized material, such as an alkali metal vapor, is added to the products of combustion, the conductivity of the gas in the generator would be about 10 mhos per meter. Even this very low conductivity is adequate for power generation in combination with a velocity of 5000 feet per second and a magnetic field strength of 30 kilogauss. The velocity can be easily achieved by expanding the gas through a nozzle. In a practical application, cryogenic cooling would be required for the 30-kilogauss magnet.

Several combustion-fired MHD experiments have been run. As a matter of fact, the feasibility of MHD power generation was demonstrated in a combustion-fired experiment conducted at Westinghouse about 10 years ago. The largest system of this type tested to date was built by the AVCO Corporation under Air Force sponsorship and operated in late 1964. The operating characteristics of the combustion-fired MHD generator are as follows:

Inlet gas temperature, $^\circ$F . . . . ~4500
Exit gas temperature, $^\circ$F . . . . ~4000
Gas velocity, ft/sec 5600
Magnetic field strength, G 33 000
Gross power, MW_e 32.6
Net power, MW_e 23.5

The generator was rocket-driven, burning ethyl alcohol and gaseous oxygen. Potassium seed was used. The system developed a gross power output of 32.6 megawatts at 20 000 amperes and 1630 volts. Of this, 9.1 megawatts were supplied to the magnet resulting in a net power output of 23.5 megawatts electric. Based on net power output and total thermal power input, the overall efficiency of the system was 6 percent. The system was designed to meet an Air Force requirement for high-power pulse operation so that operating times were very short ranging from 10 to 60 seconds.

An overall view of the system is presented in figure 10-12. The combustor and nozzle are on the left. The generator is located in the center section and is enclosed by the magnet. The magnet, which weighed over 70 tons, is supported by heavy steel straps. The generator channel was 10 feet long and 2 feet square at the exit. Products of combustion were exhausted to the atmosphere.

Experiments of this type, in which large amounts of power were generated, prompted considerable interest in the possible use of combustion-fired systems for topping conventional steam plants.

292

One of the very important questions which remains to be answered is related to life. AVCO tested a small generator channel with flowing combustion products. This test, which ran for 200 hours, is the longest test to data. The channel was in acceptable condition after the test, but much longer life must be demonstrated before combustion-fired systems can be considered for commercial use.

For closed-cycle applications, peak temperatures must be limited to values well below 5000° F. Even if a peak temperature of 3000° F were achievable, the seeded gas in the generator, if ionized thermally, would have an electrical conductivity of only 1 mho per meter and it would finally become impractical to build an MHD generator.

In closed systems, ionization techniques other than thermal must be used to improve conductivity. These techniques involve accelerating electrons to sufficiently high velocities so that the seed material atoms can be ionized by collisions with the electrons.

The approach receiving most attention is one in which electric fields existing within the generator itself are used to accelerate the electrons. At present, this is a basic research problem and is being investigated at Lewis and by other organizations. The generator channel used in the NASA program is shown in figure 10-13. It is now being tested with argon at 3100° F. The generator, which has a volume of 1/4 cubic foot, could theoretically produce 500 kilowatts electric if predicted levels of conductivity can be realized.

Progress toward achieving this so-called nonequilibrium ionization is still in its infancy. Much more research is required before any realistic evaluation of closed-cycle gas systems can be made.

SUMMARY

Of the direct energy conversion methods discussed, the only one which may possibly have an influence on the electric power industry in the relatively near future is the battery. This, however, represents a new market for electricity, rather than a new technique for manufacturing it.

Fuel cells, thermionics, and MHD do represent potential changes in production techniques which could result in lower production costs. For each one of these, deficiencies were indicated, either technical or economic, which make them unattractive in their present state of development. However, as technology continues to be developed in these areas, reassessment of these techniques by the utilities industries will be required.

TABLE 10-I. - RECHARGEABLE BATTERIES FOR SPACE USE

System	Energy density, W-hr/lb		Cycle life at 25 percent depth of discharge
	Theory - reactants only	Actual - complete battery	
Nickel-cadmium	107	12	10 000
Silver-cadmium	120	20	3 000
Silver-zinc	208	40	400
Lead-acid[a]	81	10	400

[a]For comparison.

TABLE 10-II. - COST AND AVAILABILITY OF BATTERY MATERIALS

Class	Battery couple	Raw material cost, $/(kW-hr)	Availability
I.	Lead-acid	5.50	Lead: fair
II	Nickel-cadmium	10.1	Cadmium: poor
	Nickel-zinc	5.30	Nickel and zinc: good
III	Silver-zinc	101	Silver: poor
	Zinc-air[a]	.90	Zinc and air: good
IV	Sodium-sulfur	1.08	Sodium and sulfur: excellent
	Lithium-chlorine	2.80	Lithium: good
	Organic-electrolyte	3.41	Lithium: good

[a]$500/kW for catalyst alone.

294

TABLE 10-III. - MAJOR COST ELEMENTS FOR

COMMERCIAL FUEL CELLS

Temperature, ^{o}F	Temperature range	Material	Use	Cost, $/kW	Remarks
200	Low	Platinum, silver	Catalyst	500 to 1000	Limited supply
300 to 450	Moderate	Palladium, silver	Hydrogen purifier	120	Limited supply
1000 to 1500	Intermediate	Platinum, silver	Electrodes	200	Corrosion; low efficiency
1800	High	Several	Cell parts	High	Fabrication; low efficiency

TABLE 10-IV. - THERMOELECTRIC

MATERIAL CHARACTERISTICS

Material	Maximum useful temperature, ^{o}F	Efficiency (cold-junction temperature, 100° F), percent
Bismuth telluride	500	6
Lead telluride	1000	10
Silicon-germanium	1800	10

TABLE 10-V. - TYPICAL MHD GENERATOR

DESIGN PARAMETERS

Fluid	Peak temperature, ^{o}F	Electrical conductivity, mhos/m	Velocity, ft/sec	Magnetic field strength, kG
Liquid metal	2000	1 000 000	300	10
Seeded gas	5000	10	5000	30
Seeded gas	3000	1.0	----	--
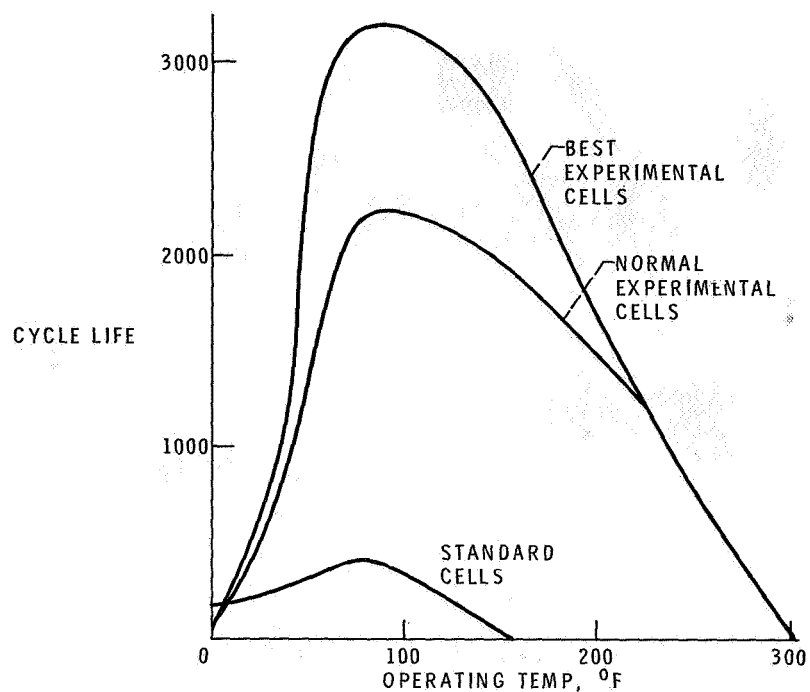
Figure 10-1. - Performance of experimental silver-zinc cell for 25 percent depth of discharge.
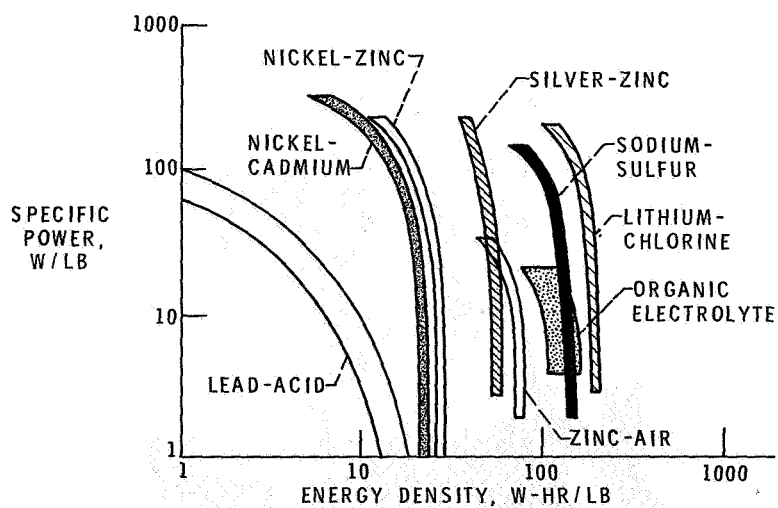
Figure 10-2. - Performance of batteries for electric vehicles. (Taken from 1967 Department of Commerce study: "The Automobile and Air Pollution".)
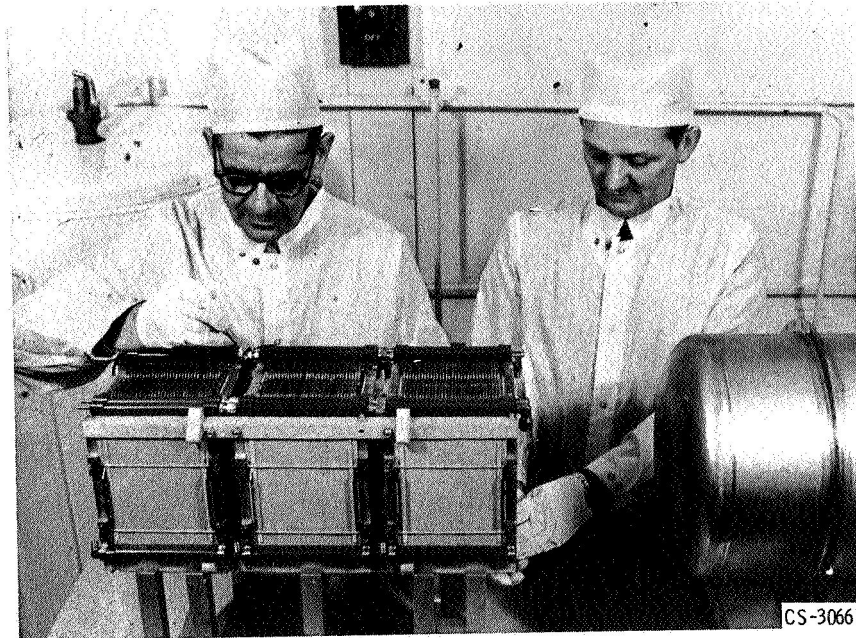
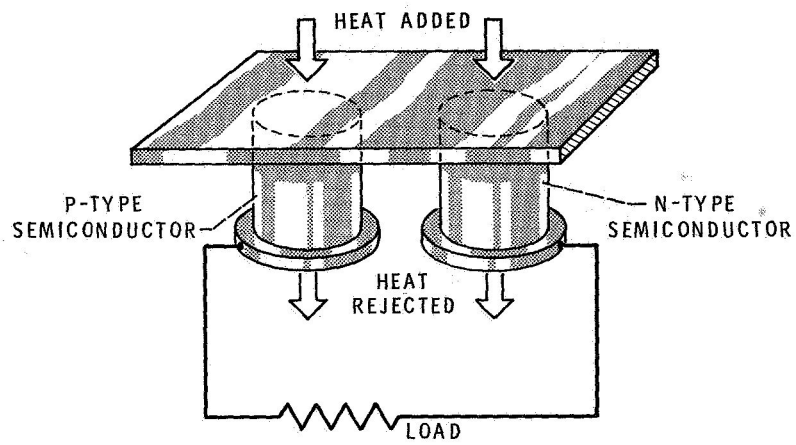Figure 10-3. - Gemini fuel cell.
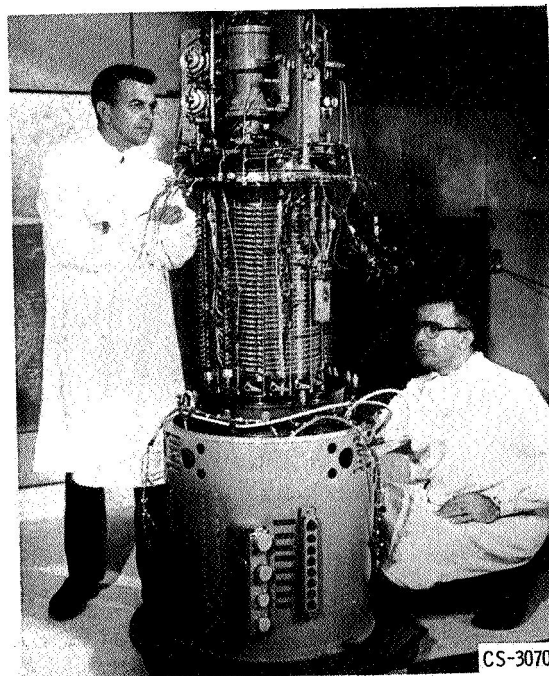
Figure 10-4. - Apollo fuel cell.

298

Figure 10-5. - Thermoelectric conversion.

CS-47435
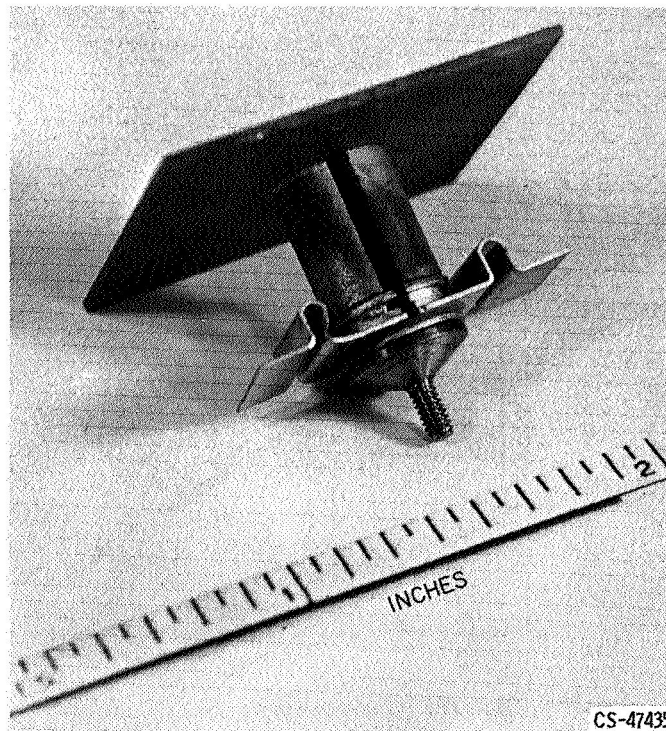
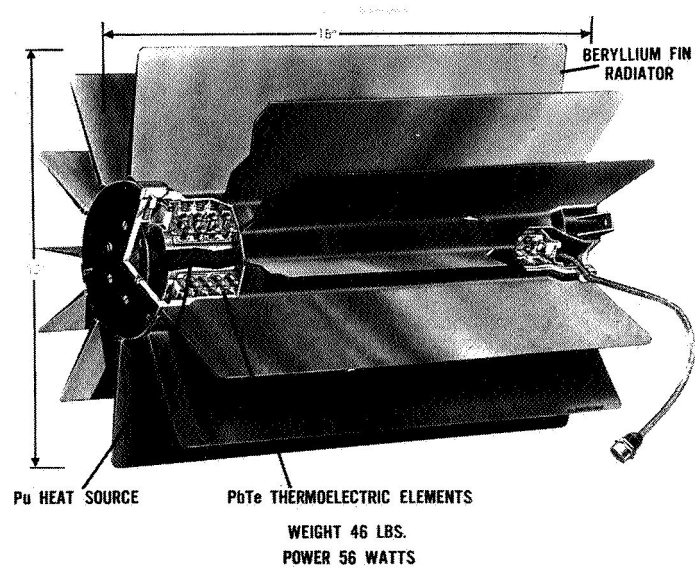Figure 10-6. - Silicon-germanium thermoelectric couple.

BERYLLIUM FIN RADIATOR

Pu HEAT SOURCE   PbTe THERMOELECTRIC ELEMENTS

WEIGHT 46 LBS.
POWER 56 WATTS

Figure 10-7. – SNAP-27 generator.   CS-40581

HOT EMITTER

HEAT
ADDED

COLD
COLLECTOR

$\ominus$

$\oplus$
Cs

HEAT
REJECTED

LOAD
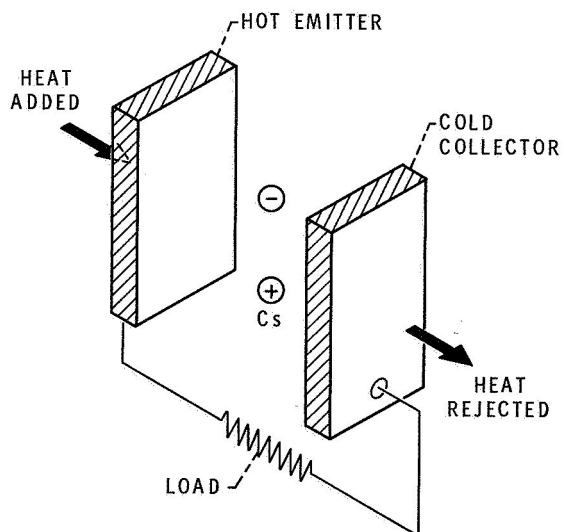
Figure 10-8. – Thermionic conversion.

CS-47722
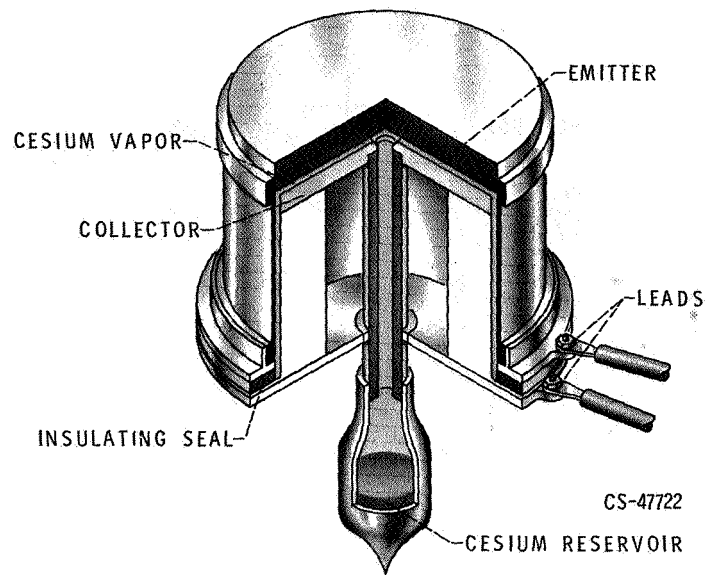
Figure 10-9. - Experimental thermionic converter.
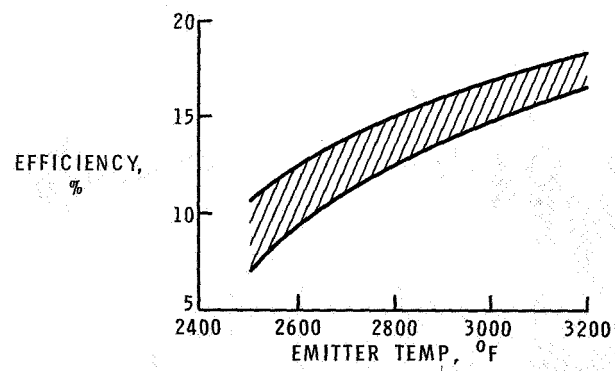
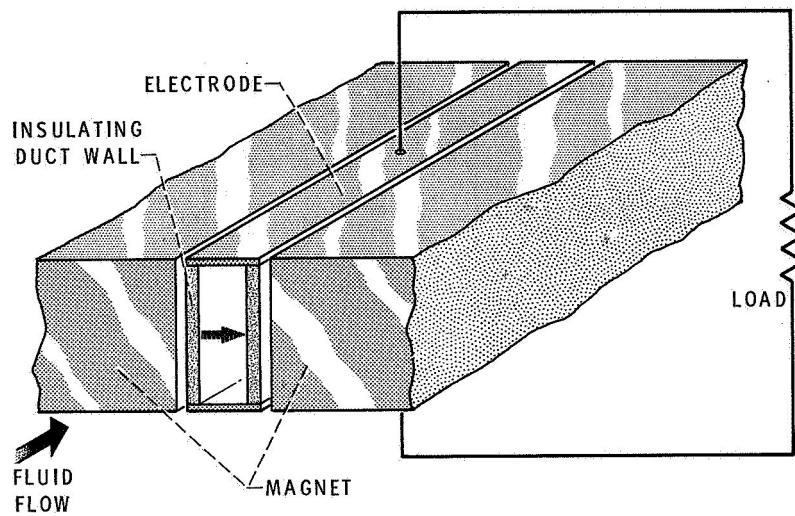Figure 10-10. - Thermionic conversion efficiency. Collector temperature, 1400° F.

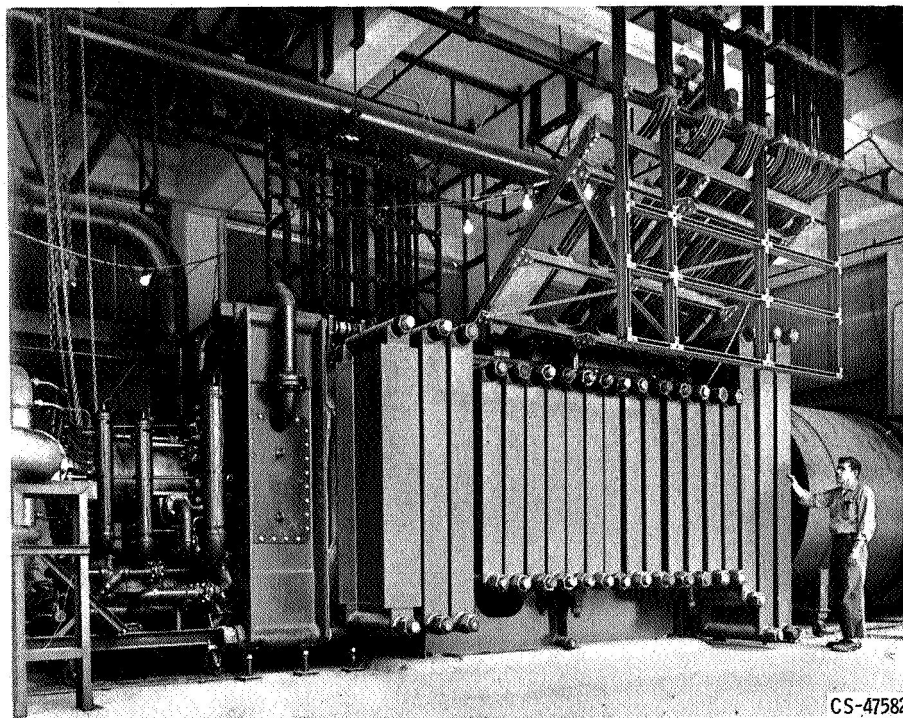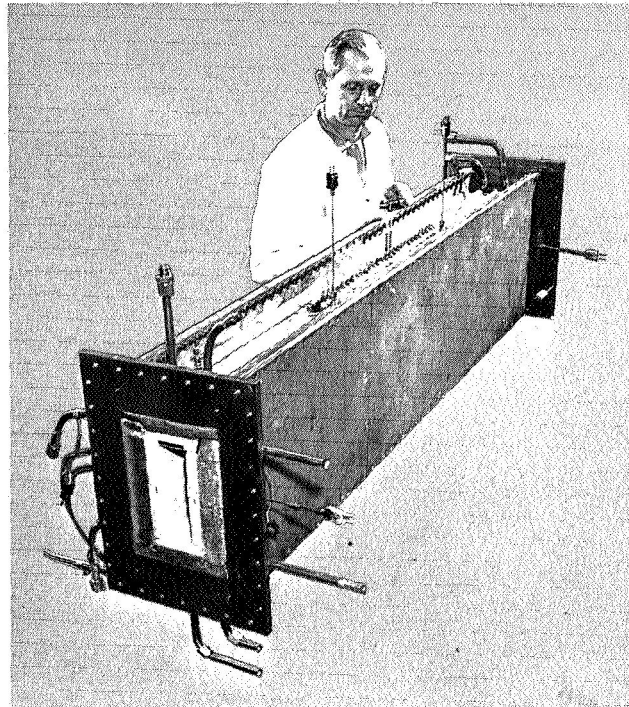Figure 10-11. - Magnetohydrodynamic (MHD) conversion.

CS-47582

Figure 10-12. - 23-Megawatt-electric combustion-fired MHD generator.

302

CS-47721

Figure 10-13. – 500-Kilowatt-electric argon MHD generator.

11. SUMMARY OF CONFERENCE

Bernard Lubarsky

This conference has presented a one and one-half day sample of aerospace technology of interest to the electric power industry. Only a limited amount of the technology of interest was covered. Because of time restrictions, many subjects were omitted or abbreviated, for example, discussions of fabrication techniques, solid-state devices and circuits, high-temperature electrical materials, heat pipes, solid lubricants, emissivity coatings, fluidic controls, gas bearings, single-phase heat transfer, combustion, etc. The relevance of a considerable body of aerospace technology to the electric power industry has been clearly displayed. Opinions might vary as to the relative importance of the various parts of the conference; some of the highlights, as seen by the writer, are presented here.

The substantially lower fuel cost associated with breeder reactors is interesting because it will modify the balance of emphasis between efficiency, first cost, and reliability to which the power industry is currently accustomed; low fuel costs will reduce the importance of efficiency relative to the other factors of overall cost. The step from current burner reactors to future breeders is a large one and considerable technology work will have to be done before the breeder reactor is ready for service. A word of caution about liquid-metal systems is necessary. Liquid metals are unforgiving fluids. Failure to follow acceptable procedures rigorously almost always leads to trouble.

The smaller boilers discussed in connection with the Rankine system are feasible for use with pressurized water or liquid-metal-cooled reactors. Smaller boilers would not only decrease first cost but would reduce boiler failures by reducing the number of tubes that can fail which permits better quality control to be exercised.

The advance in the last two decades in dynamic analysis has been very substantial. The ability to predict and eliminate boiler instabilities and to analyze the dynamic behavior during the startup of complex systems is impressive evidence of that advance.

The gas turbine should have a larger place in power generation than it now occupies. The gas-fired open-cycle gas turbine described can achieve efficiencies

in excess of 40 percent and represents a very attractive plant for regions where natural gas is readily available. Plants smaller than the 1000-megawatt plant discussed might be an attractive export item to countries with large available supplies of inexpensive gas or oil. The attractiveness of the high-temperature gas turbine suggests that efforts to use coal in gas turbines should receive greater emphasis. Perhaps the suggestion for using coal in a combined gas-turbine - steam-turbine system is interesting; perhaps a method for direct use of coal in gas turbines can be found.

The coupling of a closed-cycle gas turbine with a gas-cooled breeder reactor has an attractive simplicity when compared with three-loop systems, two of which are liquid-metal loops. Efficiencies in the high thirties, though lower than that of steam plants, may be acceptable because of the lower cost of breeder fuel. However, the implications of the higher reactor-temperature requirements and the cost of the heat exchangers, particularly the recuperator, need to be examined more thoroughly.

Because of economics, the methods used by NASA in achieving reliability are not all applicable to the electric power industry. However, some of the techniques should be considered. The searching review of all equipment designs in detail at the various stages of design with an eye toward reliability is extremely useful. One competent engineer charged with no other responsibility than reliability can do a great deal of good. A word of warning, however, is necessary. A routine, unimaginative reliability and quality assurance program increases costs with no real gains in reliability. The type of person selected for this function is the most important determinant of the result. Testing in the actual environment in which the hardware will perform is extremely important.

Automated checkout, startup, and operation is the current trend in many industries. NASA has recently started in this direction. More is being done and these experiences will probably be useful to industry. As an example (not described), a liquid-metal loop pumping sodium-potassium eutectic, or NaK, at 1100° F was operated completely unattended for a total loop operating time of about 14 000 hours, or more than 18 months. The test operator is called "the engineer with the four green eyes". The loop is automated, but since there are almost always people on site, a man takes a look in the control room once every few hours. If he sees that four adjacent green lights are all lit, then no major malfunction has occurred. Unattended operation will be extended to more complicated loops.

In all NASA work, advanced technology in instruments, materials, bearings and seals, and other such areas is often critical for the success of a new engine or system. Of the new technologies discussed, the extension of the use of infrared for temperature surveys is particularly interesting. This very powerful tool can be

306

used in many ways in the electric power industry. The optical torquemeter is an interesting device. The use of rotary transformers to eliminate slip rings and thus permit the reliable instrumentation of turbogenerator rotors is an intriquing prospect.

In the mechanics of materials area, some of the failures encountered in engines have been caused by thermal fatigue. The average engineer is usually unaware of the thermal fatigue problem or how to analyze it. Even experienced developmental stress analysts, most of whose work deals with elastic rather than plastic phenomena, are often unfamiliar with the modern methods of analyzing thermal fatigue. The strength and cost of fiber-glass composites make them very attractive materials particularly for outdoor or underground service where their corrosion resistance offers added attraction.

The work in aerospace technology to increase the life of rolling-element bearings and low-leakage seals is extremely interesting. Today, these bearings and seals are used in situations which a decade ago would have been untenable. Service life is being greatly extended; however, the sizes and lifetimes are still short of that required for utility service. Considerable test experience in this direction is required before their use would be recommended. However, they are attractive and work is continuing.

In the more advanced areas of cryogenic electrical components and direct conversion, ultimate utility becomes harder to predict. In the case of cryogenic electrical components, considerable cryogenic technology is available and has been reduced to practice. A cryogenic transmission line, for example, can be built. When it is properly designed, it will work, and it will last. Although economics for utility use has not been analyzed, it should be considered carefully when a specific application indicates its possible desirability.

Direct conversion is a tantalizing area. A level of technology has not yet been achieved where it will soon make a major impact, but it is often ''one discovery away.'' There are several rechargeable batteries which might make an excellent electric car if one or two of their problems can be solved. A low-cost, long-lived fuel cell making generation of electric power by this means economically attractive is perhaps one discovery short of feasibility. Thermoelectrics can be used today for special applications requiring a very small amount of power which is very reliable and simple. Thermionics and magnetohydrodynamics (MHD) operate at very high temperatures, and their practical utilization depends on the ability to build long-lived high-temperature devices at acceptable cost. This technology is not available today, but work is proceeding with those goals in mind. The fossil-fuel fired MHD appears to be of nearer term interest than any of the other MHD and thermionic systems.

12. INFORMATION SOURCES AND PROGRAMS

James E. Burnett

Aerospace related technology can often contribute significantly to seemingly unrelated fields. The rapid dissemination of aerospace related information that is of potential value to private industry is highly desirable.

Of course, communicating this information requires some underlying organization of the data. To this end, NASA has made its existing information storehouse (fig. 12-1) available to American industry. There are some 700 000 documents in this data bank, and about 8000 additions are made each month. The documents are under full bibliographic control; that is, they are categorized by subject, indexed and multiple cross-indexed based on selected key words, microfilmed, and indexed on magnetic tape for computer search and retrieval.

The 8000 new documents per month are covered in two abstract journals (fig. 12-2). The first of these is STAR, the Scientific and Technical Aerospace Reports, and the other is IAA, the International Aerospace Abstracts. Together, these two abstract journals provide comprehensive, current coverage of the world output of aerospace related scientific and technical information.

The STAR journal (fig. 12-3), published by NASA, is issued twice each month and covers report type literature. The source of the technical documents abstracted in STAR is about one-fourth NASA and NASA contractors, one-fourth Department of Defense and its contractors, and one-fourth from other domestic sources. The balance comes from Russia, Eastern Europe, and other foreign countries. STAR is available on subscription at $33 per year.

The companion journal (fig. 12-4), International Aerospace Abstracts, is published by the American Institute of Aeronautics and Astronautics under agreement with NASA. It, also, is issued twice each month, and it covers documents reported in technical society and professional journals. STAR and IAA have identical formats and indexing systems. The source of the technical documents abstracted in IAA is 53 percent domestic and 47 percent foreign. Russia and Great Britain are the largest individual foreign sources. Like STAR, IAA is available on subscription at $33 per year.

Subscribing to these two abstract journals can be a workable method of keeping abreast of new aerospace related technology. Subscribing is, of course, the easy part. The more difficult part is in taking those necessary steps that will actually

make the journals of constructive use and value inside your company.

Something quite different in the way of information services is the NASA Technology Utilization Program. The NASA TU Program is a continuing effort to make aerospace-related innovations, new scientific knowledge, and new technical skills broadly available to industry and the public. The key word here is "available," and technology is broadly or truly available only if there are effective means for communicating or transferring it. Consequently, the NASA TU Program seeks to develop new and effective communication methods of lasting value.

A special Technology Utilization conference, such as this one, is one such method. It is hoped that an awareness of certain new, interesting, and valuable technology results from these meetings and that the reader will wish to delve further into selected technical areas.

An approach to further technical inquiry is to contact a NASA Technology Utilization Office (fig. 12-5). Major NASA field centers are located in various parts of the country, ranging from Cambridge to Houston to Pasadena. Each center has a Technology Utilization Office. The office follows the technical work being done both at the center and by its contractors, and helps to identify those innovations and new developments of most industrial interest. As a result of this work, a variety of special TU publications are issued ranging from one page Tech Briefs, which cover single innovations, to Technology Surveys, which summarize the strong forward thrust of space technology in complete fields.

An additional important area of service by each of these TU Offices is that of working directly with interested industry. The offices answer questions, supply data, arrange for technical meetings or conferences, and, in general, work to improve technical communications.

Another, and very interesting, way of keeping informed of aerospace related technology is through an NASA Regional Dissemination Center. At the Center, NASA, industry, and university cooperation makes the total NASA data bank fully and selectively available to fee paying member companies on a regular working basis.

There are presently seven Regional Dissemination Centers. They are located at the universities of Indiana, Pittsburgh, New Mexico, Southern California, and Connecticut, and at Southeastern State College, Durant, Oklahoma, and the North Carolina Science and Technology Research Center. The first of these centers was established about 5 years ago, and there are now over 350 industrial member companies, each paying annual fees ranging from $500 to over $18 000. The amount of the annual fee depends on the amount and kind of services purchased. The membership includes both small businesses and a substantial number of blue-ribbon companies. The annual membership renewal rate is well over 90 percent, a pretty fair measure of the success of the centers.

NASA input to the centers is in two parts. First, the entire NASA data bank, including the new data acquired each month is made available. Second, NASA provides funds for about one-third of the operating cost of the center. The balance of the funds comes from the universities and from the membership fees paid by private companies. NASA funding is, however, a temporary situation. The clearly stated goal is for the centers to become financially self-supporting based on membership fees alone in about 5 years.

The services provided by these centers to their member companies include the current literature service and the retrospective library search. The current literature service keeps the individual member company informed of incoming new reports and journal articles appearing in the literature in those specific areas of interest defined by the company. The areas of interest definitions are, of course, a most important part of the process. They are carefully developed by each company working with specialists from the Dissemination Center staff. Each defined area of interest is then reduced to a computer search language and is used to automatically search the magnetic index tapes furnished each month by NASA. Relevant subject matter is retrieved and furnished to the member company. This current literature service may be used to obtain pertinent incoming reports in areas such as batteries or other direct-energy conversion methods, new steam or gas-turbine developments, automatic checkout systems, or any area of specific interest to the company.

The retrospective library search is, also, a specific technical information search and selection process. In this case, however, the total existing NASA data bank is computer searched against an area of interest definition usually developed to define one particular problem area, for example, nonstick O-ring seals or plastic to metal bonding techniques.

The relation between each member company and the Regional Dissemination Center is fully confidential, and this includes such things as the company's definition of its fields of interest.

Each Regional Dissemination Center member company receives a personalized service which includes an assigned technical coordinator to maintain personal contact. The technical coordinator provides person-to-person dialogue and professional information handling judgment. The combination of personal service and computerized information storage and retrieval is making these Regional Dissemination Centers a new and useful communication link, a link that makes aerospace related technology truly available to nonaerospace industry on a regular working basis.
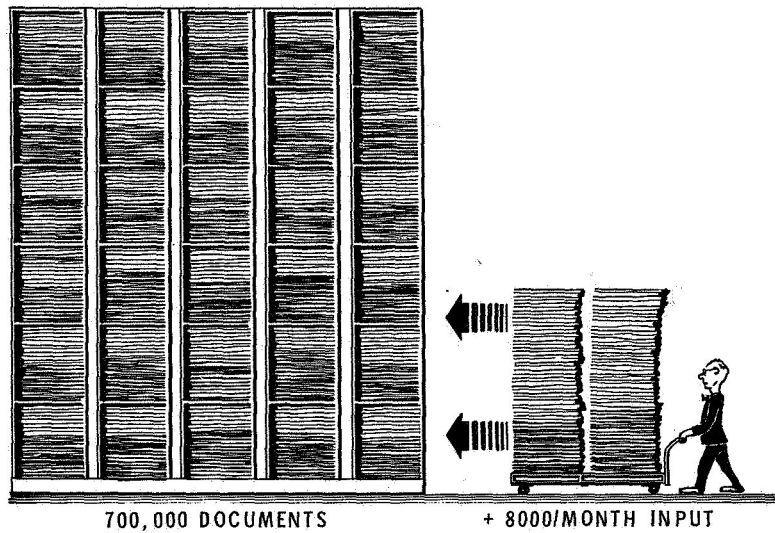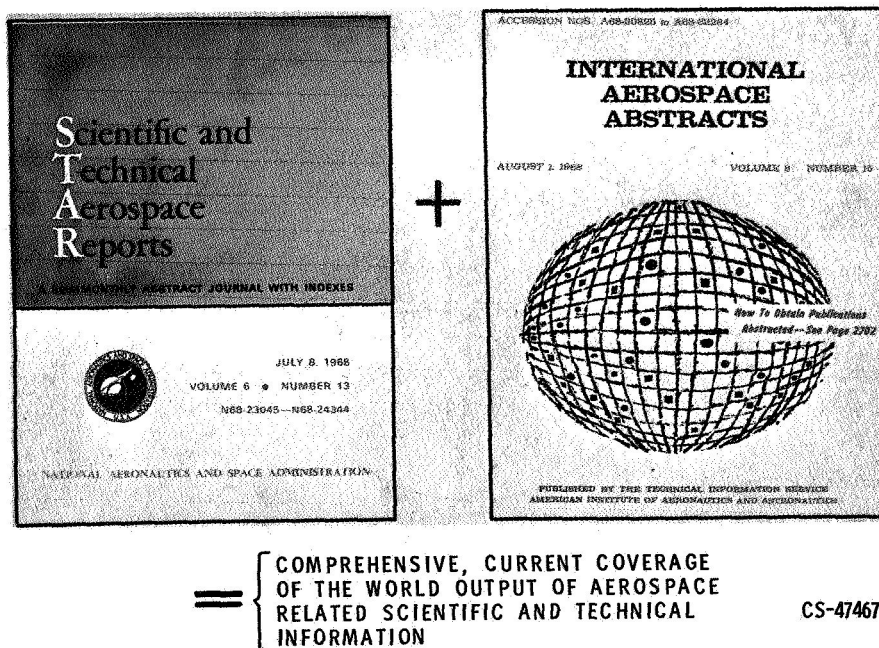
700,000 DOCUMENTS   + 8000/MONTH INPUT

Figure 12-1. - Current NASA data bank.

= { COMPREHENSIVE, CURRENT COVERAGE
OF THE WORLD OUTPUT OF AEROSPACE
RELATED SCIENTIFIC AND TECHNICAL
INFORMATION

CS-47467

Figure 12-2. - Abstract journals.
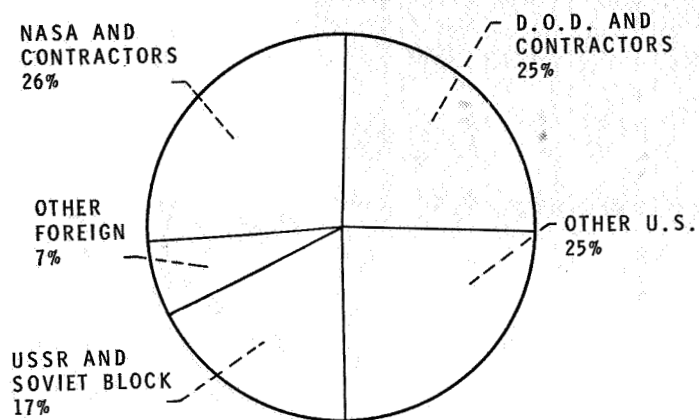
Figure 12-3. - STAR - abstracts of report literature.

NASA AND CONTRACTORS 26%

D.O.D. AND CONTRACTORS 25%

OTHER FOREIGN 7%

OTHER U.S. 25%

USSR AND SOVIET BLOCK 17%

U.S. 53%

USSR 15%

OTHER FOREIGN 22%

BRITAIN 10%
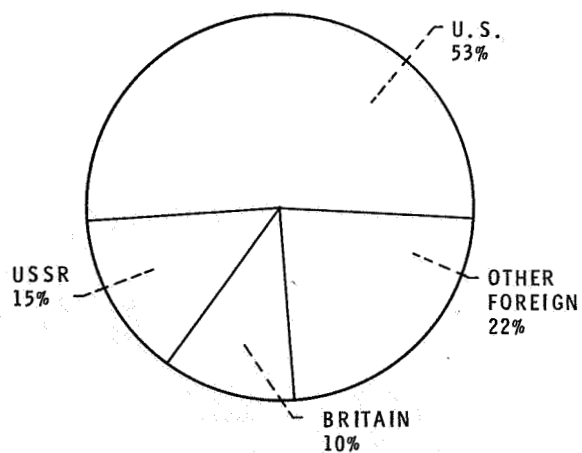
Figure 12-4. - IAA - abstracts of journal literature.

314
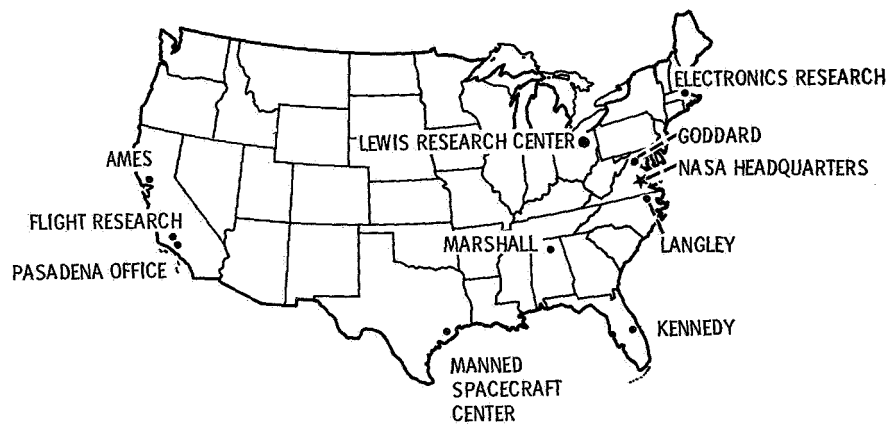
Figure 12-5. - Technology utilization offices at NASA field centers.
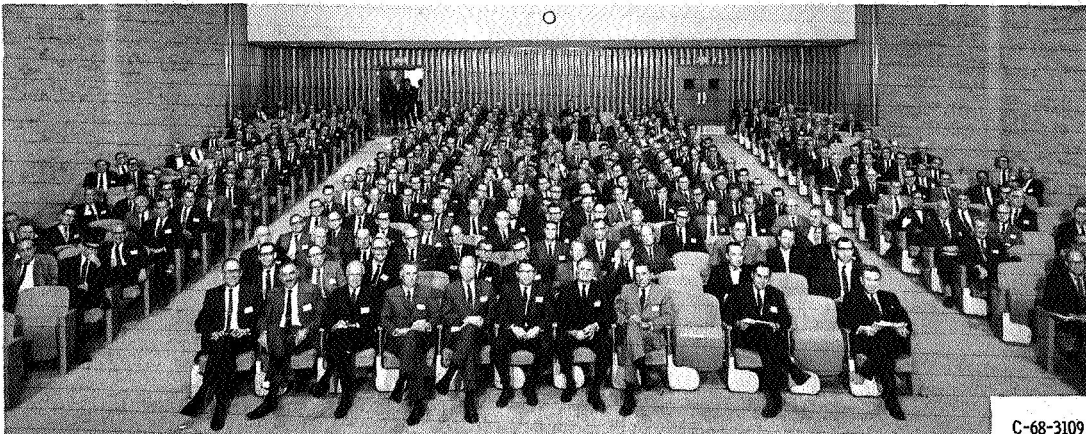
C-68-3109

Administrative and technical managers of major power companies attending the NASA Lewis Conference on Selected Technology for the Electric Power Industry.
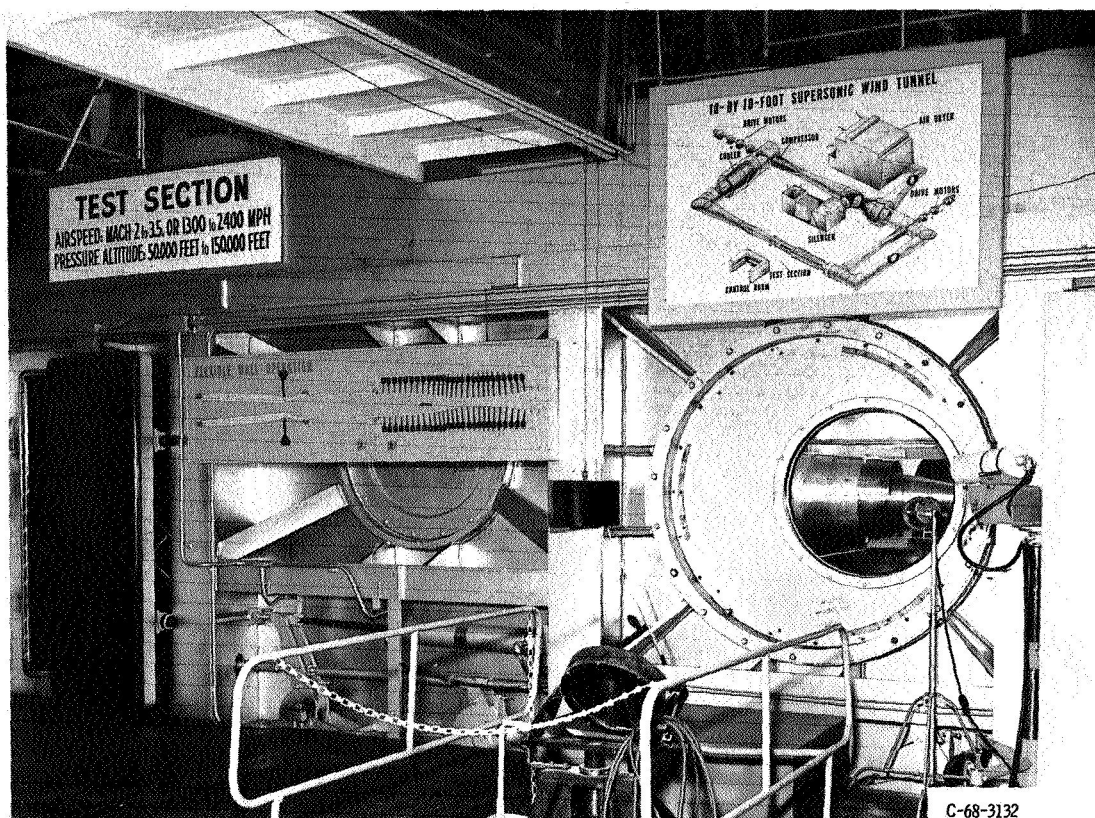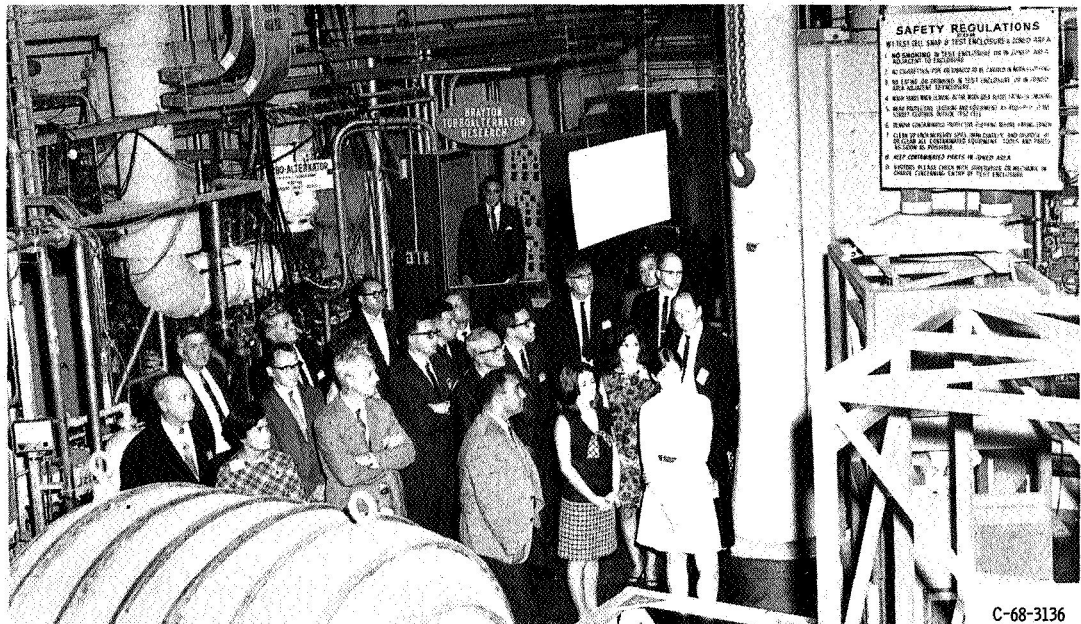

C-68-3132

10- BY 10-FOOT SUPERSONIC WIND TUNNEL: The 10- by 10-foot Supersonic Wind Tunnel tests the performance of aircraft and rocket vehicle propulsion systems at speeds ranging from 1300 to 2400 mph and altitudes ranging from 50 000 to 150 000 feet. Supersonic speeds are obtained in the 40-foot test section by expanding airflow through a 75-foot flexible wall nozzle. During the past decade, models of many supersonic aircraft, rocket boosters, and upper-stage vehicles have been tested in this facility. At present, models of airbreathing propulsion systems for advanced supersonic aircraft are being tested.

317
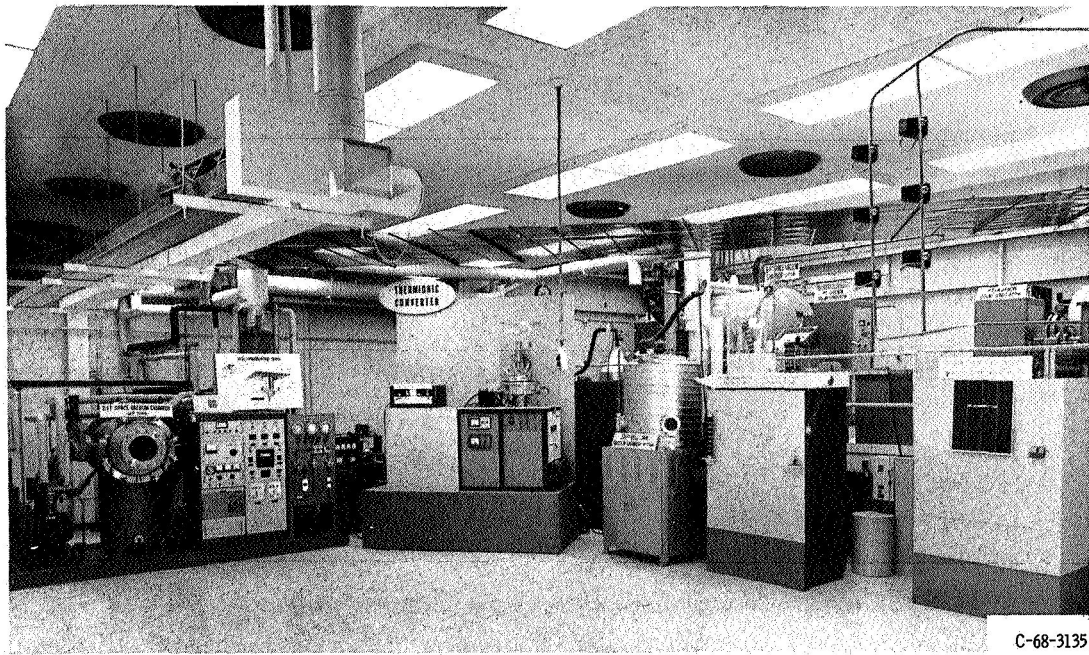
C-68-3135

DIRECT ENERGY CONVERSION: The Lewis Research Center conducts energy conversion research in many areas including thin film solar cells, advanced silicon solar cells, thermionic diodes, thermoelectric converters, high-density batteries, and batteries for use under extreme conditions of heat and cold. Several of these items were demonstrated including an experimental array of 200 cadmium sulfide thin film solar cells and batteries capable of operating at temperatures as low as -90° and as high as 840° F.

C-68-3136

BRAYTON AND RANKINE SYSTEMS: Two closed loop power conversion cycles under development to meet the future needs for large amounts of electrical power in space are the Rankine cycle and the Brayton cycle systems. Nuclear reactors can be used as a heat source for both systems. The largest Rankine cycle system under development at Lewis is the 35-kilowatt SNAP-8 (System for Nuclear Auxiliary Power). To obtain greater efficiency and lighter weight than steam plants, the SNAP-8 system uses liquid metals instead of water as a working fluid. The experimental Rankine system facility at Lewis using SNAP-8 components has logged more than 1500 hours of successful operation. An experimental 12- to 33-kilowatt Brayton system combining the turbine, alternator, and compressor on a single shaft is also in operation at Lewis. Using gas lubricated bearings, the shaft turns at 36 000 rpm.

318
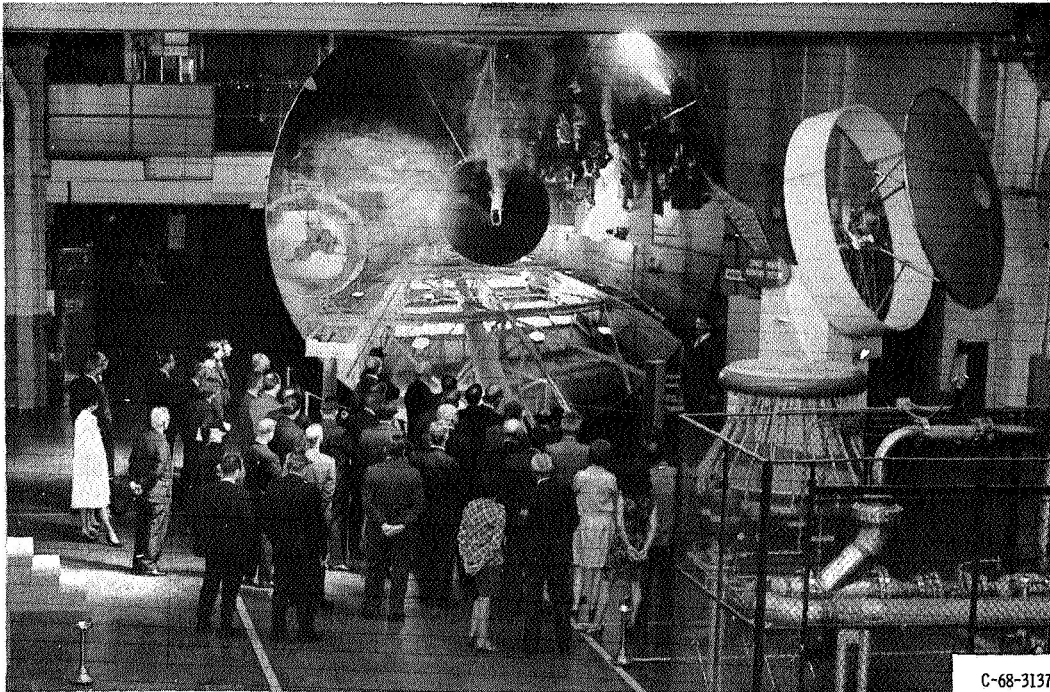
C-68-3137

SOLAR MIRROR: One way of making use of the vast amounts of energy coming from the Sun is to use it as a heat source by concentrating its rays with a parabolic mirror. Such a mirror must have good rigidity, resistance to impact by small particles, and be light enough to launch economically. A prototype concentrating mirror meeting these requirements has been constructed at Lewis. Machined from 1-inch magnesium plate, the 12 sectors of the mirror were shaped using a unique forming process developed at Lewis. Each section was then coated with an epoxy and plated with aluminum. The mirror would concentrate the Sun's rays on a heat storage receiver containing lithium fluoride. Here the inert gas working fluid of the system is heated to produce power in a turbogenerator system, while additional heat is stored for use when the unit is in the Earth's shadow. The complete system would fold into a compact disk shape. Several could be stacked for launch.


C-68-3139

ADVANCED COMPRESSORS: Increasing the pressure ratio and stable flow range of compressor stages is one of the goals of research at Lewis. Three research rotors were displayed which are designed for the study of improved blade shapes for high-speed operation with tip speeds of approximately 1400 feet per second. The best performing compressor rotor develops a pressure ratio of 1.82 at peak efficiency at 90 percent of design speed. This compares with an average stage pressure ratio of 1.3 for current aircraft engines and represents a significant advance in compressor technology.

319
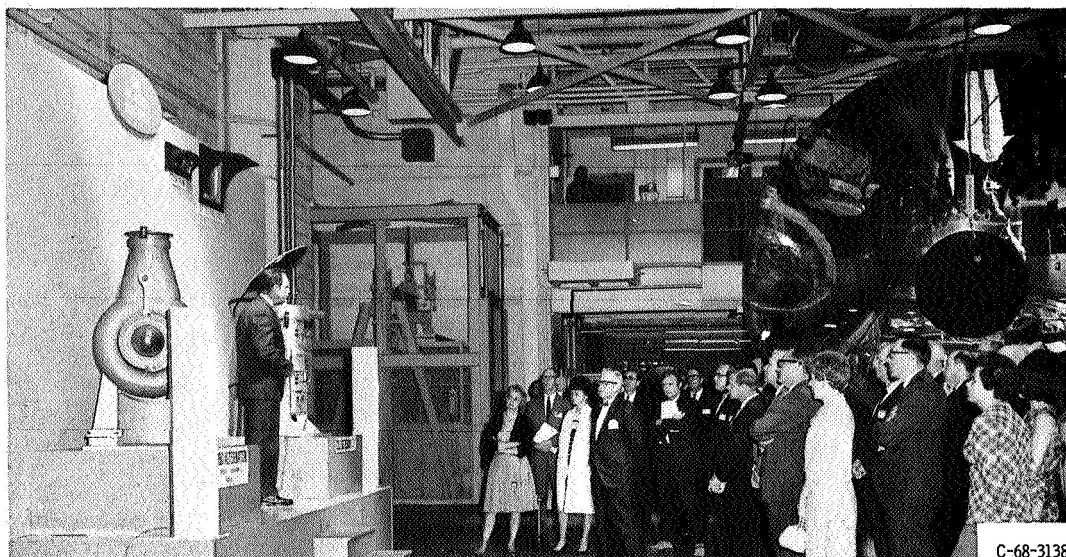
GAS BEARINGS: Lewis investigation of gas lubricated bearings has resulted in increased confidence that they may be used for space power systems. A 10-kilowatt turboalternator containing gas bearings is shown along with a bearing test rig constructed at Lewis. The bearing test rig uses internal probes to sense the motion of the shaft in relation to the bearing center and displays the position on an oscilloscope screen.
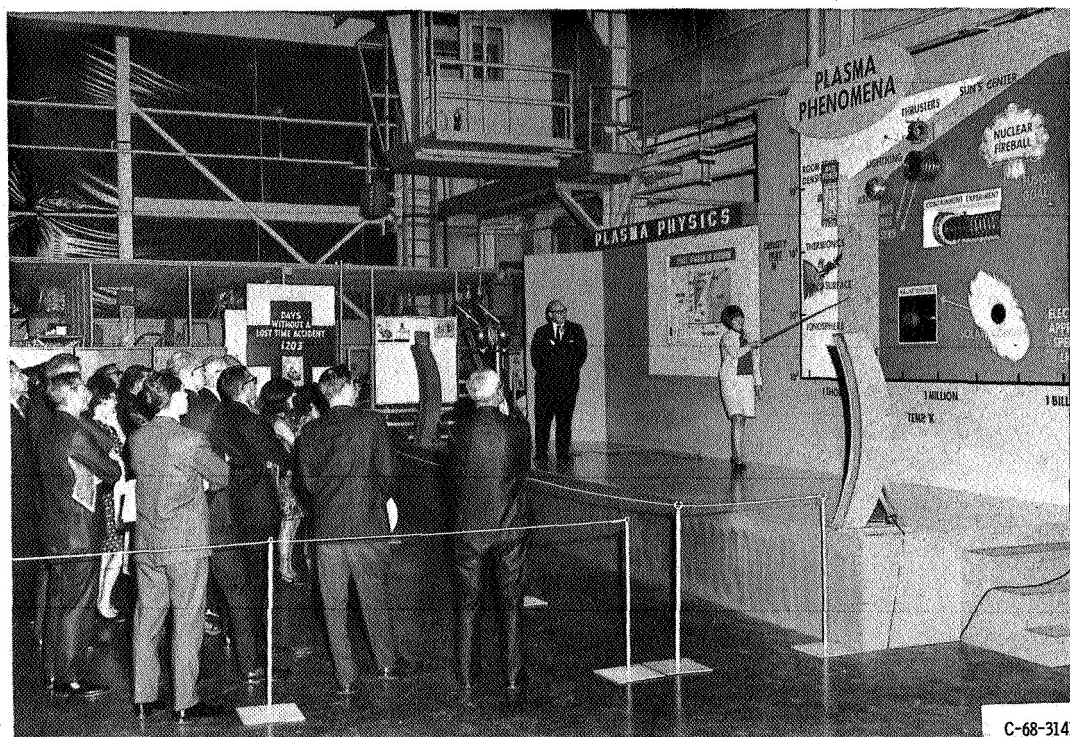
ELECTRIC PROPULSION LABORATORY: Plasma, the gaseous fourth state of matter made up of positively charged ions and free electrons, is being investigated at Lewis for use in both propulsion systems and space power generation systems. Since plasma is an electrical conductor, it can be acted upon by the interaction of a current with a magnetic field. This electromagnetic body force can be used to accelerate a plasma in a plasma thruster, to decelerate a plasma in a magnetohydrodynamic generator, or to contain a plasma in a "magnetic bottle." Both basic research into the nature of plasmas and applied research into methods of using their properties are conducted at Lewis. One interesting experiment recently was the use of a plasma rocket engine to simulate and study the interaction of the solar wind with the Earth's magnetosphere.

320
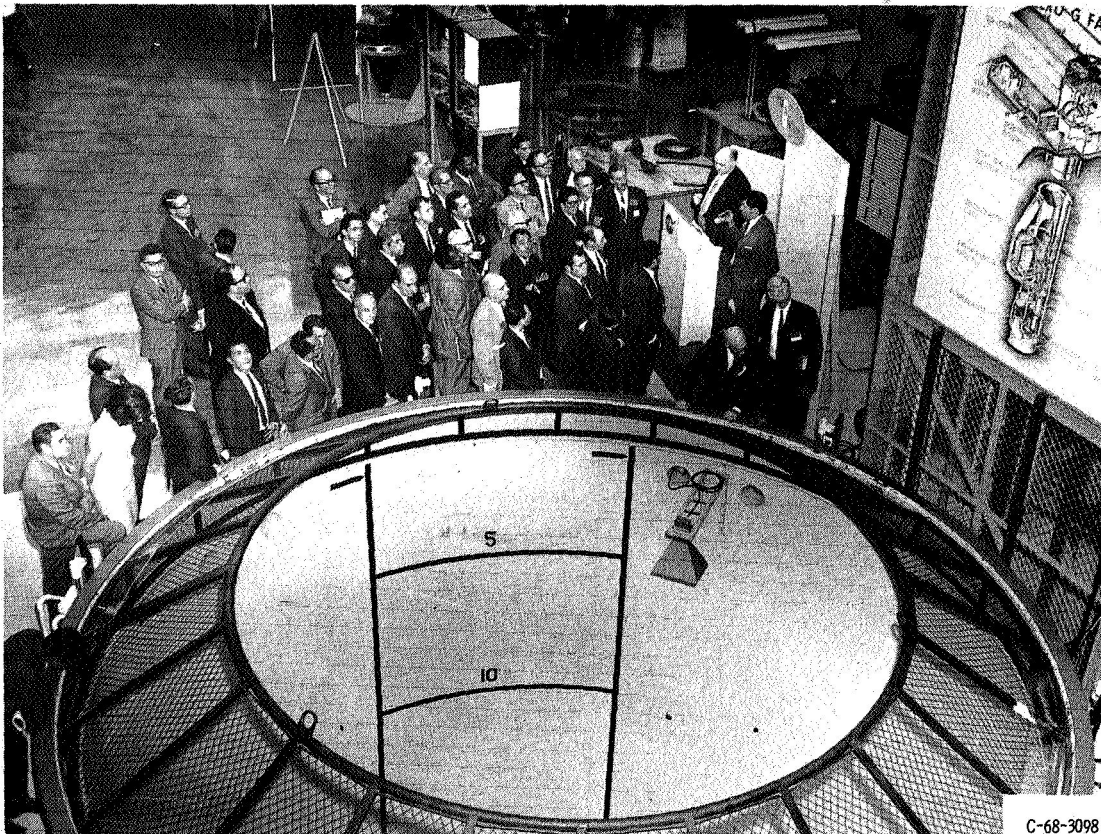
C-68-3098

ZERO GRAVITY FACILITY: The Lewis Zero Gravity Facility is the largest drop tower in the United States for producing the weightless conditions of outer space. Actual free-fall distance is 450 feet, producing 5 seconds of weightlessness. This time is doubled when experiment packages are projected upward from the bottom of the shaft and then fall back to be caught in the decelerator cart. The experiment packages are caught in a decelerator 19 feet deep and 12 feet in diameter filled with millions of polystyrene pellets. Experiments can vary in weight from 500 to 6000 pounds. Shaft air pressure is reduced during testing to eliminate the need for a drag shield. Typical experiments are for the study of the behavior of fluids in a tank or during a pumping process in the weightless environment. Data are recorded primarily on motion picture film.

"*The aeronautical and space activities of the United States shall be conducted so as to contribute . . . to the expansion of human knowledge of phenomena in the atmosphere and space. The Administration shall provide for the widest practicable and appropriate dissemination of information concerning its activities and the results thereof.*"

— NATIONAL AERONAUTICS AND SPACE ACT OF 1958

NASA TECHNOLOGY UTILIZATION PUBLICATIONS

These describe science or technology derived from NASA's activities that may be of particular interest in commercial and other non-aerospace applications. Publications include:

TECH BRIEFS: Single-page descriptions of individual innovations, devices, methods, or concepts.

TECHNOLOGY SURVEYS: Selected surveys of NASA contributions to entire areas of technology.

OTHER TU PUBLICATIONS: These include handbooks, reports, notes, conference proceedings, special studies, and selected bibliographies.

Details on the availability of these publications may be obtained from:

National Aeronautics and
Space Administration
Code UT
Washington, D.C. 20546

Technology Utilization publications are part of NASA's formal series of scientific and technical publications. Others include Technical Reports, Technical Notes, Technical Memorandums, Contractor Reports, Technical Translations, and Special Publications.

Details on their availability may be obtained from:

National Aeronautics and
Space Administration
Code US
Washington, D.C. 20546

NATIONAL AERONAUTICS AND SPACE ADMINISTRATION
Washington, D.C. 20546